Functional Characterization of Dermokine in Epidermal Differentiation

Canbay, Vahap

Publication date:
2023

Document Version
Publisher's PDF, also known as Version of record

Doctor of Philosophy

Doctoral thesis in Biotechnology and Biomedicine

Functional Characterization of Dermokine in Epidermal Differentiation

Vahap Canbay

DTU

A dissertation submitted to
Technical University of Denmark
for the degree of
Doctor of Philosophy

presented by

VAHAP CANBAY

M.Sc.Eng. - Biotechnology and Biomedicine
Technical University of Denmark
born August 13, 1993
Citizen of Austria

Supervisor: Prof. Ulrich auf dem Keller
Co-supervisor: Prof. Steffen Goletz

Chair: Assoc. Prof. Chiara Francavilla
Co-examiner: Prof. Mads Gyrd-Hansen
Co-examiner: PD. Dr. Hans-Dietmar Beer

2023

"Man is nothing else, but what he makes of himself."

-

Jean-Paul Sartre

Preface

This dissertation is submitted for the consideration of a PhD degree at the Technical University of Denmark. The work described herein was the product of a PhD project undertaken at the Department of Biotechnology and Biomedicine, under the main supervision of Prof. Ulrich auf dem Keller. The dissertation is divided into three main parts. The initial section offers an introduction, outlining the underlying objectives and extent of the project.

The introductory segment comprises a published commentary examining a novel mechanism for limited proteolysis in epidermal differentiation. Additionally, it culminates in a published overview discussing new insights into the mass spectrometry-based proteomics analysis of protease substrates. We also outline dermokine, previously identified as a MMP10 substrate, aiming to clarify the genuine functionality of this bioactive extracellular protein and its multiple isoforms in the process of epidermal differentiation.

The outcomes are segmented into three unpublished papers, the initial one exploring the methodology of optimized gene-editing techniques for application in human keratinocytes. Concurrently, we partnered with CytoSurge AG (Switzerland) to utilize their proprietary system that allows the direct injection of RNP-Cas9 moleclues into the nucleus of keratinocytes. Both approaches culminated in the generation of dermokine isoform truncations, ablating its cytokine-like domain. The second manuscript presents the application of human skin organoids and subsequent monitoring of dermokine-specific peptides as well as mapping of the exact MMP10-dependent cleavage site in human dermokine utilizing targeted degradomics. The third and final unpublished manuscript describes a phosphoproteomic approach to study dermokine-

dependent signalling events, utilizing the previously generated dermokine knockouts.

The manuscripts part of this thesis and all additional passages are the outcomes of original research, published or unpublished, carried out by myself and various colleagues with whom we collaborated for the duration of the project, mainly in Prof. Ulrich auf dem Keller's laboratory, as well as in Prof. Steffen Goletz's laboratory and the laboratory of Prof. Jörn Dengjel.

Dr. Weihua Tian assisted in the generation of the human keratinocyte knockouts with critical contributions to experimental design and manuscript revision. Dr. Tobias Beyer from CytoSurge AG (Switzerland) designed, implemented, and carried out the experiments to obtain the RNP-Cas9-based dermokine isoform knockouts. He was pivotal in this study and contributed critically to the manuscript revision.

Prof. Jörn Dengjel and his team were instrumental in the conception, design, implementation, enrichment, and acquisition of the phosphoproteomics experiment carried out in this project as well as the specific manuscript revision. In particular, Dr. Michael Stumpe and his guidance in the semi-automatic enrichment of phosphopeptides were critical.

Copenhagen, 30$^{\text{th}}$ June 2023

Vahap Canbay

Vahap Canbay

Summary

The most outer layer of the skin, the epidermis, acts as a protective barrier between the organism and its surrounding environment, operating as a boundary against detrimental substances, while also obstructing water loss and withstanding mechanical stress. The epidermis can be divided into four layers, related to the differentiation status of keratinocytes, ultimately resulting in formation of the cornified envelope. This process is heavily influenced by post-translational modifications, whereby limited proteolysis is critical not only for processing of structural proteins, such as filaggrin, but also regulatory mediators involved in several signalling events. An example of such a processing event that has been recently identified in Prof. Ulrich auf dem Keller's research group is the proteolytic cleavage of the bioactive mediator dermokine by matrix metalloproteinase 10. This cleavage event might be related to keratinocyte migration and differentiation.

As an essential member of the secreted protein gene complex family, dermokine and its various gene products play a vital role in development and stratification of suprabasal layers of the epidermis. In humans, the highly spliced dermokine exists in three major isoforms, dermokine-α, dermokine-β and dermokine-γ, whereas the C-terminal cytokine-like domain, present in dermokine-β and dermokine-α, substantially shapes the biological function of this secreted protein within the extracellular space. This cytokine-like domain is likely responsible for dermokine's bioactivity, acting as a ligand to control intracellular phosphorylation events, including the modulation of extracellular signal-regulated kinase 1/2 phosphorylation. However, the intricate mecha-

nism through which dermokine regulates keratinocyte differentiation remains elusive.

In this work, we addressed this issue by employing optimized CRISPR/-Cas9 gene editing strategies. We engaged two main gene editing methods, a transfection-based technique and an atomic force microscopy procedure utilizing FluidFM® technology. The transfection-based approach comprises an improved protocol for virus-independent delivery of CRISPR/Cas9 plasmids and the selection of single-cell mutants. The FluidFM® method enables the direct nuclear introduction of multiple gRNA CRISPR/Cas9 ribonucleoprotein complexes. Applying these designs, we generated *Dmkn* $\beta\gamma^{-/-}$ and *Dmkn* $\alpha\beta^{-/-}$ keratinocytes with high gene-editing efficiency and minimal off-target effects. This study provides novel and optimized reliable gene editing techniques to generate keratinocyte CRISPR-based knockouts.

After establishment of the *Dmkn* $\beta\gamma^{-/-}$ and *Dmkn* $\alpha\beta^{-/-}$ keratinocytes, we aimed to investigate the role of dermokine in the course of epidermal differentiation in a human model. Thereby, we took advantage of skin organoids, which were applied to explore dermokine-β's and dermokine-α's role in epidermal stratification. Histological assessments observed a non-stratified epidermis along the dermokine-specific expression gradient, which was confirmed by immunohistochemical staining. Mass spectrometry-based proteomics techniques further monitored several molecular changes due to isoform-specific dermokine truncations that we validated at the protein level by parallel reaction monitoring. A subsequent unbiased proteomics screen on *Dmkn* $\beta\gamma^{-/-}$ skin organoids unveiled changes in proteins linked to cornified envelope assembly, filaggrin processing, and desquamation in comparison to the wildtype. These changes were validated in *Dmkn* $\alpha\beta^{-/-}$ using internal standard triggered parallel monitoring, which corroborated significant reductions in filaggrin modulating proteases and proteins governing cornified envelope assembly upon cytokine-like domain depletion. With help of targeted degradomics and heavy reference peptides, we confirmed dermokine cleavage by matrix metalloproteinase 10 and for the first time mapped the cleavage site in the human protein.

Next, we analyzed how the extracellular dermokine isoforms modulate intracellular phosphorylation events. Applying automation-assisted sample preparation and cutting-edge LC-MS/MS instrumentation together with advanced data analysis strategies, we investigated phosphorylation events in *Dmkn* $\beta\gamma^{-/-}$ and *Dmkn* $\alpha\beta^{-/-}$ in comparison to wildtype keratinocytes. This system-wide comparison enabled us to confidently link differentially phosphorylated serines, threonines, or tyrosines to their specific kinases. In addition, we recorded the to our knowledge deepest phosphoproteome of keratinocytes established as of now, comprising 15468 quantified phosphosites. We could observe enhanced phosphorylation levels of various crucial receptors, such as proto-oncogene, receptor tyrosine kinase Met at S990, erb-b2 receptor tyrosine kinase 2 at T701, and insulin like growth factor 2 receptor at S2409, under endogenous dermokine levels in comparison to $\alpha\beta^{-/-}$ keratinocytes. These changes illustrate dermokine's proposed role in main physiological mechanisms in keratinocytes, including receptor activity and adhesion dynamics. Concomitantly, we identified differential dermokine-associated phosphorylation events in both the proto-oncogene tyrosine-protein kinase Src at S17, which has been detected as a key factor in cellular migration, as well as protein tyrosine phosphatase receptor type κ. Subsequently, an increase in phosphorylation of catenin δ 1 was observed when dermokine was ablated. This alteration suggests its impact on the associative state with cadherin 1 and therefore, the adhesive strength of the cells, which is known to increase upon the dephosphorylation of catenin δ 1, which might be mediated by differentially phosphorylated protein tyrosine phosphatase receptor type κ.

Overall, our findings indicate that the modulated phosphorylation of catenin δ 1 upon ablation of dermokine has potential impact on keratinocyte adhesion mediated by dermokine activity.

Oversigt

Den yderste del af huden, epidermis, er en beskyttende barriere mellem organismen og dens omgivelser, der fungerer som en barriere mod skadelige stoffer, og samtidig forhindrer vandtab og modstår mekanisk stress. Epidermis kan opdeles i fire unikke segmenter, der omfatter basale keratinocytters opadgående migration, hvilket fører til udvikling af suprabasale niveauer og kulminerer i etableringen af det yderste hornlag. Komplekse post-translationelle processer, der styrer de dynamiske ændringer af proteomet, er essentielle for opretholdelse af den epidermale homeostase. Kontrolleret proteolyse er afgørende for modificering af visse proteiner, såsom filaggrin og regulatoriske proteiner, der er involveret i adskillige signaleringer, hvilket regulerer komplekse proteolytiske netværk som f.eks. det epidermale protease-netværk. Et fremragende eksempel på en sådan molekylær ændring, der for nylig er blevet identificeret i Prof. Ulrich auf dem Kellers forskningsgruppe, er matrix metalloproteinase 10s proteolytiske kløvning af dermokin. Denne kløvning formodes at være relateret for migration af keratinocytter.

Dermokin og dets forskellige genprodukter er en essentiel del af familien af sekretoriske protein-gener, og spiller en vital rolle i udviklingen og stratifikationen af det stratificerede epitels suprabasale lag. Især det cytokinlignende domæne, der er placeret tæt på C-terminalen af dermokin-β og også er til stede i dermokin-α, er vigtig for den biologiske funktion af det sekretoriske protein ekstracellulært. Dette cytokinlignende domæne er sandsynligvis ansvarlig for dermokins bioaktivitet, der fungerer som en ligand for at fremkalde intracellulære fosforyleringer, herunder modulering af ERK 1/2-fosforylering. Det er

dog stadig uklart hvordan dermokin regulerer den komplekse differentiering af keratinocytter.

I dette projekt, undersøgte vi dette ved at anvende optimerede CRISPR/-Cas9 genredigeringsstrategier. Vi benyttede to redigeringsmetoder, nemlig en transfektionsbaseret teknik og en atomkraftmikroskopiprocedure, der anvendte FluidFM®-teknologien. Den transfektionsbaserede tilgang omfattede en forbedret protokol for indsættelse af CRISPR/Cas9-plasmider uafhængig af virus, samt valg af enkeltcellemutanter. Samtidigt gjorde FluidFM®-metoden det muligt at introducere flere gRNA CRISPR/-Cas9 ribonukleinprotein komplekser direkte i kernen. Ved at anvende disse teknikker genererede vi *Dmkn* $\beta\gamma^{-/-}$ og *Dmkn* $\alpha\beta^{-/-}$ keratinocytter med høj genredigeringseffektivitet og minimale off-target effekter. Herved blev der fundet en pålidelig genredigeringsteknik til at generere keratinocyt knockouts. Efter etablering af *Dmkn* $\beta\gamma^{-/-}$ og *Dmkn* $\alpha\beta^{-/-}$ keratinocytterne, var formålet at undersøge dermokins rolle i den epidermale differentiering. Vi benyttede os af hudorganoider, der blev anvendt til at undersøge dermokin-β's og dermokin-α's rolle i epidermal stratifikation. Ved histologisk vurdering blev der observeret en ikke-stratificeret epidermis langs den dermokin-specifikke gradient, hvilket blev bekræftet ved immunohistokemisk farvning. Massespektrometri (MS)-baserede proteom teknikker blev brugt til at kortlægge flere biokemiske ændringer forårsaget af dermokin-trunkeringer, hvor parallel reaktion monitoring MS teknologien i første omgang viste betydelige ændringer i dermokin-domænespecifikke peptider på grund af trunkeringen. Især var C-terminal peptidet af det cytokinlignende domæne fraværende i *Dmkn* $\alpha\beta^{-/-}$ organoider, men var stadig detekterbart i *Dmkn* $\beta\gamma^{-/-}$ organoider. En efterfølgende unbiased proteomics screening på *Dmkn* $\beta\gamma^{-/-}$ hudorganoider afslørede ændringer i proteiner knyttet til etablering af det yderste hornlag, filaggrin-bearbejdning, og afstødning af hudceller sammenlignet med vildtypen. Disse ændringer blev valideret i *Dmkn* $\alpha\beta^{-/-}$ ved hjælp af internal standard triggered parallel monitoring MS-teknologien, og bekræftede signifikante reduktioner i filaggrin-modulerende proteaser og proteiner, der styrer etableringen af det yderste hornlag, når det

cytokin-lignende domæne ikke var til stede. Ved anvendelse af i taargeted degradomics og isotop mærkede referencepeptider var vi i stand til at bekræfte, som tidligere demonstreret i murine modeller og western blot-analyser, at matrix metalloproteinase 10 kløver menneskelig dermokin to aminosyrer efter P 201, hvilket stemmer overens med enzymets etablerede præference for P ved P3.

Derefter undersøgte vi den komplicerede mekanisme, hvorved ekstracellulær dermokin initierer intracellulære fosforyleringer. Ved at bruge automatiseret prøveforberedelse og avanceret LC-MS/MS-instrumentering, samt avancerede dataanalysestrategier, undersøgte vi fosforyleringer i *Dmkn* $\beta\gamma^{-/-}$ og *Dmkn* $\alpha\beta^{-/-}$ såvel som vildtype keratinocytter. Ved systematiske sammenligning kunne vi knytte fosforylerede seriner, threoniner eller tyrosiner til deres specifikke kinaser med sikkerhed. Derudover registrerede vi det til dato største keratinocyt fosfoproteom, herunder 15468 kvantificerede fosfosites. Vi observerede forhøjede fosforyleringsniveauer af forskellige afgørende receptorer, såsom proto-onkogenet, receptor tyrosinekinase Met på S990, erb-b2 receptor tyrosinkinase 2 på T701 og insulin-lignende vækstfaktor 2 receptor på S2409, under endogene dermokin niveauer i forhold til $\alpha\beta^{-/-}$ keratinocytter. Disse ændringer bekræfter dermokins påståede rolle i essentielle fysiologiske mekanismer i keratinocytter, herunder receptoraktivitet og adhæsionsdynamik. Samtidig identificerede vi forskellige dermokin-associerede fosforyleringer i både proto-onkogenet Src på S17, som er blevet identificeret som en nøglefaktor i cellulær migration, og protein-tyrosin-fosfatase-receptor-typen κ. Efterfølgende blev der observeret en stigning i fosforyleringen af catenin δ 1, når dermokin blev fjernet. Denne ændring antyder en indflydelse på associationen med cadherin 1 og hermed cellernes tiltrækningskraft, der er kendt for at øges ved defosforylering af catenin δ 1, som kan faciliteres af forskellige protein-tyrosin-fosfatase-receptor-type κ forforyleringer.

Endelig antyder vores resultater, at den modulerede fosforylering af catenin δ 1 efter fjernelse af dermokin potentielt påvirker keratinocyt-adhæsionen, som formidles af dermokin.

Acknowledgments

To begin with, I want to pay my utmost thanks to my mentor and supervisor Prof. Ulrich auf dem Keller. Ulrich, you provided me the freedom I needed to develop as a scientist and when I needed you most, you were always present. You not only provided intellectual advice to tackle my problems but also offered the scientific stimulation I needed to carry on. Your support, especially towards the end, which I perceived as the most difficult time, was unwavering. You gave me the opportunity to attend multiple conferences and acquire invaluable communication skills, which I deeply value. I am ever grateful to have found such a mentor and friend. Your lessons were valuable and I hold them dear. I wish you all the best for your future.

I want to thank Dr. Farrell McGeoghan and Dr. Fabio Mira Rocha Sabino for their valuable supervision at the beginning of my PhD project. Especially I would like to acknowledge Dr. Weihua Tian and his critical contributions to this work.

Many thanks go to my external research stay supervisor Prof. Dengjel, for the fruitful discussions we had.

I would like to thank the DTU proteomics core facility for their help, especially Maike Wennekers Nielsen and Dr. Marie Vestergaard Lukassen.

I am thankful to Prof. Ulrich auf dem Keller for proof-reading my thesis and offering comments regarding the content of the thesis. I am also grateful to Assist. Prof. Louise Bundgaard for providing corrections regarding the Danish summary.

I want to thank my current and former colleagues as well as my friends,

Dr. Elizabeta Madzharova, Dr. Konstantinos Kalogeropoulos, Aleksander Moldt Haack, Chatpakorn Rassameena Christiansen, Dr. Philipp Kastl, Dr. Simonas Savickas, Deniz Tohumcu, Vinzenz Maximilian Lenhart and Runar Haaskjold.

Many thanks go to all my bachelor's and master's students I had the chance to supervise, especially Chrysillis Judy Magaard Polhaus.

Lastly, I would like to thank Skintegrity.CH for their tremendous meetings and scientific stimulation.

I want to thank Charlotte Friederike Barbara Trautmann for her unyielding support throughout the PhD especially in the last six months and to her gentle love.

Many thanks to my family, especially my siblings, Yasemin and Yakub Ali Canbay for their support.

List of Publications

Publications

This PhD thesis resulted in the following manuscripts:

- **Canbay V** and auf dem Keller U (2021) New strategies to identify protease substrates. *Curr Opin Chem Biol*, 60, pp. 89-96, **doi.org/10.1016/j.cbpa.2020.09.009**.

- **Canbay V** and auf dem Keller U (2023) New links for meprin β within the protease web. *FEBS J*, 290: 76-79, **doi.org/10.1111/febs.16621**.

- **Canbay V**, Tian W, Beyer TA, Migenda Herranz A, Mailand S, Goletz S and auf dem Keller U (2023) Efficient virus-free CRISPR/Cas9 genetic editing of human keratinocytes. *In preparation.*

- **Canbay V** and auf dem Keller U (2023) Cell autonomous functions of dermokine in human keratinocytes in the differentiating epidermis. *In preparation.*

- **Canbay V**, Stumpe M, Dengjel J and auf dem Keller U (2023) Dermokine drives keratinocyte differentiation by phosphorylation-dependent modulation of cell adhesion. *In preparation.*

This PhD thesis resulted in the following conference abstract:

- **Canbay V**, Tian W, Goletz S and auf dem Keller U (2022) Functional characterization of dermokine in epidermal differentiation, *Wound Repair and Regeneration* Volume 30, Issue 5, pp. A14-A15, **doi.org/10.1111/wrr.13041**.

Additional peer-reviewed publications resulting from work at DTU that have not been included as integral parts of this thesis:

- Ahmadi S, Pachis S, Kalogeropoulos K, McGeoghan F, **Canbay V**, Hall S, Crittenden P, Dawson C, Bartlett K, Gutiérrez J, Casewell N, auf dem Keller U, Laustsen A (2022) Proteomics and histological assessment of an organotypic model of human skin following exposure to *Naja nigricollis* venom. *Toxicon* Volume 220, 106955, ISSN 0041-0101, **doi.org/10.1016/j.toxicon.2022.106955**.

- Noddeland H, Lind M, **Canbay V**, Savickas S, Petersson K, Malmsten M, Dawson C, auf dem Keller U, Heinz A (2023) Mapping the matrix metalloproteinase landscape of imiquimod-induced mouse model using targeted proteomics. *In preparation.*

- Dohnalek J, **Canbay V**, Christiansen R C, Tian W, auf dem Keller U, Strisovksy K (2023) The function of RHBDL2 in human keratinocyte development: *In preparation.*

- Tian W, **Canbay V**, auf dem Keller U, Goletz S (2023) The role of glycosyltransferases in exosomal proteome composition. *In preparation.*

- Sabino F, Madzharova E, **Canbay V**, auf dem Keller U (2021) Protease signaling in contact inhibition of proliferation (CIP). *In preparation.*

- Nyström E E L, Smith M, **Canbay V**, Kalogeropoulos K, Hansson G, auf dem Keller U, Becker-Pauly C (2023) Increased Cathepsin S mediated activation of *Clca1* induces mucus barrier defects in colitis. *In preparation.*

Contents

CHAPTER 1

Introduction

1.1 Skin

The skin is the largest organ of the human body. Human skin serves as the interface between the body and the surrounding environment and provides essential functions, such as sensing and immunological protection. It is constituted of three layers, which are the **epidermis**, the **dermis** and the hypodermis.

1.1.1 Epidermis

The outermost layer of the skin is represented by the epidermis, which is responsible for maintaining the defensive barrier between the organism and its immediate environment. The epidermal barrier protects the human body not only against detrimental substances, UV irradiation and pathogenic microorganisms but also prevents water loss and resists mechanical stress (Candi et al., 2005; Proksch et al., 2008). Epidermal thickness is frequently between 75 µm to 96 µm (Sandby-Møller et al., 2003). Although keratinocytes are the main cell population, the epidermis comprises also melanocytes, responsible for melanin production, the pigment that is providing skin color and UV light protection; Langerhans cells and $\gamma\delta$ T cells, immune system cells of the skin; and Merkel cells which are associated with the peripheral nervous system and attached to nerve endings, causing Merkel cells to be sensitive to touch. The epidermis can be subdivided into four distinct strata due to the constant terminal keratinocyte differentiation process establishing a continuous renewal of the epidermis, via the outward migration of basal keratinocytes (Fuchs & Raghavan, 2002). Throughout the stratified epithelium, each layer is distinguishable by distinct biochemical and morphological hallmarks, indicated by the specific stratification status of keratinocytes (Watt, 1998). Hereby, distinct differentiation markers can be used to spatially distinguish the epidermal strata by the differential abundance of cellular components, for instance different intermediate filaments such as keratins (K) (Simpson et al., 2011).

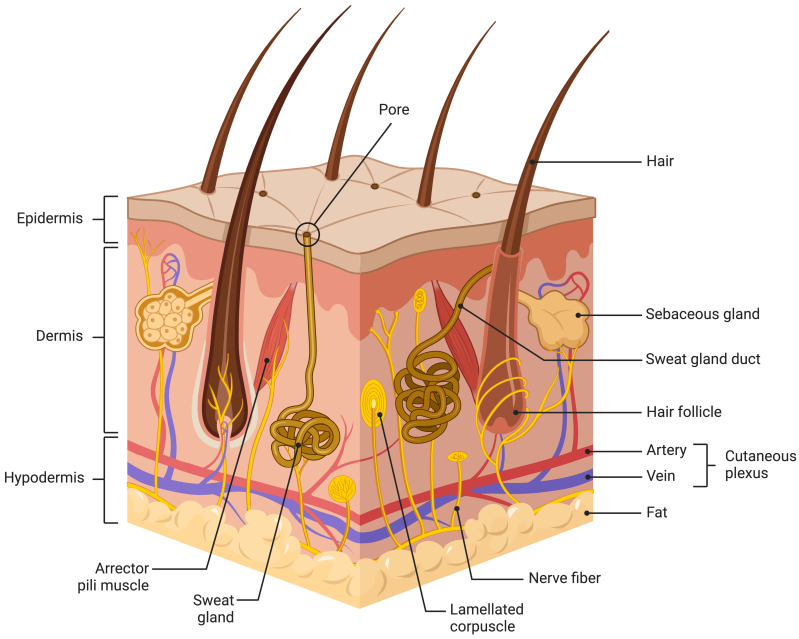

Figure 1.1. **Structure of the skin.** The constantly renewed human epidermis can be characterized by four distinct layers: stratum basale, stratum spinosum, stratum granulosum and stratum corneum. Adapted from "Anatomy of the Skin" from BioRender.com (2023)

The stratum basale (basal layer), also known as the basal layer, accommodates proliferative keratinocytes, renewed from a small population of stem cells undergoing mitosis, and is in contact with the dermis. The beginning of terminal differentiation is marked by the withdrawal of keratinocytes from the cell cycle and the disintegration of hemidesmosomes, which are protein complexes that anchor keratinocytes to the basement membrane (Segre, 2006). The expression profile of newly formed keratinocytes is characterized by up-regulated basal cytokeratins 5 and 14 (K5 and K14) and changes at the onset of stratification to up-regulated suprabasal cytokeratins 1 and 10 (K1 and K10) and down-regulated K5 and K14 (Freedberg et al., 2001). Cytokeratins merged with microfilaments and microtubules form the cytoskeleton of epithelial cells,

and several cytokeratins assemble into keratin intermediate filaments, which span from the nuclear lamina to desmosomes (Candi et al., 2005).

Suprabasal layers include the stratum spinosum (spinous layer) and stratum granulosum (granular layer). The keratinocytes of the spinous layer become polyhedral, are non-proliferative yet metabolically immensely active, and are held together by several cell-cell adhesion complexes like numerous desmosomes (Burns et al., 2010).

The granular layer is distinguishable by the presence of keratohyalin granules, containing profilaggrin, which later is responsible for the aggregation of keratin filaments, forming a waterproof layer (Simpson et al., 2011). Another differentiation marker of suprabasal keratinocytes is cytokeratin 2 (K2), which is up-regulated towards the granular layer.

The outermost layer of the epidermis is termed the stratum corneum (cornified layer) and forms the cornified envelope. Keratinocytes of the cornified envelope are terminally differentiated and named corneocytes, which are both flattened and anucleated and metabolically inactive. The dead cells further release lipid-filled granules into the extracellular space of the corneocytes to strengthen the cornified envelope's water impermeability, preventing critical loss of water from the human body (Candi et al., 2005). Hereby, transglutaminases assemble a compact protein network, through the formation of isopeptide bonds between lysine side chains and glutamine residues. The constant proliferation of basal keratinocytes requires the corneocytes to shed off, further maintaining the cornified envelope at a constant width by underlying cells.

The **basement membrane** is the connecting structure between the epidermis and the dermis, a region that physically segregates the two compartments while stabilizing the skin. The mechanical strength stems from the cross-linked collagen IV network and hemidesmosomes attaching basal cellular keratin filaments to anchoring filaments for cell-matrix contacts.

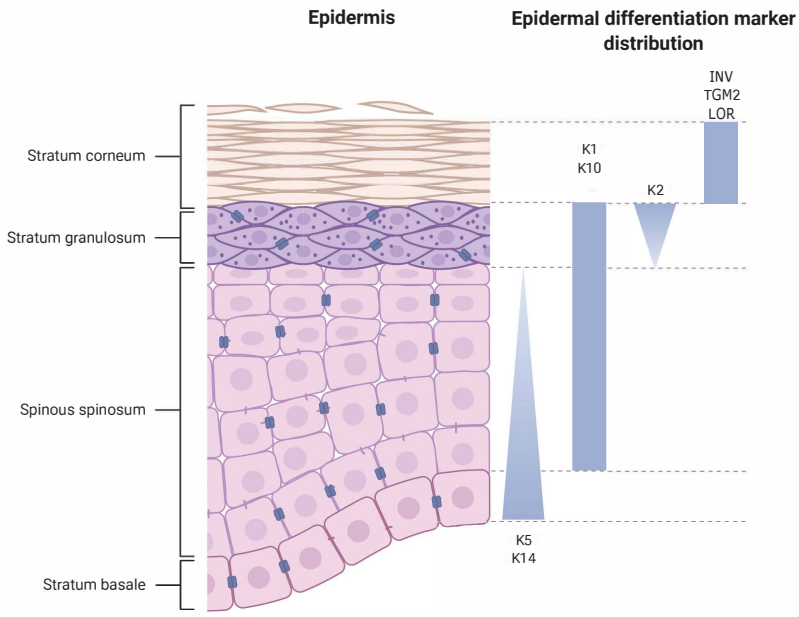

Figure 1.2. Structure of the epidermis. The constantly differentiating human epidermis is characterized by four distinct layers: stratum basale, stratum spinosum, stratum granulosum and stratum corneum. While basal keratinocytes are constantly subdividing and migrating outwards, desquamation keeps the cornified layer at a constant thickness. Each layer has its own role and can be defined by the exclusive expression of cytoskeletal proteins like keratins (K) and cross-linking enzymes such as transglutaminases (TGM2), involucrin (INV) and loricrin (LOR). Adapted from "Desmosomal Protein Distribution in the Epidermis" with Biorender.com

1.1.2 Dermis

Underneath the epidermis is the dermis dominated by fibroblasts, which produce most of the extracellular matrix resulting in the production of connective tissue. Besides fibroblasts, the dermis is home to immune cells such as macrophages and mast cells, containing lymphatic and blood vessels, as well as tightly connected nerves and nerve endings. In addition, skin appendages are localized in the dermis, such as hair follicles, sweat glands, sebaceous glands and nails and extend throughout the epidermis. The skin's tensile

strength results from fibroblast-derived type I collagen and elastin fibers, yet complementary elasticity is provided by proteoglycans and glycosaminoglycans, arranging a glycoprotein matrix that plays a crucial role in maintaining hydration (Burns et al., 2010).

Below the dermis is a layer of subcutaneous tissue, termed **hypodermis**, which is populated by adipocytes and fibroblasts, functioning both as a thermal insulator and a central figure for the energy metabolism as well as a barrier against physical trauma.

1.2 Cutaneous Wound Healing

As a result of a mechanical injury, e.g. unforeseen incidents or surgical procedures, the most outer damaged tissue is the skin, whereby the damage triggers the highly convoluted biological process of healing, helping the skin to regain its original purpose. The moment an injury appears, the process of healing begins by ceasing the bleeding. The overall healing process can take several years, until the wound has fully recovered, but leaves a permanent scar.

The cutaneous healing process is made up of multiple overlapping stages that involve multiple types of cells, releasing growth factors, cytokines, proteases as well as extracellular matrix proteins, and must be precisely coordinated in both space and time to guarantee correct wound recovery. In the early stages of the healing process inflammatory cells help to reduce inflammation, keratinocytes are required to proliferate for the restoration of the epidermis, fibroblasts assist in the formation of new granulation tissue and in the contraction of the wound, and endothelial cells are committed to forming new blood vessels.

Hemostasis and **inflammation**, the formation of new tissue through cellular **proliferation**, and tissue **remodeling**: These three separate, yet interwoven phases characterize the healing of skin wounds.

1.2.1 Hemostasis and Inflammatory Reaction

Upon injury, the first phase begins within minutes with the arrival of platelets at the wound site, contributing to formation of a blood clot that contains cross-linked fibrin, plasma fibronectin, extracellular matrix proteins, vitronectin and thrombospondin, causing vasoconstriction, which effectively leads to reduced blood loss and a brief sealing of the wound. The blood clot serves as a storage area for cytokines and growth factors and provides a temporary support structure for leukocytes, fibroblasts, and endothelial cells to move through. Subsequent to the primary hemostasis, blood vessels expand and allow for recruitment of more platelets, which in turn attract immune cells by releasing chemo-attractants.

The newly recruited neutrophils and activated macrophages sweep through the damaged region to remove foreign objects and microorganisms that have entered the wound. The main purpose of inflammatory cells is the protection against bacterial cells by phagocytosis and secreting proteases and growth factors, thereby initiating keratinocytes and fibroblasts marking the onset of the second stage of wound healing.

1.2.2 Proliferation

The second stage of healing lasts from day 3 to day 10 after wounding and is primarily prevailed by proliferation and migration of cells, involving angiogenesis and the development of new tissue. The release of immune cell- and epithelial cell-derived growth factors and cytokines prompt the relocation of actively proliferating keratinocytes toward the wound edge above the temporary blood clot to induce re-epithelization and efficiently seal the open wound with a new epidermis.

Simultaneously, the wound begins the formation of new stroma, granulation tissue that is rich in migrating fibroblasts from adjacent healthy tissue in response to growth factors such as TGF-β. In addition, the available growth

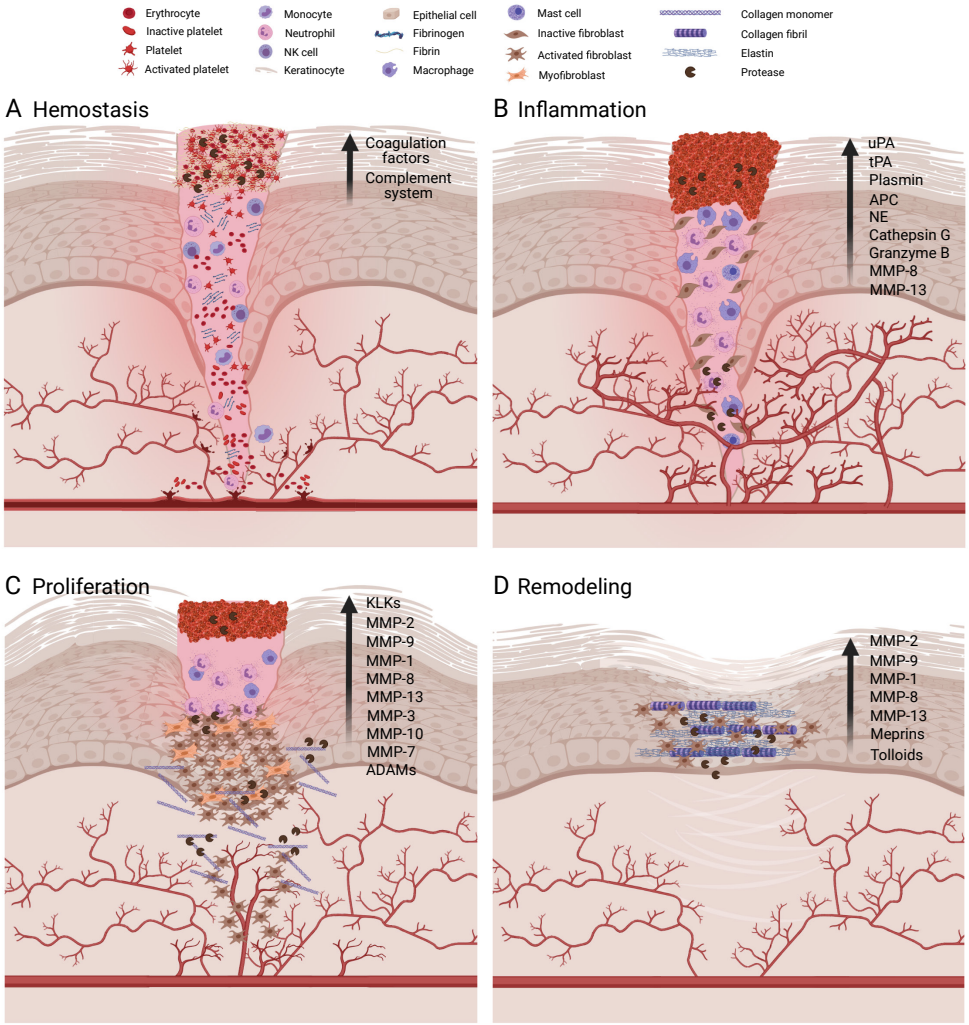

Figure 1.3. **Phases of cutaneous wound healing.** Adapted from (Kalogeropoulos et al., 2022). **A** illustrates the hemostasis, marked by the infiltration of platelets at the wound bed. **B** denotes the inflammatory phase, characterized by the presence of immune cells to the wound site. **C.** The third stage, the proliferative phase is marked by the formation of new tissue induced by proliferation of keratinocytes and fibroblasts. **D.** The final stage involves tissue remodeling, mediated through metalloproteinases, remodeling the extracellular matrix.

factors promote the sprouting of new blood vessels in close proximity to the wound, which precipitates the growth of further blood vessels, providing vital oxygen and supplements to the forming skin.

The invading fibroblasts metabolize collagen and other extracellular matrix components, allowing for the replacement of the interim tissue. A few fibroblasts progressively differentiate into myofibroblasts, depositing further extracellular matrix molecules and mirroring smooth muscle cells, thereby being able to contract, reducing the size of the wound surface (Gurtner et al., 2008).

1.2.3 Tissue Remodeling

The third and last stage of skin repair is called tissue remodeling, occurring two weeks after injury and may persist for as long as several years. Hereby, wound contraction and re-epithelization are largely complete, and the healing is characterized by remodeling of the collagenous dermis. The remaining fibroblasts, as well as immune, epithelial and endothelial cells secret matrix metalloproteinases, which in turn degrade the plethora of collagen type III, replaced by the fibroblast-mediated synthesis of collagen type I and further intermolecularly cross-linked to reinforce tensile strength. Nearly all macrophages, myofibroblasts and endothelial cells become apoptotic or abandon the wound, which ceases the formation of new stroma and concludes angiogenesis, eventually followed by the formation of a scar. Overall, wound repair contrarily to full regeneration is imperfect, as healed skin is deficient in tensile strength compared to its original counterpart and absent in skin appendage structures like hair follicles, sweat and sebaceous glands (Singer & Clark, 1999).

1.3 Proteases

Proteases are a big family of enzymes that catalyze the hydrolysis of scissile peptide bonds of targeted proteins, introducing an irreversible post-translational

modification. Apart from degradation of food-related consumed proteins, concluding in the presence of available amino acids that serve as building blocks for new protein translation, proteases regulate essential physiological processes by limited proteolysis.

Within limited proteolysis, proteases cleave their precisely defined protein substrates, producing smaller peptides that exert their own biological activity. These irreversible amendments cause alterations in various biological processes, allowing proteases to play a vital role in physiologically relevant mechanisms, like control of the cell cycle and apoptosis through activation or inactivation of a protease substrate.

Inherently, proteases can be classified as either exopeptidases, proteases that cleave amino acids positioned at the protein termini, or endopeptidases, which are proteases that catalyze the cleavage of amino acids in between the termini of substrates. Six clusters of proteases exist, which can be grouped by their catalytic mechanism; aspartate-, cysteine-, glutamate-, **metallo-**, serine- and threonine proteases.

1.3.1 Matrix Metalloproteinases

Matrix metalloproteinases (MMPs) are defined as both endopeptidases and zinc ion dependent metalloproteases that cleave either secreted or cell-bound extracellular proteins. MMPs can not only be grouped by their domain architecture but also based on their historical substrate preference into the subsequent sub-categories, stromelysins (MMP3, MMP10, MMP11), matrilysins (MMP7, MMP26), collagenases (MMP1, MMP8, MMP13), gelatinases (MMP2, MMP9), membrane-type (MT) MMPs (MMP14, MMP15, MMP16, MMP17, MMP24, MMP25) and other MMPs (MMP12, MMP19, MMP20, MMP21, MMP23, MMPP27, MMP28).

MMP activity is rigidly coordinated by several systems at gene and protein levels. Individual cell types, like fibroblasts, keratinocytes, immune and endothelial cells regulate proMMP activity by controlling gene expression re-

ceptive to external stimuli, like growth factors, cytokines, hormones, contact inhibition or contact with extracellular matrix molecules. Virtually, all MMPs, which are expressed as inactive zymogens, need additional post-translational processing through proteolytic activation by other proteases, such as furins, plasminogens or other MMPs to remove the pro-domain, unlocking the catalytic domain. The last level of physiological control is monitored by tissue inhibitors of metalloproteinases (TIMPs), a heterogeneous family of four endogenously secreted protease inhibitors with the innate capacity to reversibly inhibit MMP function.

Partly, due to the capacity of MMPs to cleave extracellular matrix proteins, MMP expression and pro-domain removal are of the highest importance in wound healing. Invading inflammatory cells secreting MMPs act on damaged tissue and deposited extracellular matrix components to purge the wounding site within the first days. Moreover, MMPs contribute to a properly regulated inflammatory response, modulating chemokines, cytokines and growth factors. Simultaneously, MMPs exert other functions, such as helping to produce granulation tissue to aid transient endothelial cells entering the wound base, which are responsive to growth factors releasing MMPs to increase both cellular mobility and proliferation of endothelial cells mediated by extracellular matrix cleavage. In addition, transiently amplifying keratinocytes at the wound edge release MMP1, MMP2, MMP9 and MMP10 contributing to re-epithelization. Further along the healing process, myofibroblasts and fibroblasts generate MMPs that positively contribute to contraction of freshly generated scar tissue by degrading aberrant fragments of the extracellular matrix.

The fact that MMPs are able to digest connective tissue highlights the relevance of MMPs in carcinogenesis and events that include the genesis of both tumor-related vascular and lymphatic systems as well as metastasis, showcasing ideal candidates to target cancer progression via suppression of MMP functionality. To date, there is no broad-spectrum anticancer MMP inhibitor drug, due to the plethora of unknown physiological processes MMPs are involved in,

considering the ambiguous inhibition leading to unwarranted adverse effects.

1.3.1.1 Stromelysin-2

The discovery of human MMP10 dates back to 1988, when the matrix metalloproteinase was cloned from a human tumor cDNA library (Muller et al., 1988). The original terminology dates back to its evident substrate specificity for a wide spectrum of extracellular matrix proteins, which is common among the stromelysin sub-cluster of matrix metalloproteinases, namely stromelysin-1 (MMP3) and stromelysin-3 (MMP11). The proteolysis of ECM macromolecules of the stroma, such as different collagen types, laminins, elastins in combination with the 78 % sequence similarity to stromelysin-1 was decisive for the naming of "stromelysin-2" (Bertini et al., 2004; Murphy et al., 1991; Nicholson et al., 1989).

Similar to all MMPs, the inactive form of MMP10, i.e. proMMP10 requires removal of the pro-domain, which in this case can be mediated both by other proteases or spontaneously by itself through autolytic cleavage (Nakamura et al., 1998). Coupled with this, MMP10 further activates other members of the MMP group, such as MMP1, MMP8, MMP7 and MMP9, which in turn cleave further substrates, initiating a convoluted signaling cascade (Nakamura et al., 1998). The activity of human MMP10 under normal conditions has been measured in several tissues, such as the menstrual endometrium and in T cells, yet elevated levels of MMP10 have been reported in various pathophysiological processes, e.g. carcinogenesis and wound healing (Kerkela et al., 2001; Murphy et al., 1991). Interestingly, the up-regulation of MMP10 activity in cancers can be linked to epithelial neoplasms such as squamous and basal cell carcinomas of the skin, esophageal and oral squamous cell carcinoma as well as non-small cell lung cancer (Gill et al., 2004; Impola et al., 2004; Mathew et al., 2002; O-charoenrat et al., 2001). The association of increased MMP10 expression and skin carcinogenesis results in part from its co-localization with laminin-5 as well as the latters MMP10-mediated cleavage (Kerkela et al., 2001).

Recently, the application of state-of-art degradomics technologies allowed for the elucidation of the human MMP10 *in-vivo* and *in-vitro* substrate repertoire of mouse primary keratinocyte secretomes and of mice epidermal lysates that have been genetically modified to consistently generate an active form of the enzyme stromelysin-2 (Schlage et al., 2015). Hereby, multiple novel MMP10-dependent cleavage sites were reported, which can be directly linked to the facilitation of keratinocyte release and migration along the injured dermis, supporting the hypothesis that MMP10 functionally controls migratory keratinocytes in the wound edge (Krampert et al., 2004). Hence, the cleavage of the hemidesomosome and desmosome complex together with proteolytic processing of cell adhesion molecules facilitate the release of migrating and amplifying keratinocytes (Schlage et al., 2015). Finally, another layer of MMP10-dependent control of keratinocyte migration is represented by the direct cleavage of the bioactive mediator **dermokine** (Schlage et al., 2015). Despite the novel cleavage site, no impact of dermokine modulation on epidermal differentiation in transgenic mice has been demonstrated (Utsunomiya et al., 2020).

1.3.2 Epidermal Proteases

The large family of proteases and their inhibitors play a crucial part in the terminal differentiation of keratinocytes in the epidermis. **Epidermal homeostasis** heavily relies on both the ordered processing of proteases and activation of their substrates but also the regulation of protease inhibitors, plainly representing a vital model for proteolytic pathways (Fortelny et al., 2014). For instance, proteases are responsible for the activation of differentiation, initiating cross-linking components in the cornified envelope and desquamation as well as barrier recovery in the wound healing process.

The early phases of the keratinocyte development process indicate reliance on proteases to disengage from mitosis to further execute terminal differentiation. This process is partly mediated by proteases, which cleave membrane-

bound molecules to modulate downstream signalling pathways. A prominent example of such a protease is a disintegrin and metalloproteinase (ADAM) 10 which not only frees epidermal growth factor (EGF) from the membrane but also cleaves exposed ligand-bound Notch receptors, which induces the switch from mitosis to differentiation (Blanpain & Fuchs, 2009; Blanpain et al., 2006; Rangarajan et al., 2001). Subsequently, γ-secretase liberates the intracellular domain of the Notch receptor, which translocates to the nucleus and induces the alteration of transcription (Weber et al., 2011).

Throughout the entire epidermal differentiation process, a major process is the step-wise disintegration of pro-filaggrin (FLG) (Elias et al., 2019). This massive protein requires meticulous proteolytic cleavage and is kept in place by checks and balances like phosphorylation, preventing altered FLG proteolytic processing which might contribute to impairments such as atopic dermatitis (Hoste et al., 2011). The initial N-terminal cleavages involved in pro-FLG processing can be attributed to furin and paired basic amino acid cleaving enzyme 4 (PACE4), emancipating the S100 domain, yet this is preceded by dephosphorylation of pro-FLG in a multi-step fashion by a protein phosphatase 2A family (Kam et al., 1993; Sandilands et al., 2009).

Overall, the proteolytic processing of FLG is a convoluted process that involves multiple proteases such as calpain-1, elastase-2, kallikrein-related peptidase 5, senescence-associated subtilisin protease, caspase-14 and bleomycin hydrolase but the exact cleavage sequence remains elusive and indeed new modulation interactions continue to be identified. Finally, the third post-translational modification, deimination, results in the conversion of arginine residues to citrulline by peptidylarginine deiminase enzymes. The accumulation of events leads to the limited proteolysis of pro-FLG into initial FLG fragments and ultimately, the complete degradation of FLG into free amino acids which together with their derivatives and other metabolites are processed into natural moisturizing factors, ensuring not only cornified envelope hydration and proper pH but also protection against UV radiation.

In addition, to ensure correct **corneocyte** development, multiple other

processes are active in parallel, like the activation of ADAM17 which is involved in the cleavage of EGF receptor (EGFR) interacting proteins like transforming growth factor - α (TGF-α) and heparin-binding EGF (HB-EGF) (Sahin et al., 2004). Typical proteases common in terminal cellular processes are caspases, as such caspase-14 and Caspase-8 are actively contributing to the differentiation. Another eminent family of proteases at play are cathepsins, namely cathepsin D, cathepsin L and cathepsin V and its inhibitor cystatin M/E, being responsible for the modulation of transglutaminase activity. Upon the final moments, proteases completely occupy the molecular situation and complete the full cycle of epidermal homeostasis. Desquamation outlines the shedding of corneocytes from the epidermal surface, subduing the redundant proliferation of basal keratinocytes. This process requires proteolytic processing of corneodesmosomes, orchestrated by the kallikrein-related peptidase (KLK) cascade, which involves KLK5, KLK7 and KLK14 and the pH-dependent serine peptidase inhibitor Kazal type 5 (SPINK5) (de Veer et al., 2014).

1.4 Epidermal Proteolytic Pathways - Manuscript 1

MANUSCRIPT 1 - SUMMARY

Intertwined Proteolytic Networks and their Implications for Skin Health. Proteases operate in co-dependent systems, introduced as the protease web, thus any disturbance within this network can deeply impact tissue balance and environmental cues. Sheddases, a subgroup of proteases linked to the membrane, can themselves be cleaved into the surrounding space through a process known as ectodomain shedding. *Werny et al.* uncovered stunning flexibility in the ectodomain shedding of meprin β, a metalloprotease indispensable to inflammation and fibrosis, suggesting new connections within convoluted proteolytic webs such as the epidermal protease network, with potential associations for skin health and injury response.

New links for meprin β within the protease web

Vahap Canbay and Ulrich auf dem Keller

Department of Biotechnology and Biomedicine, Technical University of Denmark, DK-2800, Kongens Lyngby, Denmark

Published in

Canbay V. and auf dem Keller U. (2023) New links for meprin β within the protease web. *The FEBS Journal* doi: 10.1111/febs.16621. Commentary.

Contribution by VC:
Manuscript writing.

1.4.1 Abstract

Proteases are organised in interconnected networks, together forming the protease web whose disturbance can have detrimental consequences for tissue homeostasis and response to environmental insults. Membrane-anchored sheddases are proteases that themselves can be released into the pericellular space by ectodomain shedding. *Werny et al.* have uncovered unexpected promiscuity in ectodomain shedding of meprin β, a metalloprotease with critical functions in inflammation and fibrosis. These findings suggest new links within complex proteolytic networks like the epidermal protease network with potential implications for skin homeostasis, inflammation and response to injury.
Comment on: https://doi.org/10.1111/febs.16586

1.4.2 Commentary

Proteases play pivotal roles in development, cellular signalling, tissue homeostasis and responses to environmental stimuli in health and disease. Either by degradation or by specific processing of target substrates, they irreversibly modulate extracellular environments or orchestrate intracellular processes to critically determine cell behaviour. Together with their inhibitors, proteases do not act alone but in cascades, circuits and complex networks, mutually affecting activity, localization and substrate repertoires. Classic examples of interconnected protease networks are blood coagulation and caspase-mediated programmed cell death, which control seminal tissue and cellular responses and whose disturbance is inevitably associated with life-threatening diseases. However, they are only parts of a higher order network, termed the protease web, that integrates all proteases (> 550 in humans) and inhibitors (> 150 in humans) and their complex interactions (Fortelny et al., 2014). Despite rapid advances in high-throughput degradomics technologies that have significantly contributed to deconvolution of the protease web (Canbay & auf dem Keller, 2021), only a tiny fraction of its complexity has been unravelled. Hence,

many missing links need to be established to devise effective strategies for personalised treatment for aberrant proteolysis in devastating diseases, such as cancer, neurodegeneration and chronic inflammatory disorders.

In this issue of The FEBS Journal, *Werny et al.* (Werny et al., 2023) provide new insight into the intricate interplay of the membrane-anchored proteases meprin β, MT1-MMP (membrane-type-I matrix metalloproteinase) and ADAMs 10/17 (a disintegrin and metalloproteinase) that have all been associated with carcinogenesis, inflammation and Alzheimer's disease (AD). Acting in the pericellular space, meprin β, MT1-MMP and ADAMs 10/17 are sheddases, which can modulate extracellular environments by releasing bioactive ligands from the cell surface. Interestingly, the catalytically active ectodomains of all these sheddases are also shed themselves, not only controlling their activity in close proximity to the plasma membrane, but also extending their proteolytic activity further into the protease-rich extracellular space. As shedding is mediated by proteolysis, these shedding events are critical links within the protease web and significantly contribute to dynamics of protease signal propagation. Thus, they must be tightly regulated in space and time to prevent uncontrolled proteolysis, potentially causing, or resulting from disease.

High flexibility in controlling ectodomain shedding can be conferred by multiple proteases cleaving the same substrate, allowing individual spatiotemporal regulation of expression and activity in complex tissue responses. Werny et al. now provide evidence for a striking overlap of ADAM10/17 and MT1-MMP activity towards meprin β ectodomain shedding, using the exact same cleavage site. Consistently, all three sheddases can only release inactive but not active meprin β from the cell surface, indicating a similar effect of the meprin β propeptide on susceptibility to proteolysis by ADAM10/17 and MT1-MMP. With MT1-MMP, a new meprin β sheddase has been discovered, which allows fine-tuning both the cell surface sheddase activity of meprin β to cleave bioactive mediators, such as IL6R (interleukin-6 receptor), CD109 (cluster of differentiation 109) and TREM2 (triggering receptor expressed on myeloid

cells 2), and the amount of soluble pro-meprin β that eventually is activated by secreted tryptic proteases to functionally modulate the extracellular matrix (Arnold et al., 2017).

Another and particularly interesting new link that has been established for meprin β within the protease web is its vice versa activity on MT1-MMP to shed the ectodomain of this major collagenase, sheddase of bioactive ligands and facilitator of MMP activation (Itoh, 2015). Interestingly, MT1-MMP ectodomain shedding has been described as a physiological event (Toth et al., 2005), generating an active soluble protease with enhanced activity in the pericellular space (Pahwa et al., 2019). Data suggest that the MT1-MMP ectodomain sheddase is a membrane-anchored metalloprotease, but a defined candidate has not been identified yet (Toth et al., 2006). Although focussing on meprin β rather than MT1-MMP ectodomain shedding, *Werny et al.* now present convincing data that suggest meprin β as a potent candidate to fill this void. Importantly, in addition to taking part in proMMP9 activation (Geurts et al., 2012), meprin β now connects to the complex MMP network also through MT1-MMP, one of whose major functions is the zymogen activation of proMMP2 that in turn can activate other MMPs, thereby further transmitting the proteolytic signal (Itoh, 2015).

As the authors have established these new links within the protease web in cell-based systems, major questions arise on whether, where and under which conditions they are relevant in vivo. Since MT1-MMP, as well as ADAM10/17, are expressed with low tissue specificity in many cell types and under many conditions, there might be hardly situations where meprin β ectodomain shedding is exclusively mediated by either of the three sheddases. Thus, the tissue specificity of meprin β will guide the search for the most relevant tissues and responses to physiological or pathological stimuli. Meprin β is part of protease networks in the brain, intestine, kidney and skin with high expression in the epidermal compartment (Arnold et al., 2017). The latter is of special interest, since, in addition to MT1-MMP and ADAM10/17, it includes several member proteases such as kallikreins that are involved in the regulation of

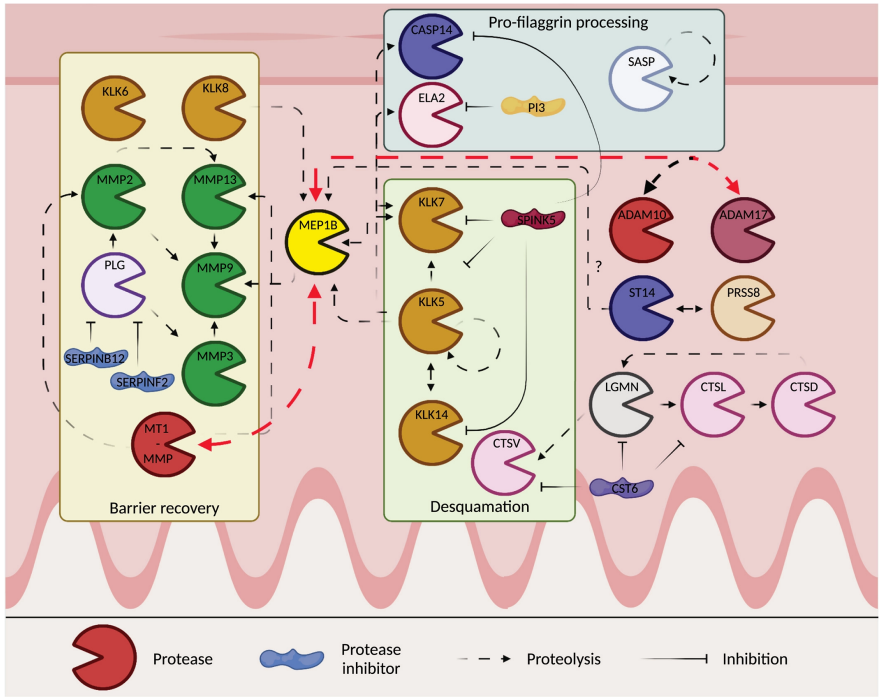

Figure 1.4. Connectivity of meprin β within the epidermal protease network. Red connections indicate new links analysed by *Werny et al.* (Werny et al., 2023). Figure inspired by (de Veer et al., 2014). Created with BioRender.com. ADAM, a disintegrin and metalloproteinase; CASP, caspase; CST, cystatin; CTS, cathepsin; ELA, elastase; LGMN, legumain; MEP, meprin; MMP, matrix metalloproteinase; MT1-MMP, membrane-type-I matrix metalloproteinase; PLG, plasmin; PRSS8, prostasin; SASP, senescence-associated subtilisin protease; SERPIN, serine protease inhibitor; SPINK, serine protease inhibitor Kazal-type; ST14, suppressor of tumorigenicity 14; TMPRSS6, trans-membrane serine protease 6.

meprin β activity (de Veer et al., 2014; Nauroy & Nyström, 2020) (Fig. 1.4). Upon injury or in inflammatory skin diseases, the epidermal protease network undergoes significant changes in expressed proteases and proteolytic interactions. Wound healing phenotypes in mice with genetic ablation of either MT1-MMP or meprin β in epidermal keratinocytes are mild (Kruppa et al., 2021; Zigrino et al., 2012), but both proteases are increased in abundance during the redifferentiation phase, whereas ADAM17 also plays important roles in keratinocyte differentiation (Tholen et al., 2016). Activities with similar functional consequences have been assigned to matriptase-1 (ST14 (suppressor of tumorigenicity 14)) (Touati et al., 2020) that is closely related and shares cleavage specificity with matriptase-2 (TMPRSS6), a major activator of membrane-anchored meprin β (Arnold et al., 2017), making it a potential candidate for meprin β activation in the epidermal compartment. As a caveat, most of these studies have been performed using mouse models, whereas *Werny et al.* could only demonstrate mutual shedding of meprin β and MT1-MMP using human proteins. However, as the authors mention, this might be related to dynamic O-glycosylation and thus could add another level of control to the complex system. Together, current evidence and the high connectivity of meprin β within the epidermal protease network (Fig. 1.4) warrant further analyses of its contributions to this very robust network with interconnected and redundant proteolytic activities. These might be addressed using humanised model systems and multiplexed gene editing strategies to understand complex rewiring of epidermal protease signalling in healing impairments and inflammatory skin disorders.

1.4.3 Acknowledgments

The authors acknowledge support by a Novo Nordisk Foundation Young Investigator Award (NNF16OC0020670) to UadK and funding from the LEO Foundation (LF-OC-19-000033).

1.5 Degradomics Technologies - Manuscript 2

MANUSCRIPT 2 - SUMMARY

Implications for the Future of Protease Substrate Analysis. The continuous progress in the identification of proteolytic proteoforms has emphasized the significance of limited proteolysis in elucidating cellular signaling events and discovering novel biomarker proteoforms. Modern degradomics strategies have not only enhanced the appreciation of cleavage events but also triggered the development of new methods. Yet, revealing protease substrates remains a convoluted effort, emphasizing the potential of novel approaches such as targeted degradomics, achieved by contemporary mass spectrometers, in quantifying proteoforms. With the accumulation of knowledge about protease substrates and their cleavages, concurrent with advancements in computation and instrumentation, the application data-independent acquisition for the generation of digital proteome maps for protease substrates is within reach.

New strategies to identify protease substrates

Vahap Canbay and Ulrich auf dem Keller

Department of Biotechnology and Biomedicine, Technical University of Denmark, DK-2800, Kongens Lyngby, Denmark

Published in

Canbay V. and auf dem Keller U. (2021) New strategies to identify protease substrates. *Current Opinion in Chemical Biology* doi: 10.1016/j.cbpa.2020.09.009. Review.

Contribution by VC:
Manuscript writing.

1.5.1 Abstract

Proteome dynamics is governed by transcription, translation, and post-translational modifications. Limited proteolysis is an irreversible post-translational modification that generates multiple but unique proteoforms from almost every native protein. Elucidating these proteoforms and understanding their dynamics at a system-wide level is of utmost importance because uncontrolled proteolytic cleavages correlate with many pathologies. Mass spectrometry–based degradomics has revolutionized protease research and invented workflows for global identification of protease substrates with resolution down to precise cleavage sites. In this review, we provide an overview of current strategies in protease substrate degradomics and introduce the concept of workflow, mass spectrometry–based and in silico enrichment of protein termini with the perspective of full deconvolution of digital proteome maps for precision medicine, and degradomics biomarker diagnostics.

1.5.2 Introduction

Data from the human genome project impressively demonstrated that in addition to canonical proteins an enormous number of diverse proteoforms generated by alternative splicing and protein post-translational modifications (PTMs) contribute to the complexity of the human proteome (Paik et al., 2018). To globally understand the myriads of human proteins and proteoforms, the Human Proteome Organization and its associated Human Protein Project have been established. The chromosome-centric Human Protein Project aims at characterizing the leading proteoforms, which have distinct and, sometimes, even contradictory biological activities in a physiological context compared with their unmodified protein of origin. The proteome analysis of dynamic regulation of proteoforms in a biological system could be a potential approach to discover novel biomarkers, unveiling differential abundance in specific diseases and provide solutions for the treatment of cancer and other disorders

(Macklin et al., 2020).

Over the last few years, cutting-edge mass spectrometry (MS)-based proteomics has become a robust and versatile tool to scrutinize the biological functions of proteins and for the quest for biomarkers (Aebersold & Mann, 2016)[3]. Particularly, MS-based proteomics is used to investigate divergent proteoforms generated from PTMs with phosphoproteomics as the most prominent example (Hosp & Mann, 2017) [4]. Yet, these proteoforms are frequently undersampled and thus neglected without proper enrichment protocols (Pieroni et al., 2020).

With roughly 560 estimated proteases derived from 3 % of human protein-coding genes, this enzyme class is characterized by hydrolysis of the peptide bond linkage of amino acid residues in a polypeptide chain (Vizovišek et al., 2018). If uncontrolled, for example, through disturbances of protease regulation, proteolysis might be associated with pathologies, such as cancer, neurodegenerative and chronic inflammatory diseases (Eckhard et al., 2016). Therefore, pathological protease cleavage events might be a manifestation of a continuous disease, making proteases important candidates for drug targets (Drag & Salvesen, 2010).

Limited proteolysis is a pivotal biological mechanism in maintaining cellular homeostasis through control of protein activities and contributes to decisive biological processes, such as cell cycle regulation and apoptosis (Turk et al., 2012). Generation of protein neo-N and neo-C termini is a result of proteolytic cleavage, and thus characterization of protein termini is critical in revealing novel protease–substrate relations and understanding of regulatory proteolytic networks. The broad interest in proteases and their substrates established the field of degradomics, aiming at identifying not only proteases but also their substrates using system-wide analytical methods and, in particular, MS-based proteomics (Klein et al., 2018).

However, the low abundance of these PTMs is a hindrance in their identification, and therefore specific protocols are necessary to record proteolytic signatures. Hereafter, we will focus on extensive protease substrate enrich-

ment workflows and give an outlook on targeted degradomics and in silico enrichment.

1.5.3 Degradomics Technologies

Typically, to characterize proteome dynamics in a biological system, a discovery-driven proteomics approach is put into practice (Aebersold & Mann, 2016). A classical bottom–up proteomics workflow involves seclusion of the proteome from the biological sample and subsequent digestion into peptides using sequence-specific proteases, such as trypsin, LysargiNase, LysN, or GluC (Huesgen et al., 2014). The newly generated peptides are fractionated by reversed-phase (RP) liquid chromatography (LC), ionized, and fragmented to be analyzed by tandem mass spectrometry (MS/MS) based on their mass-to-charge (m/z) ratio. Both identified peptide sequences and their abundances are used to computationally infer and relatively quantify the original protein. Still, the complexity of the whole biological sample proteome prevents comprehensive identification of low-abundance proteins because of the intrinsic mechanisms of the MS analysis, masking low-abundance peptides by peptides generated from highly abundant proteins. Consequently, the differentiation of sparse proteolytically spawned proteoforms requires additional experimental workflows to reduce sample complexity, such as supplementary sample fractionation and prior enrichment of protein termini (Luo et al., 2019).

Identification of crucial spatiotemporally confined proteolytic processes resulting in scarce neo-N– and neo-C–terminal proteoforms is challenging, and dedicated positional degradomics techniques have been developed to limit purification steps leading to general protein losses and prevent redundant contaminations of enriched fractions (Klein et al., 2018). Positional degradomics methods follow either a positive enrichment strategy to directly select protein termini or negative selection protocols, removing internal tryptic peptides to enrich for proteolytically generated neo-N and neo-C termini. Whereas positive enrichment methods focus on selective affinity tagging of protein

N-terminal α-amines over lysine side-chain ϵ-amines, negative selection approaches chemically label both free ϵ- and α-amines at the protein level and subsequently remove internal tryptic peptides exploiting reactivity of their newly generated N-terminal primary amine groups.

Positive Enrichment Strategies

Various positive enrichment workflows have been developed to selectively enrich N-terminal peptides relying on biotin–avidin affinity purification (Figure 1.5). With great success, subtiligase has been engineered to enzymatically label protein N termini with a biotinylated tagging peptide, while chemical biotinylation exploits differences in reactivity of ϵ- and α-amines toward amine-reactive coupling groups (Timmer et al., 2007; Yoshihara et al., 2008). Subtiligase-based N-terminomics has been applied to record the first N-terminome of human blood (Wildes & Wells, 2010), extensively map caspase cleavages in apoptosis (Mahrus et al., 2008) and monitor proteolytic fragments as biomarkers in serum from cancer patients (Wiita et al., 2014). Recently, efficacy and versatility of subtiligase for global enzymatic modification of protein N termini in complex samples have been further extended by introduction of novel engineered mutant enzymes, which expand its application in several fields of research including protease substrate discovery (Weeks & Wells, 2020).

As an alternative strategy for positive enrichment of N-terminal peptides, N-terminalomics by chemical labeling of the -amine of proteins (N-CLAP) uses selective deblocking of N-terminal -amines after whole protein full amine labeling followed by chemical biotinylation and avidin-functionalized solid-phase extraction (Xu et al., 2009). More recently, Griswold et al. (Griswold et al., 2019) used a 2-pyridinecarboxaldehyde–biotin probe to selectively label protein N termini in a chemical approach termed chemical enrichment of protease substrates (CHOPS) that is particularly suited to study dipeptidyl peptidases because binding is prohibited by proline as the penultimate

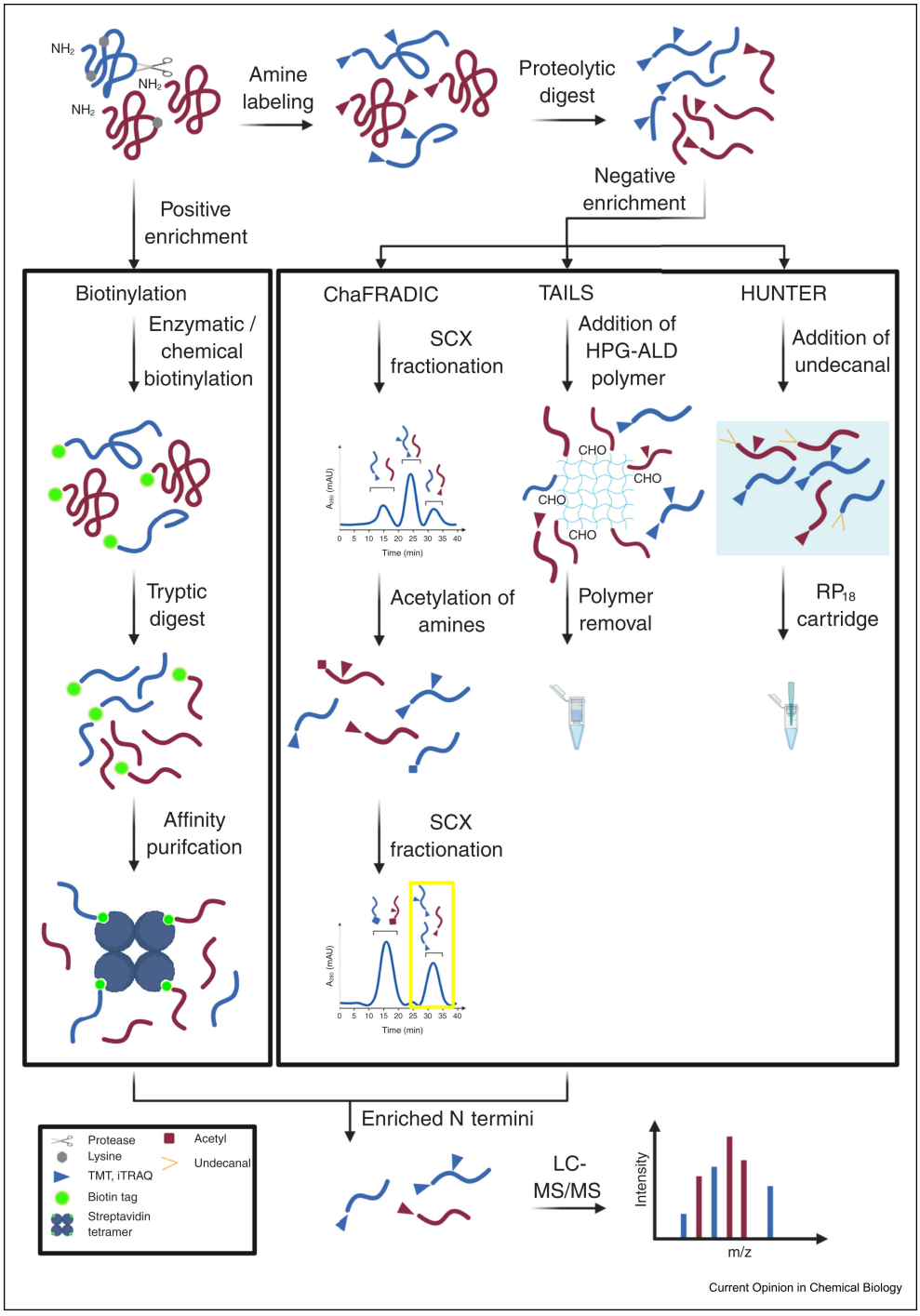

Figure 1.5. (Continued on the following page.)

Figure 1.5. Overview of N-terminal enrichment workflows. Positive enrichment strategies selectively attach affinity tags to N-terminal primary peptide -amines allowing for affinity purification. Negative enrichment workflows rely on whole protein amine-labeling and subsequent removal of internal endoproteinase-generated peptides using amine-reactive polymers (TAILS) or exploiting changes in chromatographic elution times upon chemical derivatization (ChaFRADIC, HUNTER). Created with BioRender.com. ChaFRADIC, charge-based fractional diagonal chromatography; HPG-ALD, amine-reactive soluble hyperbranched polyglycerol aldehyde polymer; HUNTER, high-efficiency undecanal-based N-termini enrichment; LC, liquid chromatography; MS, mass spectrometry; SCX, strong cation exchange; TAILS, terminal amine isotopic labeling of substrates.

N-terminal residue.

Despite constant development of novel workflows, an inherent drawback of most positive enrichment strategies is the need of customized reagents, complicating introduction of isotopic labels and often limiting multiplexing capabilities. Some of these limitations have been addressed by a novel immuno-N-terminomics (miNterm) approach using tandem mass tags (TMTs) for whole protein labeling and anti–TMT-antibody resins for N-terminal enrichment (Shin et al., 2020). On the other hand, positive enrichment has advantages in identification of intracellular neo-N termini that might be masked by the huge number of naturally Nα-acetylated protein N termini co-enriched in negative enrichment workflows.

Negative Enrichment Strategies

Negative enrichment workflows rely on removal of internal tryptic peptides rather than capture of chemically modified protein termini and thus also allow for annotation of natural N-terminal modifications, such as N -acetylation and N-terminal glutamine cyclization (Rogers & Overall, 2013). Widely applied negative enrichment strategies use either fractional chromatography, amine-reactive polymers, or solid-phase extraction upon chemical alteration of hydrophobicity and focus on N-terminal peptides for protease substrate discovery. Of these, combined fractional diagonal chromatography (COFRADIC)

and terminal amine isotopic labeling of substrates (TAILS) have been extensively applied in positional proteomics (Savickas et al., 2020), whereby high-efficiency undecanal-based N-termini enrichment (HUNTER) has been introduced more recently (Weng et al., 2019).

Combined Fractional Diagonal Chromatography

COFRADIC depends on chemical conversion of internal peptides altering their hydrophobicity, subsequently using two consecutive chromatography steps, which in turn enrich for proteolytically generated protein N termini (Staes et al., 2017). Essentially, all primary amines of proteins are acetylated; subsequently the sample is tryptically digested and prefractionated by strong cation exchange (SCX) chromatography, which is used to enrich for acetylated N termini because of the low binding capacity of neo-N–terminal peptides to the SCX resin in comparison with unblocked, tryptic peptides. The fractions undergo a primary RP high-performance liquid chromatography (HPLC) separation, and 2,4,6-trinitrobenzenosulfonic acid is introduced to each enriched fraction, hydrophobically tagging the remaining internal peptides and thus enabling their efficient depletion in a consecutive RP-HPLC run, while initially acetylated neo-N termini are collected based on their shorter retention time on the RP-HPLC resin.

The initial acetylation step limits multiplexing capabilities of COFRADIC, which has been overcome by a more recent variant termed charge-based fractional diagonal chromatography (ChaFRADIC) (Venne et al., 2013). The ChaFRADIC approach can use isobaric tags for relative or absolute quantitation (iTRAQ) or TMTs for labeling of N-terminal peptides, followed by a primary SCX run to fractionate peptides based on their charge state, deuteroacetylation of tryptic peptides upon digest and an additional SCX step to pull out fractions exclusively containing blocked neo-N–terminal peptides (Venne et al., 2015; Venne et al., 2013). Simplifying ChaFRADIC, charge-based fractional diagonal chromatography in tip format (ChaFRAtip) miniaturizes the

workflow, requiring only a pipette tip and SCX beads to significantly decrease sample amounts to below 5 g total protein per sample (Shema et al., 2018). This presents a possibility to circumvent the use of expensive HPLC systems, which are linked to investment expenses and maintenance costs (Shema et al., 2018).

Terminal Amine Isotopic Labeling of Substrates

The workflow that has been most widely applied for systematic discovery of new protease substrates in complex biological samples (Savickas et al., 2020) was introduced by Kleifeld et al. (Kleifeld et al., 2010) and termed TAILS. TAILS employs commonly used reagents, such as formaldehyde (reductive dimethylation), iTRAQ and TMTs, for labeling of lysine - and protein N-terminal -amines at the protein level, enabling flexible experimental designs optimized for costs and multiplexing capabilities (Kleifeld et al., 2011). Labeled proteomes are combined, digested with site-specific endoproteinases (mostly trypsin) and the generated internal peptides covalently captured using a commercially available amine-reactive soluble hyperbranched polyglycerol aldehyde polymer (HPG-ALD). Subsequent ultrafiltration collects N-terminal peptides in the flow-through, the so-called TAILS fraction, that together with LC-MS/MS analysis of an aliquot of the nonenriched preTAILS fraction provides a comprehensive positional annotation of the sample proteome (auf dem Keller et al., 2013). TAILS' extensive multiplexing capabilities have been applied to perform time-resolved analyses (Schlage et al., 2014) and to record N-terminomes from patient samples (Klein et al., 2015).

Over the years, the TAILS workflow has been continuously improved to increase proteome and N-terminome coverage, combined with different labeling modalities (Schlage & auf dem Keller, 2015) and adapted for analysis of samples from several species, tissues, and body fluids (Bell et al., 2019; Bundgaard et al., 2020; Sabino et al., 2017). Moreover, a recent variant of the HPG-ALD polymer that is susceptible to precipitation significantly improved N-terminal

enrichment, enabling higher efficiency and lowering potential sample losses (Solis et al., 2019).

After the principle of TAILS, Ju et al. introduced a novel workflow termed iNrich that replaces the HPG-ALD polymer by N-hydroxysuccinimide beads and has been adapted to an encapsulated format with the potential for automated processing (Ju et al., 2020).

High-efficiency Undecanal-Based N-Termini Enrichment

HUNTER, a sensitive and automatable assay, is based on chemical alteration of hydrophobicity to remove internal peptides by RP-HPLC and achieved a remarkable enrichment of 1000 N-termini from as little as 2 μg total protein per biological replicate (Weng et al., 2019). HUNTER also introduced reversible capturing to magnetic SP3 beads for proteome purification and labeling (Hughes et al., 2019) to degradomics workflows and exploited data-independent acquisition for label-free quantification. Thus, through its adaptability to automatic liquid-handling systems, HUNTER has the potential to drive forward high-throughput protease substrate discovery and N-terminal proteoform mapping in clinical degradomics.

C-terminomics

Not all protease substrate cleavages are accessible by analysis of the resulting N-terminal peptide, which might not be possible to be generated in an appropriate length, might lack suitable physicochemical properties for MS-based analysis or might be too short for unambiguous identification in complex proteomes. Thereby, a particular challenge is the detection of events resulting from carboxypeptidase activities. Therefore, despite an unfavorable chemistry COFRADIC, ChaFRADIC, and TAILS have been modified for analysis of C-terminal peptides (Tanco et al., 2015).

C-terminal COFRADIC replaces 2,4,6-trinitrobenzenosulfonic acid with an amine-reactive derivate of butyrate, allowing to separately recover N- and C-terminal peptides in the second RP-HPLC run (Van Damme et al., 2010). C-TAILS removes internal tryptic and N-terminal peptides via their (1-ethyl-3-(3-dimethylaminopropyl) carbodiimide hydrochloride)–functionalized free carboxyl groups using an amine- reactive polymer upon blocking of free C-terminal and side-chain carboxyl groups at the protein and all primary amines at both the protein and the peptide level (Schilling et al., 2011). Application of multiple enzymes for site-specific proteome digest further increased identification rates of C termini using the C-TAILS approach (Zhang et al., 2018). Only recently, ChaFRADIC has been modified to allow for negative enrichment of C termini by reducing charge states of non-C–terminal peptides through enzymatic removal of trypsin-generated basic amino acids in C-terminal position (Chen et al., 2020).

Targeted Degradomics and In Silico Enrichment

Positive and negative enrichment workflows separate terminal from internal peptides in proteome digests to facilitate their detection in complex mixtures. Targeted degradomics moves this separation inside the mass spectrometer by selective analysis of predefined peptide precursors based on mass and LC retention time utilizing the principles of selected or parallel reaction monitoring (S/PRM) (Bourmaud et al., 2016). Because neo-terminal peptides are preselected in the PRM mode, targeted degradomics is mostly applied for validation of newly identified protease cleavage events rather than to discover new protease substrates (Sabino et al., 2015). However, with the rapid improvements in MS instrumentation and PRM workflows such as internal standard–triggered PRM (IS-PRM) (Gallien et al., 2015), numbers of targets that can be monitored with high sensitivity are rapidly increasing, enabling discovery-like analyses using extensive target libraries for assay development (Figure 1.6). Such peptide libraries might be synthetically produced or generated

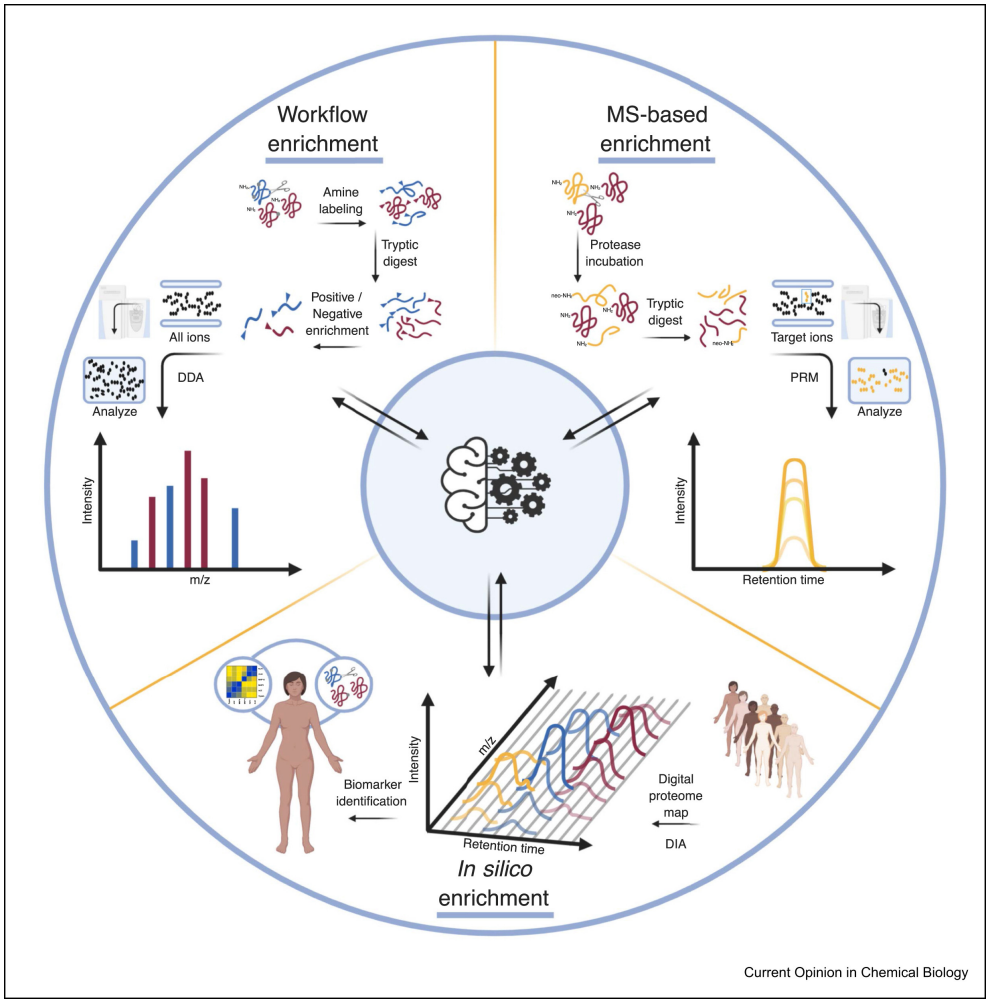

Figure 1.6. **Concept of enrichment strategies for positional proteomics.** Workflow enrichment combines chemical proteome modification with separation techniques to physically isolate protein termini before proteomics analysis. Mass spectrometry (MS)–based enrichment relies on separation of selected peptide ions within the instrument, allowing quantitative monitoring of hundreds of cleavage events by concomitant analysis of neo-termini and cleavage-site spanning peptides. In silico enrichment utilizes digital proteome maps recorded by data-independent acquisition (DIA) to correlate differential abundances of proteolytically spawned proteoforms in individual patients with large patient cohorts. Enrichment strategies use machine learning algorithms and artificial intelligence to computationally infer proteoform identification. Created with BioRender.com. DDA, data-dependent acquisition; MS, mass spectrometry; PRM, parallel reaction monitoring.

from proteomes exposed to differential protease activities. Thereby, machine learning algorithms and artificial intelligence will help to extend into the discovery domain based on growing datasets deposited in proteolysis databases, such as TopFIND (Lange & Overall, 2011).

In the future, similar libraries might be used to query digital proteome maps (Guo et al., 2015) that are recorded using DIA from cellular assay systems, animal models, and patient cohorts for proteolytic events by in silico enrichment of indicative proteoforms. This principle has recently been demonstrated by Ye et al. (Ye et al., 2019) who used glycopeptide libraries to identify and quantify hundreds of glycopeptides in human serum without prior enrichment.

1.5.4 Conclusion and Perspectives

Identification of proteolytic proteoforms has gained immense momentum over the last years, aiming at understanding limited proteolysis as a decisive signaling event and uncovering novel proteoform biomarkers generated by specific cleavage. Unveiling regulatory proteolytic networks will divulge a hidden level in the complex interplay of regulatory cellular functions.

Prevailing degradomics strategies allow unprecedented insights into cleavage events in cells and tissue and provide information about specific protease–substrate relations. Several existing degradomics methods have been improved and spun out either new techniques or modified versions. Yet, protease substrate identification proves to be challenging, and more recently developed targeted degradomics approaches have the potential to extend into the discovery domain, exploiting the increased sensitivity of state-of-the-art mass spectrometers to identify and quantify proteolytically spawned proteoforms. Growing knowledge of cleavage events and bona fide protease substrates deposited in common repositories together with advancements in machine learning algorithms and further improvements in instrumentation will pave the way for systematic querying of digital proteome maps for limited proteolysis and

significantly reduce time and efforts in global protease substrate discovery.

1.5.5 Declaration of Competing Interest

Nothing declared.

1.5.6 Acknowledgments

Ulrich auf dem Keller acknowledges support by a Novo Nordisk Foundation Young Investigator Award [NNF16OC0020670].

1.6 Advances in Phosphoproteomics and Data Interpretation

Recent developments in mass spectrometry-based proteomics technologies have enabled the identification and quantification of a plethora of post-translational modifications on an unforeseen scale (Olsen & Mann, 2013). This is especially the case for the enrichment and analysis of phosphorylated peptides and their inferred phosphorylated proteins via quantitative mass spectrometry, which has gained significant traction and benefited from continuous advances in instrumentation (Franciosa et al., 2023). Modern experimental approaches for the large-scale identification of kinase substrates comprise not only the application of state-of-the-art affinity-based chromatography exploiting the capacity of metal ions to bind to phosphate groups but also the deployment of cutting-edge automatized workflows, increasing robustness, throughput and reproducibility (Hu et al., 2021). The favored approach for the study of phosphoproteomes has been the established data-dependent acquisition method which is usually merged with the isobaric tagging of amines for the correct quantification and identification of phospho-peptides (Riley & Coon, 2016). Yet,

technological leaps in mass spectrometry instrumentation and advances in separation techniques prompted a paradigm shift in acquisition strategies towards unbiased data-independent acquisition, which allows for unprecedented depth in the phospho-proteome as well as higher quantification accuracy (Bruderer et al., 2015; Fernández-Costa et al., 2020). In concert with cutting-edge developments in spectral deconvolution and the introduction of deep neural network architectures allow for the prediction of mass spectrometry spectra of phosphopeptides in an unprecedented fashion, thus gaining extensive comprehensive insight into the phosphoproteome (Bekker-Jensen et al., 2020).

Translating high-throughput phosphoproteomics datasets into understandable biological insights often involves associating identified phosphopeptides with their corresponding upstream kinases, a task that poses a significant challenge. One potential solution is to use computational methods, such as kinase substrate enrichment analysis (KSEA), which allows for the inference of kinase activity through grouping identified phosphosites based on either their known target sites for specific kinases or shared phosphorylation motifs (Casado et al., 2013; Kim et al., 2021). Such a computational approach involves a few critical steps. First, each phosphosite's quantification needs to be z-transformed, standardizing the values for comparison. Next, each phosphosite is aligned to any known *in-vitro* or *in-vivo* kinase that targets the site. This process involves intersecting quantified substrate-kinase pairs from comprehensive databases, such as PhosphoSitePlus®. Subsequently, matching scores are calculated using statistical measures, such as Pearson's correlation, to determine the degree of association between phosphosites and their kinases (Kim et al., 2021). To determine a motif matching score, the seven preceding and seven subsequent amino acids of each quantifiable phosphosite are ranked against known kinase phosphorylation preferences. The final combined score for a phosphosite in relation to a specific kinase is computed by averaging the motif and profile matching scores (Kim et al., 2021). Further, a machine learning technique is employed to further provide additional information. A process called adaptive sampling is used to minimize positive-unlabeled phosphorylated sites (Yang

et al., 2019). This method iteratively estimates the probability of class mislabeling, thus supplying a predictive score to contribute to the interpretation of kinase-substrate relationships.

1.7 Dermokine in Epidermal Differentiation

Together with suprabasin (SBSN) and keratinocyte differentiation-associated protein (KRTDAP), dermokine (DMKN) is part of the secreted protein gene complex (SSC) from the suprabasal layer of the stratified epithelium (Matsui et al., 2004; Moffatt et al., 2004; Oomizu et al., 2000; Park et al., 2002; Tsuchida et al., 2004). Not only do the genes of SBSN, DMKN and KRTDAP group tightly together in the genomic locus but they are also transcribed in the exact direction and their resulting gene products are concurrently synthesized with the development of the stratified epidermis. In relation to epidermal stratification, calcium serves as an omnipresent cellular messenger that is both relevant for proliferation, and development as well as for differentiation but in addition, previous studies have illustrated a decisive calcium gradient along the stratified layers (Menon et al., 1985). With this purpose in mind, DMKN-β has been identified as calcium-inducible in cultured keratinocytes, up-regulated in high calcium concentrations (Higashi et al., 2012).

Several transcripts have been denoted for the DMKN gene resulting in multiple isoforms, generated not only by differential splicing but also by the use of various distinct promoters. The longest stranding DMKN isoform DMKN-β, which is encoded by 16 exons and 45 kDa big, as well as the C-terminally truncated isoform DMKN-γ are both expressed in the spinous and granular layer whereas the smaller (7 kDa) N-terminally truncated isoform DMKN-α, revealing the almost identical C-terminal domain of DMKN-β is generated throughout the stratified epithelium (Figure 1.7). Furthermore, it is important to consider that the α-, β- and γ- isoforms accommodate signal sequences that allow them to be secreted into the extracellular space. The complex biol-

ogy of the DMKN gene can be further illustrated by the existence of two other family of transcripts, the δ- and ϵ- isoforms, which are lacking signal sequences and are non-secreted. For additional convolution, a total of 16 isoforms are reported and further 18 potential DMKN isoforms are computationally mapped, rapidly increasing the ramifications of this gene's biology.

Overall, even though various human DMKN transcript variants exist, several isoforms share common protein domains. Apart from the N-terminal DMKN-β and -γ specific signal peptide and the unique DMKN-α signalling molecule, the isoform genus DMKN-β contains both the amino- and carboxyl-terminal globular domains, of which the N-terminal globular domain is alike DMKN-γ and the C-terminal domain is shared with DMKN-α (Naso et al., 2007b). In between these two domains, further two domains segregate the N- and C-terminus, firstly a coiled-coil collagen-like domain that includes uncontinuous glycine triplet repeats (G-X-Y) and an alternatively spliced keratin-like domain containing a glycine- and serine- abundant area (Brodsky & Shah, 1995; Naso et al., 2007b; Steinert et al., 1991).

Keratinocyte differentiation and epidermal renewal are decisive for skin homeostasis and maintenance of the skin's barrier capacity, which is disturbed upon injury and in inflammatory skin diseases. DMKN, is strikingly increased in abundance under these conditions, but its functional contribution to epidermal stratification has only been poorly understood (Leclerc et al., 2014). Within the first five days upon wounding, a relatively high abundance of DMKN-β and -γ was found within the wound margin, lasting throughout the wound healing-induced re-epithelization process, indicating a functional role of DMKN in the terminal differentiation program of keratinocytes (Leclerc et al., 2014). Analogously, the overall structure of DMKN, in particular the keratin-like domain, spanning a glycine- and serine-rich central portion is similar to intermediate filaments such as keratins and other cornified envolope proteins such as filaggrin, loricrin and involucrin (Kalinin et al., 2002; Naso et al., 2007a).

For this reason, genetic abscission of DMKN-β and -γ in mice culminated

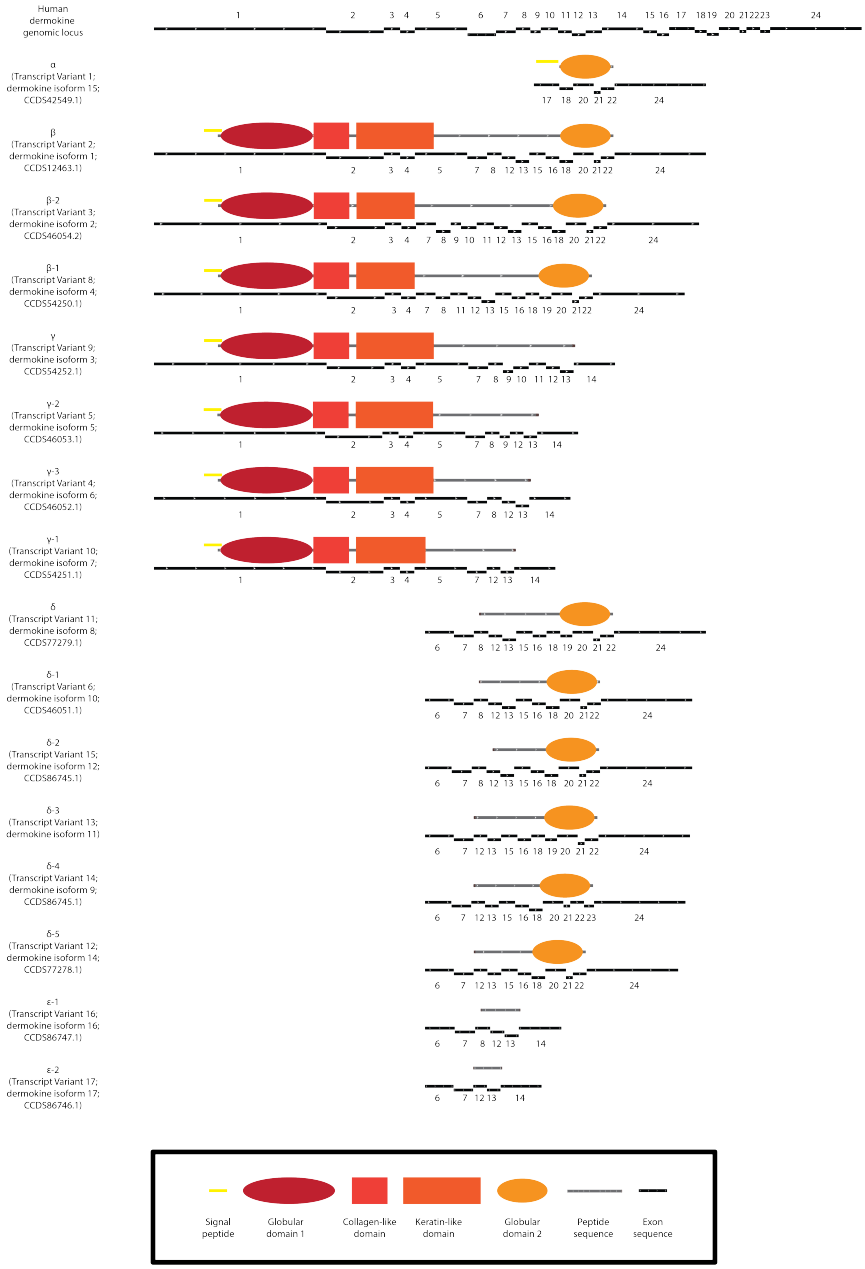

Figure 1.7. (Continued on the following page.)

Figure 1.7. Human dermokine isoforms. Current dermokine isoform annotation. Based on alternative splicing and the usage of alternative promoters a total of 34 dermokine isoforms have been denoted. Due to convoluted domain architecture, 4 unique dermokine domains are recorded - the globular domain 1, the collagen-like and keratin-like domain as well as the globular domain 2, similar to a cytokine-like domain. Adapted from (Leclerc et al., 2014) and (Matsui et al., 2004).

in the formation of transient scaly epidermal phenotypes, indicating defective cornified envelope development but even so the knockout mice did not display any apparent impact on cutaneous wound healing (Leclerc et al., 2014; Utsunomiya et al., 2020). To elaborate further, DMKN-α, -β and -γ deficient mice unearthed an epidermal transcriptome comparable to psoriasis or congenital ichthyosis, similarly the skin phenotype of DMKN-α, -β and -γ ablation results in both hyperkeratosis in neonatal mice and dyskeratosis in later stages (Utsunomiya et al., 2020). In parallel, DMKN β and γ knockout mice exhibited highly elevated levels of DMKN-α and other SSC mRNA, such as SBSN and keratinocyte differentiation-associated protein, indicating a compensatory role of DMKN-α, rectifying the loss of the other isoforms. This could be of interest, due to the suggested cytokine-like function of the C-terminal domain of DMKN-β and DMKN-α, explained by the high pI value (10.3) which is common among cytokines (Matsui et al., 2004). Fittingly, previous studies have shown that the globular C-terminal domain of DMKN-β was crucial for the inhibitory effects on phosphorylation of ERK1/2 in cultured keratinocytes, however, the incubation of DMKN-β on cultured keratinocytes had no consequence on Akt phosphorylation levels. In light of this information, the authors inferred a functional role of calcium-induced DMKN-β expression in the keratinization of the epidermis (Higashi et al., 2012). It is important to note that DMKN expression is less complex in mice due to the absent δ- and ϵ- isoform families, thus the functional contribution of DMKN in human skin diseases remains elusive (Naso et al., 2007b). These convoluted insights demonstrate the need for the mechanistic elucidation of DMKN functionality in human epidermal stratification.

1.8 Research Objectives

Since our laboratory aims to elucidate the function of proteases and the function of proteases is ultimately governed by its substrate repertoire, we sought to expand upon a previously discovered protease substrate.

DMKN - a member of the SSC family - has piqued our particular curiosity because of its deemed functional contribution in epidermal differentiation. Previous wound healing experiments have reported a putative role of MMP10 in keratinocyte migration throughout the re-epithelization process (Krampert et al., 2004; Murphy et al., 1991). Hereby, our laboratory reported MMP10-dependent proteolytic alteration of DMKN *in-vitro* and *in-vivo*, suggesting an alleged function of DMKN in migratory keratinocytes (Schlage et al., 2015). In alignment with these results, DMKN is purported to be involved in the terminal differentiation of epithelial keratinocytes (Higashi et al., 2012).

Genetic truncation of the DMKN-β and DMKN-γ isoforms in mice defined only a transient cornification impairment, which was most likely rescued by a compensatory isoform through elevated DMKN-α expression. To clearly reveal the role of DMKN in human keratinocyte differentiation, genetic ablation of all three isoforms in human keratinocytes is necessary. Furthermore, to observe the function of the cytokine-like domain a comparative evaluation between a DMKN-β/γ truncated mutant and a DMKN-α/β truncated mutant is essential.

Subsequent analysis of the consequences of truncated DMKN expression in keratinocytes will help to elucidate its contribution to epidermal phenotypes in inflammatory skin disorders. Due to the secretion of a multitude of proteins, especially in keratinocytes and fibroblasts, we employed organotypic skin cultures. Hereby we want to implement the *Dmkn* $\alpha\beta^{-/-}$ and *Dmkn* $\beta\gamma^{-/-}$ human N/TERT keratinocyte mutants into organotypic cultures so it can stratify through the air-liquid interface and be compared to wildtype keratinocyte organoid cultures. This allows us to utilize histological evaluations and employ LC MS/MS-based proteomics technologies to elucidate the role of DMKN

in human keratinocytes.

Secretion of DMKN-β from keratinocytes has been established, and previous studies strongly indicate a function of DMKN as a soluble mediator upon binding to a cell surface receptor, inducing downstream phosphorylation events. However, receptor candidates do not explain the pleiotropic functions of DMKN in epidermal differentiation, suggesting alternative or additional surface receptors on keratinocytes.

The major objectives of this thesis were the following:

1. **Optimization of human keratinocyte CRISPR/Cas9-based gene editing and generation of dermokine isoform-specific knockouts**

2. **Dissection of dermokine isoform contributions to epidermal differentiation in human skin models**

3. **Elucidation of dermokine's role in kinase-dependent signaling in keratinocytes**

Ultimately, the functional elucidation of the MMP10 substrate DMKN will support our understanding of epidermal differentiation and the underlying mechanism of DMKN in inflammatory skin disorders.

1.9 References

Aebersold, R., & Mann, M. (2016). Mass-spectrometric exploration of proteome structure and function. *Nature*, *537*(7620), 347–355.

Arnold, P., Otte, A., & Becker-Pauly, C. (2017). Meprin metalloproteases: Molecular regulation and function in inflammation and fibrosis. *Biochimica et biophysica acta. Molecular cell research*, *1864*(11 Pt B), 2096–2104.

auf dem Keller, U., Prudova, A., Eckhard, U., Fingleton, B., & Overall, C. M. (2013). Systems-level analysis of proteolytic events in increased vascular permeability and complement activation in skin inflammation. (2013/01/17). *Sci Signal*, *6*(258), rs2.

Bekker-Jensen, D. B., Bernhardt, O. M., Hogrebe, A., Martinez-Val, A., Verbeke, L., Gandhi, T., Kelstrup, C. D., Reiter, L., & Olsen, J. V. (2020). Rapid and site-specific deep phosphoproteome profiling by data-independent acquisition without the need for spectral libraries. *Nature Communications*, *11*(1), 1–12.

Bell, P. A., Solis, N., Kizhakkedathu, J. N., Matthew, I., & Overall, C. M. (2019). Proteomic and N-Terminomic TAILS Analyses of Human Alveolar Bone Proteins: Improved Protein Extraction Methodology and LysargiNase Digestion Strategies Increase Proteome Coverage and Missing Protein Identification. *Journal of Proteome Research*, *18*(12), 4167–4179.

Bertini, I., Calderone, V., Fragai, M., Luchinat, C., Mangani, S., & Terni, B. (2004). Crystal structure of the catalytic domain of human matrix metalloproteinase 10 (2004/04/21). *J Mol Biol*, *336*(3), 707–716.

Blanpain, C., & Fuchs, E. (2009). Epidermal homeostasis: a balancing act of stem cells in the skin. *Nature reviews. Molecular cell biology*, *10*(3), 207.

Blanpain, C., Lowry, W. E., Pasolli, H. A., & Fuchs, E. (2006). Canonical notch signaling functions as a commitment switch in the epidermal lineage. *Genes & development*, *20*(21), 3022–3035.

Bourmaud, A., Gallien, S., & Domon, B. (2016). Parallel reaction monitoring using quadrupole-Orbitrap mass spectrometer: Principle and applications. *PROTEOMICS*, *16*(15-16), 2146–2159.

Brodsky, B., & Shah, N. K. (1995). Protein motifs. 8. The triple-helix motif in proteins. *FASEB journal : official publication of the Federation of American Societies for Experimental Biology*, *9*(15), 1537–1546.

Bruderer, R., Bernhardt, O. M., Gandhi, T., Miladinović, S. M., Cheng, L.-Y., Messner, S., Ehrenberger, T., Zanotelli, V., Butscheid, Y., Escher, C., Vitek, O., Rinner, O., & Reiter, L. (2015). Extending the Limits of Quantitative Proteome Profiling with Data-Independent Acquisition and Application to Acetaminophen-Treated Three-Dimensional Liver Microtissues * [S]. *Molecular & Cellular Proteomics*, *14*(5), 1400–1410.

Bundgaard, L., Savickas, S., & auf dem Keller, U. (2020). Mapping the N-Terminome in Tissue Biopsies by PCT-TAILS. *Methods in Molecular Biology*, *2043*, 285–296.

Burns, D. A., Cox, N. H., & Hill, P. B. (2010). Comparative Dermatology.

Canbay, V., & auf dem Keller, U. (2021). New strategies to identify protease substrates. *Current Opinion in Chemical Biology*, *60*, 89–96.

Candi, E., Schmidt, R., & Melino, G. (2005). The cornified envelope: a model of cell death in the skin. *Nature Reviews Molecular Cell Biology 2005 6:4*, *6*(4), 328–340.

Casado, P., Rodriguez-Prados, J.-C., Cosulich, S. C., Guichard, S., Vanhaesebroeck, B., Joel, S., & Cutillas, P. R. (2013). Kinase-substrate enrichment analysis provides insights into the heterogeneity of signaling pathway activation in leukemia cells. *Sci Signal*, *6*(268), rs6.

Chen, L., Shan, Y., Yang, C., Sui, Z., Zhang, X., Zhang, L., & Zhang, Y. (2020). Carboxypeptidase B-Assisted Charge-Based Fractional Diagonal Chromatography for Deep Screening of C-Terminome. *Analytical Chemistry*, *92*(12), 8005–8009.

de Veer, S. J., Furio, L., Harris, J. M., & Hovnanian, A. (2014). Proteases: Common culprits in human skin disorders.

Drag, M., & Salvesen, G. S. (2010). Emerging principles in protease-based drug discovery. *Nat Rev Drug Discov*, *9*(9), 690–701.

Eckhard, U., Huesgen, P. F., Schilling, O., Bellac, C. L., Butler, G. S., Cox, J. H., Dufour, A., Goebeler, V., Kappelhoff, R., auf dem Keller, U., Klein, T., Lange, P. F., Marino, G., Morrison, C. J., Prudova, A., Rodriguez, D., Starr, A. E., Wang, Y., & Overall, C. M. (2016). Active site specificity profiling datasets of matrix metalloproteinases (MMPs) 1, 2, 3, 7, 8, 9, 12, 13 and 14. *Data Brief*, *7*, 299–310.

Elias, M. S., Wright, S. C., Nicholson, W. V., Morrison, K. D., Prescott, A. R., Ten Have, S., Whitfield, P. D., Lamond, A. I., & Brown, S. J. (2019). Functional and proteomic analysis of a full thickness filaggrin-deficient skin organoid model. *Wellcome Open Research*, *4*, 134.

Fernández-Costa, C., Martínez-Bartolomé, S., McClatchy, D. B., Saviola, A. J., Yu, N.-K., & Yates, J. R. I. I. I. (2020). Impact of the Identification Strategy on the Reproducibility of the DDA and DIA Results. *Journal of Proteome Research*, *19*(8), 3153–3161.

Fortelny, N., Cox, J. H., Kappelhoff, R., Starr, A. E., Lange, P. F., Pavlidis, P., & Overall, C. M. (2014). Network analyses reveal pervasive functional regulation between proteases in the human protease web (2014/05/29). *PLoS Biol*, *12*(5), e1001869.

Franciosa, G., Locard-Paulet, M., Jensen, L. J., & Olsen, J. V. (2023). Recent advances in kinase signaling network profiling by mass spectrometry. *Current Opinion in Chemical Biology*, *73*, 102260.

Freedberg, I. M., Tomic-Canic, M., Komine, M., & Blumenberg, M. (2001). Keratins and the keratinocyte activation cycle (2001/05/12). *J Invest Dermatol*, *116*(5), 633–640.

Fuchs, E., & Raghavan, S. (2002). Getting under the skin of epidermal morphogenesis. *Nature reviews. Genetics*, *3*(3), 199–209.

Gallien, S., Kim, S. Y., & Domon, B. (2015). Large-Scale Targeted Proteomics Using Internal Standard Triggered-Parallel Reaction Monitoring (IS-PRM). *Mol Cell Proteomics*, *14*(6), 1630–1644.

Geurts, N., Becker-Pauly, C., Martens, E., Proost, P., Van den Steen, P. E., Stöcker, W., & Opdenakker, G. (2012). Meprins process matrix metalloproteinase-9 (MMP-9)/gelatinase B and enhance the activation kinetics by MMP-3. *FEBS letters*, *586*(24), 4264–4269.

Gill, J. H., Kirwan, I. G., Seargent, J. M., Martin, S. W., Tijani, S., Anikin, V. A., Mearns, A. J., Bibby, M. C., Anthoney, A., & Loadman, P. M. (2004). MMP-10 is overexpressed, proteolytically active, and a potential target for therapeutic intervention in human lung carcinomas (2005/02/22). *Neoplasia*, *6*(6), 777–785.

Griswold, A. R., Cifani, P., Rao, S. D., Axelrod, A. J., Miele, M. M., Hendrickson, R. C., Kentsis, A., & Bachovchin, D. A. (2019). A Chemical Strategy for Protease Substrate Profiling. *Cell Chemical Biology*, *26*(6), 901–907.

Guo, T., Kouvonen, P., Koh, C. C., Gillet, L. C., Wolski, W. E., Röst, H. L., Rosenberger, G., Collins, B. C., Blum, L. C., Gillessen, S., Joerger, M., Jochum, W., & Aebersold, R. (2015). Rapid mass spectrometric conversion of tissue biopsy samples into permanent quantitative digital proteome maps. *Nature Medicine*, *21*, 407.

Gurtner, G. C., Werner, S., Barrandon, Y., & Longaker, M. T. (2008). Wound repair and regeneration (2008/05/16). *Nature*, *453*(7193), 314–321.

Higashi, K., Hasegawa, M., Yokoyama, C., Tachibana, T., Mitsui, S., & Saito, K. (2012). Dermokine-β impairs ERK signaling through direct binding to GRP78. *FEBS Letters*, *586*(16), 2300–2305.

Hosp, F., & Mann, M. (2017). A Primer on Concepts and Applications of Proteomics in Neuroscience.

Hoste, E., Kemperman, P., Devos, M., Denecker, G., Kezic, S., Yau, N., Gilbert, B., Lippens, S., De Groote, P., Roelandt, R., Van Damme, P., Gevaert, K., Presland, R. B., Takahara, H., Puppels, G., Caspers, P., Vandenabeele, P., & Declercq, W. (2011). Caspase-14 is required for filaggrin degradation to natural moisturizing factors in the skin. *J Invest Dermatol*, *131*(11), 2233–2241.

Hu, Z., Sankar, D. S., Vu, B., Leytens, A., Vionnet, C., Wu, W., Stumpe, M., Martínez-Martínez, E., Stork, B., & Dengjel, J. (2021). ULK1 phospho-

rylation of striatin activates protein phosphatase 2A and autophagy. *Cell Reports*, *36*(13).

Huesgen, P. F., Lange, P. F., Rogers, L. D., Solis, N., Eckhard, U., Kleifeld, O., Goulas, T., Gomis-Rüth, F. X., & Overall, C. M. (2014). LysargiNase mirrors trypsin for protein C-terminal and methylation-site identification. *Nature Methods*, *12*(1), 55–58.

Hughes, C. S., Moggridge, S., Müller, T., Sorensen, P. H., Morin, G. B., & Krijgsveld, J. (2019). Single-pot, solid-phase-enhanced sample preparation for proteomics experiments. *Nature Protocols*, *14*(1), 68–85.

Impola, U., Uitto, V. J., Hietanen, J., Hakkinen, L., Zhang, L., Larjava, H., Isaka, K., & Saarialho-Kere, U. (2004). Differential expression of matrilysin-1 (MMP-7), 92 kD gelatinase (MMP-9), and metalloelastase (MMP-12) in oral verrucous and squamous cell cancer. *J Pathol*, *202*(1), 14–22.

Itoh, Y. (2015). Membrane-type matrix metalloproteinases: Their functions and regulations. *Matrix biology : journal of the International Society for Matrix Biology*, *44-46*, 207–223.

Ju, S., Kwon, Y., Kim, J.-M., Park, D., Lee, S., Lee, J.-W., Hwang, C.-S., & Lee, C. (2020). iNrich, Rapid and Robust Method to Enrich N-Terminal Proteome in a Highly Multiplexed Platform. *Analytical Chemistry*.

Kalinin, A. E., Kajava, A. V., & Steinert, P. M. (2002). Epithelial barrier function: assembly and structural features of the cornified cell envelope. *BioEssays : news and reviews in molecular, cellular and developmental biology*, *24*(9), 789–800.

Kalogeropoulos, K., Bundgaard, L., & auf dem Keller, U. (2022). Proteolytic signaling in cutaneous wound healing. *Proteolytic Signaling in Health and Disease*, 131–164.

Kam, E., Resing, K. A., Lim, S. K., & Dale, B. A. (1993). Identification of rat epidermal profilaggrin phosphatase as a member of the protein phosphatase 2A family. *Journal of cell science*, *106 (Pt 1)*(1), 219–226.

Kerkela, E., Ala-aho, R., Lohi, J., Grénman, R., M-Kähäri, V., Saarialho-Kere, U., Grenman, R., V, M. K., & Saarialho-Kere, U. (2001). Differential patterns of stromelysin-2 (MMP-10) and MT1-MMP (MMP-14) expression in epithelial skin cancers. *Br J Cancer*, *84*(5), 659–669.

Kim, H. J., Kim, T., Hoffman, N. J., Xiao, D., James, D. E., Humphrey, S. J., & Yang, P. (2021). PhosR enables processing and functional analysis of phosphoproteomic data. *Cell Reports*, *34*(8).

Kleifeld, O., Doucet, A., auf dem Keller, U., Prudova, A., Schilling, O., Kainthan, R. K., Starr, A. E., Foster, L. J., Kizhakkedathu, J. N., & Overall, C. M. (2010). Isotopic labeling of terminal amines in complex samples identifies protein N-termini and protease cleavage products. *Nature Biotechnology*, *28*(3), 281–288.

Kleifeld, O., Doucet, A., Prudova, A., auf dem Keller, U., Gioia, M., Kizhakkedathu, J. N., & Overall, C. M. (2011). Identifying and quantifying proteolytic events and the natural N terminome by terminal amine isotopic labeling of substrates. *Nature Protocols*, *6*(10), 1578–1611.

Klein, T., Fung, S. Y., Renner, F., Blank, M. A., Dufour, A., Kang, S., Bolger-Munro, M., Scurll, J. M., Priatel, J. J., Schweigler, P., Melkko, S., Gold, M. R., Viner, R. I., Regnier, C. H., Turvey, S. E., & Overall, C. M. (2015). The paracaspase MALT1 cleaves HOIL1 reducing linear ubiquitination by LUBAC to dampen lymphocyte NF-kappaB signalling. *Nat Commun*, *6*, 8777.

Klein, T., Eckhard, U., Dufour, A., Solis, N., & Overall, C. M. (2018). Proteolytic Cleavage - Mechanisms, Function, and "omic" Approaches for a Near-Ubiquitous Posttranslational Modification. *Chemical Reviews*, *118*(3), 1137–1168.

Krampert, M., Bloch, W., Sasaki, T., Bugnon, P., Rulicke, T., Wolf, E., Aumailley, M., Parks, W. C., & Werner, S. (2004). Activities of the matrix metalloproteinase stromelysin-2 (MMP-10) in matrix degradation and keratinocyte organization in wounded skin (2004/09/17). *Mol Biol Cell*, *15*(12), 5242–5254.

Kruppa, D., Peters, F., Bornert, O., Maler, M. D., Martin, S. F., Becker-Pauly, C., & Nyström, A. (2021). Distinct contributions of meprins to skin regeneration after injury - Meprin α a physiological processer of pro-collagen VII. *Matrix biology plus*, *11*, 100065.

Lange, P. F., & Overall, C. M. (2011). TopFIND, a knowledgebase linking protein termini with function.

Leclerc, E. A., Huchenq, A., Kezic, S., Serre, G., & Jonca, N. (2014). Mice deficient for the epidermal dermokine β and γ isoforms display transient cornification defects. *Journal of Cell Science*, *127*(13), 2862–2872.

Luo, S. Y., Araya, L. E., & Julien, O. (2019). Protease Substrate Identification Using N-terminomics. *ACS Chemical Biology*, *14*(11), 2361–2371.

Macklin, A., Khan, S., & Kislinger, T. (2020). Recent advances in mass spectrometry based clinical proteomics: Applications to cancer research.

Mahrus, S., Trinidad, J. C., Barkan, D. T., Sali, A., Burlingame, A. L., & Wells, J. A. (2008). Global sequencing of proteolytic cleavage sites in

apoptosis by specific labeling of protein N termini (2008/08/30). *Cell*, *134*(5), 866–876.

Mathew, R., Khanna, R., Kumar, R., Mathur, M., Shukla, N. K., & Ralhan, R. (2002). Stromelysin-2 overexpression in human esophageal squamous cell carcinoma: potential clinical implications. *Cancer Detect. Prev.*, *26*(3), 222–228.

Matsui, T., Hayashi-Kisumi, F., Kinoshita, Y., Katahira, S., Morita, K., Miyachi, Y., Ono, Y., Imai, T., Tanigawa, Y., Komiya, T., & Tsukita, S. (2004). Identification of novel keratinocyte-secreted peptides dermokine-α/- β and a new stratified epithelium-secreted protein gene complex on human chromosome 19q13.1. *Genomics*, *84*(2), 384–397.

Menon, G. K., Grayson, S., & Elias, P. M. (1985). Ionic calcium reservoirs in mammalian epidermis: ultrastructural localization by ion-capture cytochemistry. *The Journal of investigative dermatology*, *84*(6), 508–512.

Moffatt, P., Salois, P., St-Amant, N., Gaumond, M.-H., & Lanctôt, C. (2004). Identification of a conserved cluster of skin-specific genes encoding secreted proteins. *Gene*, *334*, 123–131.

Muller, D., Quantin, B., Gesnel, M. C., Millon-Collard, R., Abecassis, J., & Breathnach, R. (1988). The collagenase gene family in humans consists of at least four members. *Biochem J*, *253*(1), 187–192.

Murphy, G., Cockett, M. I., Ward, R. V., & Docherty, A. J. (1991). Matrix metalloproteinase degradation of elastin, type IV collagen and proteoglycan. A quantitative comparison of the activities of 95 kDa and 72 kDa gelatinases, stromelysins-1 and -2 and punctuated metalloproteinase (PUMP). *Biochem J*, *277 (Pt 1)*, 277–279.

Nakamura, H., Fujii, Y., Ohuchi, E., Yamamoto, E., & Okada, Y. (1998). Activation of the precursor of human stromelysin 2 and its interactions with other matrix metalloproteinases. *Eur J Biochem*, *253*(1), 67–75.

Naso, M. F., Liang, B., Huang, C. C., Song, X. Y., Shahied-Arruda, L., Belkowski, S. M., D'Andrea, M. R., Polkovitch, D. A., Lawrence, D. R., Griswold, D. E., Sweet, R. W., & Amegadzie, B. Y. (2007a). Dermokine: an extensively differentially spliced gene expressed in epithelial cells (2007/03/24). *J Invest Dermatol*, *127*(7), 1622–1631.

Naso, M. F., Liang, B., Huang, C. C., Song, X. Y., Shahied-Arruda, L., Belkowski, S. M., D'Andrea, M. R., Polkovitch, D. A., Lawrence, D. R., Griswold, D. E., Sweet, R. W., & Amegadzie, B. Y. (2007b). Dermokine: An extensively differentially spliced gene expressed in epithelial cells. *Journal of Investigative Dermatology*, *127*(7), 1622–1631.

Nauroy, P., & Nyström, A. (2020). Kallikreins: Essential epidermal messengers for regulation of the skin microenvironment during homeostasis, repair and disease. *Matrix biology plus*, *6-7*, 100019.

Nicholson, R., Murphy, G., & Breathnach, R. (1989). Human and rat malignant-tumor-associated mRNAs encode stromelysin-like metalloproteinases (1989/06/13). *Biochemistry*, *28*(12), 5195–5203.

O-charoenrat, P., Rhys-Evans, P. H., & Eccles, S. A. (2001). Expression of Matrix Metalloproteinases and Their Inhibitors Correlates With Invasion and Metastasis in Squamous Cell Carcinoma of the Head and Neck. *Archives of Otolaryngology–Head & Neck Surgery*, *127*(7), 813–820.

Olsen, J. V., & Mann, M. (2013). Status of large-scale analysis of post-translational modifications by mass spectrometry (2013/11/05). *Mol Cell Proteomics*, *12*(12), 3444–3452.

Oomizu, S., Sahuc, F., Asahina, K., Inamatsu, M., Matsuzaki, T., Sasaki, M., Obara, M., & Yoshizato, K. (2000). Kdap, a novel gene associated with the stratification of the epithelium. *Gene*, *256*(1-2), 19–27.

Pahwa, S., Bhowmick, M., Amar, S., Cao, J., Strongin, A. Y., Fridman, R., Weiss, S. J., & Fields, G. B. (2019). Characterization and regulation of MT1-MMP cell surface-associated activity. *Chemical biology & drug design*, *93*(6), 1251–1264.

Paik, Y. K., Lane, L., Kawamura, T., Chen, Y. J., Cho, J. Y., Labaer, J., Yoo, J. S., Domont, G., Corrales, F., Omenn, G. S., Archakov, A., Encarnación-Guevara, S., Lui, S., Salekdeh, G. H., Cho, J. Y., Kim, C. Y., & Overall, C. M. (2018). Launching the C-HPP neXt-CP50 Pilot Project for Functional Characterization of Identified Proteins with No Known Function.

Park, G. T., Lim, S. E., Jang, S. I., & Morasso, M. I. (2002). Suprabasin, a novel epidermal differentiation marker and potential cornified envelope precursor (2002/09/14). *Journal of Biological Chemistry*, *277*(47), 45195–45202.

Pieroni, L., Iavarone, F., Olianas, A., Greco, V., Desiderio, C., Martelli, C., Manconi, B., Sanna, M. T., Messana, I., Castagnola, M., & Cabras, T. (2020). Enrichments of post-translational modifications in proteomic studies. *Journal of Separation Science*, *43*(1), 313–336.

Proksch, E., Brandner, J. M., & Jensen, J. M. (2008). The skin: an indispensable barrier (2008/12/02). *Exp Dermatol*, *17*(12), 1063–1072.

Rangarajan, A., Talora, C., Okuyama, R., Nicolas, M., Mammucari, C., Oh, H., Aster, J. C., Krishna, S., Metzger, D., Chambon, P., Miele, L., Aguet, M., Radtke, F., & Dotto, G. P. (2001). Notch signaling is a

direct determinant of keratinocyte growth arrest and entry into differentiation (2001/07/04). *EMBO J*, *20*(13), 3427–3436.

Riley, N. M., & Coon, J. J. (2016). Phosphoproteomics in the Age of Rapid and Deep Proteome Profiling. *Analytical Chemistry*, *88*(1), 74–94.

Rogers, L. D., & Overall, C. M. (2013). Proteolytic post-translational modification of proteins: Proteomic tools and methodology. *Molecular and Cellular Proteomics*, *12*(12), 3532–3542.

Sabino, F., Hermes, O., & auf dem Keller, U. (2017). *Body Fluid Degradomics and Characterization of Basic N-Terminome* (1st ed., Vol. 585). Elsevier Inc.

Sabino, F., Hermes, O., Egli, F. E., Kockmann, T., Schlage, P., Croizat, P., Kizhakkedathu, J. N., Smola, H., & auf dem Keller, U. (2015). In vivo assessment of protease dynamics in cutaneous wound healing by degradomics analysis of porcine wound exudates (2014/12/18). *Mol Cell Proteomics*, *14*(2), 354–370.

Sahin, U., Weskamp, G., Kelly, K., Zhou, H. M., Higashiyama, S., Peschon, J., Hartmann, D., Saftig, P., & Blobel, C. P. (2004). Distinct roles for ADAM10 and ADAM17 in ectodomain shedding of six EGFR ligands. *The Journal of cell biology*, *164*(5), 769–779.

Sandby-Møller, J., Poulsen, T., & Wulf, H. C. (2003). Epidermal thickness at different body sites: relationship to age, gender, pigmentation, blood content, skin type and smoking habits. *Acta dermato-venereologica*, *83*(6), 410–413.

Sandilands, A., Sutherland, C., Irvine, A. D., & McLean, W. H. I. (2009). Filaggrin in the frontline: role in skin barrier function and disease. *J Cell Sci*, *122*(Pt 9), 1285–1294.

Savickas, S., Kastl, P., & Auf Dem Keller, U. (2020). Combinatorial degradomics: Precision tools to unveil proteolytic processes in biological systems.

Schilling, O., Huesgen, P. F., Barré, O., & Overall, C. M. (2011). Identification and relative quantification of native and proteolytically generated protein C-termini from complex proteomes: C-terminome analysis. *Methods in Molecular Biology*, *781*, 59–69.

Schlage, P., Kockmann, T., Sabino, F., Kizhakkedathu, J. N., & auf dem Keller, U. (2015). Matrix Metalloproteinase 10 Degradomics in Keratinocytes and Epidermal Tissue Identifies Bioactive Substrates With Pleiotropic Functions. *Mol Cell Proteomics*, *14*(12), 3234–3246.

Schlage, P., & auf dem Keller, U. (2015). Proteomic approaches to uncover MMP function.

Schlage, P., Egli, F. E., Nanni, P., Wang, L. W., Kizhakkedathu, J. N., Apte, S. S., & Keller, U. a. d. (2014). Time-resolved Analysis of the Matrix Metalloproteinase 10 Substrate Degradome. *Molecular & Cellular Proteomics*, *13*(2), 580.

Segre, J. A. (2006). Epidermal barrier formation and recovery in skin disorders. *Journal of Clinical Investigation*, *116*(5), 1150.

Shema, G., Nguyen, M. T., Solari, F. A., Loroch, S., Venne, A. S., Kollipara, L., Sickmann, A., Verhelst, S. H., & Zahedi, R. P. (2018). Simple, scalable, and ultrasensitive tip-based identification of protease substrates. *Molecular and Cellular Proteomics*, *17*(4), 826–834.

Shin, S., Hong, J. H., Na, Y., Lee, M., Qian, W.-J., Kim, V. N., & Kim, J.-S. (2020). Development of Multiplexed Immuno-N-Terminomics to Reveal the Landscape of Proteolytic Processing in Early Embryogenesis of Drosophila melanogaster. *Analytical Chemistry*, *92*(7), 4926–4934.

Simpson, C. L., Patel, D. M., & Green, K. J. (2011). Deconstructing the skin: cytoarchitectural determinants of epidermal morphogenesis. *Nature Reviews Molecular Cell Biology 2011 12:9*, *12*(9), 565–580.

Singer, A. J., & Clark, R. A. (1999). Cutaneous wound healing (F. H. Epstein, Ed.). *The New England journal of medicine*, *341*(10), 738–746.

Solis, N., Parambath, A., Abbina, S., Kizhakkedathu, J., & Overall, C. M. (2019). *Simplified high yield TAILS terminomics using a new HPG-ALD 800K-2000 polymer with precipitation* (1st ed., Vol. 626). Elsevier Inc.

Staes, A., van Damme, P., Timmerman, E., Ruttens, B., Stes, E., Gevaert, K., & Impens, F. (2017). Protease substrate profiling by N-terminal COFRADIC. In *Methods in molecular biology* (pp. 51–76). Humana Press Inc.

Steinert, P. M., Mack, J. W., Korge, B. P., Gan, S. Q., Haynes, S. R., & Steven, A. C. (1991). Glycine loops in proteins: their occurrence in certain intermediate filament chains, loricrins and single-stranded RNA binding proteins. *International journal of biological macromolecules*, *13*(3), 130–139.

Tanco, S., Gevaert, K., & Van Damme, P. (2015). C-terminomics: Targeted analysis of natural and posttranslationally modified protein and peptide C-termini (2014/10/16). *Proteomics*, *15*(5-6), 903–914.

Tholen, S., Wolf, C., Mayer, B., Knopf, J. D., Löffek, S., Qian, Y., Kizhakkedathu, J. N., Biniossek, M. L., Franzke, C.-W., & Schilling, O. (2016). Skin Barrier Defects Caused by Keratinocyte-Specific Deletion of

ADAM17 or EGFR Are Based on Highly Similar Proteome and Degradome Alterations. *Journal of proteome research*, *15*(5), 1402–1417.

Timmer, J. C., Enoksson, M., Wildfang, E., Zhu, W., Igarashi, Y., Denault, J. B., Ma, Y., Dummitt, B., Chang, Y. H., Mast, A. E., Eroshkin, A., Smith, J. W., Tao, W. A., & Salvesen, G. S. (2007). Profiling constitutive proteolytic events in vivo. *Biochemical Journal*, *407*(1), 41–48.

Toth, M., Osenkowski, P., Hesek, D., Brown, S., Meroueh, S., Sakr, W., Mobashery, S., & Fridman, R. (2005). Cleavage at the stem region releases an active ectodomain of the membrane type 1 matrix metalloproteinase. *The Biochemical journal*, *387*(Pt 2), 497–506.

Toth, M., Sohail, A., Mobashery, S., & Fridman, R. (2006). MT1-MMP shedding involves an ADAM and is independent of its localization in lipid rafts. *Biochemical and biophysical research communications*, *350*(2), 377–384.

Touati, A., Saeidian, A. H., Youssefian, L., Faghankhani, M., Niaziorimi, F., Pajouhanfar, S., Vahidnezhad, H., & Uitto, J. (2020). The matriptase-prostasin proteolytic cascade in dermatologic diseases. *Experimental dermatology*, *29*(7), 580–587.

Tsuchida, S., Bonkobara, M., McMillan, J. R., Akiyama, M., Yudate, T., Aragane, Y., Tezuka, T., Shimizu, H., Cruz, P. D., & Ariizumi, K. (2004). Characterization of Kdap, A Protein Secreted by Keratinocytes. *Journal of Investigative Dermatology*, *122*(5), 1225–1234.

Turk, B., Turk, D. S. A., & Turk, V. (2012). Protease signalling: the cutting edge. *EMBO J*, *31*(7), 1630–1643.

Utsunomiya, A., Chino, T., Utsunomiya, N., Luong, V. H., Tokuriki, A., Naganuma, T., Arita, M., Higashi, K., Saito, K., Suzuki, N., Ohara, A., Sugai, M., Sugawara, K., Tsuruta, D., Oyama, N., & Hasegawa, M. (2020). Homeostatic Function of Dermokine in the Skin Barrier and Inflammation. *Journal of Investigative Dermatology*.

Van Damme, P., Staes, A., Bronsoms, S., Helsens, K., Colaert, N., Timmerman, E., Aviles, F. X., Vandekerckhove, J., & Gevaert, K. (2010). Complementary positional proteomics for screening substrates of endo-and exoproteases. *Nature Methods*, *7*(7), 512–515.

Venne, A. S., Solari, F. A., Faden, F., Paretti, T., Dissmeyer, N., & Zahedi, R. P. (2015). An improved workflow for quantitative N-terminal charge-based fractional diagonal chromatography (ChaFRADIC) to study proteolytic events in Arabidopsis thaliana. *Proteomics*, *15*(14), 2458–2469.

Venne, A. S., Vögtle, F. N., Meisinger, C., Sickmann, A., & Zahedi, R. P. (2013). Novel highly sensitive, specific, and straightforward strategy for comprehensive N-terminal proteomics reveals unknown substrates of the mitochondrial peptidase Icp55. *Journal of Proteome Research*, *12*(9), 3823–3830.

Vizovišek, M., Vidmar, R., Drag, M., Fonović, M., Salvesen, G. S., & Turk, B. (2018). Protease Specificity: Towards In Vivo Imaging Applications and Biomarker Discovery. *Trends in biochemical sciences*, *43*(10), 829–844.

Watt, F. M. (1998). Epidermal stem cells: markers, patterning and the control of stem cell fate. *Philosophical Transactions of the Royal Society of London. Series B: Biological Sciences*, *353*(1370), 831–837.

Weber, S., Niessen, M. T., Prox, J., Lüllmann-Rauch, R., Schmitz, A., Schwanbeck, R., Blobel, C. P., Jorissen, E., De Strooper, B., Niessen, C. M., & Saftig, P. (2011). The disintegrin/metalloproteinase Adam10 is essential for epidermal integrity and Notch-mediated signaling. *Development (Cambridge, England)*, *138*(3), 495–505.

Weeks, A. M., & Wells, J. A. (2020). N-Terminal Modification of Proteins with Subtiligase Specificity Variants. *Current protocols in chemical biology*, *12*(1).

Weng, S. S., Demir, F., Ergin, E. K., Dirnberger, S., Uzozie, A., Tuscher, D., Nierves, L., Tsui, J., Huesgen, P. F., & Lange, P. F. (2019). Sensitive determination of proteolytic proteoforms in limited microscale proteome samples. *Molecular and Cellular Proteomics*, *18*(11), 2335–2347.

Werny, L., Grogro, A., Bickenbach, K., Bülck, C., Armbrust, F., Koudelka, T., Pathak, K., Scharfenberg, F., Sammel, M., Sheikhouny, F., Tholey, A., Linder, S., & Becker-Pauly, C. (2023). MT1-MMP and ADAM10/17 exhibit a remarkable overlap of shedding properties. *The FEBS Journal*, *290*(1), 93–111.

Wiita, A. P., Seaman, J. E., & Wells, J. A. (2014). Global analysis of cellular proteolysis by selective enzymatic labeling of protein n-termini. In *Methods in enzymology* (pp. 327–358). Academic Press Inc.

Wildes, D., & Wells, J. A. (2010). Sampling the N-terminal proteome of human blood (2010/02/23). *Proc Natl Acad Sci U S A*, *107*(10), 4561–4566.

Xu, G., Shin, S. B. Y., & Jaffrey, S. R. (2009). Global profiling of protease cleavage sites by chemoselective labeling of protein N-termini. *Proceedings of the National Academy of Sciences of the United States of America*, *106*(46), 19310–19315.

Yang, P., Ormerod, J. T., Liu, W., Ma, C., Zomaya, A. Y., & Yang, J. Y. H. (2019). AdaSampling for Positive-Unlabeled and Label Noise Learning With Bioinformatics Applications. *IEEE Transactions on Cybernetics*, *49*(5), 1932–1943.

Ye, Z., Mao, Y., Clausen, H., & Vakhrushev, S. Y. (2019). Glyco-DIA: a method for quantitative O-glycoproteomics with in silico-boosted glycopeptide libraries. *Nature Methods*, *16*(9), 902–910.

Yoshihara, H. A., Mahrus, S., & Wells, J. A. (2008). Tags for labeling protein N-termini with subtiligase for proteomics. *Bioorganic and Medicinal Chemistry Letters*, *18*(22), 6000–6003.

Zhang, Y., Li, Q., Huang, J., Wu, Z., Huang, J., Huang, L., Li, Y., Ye, J., & Zhang, X. (2018). An Approach to Incorporate Multi-Enzyme Digestion into C-TAILS for C-Terminomics Studies. *PROTEOMICS*, *18*(1), 1700034.

Zigrino, P., Ayachi, O., Schild, A., Kaltenberg, J., Zamek, J., Nischt, R., Koch, M., & Mauch, C. (2012). Loss of epidermal MMP-14 expression interferes with angiogenesis but not with re-epithelialization. *European journal of cell biology*, *91*(10), 748–756.

CHAPTER 2

Results

2.1 Dermokine-isoform Genetic Editing – Manuscript 3

MANUSCRIPT 3 - SUMMARY

Establishment of Lentivirus-Free High-Efficiency Human Keratinocyte Transfection. Dermokine, a secreted protein produced by suprabasal keratinocytes, plays a crucial role in epidermal stratification and terminal differentiation. Despite its importance, the precise functions of its multiple isoforms remain elusive. To investigate the biological roles of dermokine proteoforms in epidermal differentiation, we optimized CRISPR/-Cas9 gene editing strategies to efficiently generate dermokine isoform-specific knockouts in human keratinocytes. Creating these knockouts allows for a more in-depth understanding of the protein's functions and its roles in skin biology.

Two main CRISPR/Cas9 strategies were employed in the study: a transfection-based method and an atomic force microscopy (AFM)-based method using FluidFM® technology. The transfection method established a novel optimized transfection protocol for virus-free delivery of CRISPR/Cas9 plasmids to keratinocytes and selection of genetically modified cells by concomitant expression of green fluorescent protein (GFP). In contrast, the AFM-based method used FluidFM® nano-syringes to directly deliver multiple gRNA CRISPR/Cas9 ribonucleoprotein (RNP) complexes to the nucleus. Both methods were optimized for maximum efficiency in gene editing and minimizing off-target effects.

Multiplexed CRISPR RNP Complex Delivery Directly to the Nucleus. Using these optimized CRISPR/Cas9 strategies, we successfully generated dermokine proteoform-specific knockouts in human keratinocytes. The transfection-based method allowed for isolation of single-cell clones with

the desired genomic alterations, while the FluidFM® technology enabled multiplexed CRISPR targeting, facilitating the direct delivery of quadruple CRISPR RNP complexes into the nucleus. These strategies resulted in high-efficiency gene editing and minimized off-target effects and provided stable cell knockout models for further investigation.

This study presents a robust and efficient CRISPR/Cas9 gene editing workflow for generating dermokine proteoform-specific knockouts in human keratinocytes. These stable mutants will facilitate future research on the role of dermokine proteoforms in epidermal differentiation. Moreover, the optimized CRISPR/Cas9 strategies can be applied to other challenging cell types, expanding the applicability of this powerful gene editing tool in the study of complex biological systems.

Isoform-specific ablation of dermokine by virus-free CRISPR/Cas9 genetic editing of human keratinocytes

Vahap Canbay[1], Weihua Tian[1], Tobias A. Beyer[2], Anabel Migenda Herranz[2], Susanne Mailand[2], Steffen Goletz[1], and Ulrich auf dem Keller[1]

[1]Department of Biotechnology and Biomedicine, Technical University of Denmark, DK-2800, Kongens Lyngby, Denmark
[2]Cytosurge AG, Saegereistrasse 25, 8152 Glattbrug, Switzerland

Will be published as part of

Canbay V., Tian W., Beyer TA., Migenda Herranz A, Mailand S., Goletz S., and auf dem Keller U. (2023) Efficient virus-free CRISPR/Cas9 genetic editing of human keratinocytes *In preparation.*

Contribution by VC:
Cell culture, cloning, genotyping, data analysis, manuscript writing.

2.1.1 Abstract

The epidermis provides a vital barrier between the human body and its external environment, playing critical roles in protection, water retention, and mechanical resistance. Dermokine, a secreted protein produced by suprabasal keratinocytes, is associated with epidermal stratification and terminal differentiation but has been poorly understood due to its multiple isoforms. In this study, we employed CRISPR/Cas9 genome editing to generate isoform-specific dermokine gene disruption in human keratinocytes, allowing to investigate the biological role of various dermokine isoforms in keratinocytes. We optimized transfection efficiency and delivery strategies for CRISPR/Cas9, including lentiviral-free CRISPR/Cas9 plasmid transfection and FluidFM® technology. This enabled us to generate dermokine mutants with minimal off-target effects. Through the generation of dermokine isoform-specific knockout keratinocytes, we have established a powerful model to elucidate the function of dermokine in keratinocytes and epidermal differentiation. Our findings pave the way for a better understanding of the role of dermokine and its isoforms in epidermal biology, potentially leading to new therapeutic targets for skin disorders, and provide novel efficient protocols for genome editing of keratinocytes.

2.1.2 Introduction

The epidermis provides an effective barrier between the organism and the outer surrounding, not only shielding the human body from pathogens but also impeding water loss and defying mechanical strains (Candi et al., 2005). Epidermal differentiation is an inherently complex and tightly inter-twined process marked by the outward migration of basal keratinocytes and resulting in a stratified epithelium (Fuchs & Raghavan, 2002). In each stratum keratinocytes undergo several programs of terminal differentiation, eventually culminating in anucleated and flattened corneocytes which are shed off (Burns et al., 2010).

The secreted protein dermokine is produced by suprabasal keratinocytes and is potentially tied to epidermal stratification and terminal differentiation (Naso et al., 2007). Several transcripts have been denoted for the dermokine gene, resulting in five main gene products in the human proteome and three main isoforms in mice (Leclerc et al., 2014). Mice genetically ablated for all DMKN isoforms ($\alpha\beta$ and γ) develop neonatal hyperkeratosis and dyskeratosis in later stages of life, while several of the mice with severe skin phenotypes die 21 days postnatally, especially under low humidity (Utsunomiya et al., 2020). Their phenotypes include scaly skin with modest wrinkles until day eight, and some of the mice develop very dry skin and auto-amputation of the tail along with growth delay and transient body weight loss (Utsunomiya et al., 2020). Interestingly, mice with the dermokine $\alpha\beta\gamma$ knockout had a harsher phenotype in comparison to mice only deficient for dermokine $\beta\gamma$, insinuating a compensatory response of dermokine α (Utsunomiya et al., 2020). However, phenotypes in mice were highly dependent on an altered inflammatory response, precluding direct analysis of keratinocyte-autonomous effects, and might significantly differ from effects in human skin (Touati et al., 2020).

To further elucidate the functions of dermokine's multiple isoforms in human keratinocytes and unravel the cellular mechanism, loss of function approaches are needed.

Here, we exploit the capabilities of the CRISPR/Cas9 technology to efficiently introduce isoform-specific dermokine gene disruption in human keratinocytes. Examples of lentiviral-free CRISPR/Cas9 approaches in immortalized human keratinocytes have been established, e.g. successfully ablating ABCA12 (ATP Binding Cassette Subfamily A Member 12) (Enjalbert et al., 2020) or SPINK5 (Gálvez et al., 2020). Through optimization of several essential steps, we were able to achieve a significantly improved workflow by enhancing critical parameters, such as transfection efficiency, which in parallel with the novel method for the disruption of several isoforms and the concurrent genotyping allowed us to extend our analysis of dermokine isoform functions. First, using the primary gRNA we were able to disrupt dermokine

$\beta\gamma$, thus generating a dermokine α expressing mutant. In parallel, we utilized a secondary gRNA to successfully knockout dermokine β and ablate the α isoform, resulting in expression of only the dermokine γ isoform. Subsequently, we supplemented each construct with the complementary gRNA to generate the full dermokine $\alpha\beta\gamma^{-/-}$ mutant.

In recent years, several cellular delivery systems have been developed to address the molecular necessity of genetic engineering, consequently a mechanical strategy applying a hollow molecular cantilever coined FluidFM® was engineered (Meister et al., 2009). FluidFM® allows for the local dispensation of various molecules into single living cells under physiological conditions, making it an ideal approach to integrate the process within a CRISPR/Cas9-based genome editing setup (Guillaume-Gentil et al., 2016). Utilizing FluidFM®'s strength we designed a multiplexed workflow, enabling us to directly deliver quadruple CRISPR ribonucleoproteins with the respective gRNA into a single nucleus to delete entire exons.

Applying either Cytosurge AG's, Switzerland, proprietary FluidFM® technology or our optimized virus-free genome editing, we were able to obtain clones of knockout keratinocytes based on a single cell that inherited the genomic alterations. These two methods not only differ in terms of gRNA delivery but also vary with regard to the modality of disruption. From here on we are able to further elucidate the function of dermokine in keratinocytes and epidermal differentiation.

2.1.3 Experimental Procedures

N/TERT keratinocytes cell culture. Human keratinocyte telomerase reverse transcriptase immortalized (h/TERT immortalized) N/TERT-1 cells derived from clinically normal foreskin tissue (A et al., 2000) were a kind gift from Prof. Edel O'Toole (Queen Mary University, London, United Kingdom). N/TERT-1 keratinocytes were grown in DMEM/F-12 growth medium supplemented with RM+ (DMEM/F-12 (Thermo Fisher Scientific, Waltham,

MA, 11-320-033), 10% FBS (Thermo Fisher Scientific, 11550356), 1% penicillin/streptomycin [P/S] (Sigma-Aldrich, Darmstadt, Germany, P0781), 0.4 μg/mL hydrocortisone (Sigma-Aldrich, H4881), 0.5 μg/mL insulin (Sigma-Aldrich, I5500), 10 ng/mL epidermal growth factor (Bio-Rad, Hercules, CA, PMP89), 0.1 nM cholera toxin (Sigma-Aldrich, C8052), 5 μg/mL transferrin (Sigma-Aldrich, T2252), 20 pM liothyronine (Sigma-Aldrich, T6397)) and incubated at 37 °C, 5% CO_2. All cell lines were tested mycoplasm negative.

gRNA design. Guide RNAs (gRNAs) were designed utilizing the CHOPCHOP web tool to target specific sequences associated with either the α/β orβ/γisoforms of the gene (Labun et al., 2019). The aim was to identify CRISPR/Cas9 target sites in close proximity to the N-terminus. By adopting the general settings suggested by CHOPCHOP, a balance between specificity and efficiency in gRNA design was pursued. Consequently, the gRNAs were tailored for isoform-specific gene editing.

Table 2.1. Transfection-based gRNA for the insertion of indels in N/TERT keratinocyte.

	Strand direction	**gRNA target sequence**	**PAM**	**Sequence forward primer**	**Sequence reverse primer**
gRNA 1 - Exon 2	+	GGA TAC CCC GGA AAC TCA GC	*AGG*	TCA TTC TGG TTG CTG GCT CT	TCT ACC AGG GTC AGA GAT GGT
gRNA 2 - Exon 18	+	TCA TCA CTG CAG AAA CGT GC	*AGG*	ACC CTC ACC TGC CTT TAC TG	TAG GTA GCA CGT GGA AAG GG
gRNA 3 - Exon 19	+	AGG CAG TGG GAT ACG CAT GC	*AGG*	AGA GCT GCT TGC GTG TTT TG	AAA ATG GCC TTC GTC CGT CT

Plasmids and DNA construction. We employed a two-plasmid system to enable the assembly of gRNA and Cas9 protein inside the cells for gene editing. The Cas9 plasmid (CAS9PBKS) was obtained from Addgene (Addgene, Watertown, MA, 6837), while the gRNA plasmid was reconstructed using the U6GRNA (Addgene, 68370) vector with DMKN gRNAs (Macrogen, Seoul, Republic of Korea). To insert the gRNA target, we opened the vector through Bbs1 restriction enzyme (Thermo Fisher Scientific, ER1011) , which resulted in the linearization of the plasmid backbone with two sticky ends (GTGG and GTTT). We synthesized the gRNA oligos with complementary sticky ends and ligated them into the U6GRNA (Addgene) plasmid using T4 ligase (Thermo Fisher Scientific, EL0011). The presence of the ampicillin resistance gene (AmpR) on both plasmids allowed us to select transformed E. coli clones on an ampicillin agar plate during the gRNA cloning process. Successful insertion of the gRNA target was confirmed through Sanger sequencing (Macrogen Europe, Amsterdam, Netherlands).

Optimization of plasmid DNA transfection. N/TERT-1 keratinocytes were seeded at a density of 5 x 10^5 cells/mL in 6 wells plate one day prior to make it approximately 50-80% confluence on the day of transfection. The Cas9PBKS plasmid (Addgene, 68371), which expresses Cas9-2A-GFP and has a size of 8984 bp, was utilized to determine the transfection efficiency. Each transfection involved the use of 2 μg of the Cas9PBKS plasmid, and six commonly used commercial transfection reagents were selected for the experiment: Lipofectamine™3000 (Thermo Fisher Scientific, L3000001), X-tremeGENE™HP (Sigma-Aldrich, XTGHP-RO), FuGENE® HD (Promega, Madison, WI, E2311) and ViaFect™(Promega, E4981), PEIpro® (Polyplus, Illkirch, France, 101000017) and jetOPTIMUS® (Polyplus, 101000051). The instructions provided by the manufacturers for each reagent were followed for each transfection.

In the process of using Lipofectamine™3000 (Thermo Fisher Scientific), 5 μL of the reagent was diluted with 125 μL of Opti-MEM™(Thermo Fisher

Scientific, 31985062) in tube 1. In tube 2, 2 μg of CAS9PBKS (Addgene) plasmids were diluted into 125 μL of Opti-MEM™(Thermo Fisher Scientific), with the subsequent addition of 4 μL of P3000 reagents (Thermo Fisher Scientific). The reagent from tube 2 was then transferred to tube 1, gently mixed by finger-tapping, and incubated at room temperature for 15 min.

In the application of X-tremeGENE™HP, 2 μg of CAS9PBKS (Addgene) plasmids was diluted into 200 μL OptiPRO™SFM (Thermo Fisher Scientific,12309019) in tube 1. Subsequently, 6 μL (3:1) of the X-tremeGENE HP DNA Transfection Reagent (Sigma-Aldrich) was added directly into tube 1. The mixture was gently mixed and incubated at room temperature for 15 min.

In employing FuGENE® HD (Promega), 2 μg of CAS9PBKS plasmids was diluted into 100 μL of Opti-MEM™(Thermo Fisher Scientific), followed by a gentle mix. Then, 6 μL of FuGENE® HD Transfection Reagent (Promega) (3:1 to DNA) was added and the mixture incubated at room temperature for 15 min.

For Viafect™(Promega) usage, 2 μg of CAS9PBKS (Addgene) plasmids was diluted to 200 μL of Opti-MEM™(Thermo Fisher Scientific), after which 6 μL of ViaFect (Promega) (3:1 to DNA) was added. The mix was stirred well and incubated at room temperature for 15min.

During the utilization of PEIPro® (Polyplus), 2 μg of CAS9PBKS (Addgene) plasmids was diluted in OptiPRO™SFM (Thermo Fisher Scientific) to a final volume of 50 μL in tube 1. Similarly, 2 μL of PEIpro® reagent (Polyplus) was diluted in OptiPRO™SFM (Thermo Fisher Scientific) to a final volume of 50 μL in tube 2. The contents of the two tubes were then mixed and incubated at room temperature for 15 min.

With JetOPTIMUS® (Polyplus), 2 μg of CAS9PBKS (Addgene) plasmids were diluted in 200 μL JetOPTIMUS® buffer (Polyplus), and then 2 μL of JetOPTIMUS® (Polyplus) reagent was added. The mixture was stirred well and incubated at room temperature for 10 min.

Each transfection mixture was added to cells in one well of a 6-well plate

and incubated. Pictures were taken using a microscope (Thermo Fisher Scientific, AMF7000) one day after transfection and FACS was used two days after transfection to determine transfection efficiency. The list of CRISPR gRNA targets and PCR primers, as well as the genotyping of selected clones, are shown in Table 2.1.

FACS enrichment and single cell cloning. Two days after transfection, the cells were subjected to FACS enrichment using the Sony MA900 cell sorter (Sony Biotechnology, San Jose, CA) to isolate the top 10-15% of cells expressing GFP. This process aimed to remove the untransfected cells from the population. The enriched cell pool obtained from the FACS enrichment step was subsequently cultured for an additional 1-2 weeks to allow for cell expansion. Afterward, single-cell sorting was performed using FACS, with each GFP negative cell individually sorted into a designated well of a 96-well plate.

Genotyping through PCR and Sanger sequencing. Genotyping was performed using PCR amplification and Sanger sequencing. PCR primers were designed through chopchop online tool. The QuickExtract™DNA Extraction Solution (Lucigen®, part of LGC Biosearch Technologies, Teddington, United Kingdom) was utilized to extract cellular DNA, which served as the template for PCR amplification. Approximately 1000-10000 cells were collected, washed with PBS, and resuspended in 30-50 μL of QuickExtract™(LGC Biosearch Technologies) DNA Extraction Solution. The samples were then heated at 70 °C for 20 min to extract DNA from the cells, followed by 95 °C for 10 min to deactivate the enzyme. The PCR setup included 12.5 μL of PROFILase™2x Master Mix (COBO Technologies, Frederiksberg, Denmark, C30101), 10 μL of Nuclease-Free water (QIAGEN, Venio, Netherlands, 129117), 0.25 μL of 25 μM forward primer, 0.25 μL of 25 μM reverse primer, and 2 μL of the DNA template. The PCR tube was placed in an ABI 9902 Veriti™96-well thermocycler (Thermo Fisher Scientific, 4375305). The PCR program consisted of three stages. In stage 1, the samples were heated to 95 °C for 15 min to denature

the double-stranded DNA. In stage 2, the samples underwent cycles of denaturation at 95 °C for 30 seconds, annealing at 60 °C for 30 seconds (the primer annealing temperature), and extension at 72 °C for 45 seconds to allow for primer extension by DNA polymerase. Stage 2 was repeated 38 times to amplify the target DNA sequence. In stage 3, the sample was heated at 72 °C for 7 min to ensure complete synthesis of all ongoing templates. The PCR product was then purified using the ExoSAP-IT™PCR Product Cleanup Reagent (Thermo Fisher Scientific, 75001.40.UL) following the manufacturer's instructions. The purified PCR product was sent to Macrogen Europe BV for Sanger sequencing (Macrogen Europe, Amsterdam, Netherlands). The resulting sequencing data were analysed using the Synthego ICE online tool (Synthego Performance Analysis, ICE Analysis. 2019. version 3.0.). Mutant clones were selected based on the presence of indel mutations.

AFM-based nano-injections for the introduction of sgRNAs. The principle for the FluidFM® hollow-lever is described elsewhere (Meister et al., 2009). Single N/TERT-1 were seeded into the center of a well of a 12-well plate using a DispenCell™(SEED Biosciences, Epalinges, Switzerland). The cells were left to adhere overnight and 50-100 fL of RNP solution was nano-injected using FluidFM® technology. The injection mixture consisted of 0.5 pmol gRNA, 0.366 pmol of Cas9 and 20 ng of GFP mRNA per μL. Injection success was monitored 24 h after injection by fluorescent microscopy (GFP positive cells). Single cells were expanded in the medium described

Table 2.2. PCR Program for transfection-based *Dmkn* $\alpha\beta\gamma^{-/-}$.

Step	Temperature [°C]	Time [s]	Cycles
First denaturing step	95	900	1
Denaturation	95	30	38
Annealing	60	30	38
Extension	72	45	38
Heating	72	420	1

above aided by co-culture inserts to improve single-cell outgrowth. When cell colonies reached a size of approximately 1000 cells, cells were detached and seeded into fresh 12-well plates. 48 to 72 h later, cells were split at a 1:3 ratio and a portion was used for isolation of genomic DNA.

Table 2.3. AFM-based gRNA design for exon deletion in N/TERT keratinocytes.

	Strand direction	**gRNA target sequence**	**PAM**	**Sequence forward primer**	**Sequence reverse primer**
gRNA 4 - Exon 17	-	CTC GGG ATT GCA CAA AGC CT	*GGG*	ACC CGA GAT CTG GAA TCC CC	CAG CAT CCT GGT TCT TCG TG
gRNA 5 - Exon 17	+	ACC CGT GGG CAC TGA GAC AA	*AGG*	ACC CGA GAT CTG GAA TCC CC	CAG CAT CCT GGT TCT TCG TG
gRNA 6 - Exon 1	-	GGA AAC ACT GGG CAC GAG AT	*TGG*	TGG TGG GAG GAA GAC ACT CT	GCC ATG GCC TCC AGA AGT TT
gRNA 7 - Exon 1	-	CCA TTG GCA AAG AGG CCG GA	*GGG*	TGG TGG GAG GAA GAC ACT CT	GCC ATG GCC TCC AGA AGT TT

Analytical PCR reaction used for AFM-based nano-injections. Genomic DNA is isolated from the clones using QuickExtract (Lucigen) according to the manufacturer's instructions. Single gRNAs targeting either the *Dmkn* $\beta\gamma$ isoform or the *Dmkn* $\alpha\beta$ isoform. PCR was performed using the Platinum-Taq DNA polymerase with GC enhancer (Thermo Fisher Scientific) and an α cycler (PCRmax) using 1 μL of DNA lysate. Primer concentrations were 0.4 μM each. PCR to detect editing on exon 1 or 17, were performed using the DreamTaq polymerase (Thermo Fisher Scientific) according to the manufac-

turer's instructions.

Table 2.4. PCR program for AFM-based *Dmkn* $\alpha\beta\gamma^{-/-}$.

Step	Temperature [°C]	Time [s]	Cycles
Polymerase activation	95	240	1
Denaturation	95	30	35
Annealing	67.1	30	35
Extension	72	45	35
Final extension	72	300	1

Table 2.5. PCR program for AFM-based *Dmkn* $\alpha\beta^{-/-}$.

Step	Temperature [°C]	Time [s]	Cycles
Polymerase activation	95	240	1
Denaturation	95	30	35
Annealing	67.1	30	35
Extension	72	30	35
Final extension	68	300	1

Analytical agarose gel electrophoresis. For separation and visualization of PCR amplification products using 1.5% (w/v) agarose gels, 3 g agarose (Sigma-Aldrich, A9539) were dissolved in 200 mL TAE buffer (Sigma-Aldrich, 1.06174) by boiling in a microwave oven. After the addition of 20 μL GelGreen (Sigma-Aldrich, SCT125), gels were casted and run using a cleaver scientific agarose gel system (Cleaver Scientific, Rugby, United Kingdom). Thereby, DNA and size marker (4 μL, GeneRuler 100 bp) were separated at a constant voltage of 100 V for 25 min. Afterwards, DNA bands were documented using a UVITEC gel documentation system (Cambridge, United Kingdom).

Sanger sequencing of AFM-based nano-injections. Sequencing: 7.5 μL of PCR product (50 - 300 ng) was purified using ExoSAP-IT™(Thermo Fisher Scientific) according to the instructions. The volume of the PCR prod-

uct was adjusted to 12 μL with ultra pure water and 3 μL of sequencing primer (20 μM) added to the reaction. Either the forward or the reverse primer used for the PCR amplification was used as sequencing primer. Sanger sequencing was performed by Microsynth™(Microsynth, Balgach, Switzerland) and quality control of the sequencing was performed in Benchling™(Benchling, San Francisco, CA).

Alignment and deconvolution of sequence trace files of AFM-based nano-injections. Sequence files were aligned to the target sequence using the in-suite Benchling™(Benchling) application (Katoh & Standley, 2013). Sequences with distorted Sanger signal around the gRNA cut site were chosen for further analysis. In order to determine the signal of the individual alleles a deconvolution algorithm is applied. INDIGO™(Gear Genomics, Heidelberg, Germany) was used to determine approximately the sequence of the edited alleles.

2.1.4 Results and Discussion

Dermokine isoform-specific gene knockout experimental strategy and workflow. To better understand the biological role of dermokine and the manifold of its isoforms in the context of epidermal differentiation, it is necessary to ablate dermokine isoforms in keratinocytes, the same cells that show the highest endogenous expression of dermokine (Naso et al., 2007). Therefore, we applied a systematic approach, where we used several gene abscission technologies to ablate the various dermokine isoforms, allowing us to monitor isoform-specific changes in keratinocytes as depicted in Figure 2.1. Concomitantly, we not only followed several gRNA delivery strategies but also applied distinct abscission methods to establish knockout models, which can aid us in elucidation of dermokine's function. Firstly, we employed two different gRNA delivery strategies in parallel. The primary transfection-based method

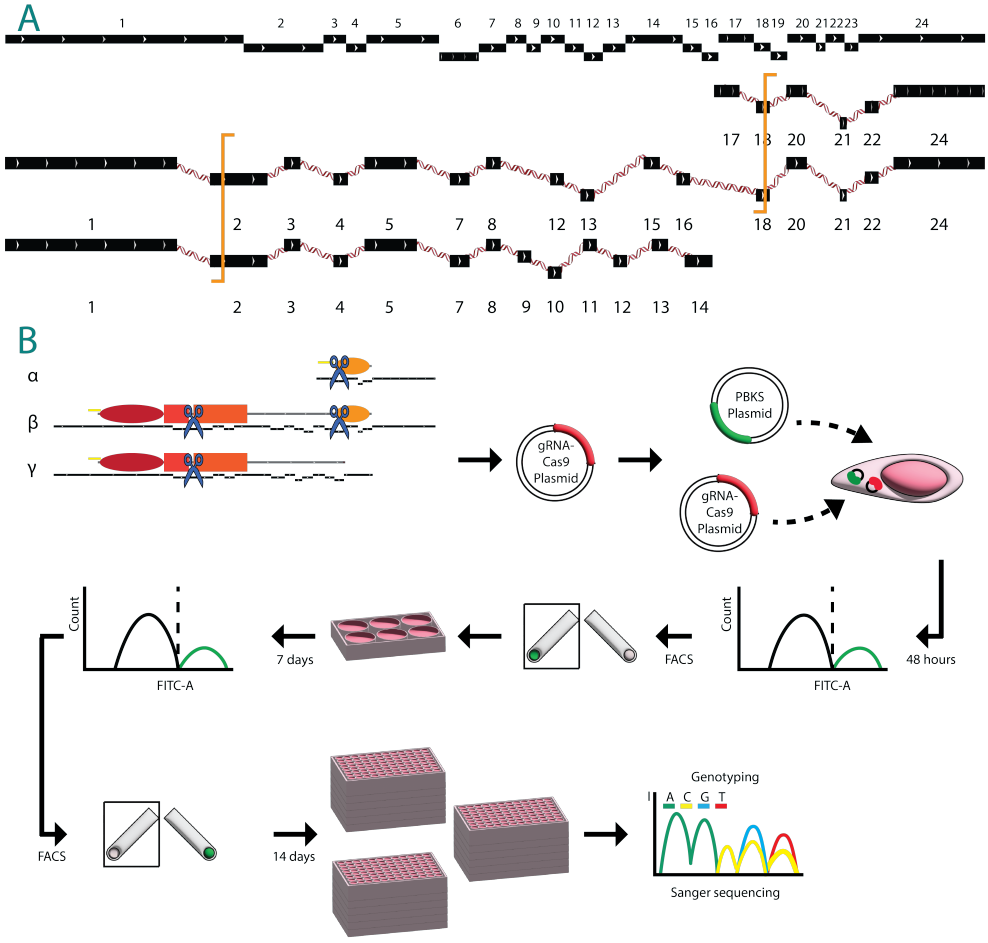

Figure 2.1. Experimental Design and Dermokine isoform gRNA construction – transfection-based method. A Presented here is the genetic locus of *Dmkn* with marked positions of gRNA 1 and gRNA 2. These positions indicate the precise locations where the indels are to be inserted into the various *Dmkn* isoforms. **B** This section describes the stepwise transfection-based workflow. It initiates with the transfection of keratinocytes using CAS9PBKS plasmids. This step induces the formation of indels and GFP expression. Following this, bulk FACS sorting by GFP is conducted, succeeded by a growth period of 7 days. The procedure then continues with single-cell FACS sorting based on non-GFP positivity, culminating in a 14-day colony growth period. This workflow offers an overview of the methodological process employed in this study to manipulate the *Dmkn* isoforms.

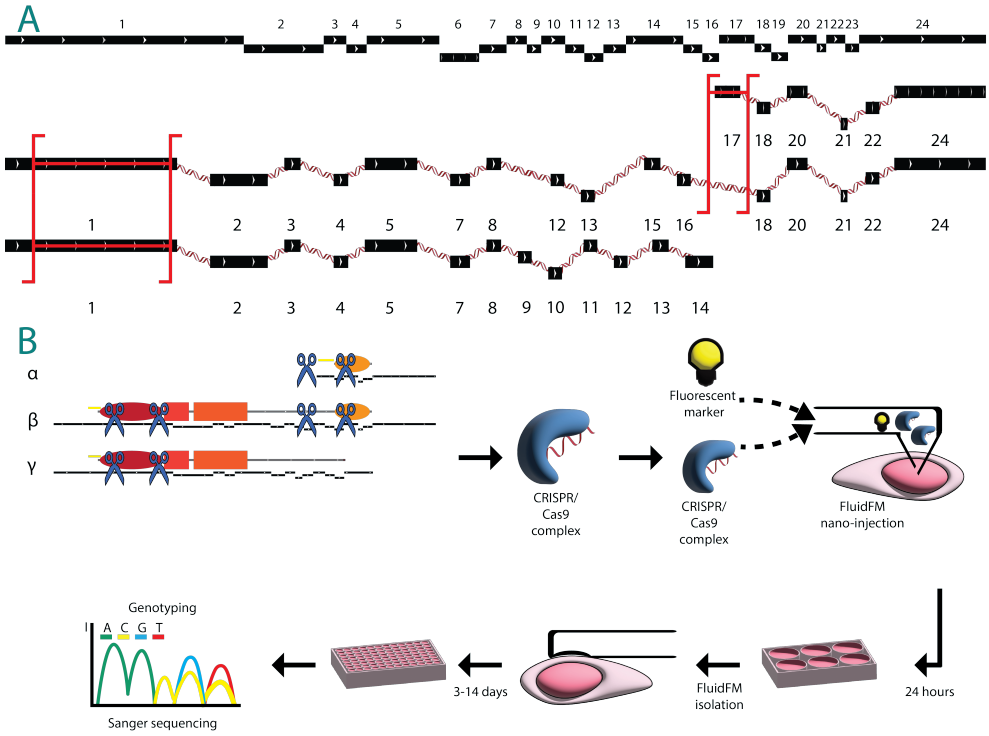

Figure 2.2. **Experimental design and dermokine isoform gRNA construction - AFM-based method.** **A**. The genetic locus of *Dmkn* is displayed, with marked positions of different gRNAs compared to the transfection-based method. Direct injection into the nucleus enables the simultaneous delivery of multiple RNP complexes with high efficiency. As a part of this strategy, gRNA 4 and 5 were used to remove exon 1 entirely. Subsequently, gRNA 6 and 7 were used on a different Ntert cell to ablate exon 17. **B** This section outlines a slightly different approach from the transfection-based method. Here, the RNP with gRNA is directly induced into the nucleus (indicated in yellow-orange). After 24 h, positive cells are selected and transferred into a new well using the hollow lever, guided by AFM. Following a 14-day period, positively exon-ablated colonies emerge from a single cell. This innovative process offers a unique approach to the manipulation of *Dmkn* isoforms.

allowed us to deliver gRNA as part of a CRISPR/Cas9 plasmid via transfection and first select a broad population of successfully genomically altered keratinocytes (Figure 2.1). Secondly, based on the modified population of cells we selected single-cell clones by FACS sorting, which we maintained in culture for 14 days and sequenced for validation. Similarly, the AFM-based method utilizes a direct transfer of the CRISPR/Cas9 RNP complex into the nucleus, thereby providing simultaneous sub-cellular delivery of several CRISPR/Cas9 RNP complex molecules, composing a high-efficiency relocation system (Figure 2.2). Upon optimization of gRNA delivery, we appropriated two distinct genomic alteration workflows. The immediate method was the introduction of a genetic frameshift on exons via gRNA targeting, either exon 2 or exon 18. Additionally, we did attempt to deploy gRNA 3 on exon 19, but our efforts did not culminate in the continuation of this clone. The alternative genetic altering method made use of the high-efficient simultaneous delivery of multiple CRISPR/Cas9 RNP complexes into the nucleus, thereby transporting two complexes that allowed for deletion of exon 1 or exon 17.

A comparison of gRNA delivery methods using cell transfection techniques and FluidFM® nano-injections. The general principle of our approach to generating a reliable dermokine isoform knockout was the optimization and comparison of several methods (Figure 2.1 and 2.2) (Lonowski et al., 2017). This experimental setup was chosen, to not solely rely on one knockout but rather have several independently produced keratinocyte clones with dermokine gene disruption, providing two defined models to investigate dermokine activity.

First, we devised several optimization strategies for the best set of parameters for the transfection-based technique, in regard to transfection efficiency and instrumentation settings. To identify the optimal transfection reagent we tested several commercially available reagents in order to find the most suitable for our approach (Figure 2.3A). By subjecting the keratinocytes to the respective transfection reagent and incubating the cells for 48 h with the

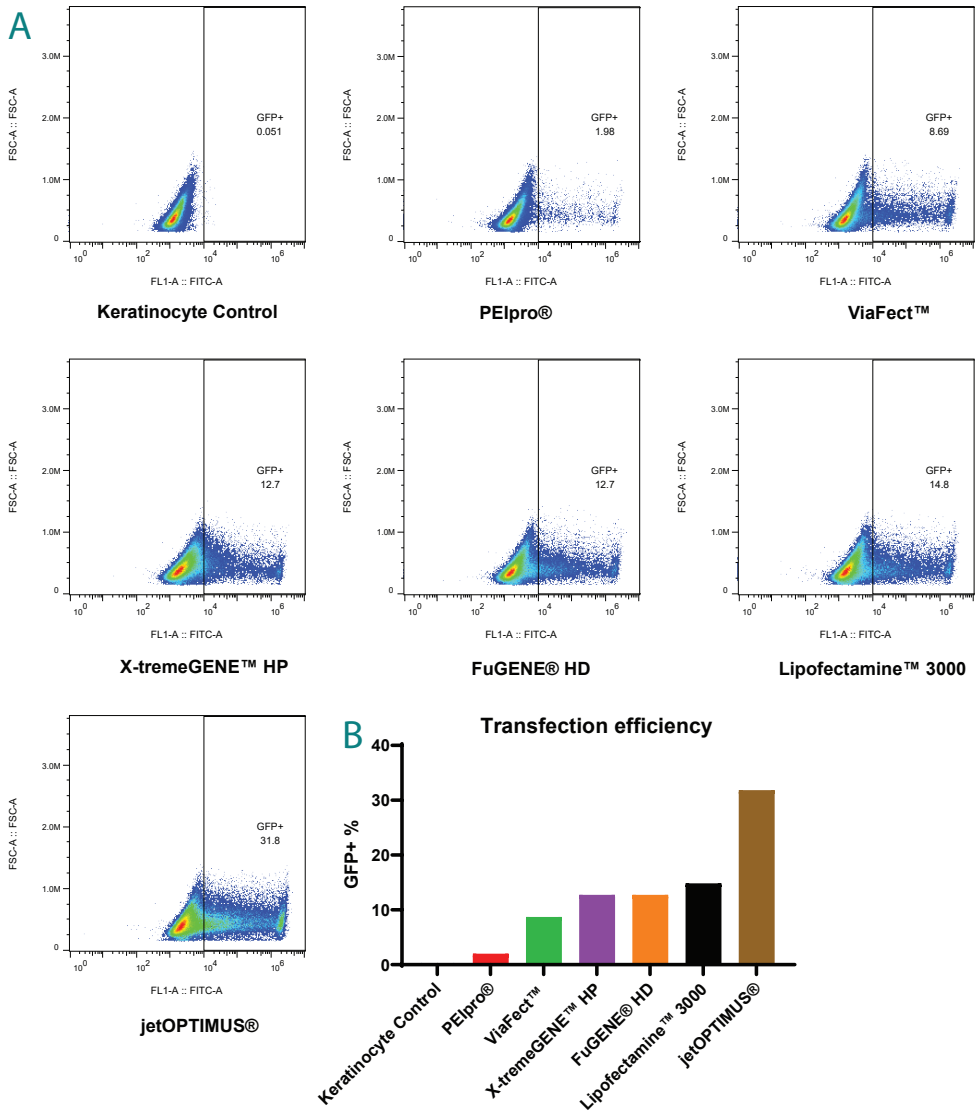

Figure 2.3. Optimization of transfection-based gene editing in N/TERT-1 keratinocytes. A This chart visualizes the progressive increases in transfection efficiency achieved by using various transfection reagents. It provides a comparative view of the different agents' performance, underscoring the influence of the transfection reagent on the success of gene editing. **B**This part of the figure offers a closer examination of the most effective transfection reagent, which achieves close to 35% efficiency. The result underscores the significance of the optimization process, ultimately contributing to a more effective approach to transfection-based gene editing in N/TERT-1 keratinocytes.

CAS9PBKS plasmids to induce GFP expression we characterized the best candidate via our FACS gating strategy which was determined with the wild-type keratinocytes. The pilot reagent was PEIpro® which displayed a parallel GFP expression pattern that closely resembled that of transfected wildtype keratinocytes. By contrast, both Viafect™, X-tremeGENE™HD, FuGENE® HD and Lipofectamine™3000 resulted in a relative GFP expression below 15%, which is comparatively high (Figure 2.3A). However, the most promising candidate was JetOPTIMUS®, which amplified the relative GFP expression two-fold, up to 31.8%, establishing an efficient protocol for virus-free transfection of this hard-to-transfect cell type (Figure 2.3B) (Freije et al., 2020).

In parallel, we used the proprietary FluidFM® technology to directly deliver the CRISPR/Cas9 RNP complexes in combination with a fluorescent marker into the nucleus (Figure 2.2). Hereby, we utilized the FluidFM® nanosyringe to transfer multiple gRNA in tandem, which in general is a non-trivial task as conventional methods commonly cause a DNA damage response, provoking low cell viability. To test this multiplexed CRISPR approach we first needed to adjust the FluidFM® CellEDIT technology to the hard-to-transfect keratinocytes. After elucidating the optimal culturing conditions we were able to apply the nano-injection and isolate mono-cultures (Figure 2.2)B.

Distinguishing between exon deletion and gene disruption using the NHEJ repair mechanism. In a next step and to finalize the generation of the dermokine isoform-specific knokckouts in keratinocytes, we designed the gRNA targeting the various isoforms. For the primary approach, we targeted either exon 2 or exon 18 by introducing a single double-strand break causing NHEJ (Figure 2.4). In detail, we selected 4 different gRNA target sites, transfected keratinocytes with the respective gRNA and subjected the GFP-positive keratinocytes to cell sorting. After one week week, we iterated the cell sorting, yet excluding the GFP-positive population, separating each cell into a segregated well. Those cells were then expanded into monoclonal cultures, and the sanger sequence of each cell population was analysed with

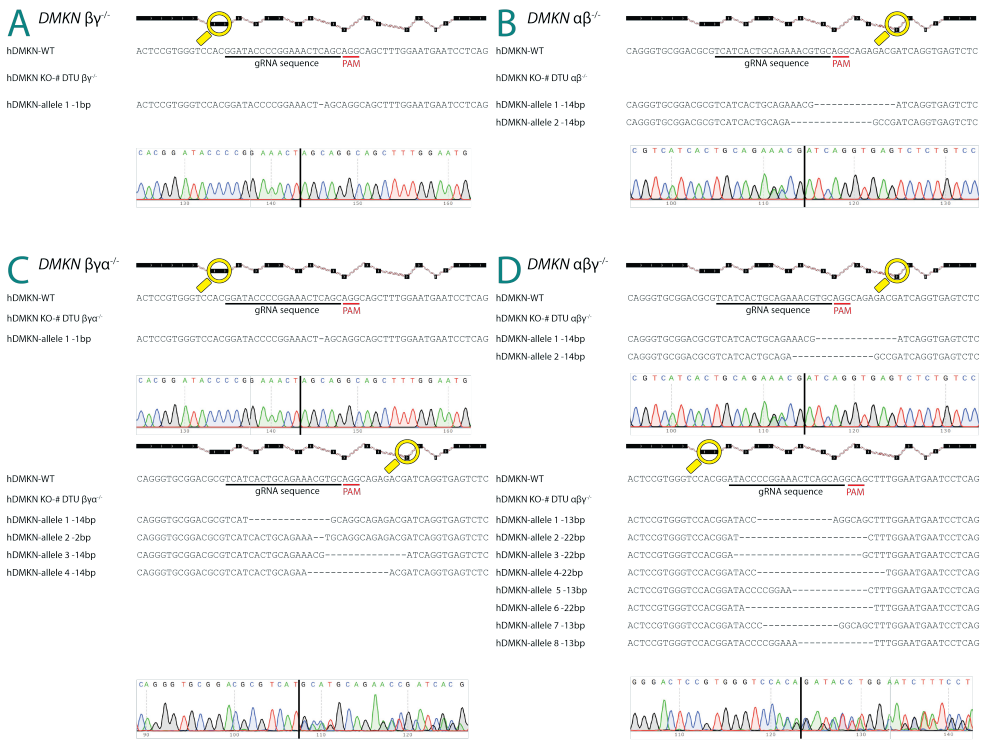

Figure 2.4. **Transfection-based gene editing of N/TERT-1 keratinocytes.** This figure delineates the results of the DNA alignment and DNA chromatograms following the introduction of guide RNAs (gRNAs) and indels into N/TERT-1 keratinocytes using the transfection method. **A.** This panel illustrates the *Dmkn* $\beta\gamma$ knockout (KO) (induced by gRNA1) and the consequential genetic sequence frameshift owing to the insertion of a missing base/nucleotide. **B.** Here, the *Dmkn* $\alpha\beta$ KO is shown, which was induced using gRNA2. This event led to the loss of a long string of nucleotides, causing frameshifts in the genetic sequence. **C.** This panel demonstrates the effects of adding the *Dmkn* α gRNA (gRNA2) to the *Dmkn* $\beta\gamma$ KO cells. This dual action truncated the complementary isoform, and the *Dmkn* $\beta\gamma$ induced truncation site was resequenced to verify this genetic modification. **D.** The analogous process is shown for the complementary case: *Dmkn* $\alpha\beta$ KO cells were subjected to gRNA1 to achieve the complementary knockout. Subsequent resequencing confirmed the expected modification.

the ICE appliance to deconvolute successful *Dmkn* $\beta\gamma^{-/-}$ or *Dmkn* $\alpha\beta^{-/-}$, which we termed transfection-based *Dmkn* $\beta\gamma^{-/-}$ and transfection-based *Dmkn* $\alpha\beta^{-/-}$ (Figure 2.4A and 2.4B). We iterated the entire workflow with transfection-based *Dmkn* $\beta\gamma^{-/-}$ or AFM-based *Dmkn* $\alpha\beta^{-/-}$ mutants, introducing the complementary gRNA to the respective clone, consequently we successfully generated a *Dmkn* $\beta\gamma\alpha^{-/-}$ and a *Dmkn* $\alpha\beta\gamma^{-/-}$, from now referred to as AFM-based *Dmkn* $\beta\gamma\alpha^{-/-}$ and DTU *Dmkn* $\alpha\beta\gamma^{-/-}$ (Figure 2.4C and 2.4D). Interestingly, the transfection-based *Dmkn* $\beta\gamma^{-/-}$ and transfection-based *Dmkn*$\alpha\beta^{-/-}$ had an apparent and uniformly modified genetic sequence while the triple isoform disrupted keratinocytes revealed a heterogeneous response to the DSB (Figure 2.4A, 2.4B, 2.4C and 2.4D). In total, we sequenced 6 transfection-based *Dmkn* $\beta\gamma^{-/-}$ and 12 transfection-based *Dmkn* $\alpha\beta^{-/-}$ clones, as well as 9 transfection-based *Dmkn* $\alpha\beta\gamma^{-/-}$ and 15 transfection-based *Dmkn* $\beta\gamma\alpha^{-/-}$ mutants (Supplemental file 1 and 2).

In parallel, the FluidFM® multiplexed CRISPR approach allowed for the unambiguous deletion of the entire exon by parallel co-injection of CRISPR RNP complexes. Here, we designed a quadruple gRNA delivery system, successfully delivering complexes that aim to eliminate partially exon 1 and entirely exon 17, resulting in AFM-based 1 *Dmkn* $\alpha\beta\gamma^{-/-}$ and AFM-based 2 *Dmkn* $\alpha\beta\gamma^{-/-}$. To ensure the success of the genetic modifications, we monitored the PCR products of both exon 1 and 17 by means of agarose gel electrophoresis and could indeed observe the missing band for both exons in comparison to the wildtype (Figure 2.5A and 2.5B). For AFM-based 2 *Dmkn* $\alpha\beta\gamma^{-/-}$ we could observe a previously not identified fragment in lane 6 which might be explained by a large re-arrangement in exon 1 (Figure 2.5B). Due to the modification of the non-coding genetic site circa exon 17, we could not retrieve a sole alpha knockout on account of the modified subsequent exon, which is shared with the β isoform. Concurrently, we tested the dual gRNA delivery approach, co-injecting two CRISPR RNP complexes, which are targeting the non-coding genetic sequence prior to and subsequent to exon 17, thus eliminating the entire exon. To validate the success of the deletion, we

monitored the DNA sequence just before the succeeding exon and indeed could verify the insertion of new nucleotides downstream of the deletion site, resulting in a frame-shift and thus genetic abscission (Figure 2.5C). In this manner, we were able to generate a homozygous AFM-based *Dmkn* $\alpha\beta^{-/-}$.

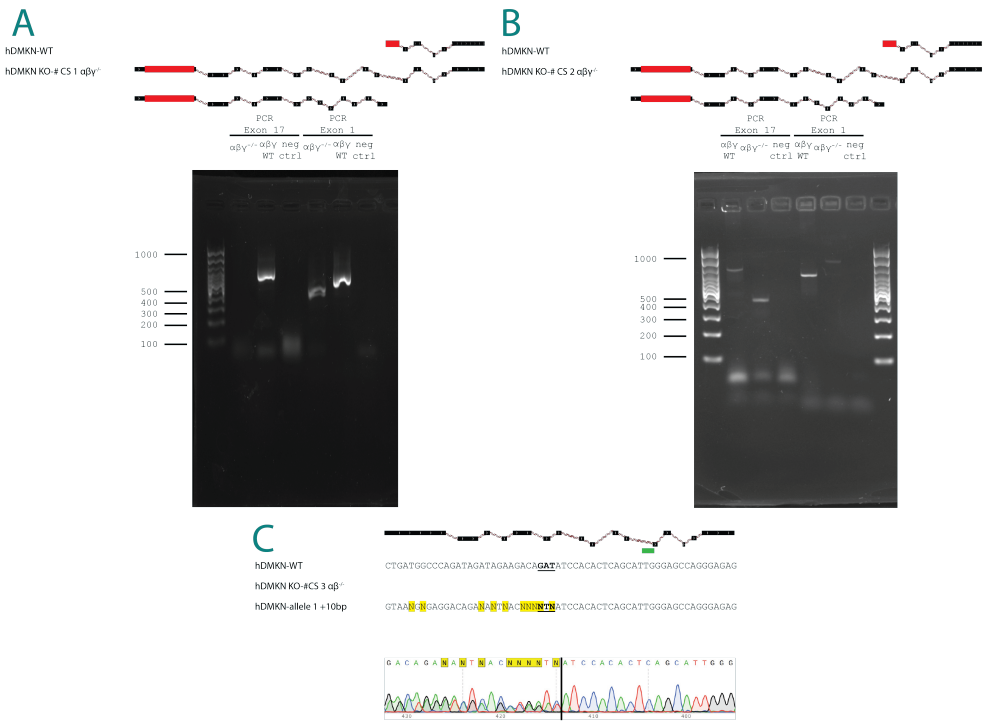

Figure 2.5. **AFM-based gene editing of N/TERT-1 keratinocytes.** This figure presents the results of the DNA chromatograms following the simultaneous introduction of guide RNAs (gRNAs) via Atomic Force Microscopy (AFM) and subsequent insertions and deletions (indels). **A.** This panel shows the *Dmkn* $\alpha\beta\gamma$ knockout (KO) achieved by ablating both exon 1 and exon 17. The PCR gel demonstrates the bands indicative of successful knockout. **B.** Depicts another single cell clone with a similar setup as in panel A, thus resulting in a comparable *Dmkn* $\alpha\beta\gamma$ knockout. **C.** The targeting of only exon 17 is shown, leading to the generation of a *Dmkn* $\alpha\beta$ KO. In this case, only the DNA chromatogram is presented, which clearly displays the introduction of additional nucleotides/bases following exon removal.

Recent advances in genome editing have enabled the reliable study of proteins in complex biological systems (Jinek et al., 2012). Evolving these power-

ful technologies further enables researchers to expand their toolkit and study increasingly intricate biochemical mechanisms (Wang & Doudna, 2023). Here, we present not only a high-efficiency gene editing workflow for the introduction of CRISPR/Cas9 plasmids into keratinocytes but also a multiplexed CRISPR approach that facilitates the direct delivery of quadruple CRISPR RNP complexes into the nucleus of the same cell type (Lonowski et al., 2017; McCarty et al., 2020).

For the optimization of the transfection-based strategy, we optimized several parameters and could improve the process, increasing transfection efficiency to twice the current approaches and decreasing overall time allocation for the whole generation of a single truncated mutant by 7 weeks, which has a current average duration of 10 weeks (Enjalbert et al., 2020; Tuladhar et al., 2019). In total, we sequenced 42 different keratinocyte populations expanded from a single-cell clone and could generate 4 reliable isoform-specific dermokine ablations (Table 2.6).

Commonly, CRISPR/Cas9-based genome editing introduces unintended off-target mutations, which could obstruct the exact elucidation of biological mechanisms of the protein of interest (Wienert et al., 2019). Thus, we engaged in a joint effort together with Cytosurge AG, Switzerland, and created an independent dermokine truncated keratinocyte using not only their proprietary FluidFM® technology that allows the direct nano-injection of CRISPR RNP complexes into the nucleus but also allows for multiplexed CRISPR (Table 2.6) (Meister et al., 2009). The findings demonstrate the feasibility of simultaneous adelivery of multiple gRNAs into targeted single cells through FluidFM® nano-injection, ablating entire exons in parallel. In addition, here we have established that the approach provided by FluidFM® significantly shortens the timeline required to develop monoclonal cell lines with multiple desired characteristics, from a span of up to 10 weeks in conventional methods.

Finally, we obtained various dermokine isoform-specific loss-of-function mutants, which can be used in follow-up experiments to elucidate the true function of dermokine in epidermal differentiation.

Table 2.6. Final selection of single-cell clones. Single-cell clones were obtained through two primary methods: transfection-based procedures and AFM-guided methods. The latter involves the direct injection of gRNA into the nucleus.

AFM-based exon deletion	Transfection-based gene editing
Dmkn $\alpha\beta^{-/-}$	*Dmkn* $\alpha\beta^{-/-}$
N/A	*Dmkn* $\beta\gamma^{-/-}$
1 *Dmkn* $\alpha\beta\gamma^{-/-}$	*Dmkn* $\alpha\beta\gamma^{-/-}$
2 *Dmkn* $\alpha\beta\gamma^{-/-}$	*Dmkn* $\beta\gamma\alpha^{-/-}$

2.1.5 Acknowledgments

We thank Dr. Edel O'Toole (Queen Mary University of London, United Kingdom) for providing the N/TERT-1 keratinocyte cell line. This work was supported by a Novo Nordisk Foundation Young Investigator Award (NNF16OC0020670 to U.a.d.K), as well as Novo Nordisk Foundation Grants (NNF19SA0056783, NNF19SA0057794 and NNF20SA0066621 to S.G.) and funding from the LEO Foundation (LF-OC-19-000033 to U.a.d.K).

2.1.6 References

A, D. M., C, H. W., Yasushi, I., Vincent, R., Y, W. J., A, W. R., N, L. D., P, L. F., & G, R. J. (2000). Human Keratinocytes That Express hTERT and Also Bypass a p16INK4a-Enforced Mechanism That Limits Life Span Become Immortal yet Retain Normal Growth and Differentiation Characteristics. *Molecular and Cellular Biology*, *20*(4), 1436–1447.

Burns, D. A., Cox, N. H., & Hill, P. B. (2010). Comparative Dermatology.

Candi, E., Schmidt, R., & Melino, G. (2005). The cornified envelope: a model of cell death in the skin. *Nature Reviews Molecular Cell Biology 2005 6:4*, *6*(4), 328–340.

Enjalbert, F., Dewan, P., Caley, M. P., Jones, E. M., Morse, M. A., Kelsell, D. P., Enright, A. J., & O'Toole, E. A. (2020). 3D model of harlequin ichthyosis reveals inflammatory therapeutic targets. *Journal of Clinical Investigation*, *130*(9), 4798–4810.

Freije, A., Sanz-Gómez, N., & Gandarillas, A. (2020). Genetic Modification of Human Primary Keratinocytes by Lentiviral Vectors. *Methods in molecular biology (Clifton, N.J.)*, *2109*, 113–123.

Fuchs, E., & Raghavan, S. (2002). Getting under the skin of epidermal morphogenesis. *Nature reviews. Genetics*, *3*(3), 199–209.

Gálvez, V., Chacón-Solano, E., Bonafont, J., Mencía, Á., Di, W. L., Murillas, R., Llames, S., Vicente, A., Del Rio, M., Carretero, M., & Larcher, F. (2020). Efficient CRISPR-Cas9-Mediated Gene Ablation in Human Keratinocytes to Recapitulate Genodermatoses: Modeling of Netherton Syndrome. *Molecular Therapy. Methods & Clinical Development*, *18*, 280.

Guillaume-Gentil, O., Grindberg, R. V. V., Kooger, R., Dorwling-Carter, L., Martinez, V., Ossola, D., Pilhofer, M., Zambelli, T., & Vorholt, J. A. A. (2016). Tunable Single-Cell Extraction for Molecular Analyses. *Cell*, *166*(2), 506–516.

Jinek, M., Chylinski, K., Fonfara, I., Hauer, M., Doudna, J. A., & Charpentier, E. (2012). A Programmable Dual-RNA–Guided DNA Endonuclease in Adaptive Bacterial Immunity. *Science*, *337*(6096), 816–821.

Katoh, K., & Standley, D. M. (2013). MAFFT multiple sequence alignment software version 7: improvements in performance and usability. *Molecular biology and evolution*, *30*(4), 772–780.

Labun, K., Montague, T. G., Krause, M., Torres Cleuren, Y. N., Tjeldnes, H., & Valen, E. (2019). CHOPCHOP v3: expanding the CRISPR web toolbox beyond genome editing. *Nucleic Acids Research*, *47*(W1), W171–W174.

Leclerc, E. A., Huchenq, A., Kezic, S., Serre, G., & Jonca, N. (2014). Mice deficient for the epidermal dermokine β and γ isoforms display transient cornification defects. *Journal of Cell Science*, *127*(13), 2862–2872.

Lonowski, L. A., Narimatsu, Y., Riaz, A., Delay, C. E., Yang, Z., Niola, F., Duda, K., Ober, E. A., Clausen, H., Wandall, H. H., Hansen, S. H., Bennett, E. P., & Frödin, M. (2017). Genome editing using FACS enrichment of nuclease-expressing cells and indel detection by amplicon analysis. *Nature Protocols*, *12*(3), 581–603.

McCarty, N. S., Graham, A. E., Studená, L., & Ledesma-Amaro, R. (2020). Multiplexed CRISPR technologies for gene editing and transcriptional regulation. *Nature Communications*, *11*(1), 1281.

Meister, A., Gabi, M., Behr, P., Studer, P., Vörös, J., Niedermann, P., Bitterli, J., Polesel-Maris, J., Liley, M., Heinzelmann, H., & Zambelli, T. (2009). FluidFM: Combining Atomic Force Microscopy and Nanofluidics in a Universal Liquid Delivery System for Single Cell Applications and Beyond. *Nano Letters*, *9*(6), 2501–2507.

Naso, M. F., Liang, B., Huang, C. C., Song, X. Y., Shahied-Arruda, L., Belkowski, S. M., D'Andrea, M. R., Polkovitch, D. A., Lawrence, D. R., Griswold, D. E., Sweet, R. W., & Amegadzie, B. Y. (2007). Dermokine: an extensively differentially spliced gene expressed in epithelial cells (2007/03/24). *J Invest Dermatol*, *127*(7), 1622–1631.

Touati, A., Saeidian, A. H., Youssefian, L., Faghankhani, M., Niaziorimi, F., Pajouhanfar, S., Vahidnezhad, H., & Uitto, J. (2020). The matriptase-prostasin proteolytic cascade in dermatologic diseases. *Experimental dermatology*, *29*(7), 580–587.

Tuladhar, R., Yeu, Y., Tyler Piazza, J., Tan, Z., Rene Clemenceau, J., Wu, X., Barrett, Q., Herbert, J., Mathews, D. H., Kim, J., Hyun Hwang, T., & Lum, L. (2019). CRISPR-Cas9-based mutagenesis frequently provokes on-target mRNA misregulation. *Nature Communications*, *10*(1), 4056.

Utsunomiya, A., Chino, T., Utsunomiya, N., Luong, V. H., Tokuriki, A., Naganuma, T., Arita, M., Higashi, K., Saito, K., Suzuki, N., Ohara, A., Sugai, M., Sugawara, K., Tsuruta, D., Oyama, N., & Hasegawa, M. (2020). Homeostatic Function of Dermokine in the Skin Barrier and Inflammation. *Journal of Investigative Dermatology*.

Wang, J. Y., & Doudna, J. A. (2023). CRISPR technology: A decade of genome editing is only the beginning. *Science*, *379*(6629), eadd8643.

Wienert, B., Wyman, S. K., Richardson, C. D., Yeh, C. D., Akcakaya, P., Porritt, M. J., Morlock, M., Vu, J. T., Kazane, K. R., Watry, H. L., Judge, L. M., Conklin, B. R., Maresca, M., & Corn, J. E. (2019). Unbiased detection of CRISPR off-targets in vivo using DISCOVER-Seq. *Science*, *364*(6437), 286–289.

Supplemental Files

List of supplemental files uploaded onto Onedrive, attached to this document:

File S1. This file provides a comprehensive list of both the 6 *Dmkn* $\beta\gamma^{-/-}$ and the 12 *Dmkn* $\alpha\beta^{-/-}$ genotyping analyses, which were carried out using transfection-based techniques.

File S2. This file provides a comprehensive list of the 9 transfection-based *Dmkn* $\alpha\beta\gamma^{-/-}$ and the 15 *Dmkn* $\beta\gamma\alpha^{-/-}$ genotyping analyses.

File S3. This collection of files contains the sequencing results obtained from the AFM-based genotyping analyses of *Dmkn* $\alpha\beta\gamma^{-/-}$ and *Dmkn* $\alpha\beta^{-/-}$.

Abbreviations and Acronyms

AFM Atomic Force Microscopy

Cas9 CRISPR Associated Protein 9

CO_2 Carbon Dioxide

CRISPR Clustered Regularly Interspaced Short Palindromic Repeats

DMKN Dermokine

FACS Fluorescence-Activated Cell Sorting

FBS Fetal Bovine Serum

GFP Green Fluorescent Protein

gRNAs Guide RNAs

NHEJ Non-Homologous End Joining

PCR Polymerase Chain Reaction

RNP Ribonucleoprotein

2.2 Dermokine Deficient Human Skin Models – Manuscript 4

MANUSCRIPT 4 - SUMMARY

Utilizing Skin Organoids of *Dmkn* $\beta\gamma^{-/-}$ and *Dmkn* $\alpha\beta^{-/-}$ as well as Wildtype Keratinocytes to Study the Epidermal Phenotype upon Truncation. This study, provides further insight into the previously established *Dmkn* $\beta\gamma^{-/-}$ and *Dmkn* $\alpha\beta^{-/-}$ keratinocytes to further investigate if dermokine absolutely plays a role in epidermal development. Here we employ skin organoids utilizing the cross-talk between keratinocytes and fibroblasts to study the function of dermokine in keratinocyte differentiation. First, we histologically assess the keratinocyte stratification allowing us to observe a non-stratified epidermis following the dermokine-expression gradient. Furthermore, immunohistochemical staining allowed us to confirm the absent dermokine expression of *Dmkn* $\beta\gamma^{-/-}$ and *Dmkn* $\alpha\beta^{-/-}$ keratinocytes. Next, we utilized a range of mass spectrometry-based proteomics techniques to investigate the various effects of dermokine truncation in the skin organoids. Initially, we monitored proteotypic dermokine peptides located in various domains employing parallel reaction monitoring to observe changes in abundance because of truncation. The peptide of most interest was the C-terminal peptide found in the cytokine-like domain, which was observed to be entirely missing in the *Dmkn* $\alpha\beta^{-/-}$ skin organoids but still present in the *Dmkn* $\beta\gamma^{-/-}$ skin organoids. Subsequently, we subjected the *Dmkn* $\beta\gamma^{-/-}$ skin organoids to an unbiased proteomics screen to observe global protein changes. In comparison to the wildtype, we could detect abundance changes in proteins associated with cornified envelope assembly, filaggrin processing and desquamation. Consequently, we wanted to validate our results in *Dmkn* $\beta\gamma^{-/-}$ skin organoids utilizing internal standard triggered parallel monitoring. We could indeed confirm that upon depletion of the cytokine-like domain, we observe a significant decrease

in filaggrin processing proteases and proteins regulating the assembly of the cornified envelope, critical for the proper development of the epidermis.

Targeted Degradomics to Validate Matrix Metalloproteinase 10-dependent Cleavage in Human Dermokine. As previously shown in murine models, matrix metalloproteinase 10 is able to cleave mouse dermokine, which was confirmed in a western blot. However, we employed targeted degradomics to elucidate the exact cleavage site utilizing heavy reference peptides. We could indeed show that the cleavage site is two amino acids subsequent to P 201 which is in accordance with the previously established preference for matrix metalloproteinase 10 for P at P3.

Cell autonomous functions of dermokine in human keratinocytes in the differentiating epidermis

Vahap Canbay[1] and Ulrich auf dem Keller[1]

[1]Department of Biotechnology and Biomedicine, Technical University of Denmark, DK-2800, Kongens Lyngby, Denmark

Planned publication

Canbay V. and auf dem Keller U. (2023) Cell autonomous functions of dermokine in human keratinocytes in the differentiating epidermis *In preparation.*

Contribution by VC:
Cell culture, skin organoid culturing, HPLC fractionation and performance of the LC-MS/MS measurements, PRM and IS-PRM assay optimization, data analysis, bioinformatics, manuscript writing.

2.2.1 Abstract

The epidermis provides a vital barrier between the human body and its external environment, playing critical roles in protection, water retention, and mechanical resistance. Dermokine, a secreted protein produced by suprabasal keratinocytes, is associated with epidermal stratification and terminal differentiation. However, its function has been poorly understood, in part due to its multiple isoforms – dermokine-α, dermokine-β, and dermokine-γ, each with unique domain architectures that contribute to diverse biological processes. In this study, we utilized human skin organoids, which allowed us to monitor epidermal stratification at endogenous dermokine isoform levels using wildtype in comparison to *Dmkn* $\alpha\beta^{-/-}$ and *Dmkn* $\beta\gamma^{-/-}$ keratinocytes. Our results identified that isoform-specific ablation of dermokine led to a disrupted suprabasal stratification detectable both in the histological assessment and various proteomics methods using a human system. By integrating this information, we corroborate that dermokine is involved in the suprabasal epidermal stratification and indirectly influences the abundance of proteins associated with the assembly of the cornified envelope including epidermal proteases.

2.2.2 Introduction

The most distal level of the skin, the epidermis, acts as a protective cover between the organism and its immediate environment, functioning as a barrier against harmful substances, while also impeding water loss and enduring mechanical stress. The epidermis can be segmented into four unique levels attributable to the upward migration of basal keratinocytes, leading to the creation of suprabasal layers, culminating in the formation of the cornified envelope (Fuchs & Raghavan, 2002; Werner & Smola, 2001). Convoluted post-translational modifications (PTMs) modulating protein function, location, and interactions are paramount for the preservation of epidermal homeostasis (de Veer et al., 2014). Hereby, limited proteolysis is critical in initia-

tion of certain proteins, such as filaggrin and regulatory proteins involved in various signalling pathways, such as protease-mediated ectodomain shedding (Lichtenthaler et al., 2018). An example of such molecular processing is the proteolytic cleavage of dermokine (DMKN) by matrix metalloproteinase 10 (MMP10) (Schlage et al., 2015). This protein is overexpressed at wound edges by keratinocytes and in the tumor stroma, indicating a possible role in tissue remodeling and tumor progression (Krampert et al., 2004). DMKN, a member of the SSC family, is implied to be critical to the epidermal differentiation process. The *Dmkn* gene instigates various isoforms through alternative splicing and alternative promoter usage. The longest-stranding isoform, DMKN-β, and the C-terminally truncated DMKN-γ, are both expressed in the stratum spinosum and granulosum, whereas N-terminally truncated DMKN-α, which shares an almost identical C-terminal cytokine-like domain with DMKN-β, is generated throughout the stratified epithelium (Naso et al., 2007). In addition, DMKN-α possesses its own distinct promoter, being independently transcribed from all the other isoforms. Each of these α, β, and γ DMKN isoforms possess signal sequences, enabling their secretion into the extracellular space (Leclerc et al., 2014).

Murine models are often utilized for mechanistic studies, but they involve certain restrictions (Mestas & Hughes, 2004; Richmond & Yingjun, 2008). Previous research on DMKN knockouts has been limited, with studies to date only having disrupted DMKN isoforms in mice (Utsunomiya et al., 2020). Hereby, the genetic removal of DMKN β in a murine model resulted in a compensatory increase in DMKN α expression, both of which contain the cytokine-like domain. However, as acknowledged by the authors, there is a clear need for additional studies to illuminate the specific roles of each DMKN isoform (Utsunomiya et al., 2020). More importantly, it is crucial to specifically study cell autonomous functionality of DMKN within keratinocytes. Especially in this context, is the development and application of skin organoids, intricate three-dimensional structures cultivated *in-vitro* that comprise solely human keratinocytes and fibroblasts (Clevers, 2016; Eckl, 2014; Enjalbert et

al., 2020).

Here, we utilize the potential of 3D skin organoids in conjunction with advanced proteomics methods to explore the cell autonomous effects upon DMKN isoform truncation in keratinocytes, non-reliant on immune activity. First, we histologically assessed the 3D skin organoids grown with *Dmkn* $\alpha\beta^{-/-}$, *Dmkn* $\beta\gamma^{-/-}$ isoform knockouts or wildtype keratinocytes, detecting substantial aberrations when DMKN isoforms were absent. Proteotyping of *Dmkn* $\alpha\beta^{-/-}$ and *Dmkn* $\beta\gamma^{-/-}$ revealed that a peptide mapped to the cytokine-like domain was exclusively elusive upon ablation of both DMKN α and β. Further, acquiring the proteome of the *Dmkn* $\beta\gamma^{-/-}$ skin organoids allowed us to identify several proteins associated with key processes involved in the epidermal stratification, which were able to confirm in *Dmkn* $\alpha\beta^{-/-}$ skin organoids via targeted proteomics assays.

2.2.3 Experimental Procedures

N/TERT keratinocytes and human primary fibroblasts cell culture. Human keratinocyte telomerase reverse transcriptase immortalized (h/TERT immortalized) N/TERT-1 cells derived from clinically normal foreskin tissue (A et al., 2000) were a kind gift from Prof. Edel O'Toole (Queen Mary University, London, United Kingdom). N/TERT-1 keratinocytes as well as the N/TERT-1 *Dmkn* $\alpha\beta^{-/-}$ and N/TERT-1 *Dmkn* $\beta\gamma^{-/-}$ keratinocytes (see chapter 2.1 for more details) were grown in DMEM/F-12 growth medium supplemented with RM+ (DMEM/F-12 (Thermo Fisher Scientific, Waltham, MA, 11-320-033), 10% FBS (Thermo Fisher Scientific, 11550356), 1% penicillin/streptomycin [P/S] (Sigma-Aldrich, Darmstadt, Germany, P0781), 0.4 μg/mL hydrocortisone (Sigma-Aldrich, H4881), 0.5 μg/mL insulin (Sigma-Aldrich, I5500), 10 ng/mL epidermal growth factor (Bio-Rad, Hercules, CA, PMP89), 0.1 nM cholera toxin (Sigma-Aldrich, C8052), 5 μg/mL transferrin (Sigma-Aldrich, T2252), 20 pM liothyronine (Sigma-Aldrich, T6397)) and incubated at 37 °C, 5% CO_2. Human primary neonatal dermal fibroblasts

(Sigma-Aldrich, 106-05N) were grown in fibroblast growth media (DMEM, 10% FBS, 1× P/S) and incubated at 37°C, 5% CO_2. All cell lines were tested mycoplasm negative.

Generation of human *Dmkn* $\alpha\beta^{-/-}$ and *Dmkn* $\beta\gamma^{-/-}$ keratinocyte skin organoids. *In-vitro* 3D skin organoids were generated by placing 600 μL of collagen/Matrigel (Corning, Corning, NY, 354236) (Corning, 354234) matrix containing 1 × 10^5 fibroblasts (210 μL of collagen I (Corning), 210 μL of matrigel (Corning), 59 μL of 10× MEM (Thermo Fisher Scientific), 59 μL of FBS (Thermo Fisher Scientific), and 59 μL of primary human fibroblasts (Sigma-Aldrich)) into a 12-well plate Transwell insert (Sigma-Aldrich, PTHT12H48) and incubating for 1 h at 37 °C. After polymerization of the dermis-like layer, 59 μL of either wildtype or *Dmkn* $\alpha\beta^{-/-}$ or *Dmkn* $\beta\gamma^{-/-}$ N/TERT keratinocytes (see chapter 2.1 for more details) (containing 1 × 10^6 cells) were seeded on top of the matrix and RM+ growth media was added below the insert. After overnight incubation at 37 °C, the 3D models were airlifted and left to grow at an air/liquid interface for 15 days with daily media changes. After 15 days, the 3D models were cut in half: one half was fixed in 4% PFA (Sigma-Aldrich, P6148) for 30 min at RT and stored in ethanol (VWR, Radnor, PA, 83801.290) until embedding in paraffin, and the other half was frozen in liquid nitrogen for proteomics. 4 μm paraffin sections were generated with a serial microtome (Shandon, Cambridge, United Kingdom) and dried overnight at 35 °C.

Hematoxylin and Eosin staining of *Dmkn* $\alpha\beta^{-/-}$ and *Dmkn* $\beta\gamma^{-/-}$ keratinocyte skin organoids. Firstly, the section was placed into tap water. Mayer's Hematoxylin (Sigma-Aldrich, H9627) was prepared by dissolving 2 grams of Hematoxylin in 2000 mL deionized water while heating and stirring and 0.4 grams of sodium iodate (Sigma-Aldrich, S4007) were added, followed by 100 grams of aluminum potassium sulfate (Sigma-Aldrich, 237086) with continued stirring. The solution was filtered before use. Mayer's Hematoxylin (Sigma-Aldrich) was applied for a duration of 5 min. Following this, the sec-

tion was washed in tap water for 5 min. 2.5 g of Eosin Y (Sigma-Aldrich, E4009) was dissolved in 1000 mL of deionized water and 10% acetic acid (Sigma-Aldrich, 71251) was added until the solution reached pH 5.2 and filtered. Subsequently, Eosin Y (Sigma-Aldrich) was applied for another 5 min. An immediate rinse in tap water was done prior to dehydration in 96% and 99% ethanol (Sigma-Aldrich, 51976), with 4 submersions in 96% ethanol (Sigma-Aldrich) and 5 submersions in 99% ethanol (Sigma-Aldrich). The section was left to air dry before being mounted with Pertex mounting medium (Histoline, Pantigliate, Italy, R0080).

Immunohistochemical staining of *Dmkn* $\alpha\beta^{-/-}$ and *Dmkn* $\beta\gamma^{-/-}$ keratinocyte skin organoids with a dermokine-specific antibody. Immunohistochemical staining was performed according to the manufacturer's instructions (Thermo Fisher Scientific, TR-015-HD). In brief, sections were heated at 60 °C for 60 min before de-paraffination. The sections were deparaffinized, rehydrated and blocked with Ultra V Block (Thermo Fisher Scientific, TA-060-UB) for 5 min. The slides were incubated with 50 μL antibody (Abcam, Cambridge, United Kingdom, ab246965) for 1 hour and rinsed twice with washing buffer (TBS) for 5 min each. Primary antibody enhancer (Thermo Fisher Scientific, TL-060-PB) was applied and incubated for 10 min before being washed 3 times with washing buffer for 5 min. HRP Polymer (Thermo Fisher Scientific, TL-060-PH) was applied and incubated for 15 min before being washed 3 times with washing buffer for 5 min. Lastly, slides were incubated with 3,3' diaminobenzidine (DAB) (Thermo Fisher Scientific, 12623957) for 10 min and washed first in washing buffer for 5 min prior to rinsing under tap water. Hematoxylin (Sigma-Aldrich) was applied onto the slides for 15 seconds and rinsed once more under tap water for 5 min before being mounted with Pertex mounting medium (Histoline).

Sample preparation for MS analysis. Lysis buffer (4 M guanidine hydrochloride (GuHCl) (Sigma-Aldrich, G3272) and 250 mM

N-2-hydroxyethylpiperazine-N-2-ethane sulfonic acid (HEPES) (pH7.8) (Sigma-Aldrich, H3375)) was prepared and cooled before mixing with skin organoids, then homogenized using the stainless steel beads (QIAGEN, Venio, Netherlands, 69989) and the TissueLyser II (QIAGEN, 85300). The mixture was processed twice for 1 min each at varying frequencies (3 Hz to 30 Hz), then the beads were removed using a magnetic rack and the suspension was heated for 5 min at 95 °C. Following this, the samples underwent five cycles of sonication and cooling. After centrifugation, the protein content was determined using Nanodrop (Thermo Fisher Scientific) and Bradford assays (Bio-Rad, 5000001). The samples were reduced and alkylated on aliquots of 50 μg protein using 5 mM tris(2-carboxyethyl)phosphin (TCEP) (Sigma-Aldrich, C4706) and 20 mM 2-chloroacetamide (CAA) (Sigma-Aldrich, C0267), sequentially. The samples were then diluted with 50 mM HEPES buffer (pH 7.8) (Sigma-Aldrich) to lower the GuHCl (Sigma-Aldrich) concentration. First, the samples were incubated with Lys-C (FUJIFILM Wako Pure Chemical Corporation, Osaka, Japan, 125-05061) for 4 h, 37 °C and subsequently, trypsin (Promega, Madison, WI, V5113) was introduced for overnight digestion at 37 °C. After the digestion, enzyme activity was blocked by addition of 1% trifluoroacetic acid (Sigma-Aldrich, T650) (TFA). For desalting, samples were applied to Solaμ 96-well plates, initially activated with 200 μL 100% ACN and equilibrated with 200 μL 0.1% TFA, both under 700 x g for 1 min. Following sample loading and centrifugation, the plate was washed once with 200 μL 0.1% TFA, then with 100 μL 0.1% formic acid. Peptides were eluted using 2 x 25 μL 80% ACN, 0.1% TFA. Samples were dried via speed-vacuum and resuspended in 12 μL of solution 0.1% formic acid.

Parallel reaction monitoring of DMKN proteotypic peptides in *Dmkn* $\alpha\beta^{-/-}$ and *Dmkn* $\beta\gamma^{-/-}$ keratinocyte skin organoids. Peptides (500 ng and 0.25 pmol for each heavy peptide) were loaded onto a 2 cm C18 trap column (Thermo Fisher Scientific, 164705), connected in-line to a 50 cm C18 reverse-phase analytical column (Thermo Fisher Scientific, ES803) using

100% Buffer A (0.1% Formic acid in water) at 750 bar, using the EasyLC 1200 HPLC system (Thermo Fisher Scientific), and the column oven operating at 30 °C. Peptides were eluted over a 70-minute gradient ranging from 10 to 95% of 80% acetonitrile, 0.1% formic acid at 250 nL/min, and the Q-Exactive instrument (Thermo Fisher Scientific) was run in scheduled parallel reaction monitoring (PRM) mode for the *Dmkn* $\beta\gamma^{-/-}$ keratinocyte skin organoids. Full MS spectra were collected at a resolution of 70000, with an AGC target of $3e^6$ or maximum injection time of 10 ms and a scan range of 350–1400 m/z. The MS^2 spectra were obtained at a resolution of 35000, with an AGC target value of $1e^6$ or maximum injection time of 128 ms, a normalised collision energy of 27. MS performance was verified for consistency by running complex cell lysate quality control standards, and chromatography was monitored to check for reproducibility. For the *Dmkn* $\alpha\beta^{-/-}$ keratinocyte skin organoids the MS^2 spectra were obtained at a resolution of 17500.

Skyline 22.2.0.351 was used to analyze the PRM data (MacLean et al., 2010). Target peptides were imported after setting filter parameters at MS^1 precursor mass analyzer to orbitrap, resolving power of 70000 at 400 m/z and MS^2 acquisition method set to PRM orbitrap resulting power of 30000 at 400 m/z. Endogenous peptides had a fixed modification of carbamidomethylation of cysteines (+57.021 Da). In addition, heavy peptides had fixed modifications of heavy lysine and heavy arginine amino acids on their C-terminus (+8.014 and +10.008 Da). The transition peak areas and their boundaries were manually adjusted and derived from the heavy peptide retention times. Endogenous peptides were normalized based on their ratio to heavy peptides. Final calculations are based on the sum of transition areas.

Proteomics screening of *Dmkn* $\beta\gamma^{-/-}$ keratinocyte skin organoids. For each resuspended skin organoid proteome, peptides were analysed using the pre-set '30 samples per day' method on the EvoSep One (EvoSep, Odense, Denmark) instrument. Peptides were eluted over an EvoSep One defined 44-min gradient and analysed by mass spectrometry, Orbitrap Exploris 480

(Thermo Fisher Scientific), adapted from *Tognetti, Sklowodski et al.* (Tognetti et al., 2021), with the following settings: Spray voltage was set to 2.3 kV, funnel RF level at 40, and heated capillary at 240 °C. Full MS spectra were collected at a resolution of 120000, with an AGC target of 300% or maximum injection time set to 'custom' and a scan range of 350–1650 m/z. The MS^2 spectra were obtained in DIA mode in the Orbitrap operating at a resolution of 15000, equipepd with FAIMS Pro™Interface (Thermo Fisher Scientific) with a CV of -35, -55 and -75 V, with an AGC target 1000% or maximum injection time set to 'auto', a normalised HCD collision energy of 30. The isolation window was set to 38 m/z with a 1 m/z overlap and window placement off. MS performance was verified for consistency by running complex cell lysate quality control standards, and chromatography was monitored to check for reproducibility.
Raw files were analysed using DIA-NN (Data-Independent Acquisition by Neural Networks, version 1.8), Spectra were matched against the homo sapiens reference FASTA database
(UP000005640; downloaded from Uniprot on 28th of June 2021) (Demichev et al., 2019). Parameters were set to permit a fragment mass-to-charge ratio (m/z) between 200 and 1400, allowing for methionine excision, in silico digestion was adjusted for cuts at lysine and arginine residues, excluding proline-followed ones, and allowed for up to two missed cleavages. The peptide lengths were constrained to 6-47 residues and considered precursors with m/z ratios between 300 and 1400, along with charge states from +1 to +4. Cysteine carbamidomethylation was included as a fixed modification, while up to three variable modifications, including oxidation at methionine (UniMod:35) and acetylation at the N-terminus (UniMod:1), were allowed. The neural networks enabled peak selection, and the software was set to generate a new in silico spectral library. The analysis also incorporated a double-search, reanalysis, and smart profiling, operating on 64 threads, with outputs filtered at 0.05 false discovery rate.

Data were processed using R (version 4.1.1) (R Core Team, 2022). Most

of the data analysis was performed using functions implemented in the data analysis pipeline of DAPAR and Prostar (version 1.30.7) (Wieczorek et al., 2017). The volcano plots were visualized using ggVolcanoR and the Gene Ontology analysis was performed using Metascape (Mullan et al., 2021; Zhou et al., 2019).

Internal-standard triggered parallel reaction monitorng of *Dmkn* $\alpha\beta^{-/-}$ keratinocyte skin organoids. For the survey scan, peptides were loaded onto a 2 cm C18 trap column (Thermo Fisher Scientific, 164705), connected in-line to a 15 cm C18 reverse-phase analytical column (Thermo EasySpray ES803) using 100% Buffer A (0.1% Formic acid in water) at 750 bar, using the Thermo EasyLC 1200 HPLC system, and the column oven operating at 30 °C. An Orbitrap Exploris 480 mass spectrometer (ThermoFisher Scientific) was operated in DDA mode containing an inclusion list of heavy peptide masses for 70 min. A sample volume corresponding to 0.3 pmol of heavy peptides was injected. MS^1 resolution was set to 120000, automatic gain control (AGC) target set to 300%, maximum injection time set to 50 ms, scan range 300 to 1500 m/z. MS^2 scans used 7500 resolution, AGC target of 1000%, maximum injection time 10 ms, an isolation window of 1 m/z and normalized collision energy of 28.

Peptides (500 ng and 0.3 pmol for each heavy peptide) were loaded onto a 2 cm C18 trap column (Thermo Fisher Scientific, 164705), connected in-line to a 15 cm C18 reverse-phase analytical column (Thermo EasySpray ES803) using 100% Buffer A (0.1% Formic acid in water) at 750 bar, using the Thermo EasyLC 1200 HPLC system, and the column oven operating at 30 °C. Peptides were eluted over a 70-minute gradient ranging from 6 to 95% of 80% acetonitrile, 0.1% formic acid at 250nL/min, and the Orbitrap Exploris 480 mass spectrometer (Thermo Fisher Scientific) was run in SureQuant™mode. Spray voltage was set to 1.8 kV, funnel RF level at 40, and heated capillary at 275 °C. The MS^1 scan parameters included a resolution of 120000, AGC target of 300%, a 50 ms injection time, and a 5-second cycle time. Following,

precursors and fragments of heavy peptides were recognized based on the list (refer to Supplemental Tables), under parameters of 7500 resolution, HCD collision energy set at 28, an AGC target of 1000%, and a 10 ms injection time. A minimum of 3 product ions detected by on-the-fly triggering initiated an offset scan. The offset scan operated at a resolution of 60000, with an HCD collision energy of 28, an AGC target of 1000%, and a 116 ms injection time, functioning in profile mode.

Skyline 22.2.0.351 was used to analyze the SureQuant™data (MacLean et al., 2010). Target peptides were imported after setting filter parameters at MS^1 precursor mass analyzer to centroided, a mass accuracy of 10 ppm and MS^2 SureQuant™centroided filtering at 20 ppm. Precursor masses were set to have a minimum of 3 transitions. Endogenous peptides had a fixed modification of carbamidomethylation of cysteines (+57.021 Da) and a variable modification of methionine-loss and acetylation at the protein N-terminus (-89.030). In addition, heavy peptides had fixed modifications of heavy lysine and heavy arginine amino acids on their C-terminus (+8.014 and +10.008 Da). The transition peak areas and their boundaries were manually adjusted and derived from the heavy peptide retention times. Endogenous peptides were normalized based on their ratio to heavy peptides. Final calculations are based on the sum of transition areas.

Targeted degradomics of MMP10-dependent cleavage of human dermokine. The recombinant MMP10 (R&D Systems, Minneapolis, MN, 910-MP-010) is auto-activated at 37 °C for 16 h in modified activation buffer (20 mM $CaCl_2$ (Sigma-Aldrich, 499609), 100 mM NaCl (Sigma-Aldrich, S9888) and 5o mM HEPES (pH 7.8) (Sigma-Aldrich, H3375)). Next, recombinant human DMKN (OriGene Technologies, Rockville, MD, TP325655) is co-incubated at a protease-substrate ratio of 1:10 (w/w) either with the auto-activated MMP10 or with an equivalent amount of modified activation buffer alone for 16 h at 37 ∘C, 600 rpm. The reaction is stopped by adding 26 μL of digestion buffer (5 M GuHCl (Sigma-Aldrich) and 50 mM HEPES (pH 7.8)

(Sigma-Aldrich)), followed by shaking for 10 min at room temperature, 1000 rpm. The sample is reduced by addition of 20x TCEP (Sigma-Aldrich) (1:100) (w/w), followed by an incubation at 65 °C for 30 min, 600 rpm. The sample is alkylated using freshly prepared CAA (Sigma-Aldrich) in a 1:50 fashion, incubated at 65 °C for 30 min, 600 rpm. The GuHCl (Sigma-Aldrich) concentration is diluted with 50 mM HEPES (pH 7.8) (Sigma-Aldrich) to less than 1 M and finally overnight incubated with trypsin (1:50) (W/w) at 37 °C. The next day the samples are acidified using 5% TFA (Sigma-Aldrich) to a pH below 3. The samples were desalted employing the C18 cleanup by stamping out two pieces of the C18 Empore disk (Sigma-Aldrich, 66883-U) using a blunt-ended syringe needle and pressing the cored pieces close to the end of a P200 pipette tip. Next, the disks are activated by subsequent washes with 40 μL MeOH and 40 μL of 80% ACN, 0.1% acetic acid (Sigma-Aldrich), followed by equilibration of the disks with 2 subsequent washes of 60 μL of 3% ACN, 1% TFA (Sigma-Aldrich). The flow-through is discarded, and the sample is loaded onto the disk and washed twice with 40 μL of 0.1% acetic acid (Sigma-Aldrich). The sample is eluted with 40 μL of 80% ACN, 0.1% acetic acid (Sigma-Aldrich). The peptide mixture is dried utilizing a speed vacuum and resuspended in 3% ACN (Sigma-Aldrich), 0.1% acetic acid (Sigma-Aldrich).

Peptides (500 ng and 0.25 pmol for each heavy peptide) were loaded onto a 2 cm C18 trap column (Thermo Fisher Scientific, 164705), connected in-line to a 50 cm C18 reverse-phase analytical column (Thermo Fisher Scientific, ES803) using 100% Buffer A (0.1% Formic acid in water) at 750 bar, using the EasyLC 1200 HPLC system (Thermo Fisher Scientific), and the column oven operating at 30 °C. Peptides were eluted over a 70-minute gradient ranging from 10 to 95% of 80% acetonitrile, 0.1% formic acid at 250 nL/min, and the Q-Exactive instrument (Thermo Fisher Scientific) was run in unscheduled parallel reaction monitoring (PRM) mode. Full MS spectra were collected at a resolution of 70000, with an AGC target of $3e^6$ or maximum injection time of 10 ms and a scan range of 350–1400 m/z. The MS^2 spectra were obtained at a resolution of 35000, with an AGC target value of $1e^6$ or maximum

injection time of 128 ms, a normalised collision energy of 27. MS performance was verified for consistency by running complex cell lysate quality control standards, and chromatography was monitored to check for reproducibility.

Skyline 22.2.0.351 was used to analyze the PRM data (MacLean et al., 2010). Target peptides were imported after setting filter parameters at MS^1 precursor mass analyzer to centroided, a mass accuracy of 10 ppm and MS^2 acquisition method set to PRM centroided at a mass accuracy of 20 ppm. Endogenous peptides had a fixed modification of carbamidomethylation of cysteines (+57.021 Da) and a variable modification of methionine-loss and acetylation at the protein N-terminus (-89.030). In addition, heavy peptides had fixed modifications of heavy lysine and heavy arginine amino acids on their C-terminus (+8.014 and +10.008 Da). The transition peak areas and their boundaries were manually adjusted and derived from the heavy peptide retention times. Endogenous peptides were normalized based on their ratio to heavy peptides.

2.2.4 Results

Experimental setup to study effects on dermokine isoform disruption on human epidermal differentiation. In this study, we exploited the applicability of skin organoids that were grown from our previously established dermokine (DMKN) isoform knockout keratinocytes (see chapter 2.1 for more details). The organoids were cultured using a multi-cellular system where primary human fibroblasts are incorporated within a matrix, followed by the addition of human keratinocytes on the embedded fibroblasts (Figure 2.6) (Enjalbert et al., 2020). This *in-vitro* epidermal system closely resembles the biological intricacies of real skin, through which fibroblasts supply crucial growth factors that direct keratinocyte stratification, thereby facilitating the emergence of distinct epidermal layers (Enjalbert et al., 2020; Werner, 1998).

The further analysis was conducted in triplicates, utilizing either *Dmkn*

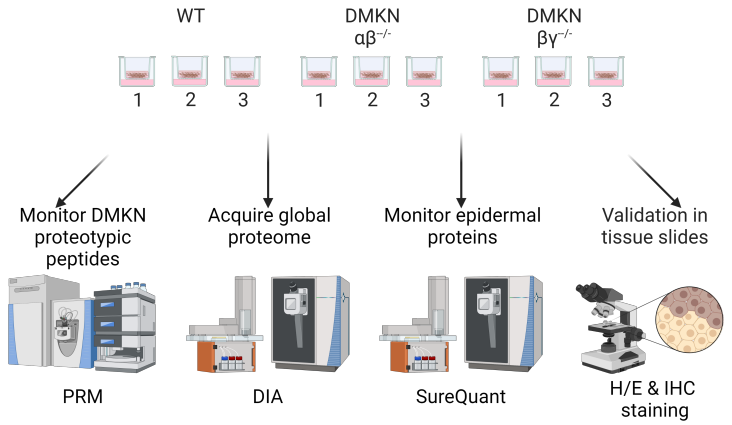

Figure 2.6. Experimental setup for the analysis of cell autonomous functions of dermokine in human keratinocytes. Employing *Dmkn* $\alpha\beta^{-/-}$, *Dmkn* $\beta\gamma^{-/-}$ and wildtype keratinocytes in skin organoids. First, the skin organoids were histologically evaluated for both the proper formation of the suprabasal layers through a hematoxylin and eosin staining while the expression of dermokine was assessed by immunohistochemical staining using an anti-dermokine antibody. All skin organoids underwent sample preparation for MS-based proteomics measurements. In *Dmkn* $\alpha\beta^{-/-}$, *Dmkn* $\beta\gamma^{-/-}$ and wildtype keratinocytes skin organoids, dermokine proteotypic peptides are monitored by parallel reaction monitoring to observe differences between isoform-specific ablations. Next, performing a global MS-based proteomics screen of *Dmkn* $\beta\gamma^{-/-}$ and wildtype keratinocyte skin organoids identified dermokine-mediated proteome changes, which were confirmed with help of internal standard triggered parallel reaction monitoring in *Dmkn* $\alpha\beta^{-/-}$ skin organoids.

$\beta\gamma^{-/-}$ (DTU $\beta\gamma^{-/-}$) or *Dmkn* $\alpha\beta^{-/-}$ (CS $\alpha\beta^{-/-}$) keratinocytes (Figure 2.14A), as well as wildtype keratinocytes (Figure 2.6). This enabled us to track the activity of DMKN's cytokine-like domain (Higashi et al., 2012). Initially, a histological analysis was conducted to visually verify the knockout, employing both H/E as well as immunohistochemical staining methods. Subsequently, the DMKN proteotypic peptides of the skin organoid lysates were measured using parallel reaction monitoring (PRM) (Picotti & Aebersold, 2012). Following this, a comprehensive proteomics screening was performed in the *Dmkn* $\beta\gamma^{-/-}$ keratinocyte orgnaoid models. Lastly, proteins relevant to the epidermal stratification process were validated in the *Dmkn* $\alpha\beta^{-/-}$ keratinocyte skin models using internal standard triggered-PRM (IS-PRM) (Gallien et al., 2015).

Analyzing histological outcomes in dermokine ablated skin organoids. To gain a better understanding of the phenotype of the keratinocytes, we processed the skin organoids for histological sectioning and performed several stainings, including hematoxylin and eosin (H/E). In order to further confirm the removal of DMKN at the protein level, we carried out immunohistochemical staining (IHC) utilizing a dermokine-specific antibody. To investigate the structure and composition of the skin organoids, we initially examined the wildtype histological stainings. Through the H/E staining, we observed the stratification of keratinocytes culminating in the formation of a stratum corneum-like stratum. A high accumulation of nuclei near the dermis-like structure suggested an active population of proliferating keratinocytes, while suprabasal layers presented the beginning of the stratification process, culminating in the corneocytes. The IHC staining confirmed an expected DMKN suprabasal expression gradient, with the peak expression visualized close to the stratum corneum. Upon analyzing the DMKN α/β knockouts, interesting deviations from the wildtype were seen. H/E stainings revealed a thinner total epidermis, with keratinocytes packed tightly together. The suprabasal layers of keratinocytes did not seem to extend beyond the stratum spinosum. This observation echoes with the known DMKN expression pattern—absent in the stratum basale, minimally present in the stratum spinosum, and most abundant in the stratum granulosum. *Dmkn* $\beta/\gamma^{-/-}$ showed results, which were similar to the results from *Dmkn* $\alpha/\beta^{-/-}$. The stratification pattern of the epidermis did not exhibit substantial differences. The lack of DMKN expression, once again confirmed by the IHC staining, was consistent with the previous knockout model, suggesting a common motif in their altered epidermal structures.

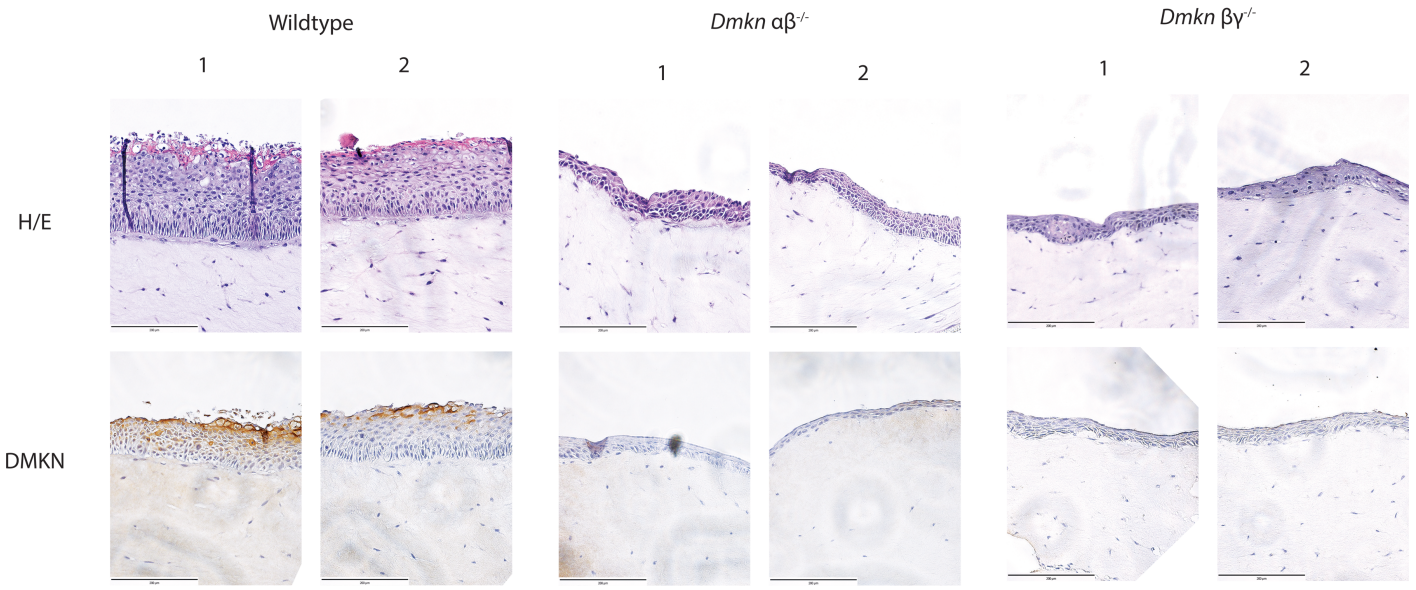

Figure 2.7. **Histology of DMKN-ablated keratinocyte 3D organoids.** The top panel shows hematoxylin and eosin (H/E) staining of histological sections from the 3D model. The bottom panel displays immunohistochemical (IHC) staining of each 3D model to validate the absence of dermokine in the knockouts, in comparison to the wildtype. The scale bar for each staining is 200 μm.

Proteotyping *Dmkn* $\alpha\beta^{-/-}$ and *Dmkn* $\beta\gamma^{-/-}$ keratinocytes in skin organoids. Next, we utilized targeted proteomics to quantify relative abundance changes of DMKN isoform expression. To ensure comprehensive coverage of the protein sequence, we utilized proteotypic peptides, which were spread across the entire DMKN sequence: two were near the N-terminus, three were after the keratin-like domain, and one was at the C-terminus (Figure S2.12). The diverse location of these peptides facilitated the detection of modulations in different parts of the DMKN protein upon the ablation of either the β and γ isoforms or the combination of the α and β isoforms. Of particular interest was the C-terminal peptide "GGVSPSSSASR", which is only 12 amino acids away from the C-terminus and shared by both the β and α isoforms (Figure 2.8A). We reasoned that if only the β isoform was truncated, leaving the α isoform intact, this peptide would still be detectable. Indeed, when comparing endogenous expression levels of this peptide in the knockout to wildtype, we observed a slight reduction in peak area when only the β isoform (in combination withγ) was truncated (Figure 2.8C). However, upon removing both the α and β isoforms, sharing the cytokine-like domain, we observed a substantial decrease in peptide abundance (Figure 2.8C). Evaluating all the peptides we monitored, we noticed changes except for all peptides, especially the cytokine-like domain and a peptide near the N-terminus that is part of the globular domain in both the α and β DMKN knockouts (Figure 2.8D). When we compared the intensity of all the proteotypic peptides and assessed the fold change, we noticed a median intensity ratio reduction of -32. This indicates an overall decline in DMKN levels after the deletion of either the α in combination with the β isoform or the truncation of the β and γ isoforms when compared to their endogenous levels.

***Dmkn* $\beta\gamma^{-/-}$ LC MS/MS-based proteomics in skin organoids.** Having validated our isoform specific dermokine knockouts at the protein level by targeted proteomics and to understand molecular differences of genotypes, we quantitatively assessed proteomes of *Dmkn* $\beta\gamma^{-/-}$ skin organoid models in

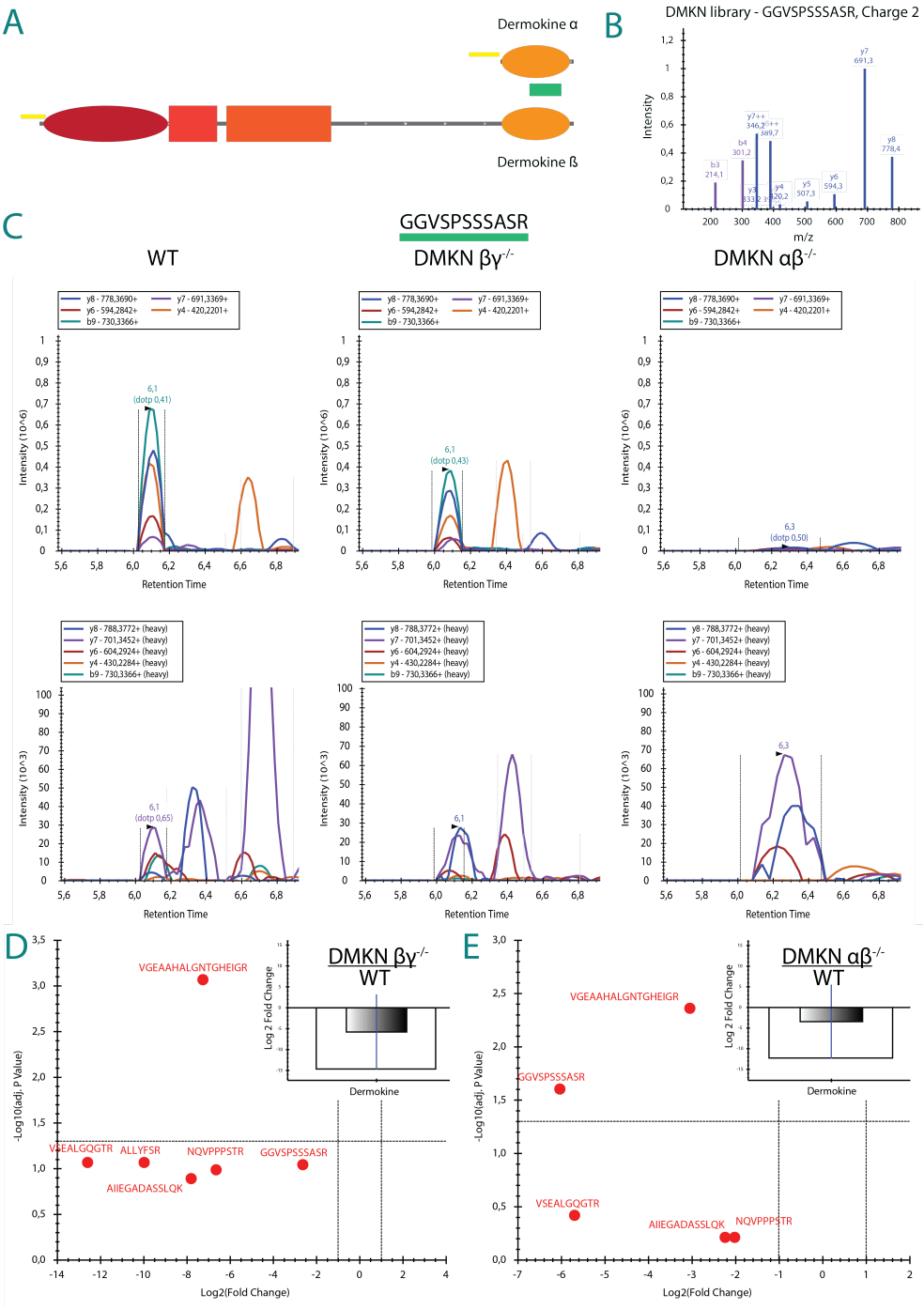

Figure 2.8. (Continued on the following page.)

Figure 2.8. Proteotpying dermokine-specific peptides of *Dmkn* $\alpha\beta^{-/-}$, *Dmkn* $\beta\gamma^{-/-}$ and wildtype keratinocytes in skin organoids. A illustrates the peptide "GGVSPSSSASR", which is unique to the cytokine-like domain, comprising the C-terminus of dermokine-β and inherent part of dermokine-α. **B** displays the *in-silico* MS/MS spectrum of peptide "GGVSPSSSASR". **C** shows the different peak areas of peptide "GGVSPSSSASR" in *Dmkn* $\alpha\beta^{-/-}$, *Dmkn* $\beta\gamma^{-/-}$ and wildtype keratinocyte skin organoids. **D** visualizes the $\log_2$ fold change of all peptide abundances in either *Dmkn* $\alpha\beta^{-/-}$ or *Dmkn* $\beta\gamma^{-/-}$ in comparison to wildtype keratinocyte skin organoids.

comparison to models grown with wildtype cells. This analysis resulted in identification of fully quantifiable 4253 proteins after processing with DIA-NN (Figure 2.9A). Our data revealed 493 proteins that significantly decreased in abundance ($-\log_2(1.5)$ and a pvalue lower than 0.05) and 411 proteins that significantly increased ($\log_2(1.5)$ with a pvalue < 0.05), resulting in a total of 904 significantly differentially abundant proteins. Among these, numerous proteins involved in epidermal stratification, especially proteases, were found to be less abundant in the knockout model than in the wildtype, suggesting a substantial role of DMKN in these processes. Particularly intriguing was the decreased abundance of proteins associated with suprabasal stratification. Gene ontology (GO) analysis further corroborated these findings, revealing decreased association of proteins involved in the formation of the cornified envelope, RHO GTPase signalling, RNA metabolism, and translation in the *Dmkn* $\beta\gamma^{-/-}$ organoids (Figure 2.9B). Interestingly, the term 'regulation of proteolysis' was common among both significantly decreased and increased proteins. The proteins that increased in abundance in the presence of dermokine, were associated with extracellular matrix organization, regulation of insulin-like growth factor transport and signalling by receptor tyrosine kinases (Figure 2.9C). These findings emphasize the implications of DMKN isoform truncations on the skin proteome and provide further insight into the critical roles this protein plays in epidermal stratification and overall skin homeostasis.

Validating *Dmkn* $\beta\gamma^{-/-}$ skin organoids proteomics screening results

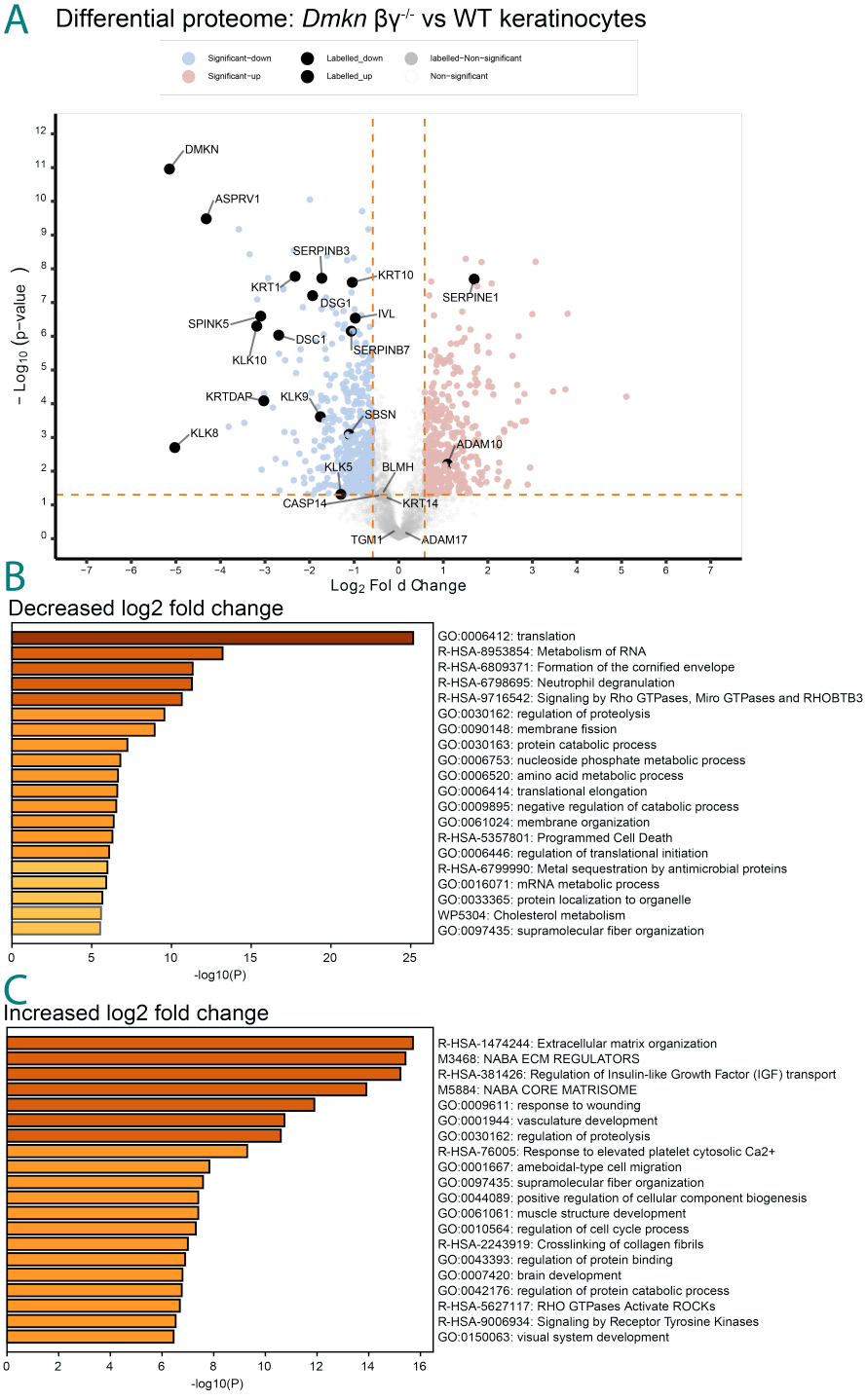

Figure 2.9. (Continued on the following page.)

Figure 2.9. LC-MS/MS-based measurements of protein abundances in *Dmkn* $\beta\gamma^{-/-}$ versus wildtype keratinocytes. A. Volcano plot illustrating the ratio in $\log_2$ fold change in *Dmkn* $\beta\gamma^{-/-}$ to wildtype keratinocyte skin organoids ($\log_2(1.5)$ and a pvalue < 0.05) **B.** Gene ontology analysis of significantly decreased proteins and **C** significantly increased proteins when comparing *Dmkn* $\beta\gamma^{-/-}$ keratinocytes to wildtype keratinocyte skin organoids.

in *Dmkn* $\alpha\beta^{-/-}$ skin organoids. Next, we utilized targeted internal-standard triggered parallel reaction monitoring (IS-PRM) on the *Dmkn* $\alpha/\beta^{-/-}$, aiming to elucidate the implications of completely eliminating the cytokine-like domain and validating our previous proteomics screening in *Dmkn* $\beta\gamma^{-/-}$ skin organoids. This analytical approach enabled us to monitor a set of 37 proteins, among which we could quantify 23 with at least one peptide. Our study incorporated a total of 107 heavy peptides, leading to the formation of 214 peptide pairs when combined with endogenous peptides. We successfully quantified 75 heavy peptides and 34 endogenous peptides over a 70-minute elution gradient. Our peptide selection was heavily influenced by the proteins present in the epidermal protease network, shedding light on the abundance of proteins involved in crucial processes spanning from barrier recovery and ENaC and PAR2 activation to pro-Filaggrin processing, desquamation, and assembly of the cornified envelope.

Of the 23 proteins quantified, we identified 4 significantly decreased proteases (BLMH, APRV1, KLK5, CASP14), all well-known for their role in filaggrin processing and subsequent contribution to the formation of the stratum corneum (Figure 2.10A and 2.10B). This observation indicates the missing suprabasal stratification arising from the ablation of DMKN's cytokine-like domain. Extending our analysis, we found 8 out of the 23 quantified proteins (TGM1, CATL1, TGM3, KLK7, CATG, KLK5, KLK14, KLK6) that showed a significant decrease in abundance. These proteins are commonly recognized for their integral roles in the assembly of the cornified envelope and the process of desquamation, both essential for ensuring proper epidermal stratification. The conclusions drawn from our targeted proteomics approach substantiate

our earlier findings corroborating that the absence of dermokine leads to a decreased abundance of key proteases involved in the epidermal stratification process.

MMP10-dependent proteolytic cleavage of human DMKN. Previous research has illustrated limited proteolysis of DMKN by MMP10 in mouse epidermis, expressing constitutively active MMP10 in basal keratinocytes as well as direct processing of recombinant human DMKN by active human MMP10 (Schlage et al., 2015). Nonetheless, the precise cleavage site in the human system remained elusive. Here, we utilized our targeted degradomics workflow, co-incubating recombinant human DMKN with recombinant human MMP10 (Figure 2.11A) (Savickas & dem Keller, 2017). Building on previous findings, we hypothesized that the cleavage site would be located two amino acids after the proline at position 201, mirroring the cleavage site observed in mouse DMKN. This assumption is based on MMP10's known preference for proline in the P3' position (Schlage et al., 2014). Consequently, the new N-terminus following MMP10 cleavage would start at phenylalanine 204, immediately succeeding asparagine 203. Our targeted degradomics validation confirmed this prediction (Figure 2.11B) by detection of the semi-tryptic peptide matching the predicted cleavage in presence of the active protease. Conversely, in the absence of MMP10, this peptide was not detected, indicating that the cleavage event was indeed MMP10-dependent. Moreover, we closely examined two specific tryptic peptides, of which one was located close to the original DMKN N-terminus, prior to the expected cleavage site, and the other mapped downstream of the cleavage site, closer to the original C-terminus. The targeted degradomics effectively visualized that in the absence of cleavage, both tryptic peptides showed a reduced peak intensity compared to their levels when MMP10 was present (Figure 2.11B).

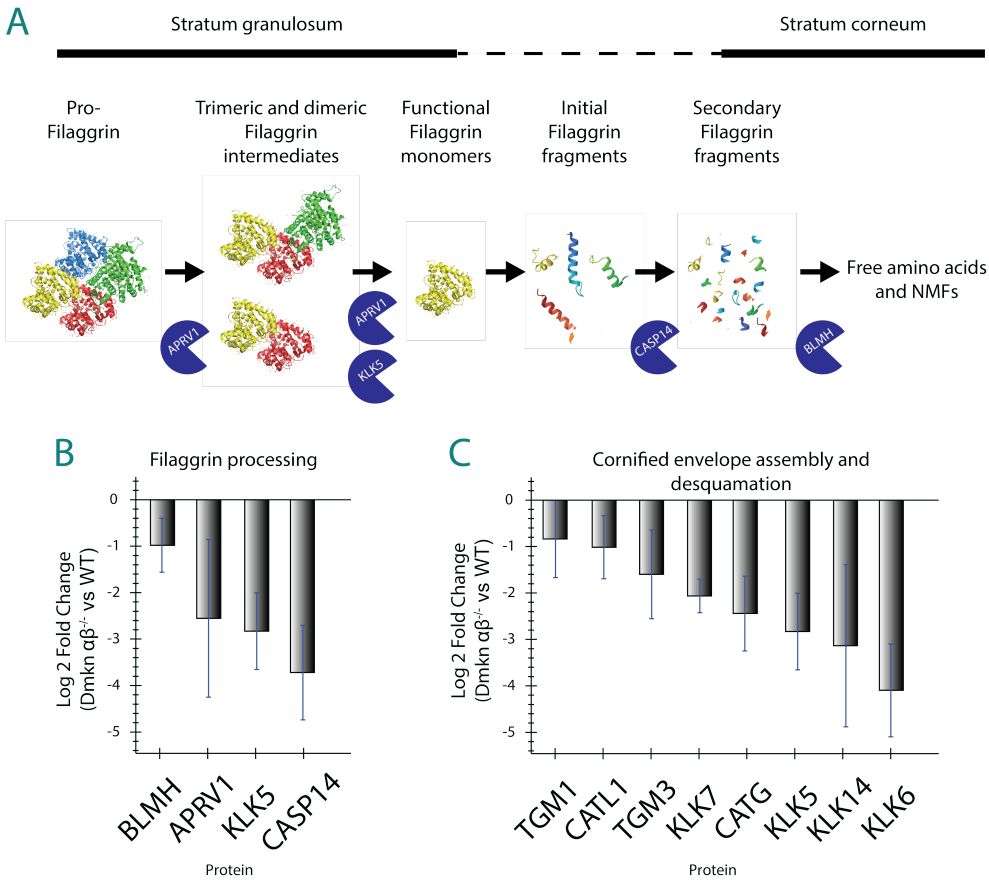

Figure 2.10. **SureQuant™targeted proteomics measurements of significantly differentially abundant epidermal proteins in wildtype keratinocytes versus *Dmkn* $\alpha\beta^{-/-}$ keratinocytes.** **A.** Adapted from (de Veer et al., 2014). Illustrates the proteolytic cleavage of filaggrin mediated by "APRV1", "KLK5", "CASP14" and "BLMH", which are contributing to the development of the stratum corneum. **B** visualizes significantly decreased filaggrin-modulating proteins when comparing *Dmkn* $\alpha\beta^{-/-}$ to wildtype keratinocyte skin organoids. **C** shows the significantly decreased proteins associated with the cornified envelope assembly and desquamation detected in the ratio *Dmkn* $\alpha\beta^{-/-}$ to wildtype keratinocyte skin organoids.

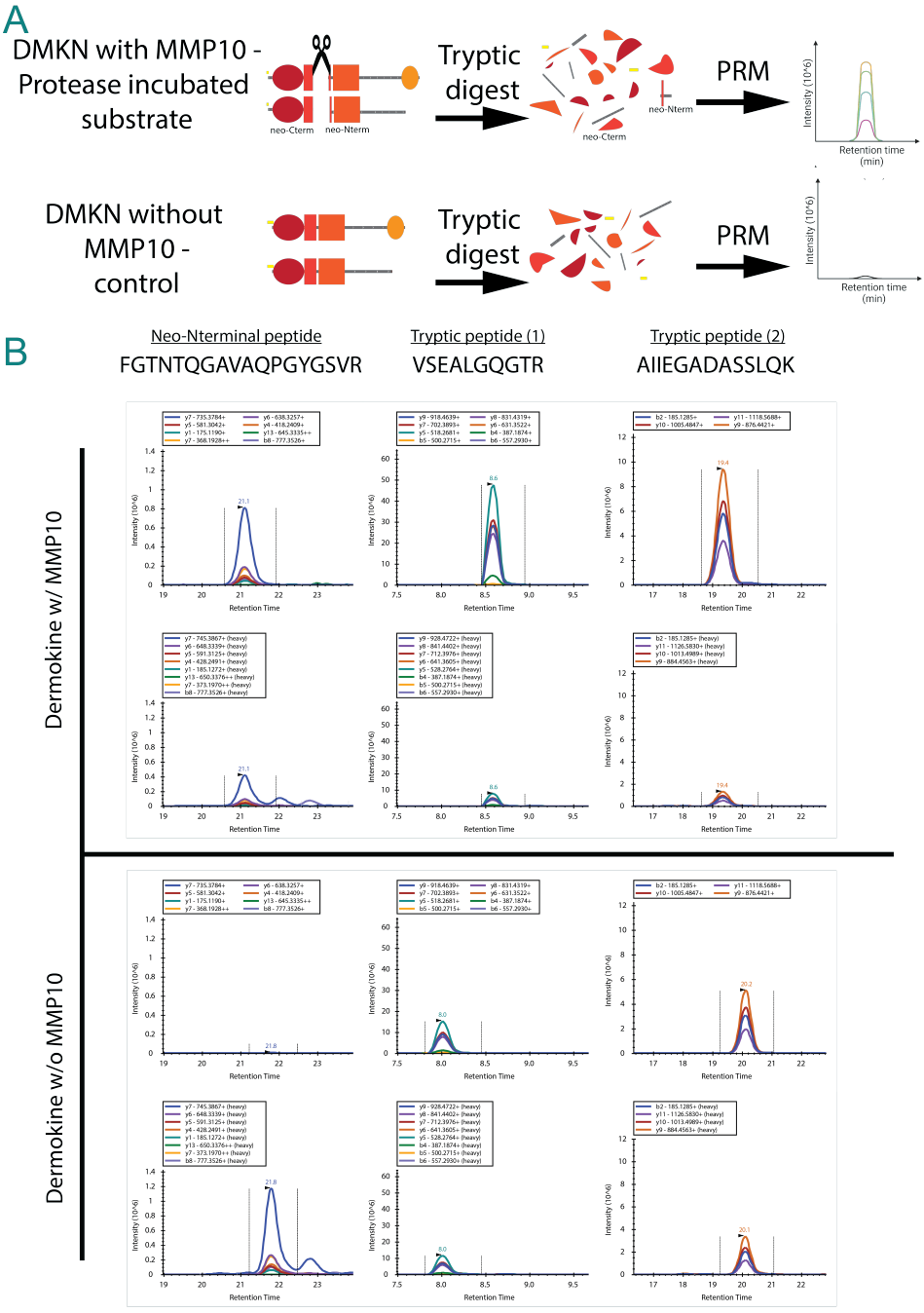

Figure 2.11. (Continued on the following page.)

Figure 2.11. MMP10 co-incubation experiment to identify the exact cleavage site in human DMKN. A illustrates the MMP10-dependent cleavage of dermokine and the generation of a unique neo-C- and neo-N-terminus, which are not detected in the absence of MMP10, seen in the exclusively tryptic digest of dermokine, quantifiable by targeted degradomics. **B.** In the presence of MMP10, the neo-N-terminal peptide is detectable, which is aligned with the heavy peptide, whereas the absence of MMP10 illustrates the lack of the MMP10-dependent neo-N-terminal peptide. Regardless of MMP10 presence, two tryptic peptides were measured in parallel.

2.2.5 Discussion

In the current study, we examined the cell autonomous effect of DMKN on the biology of keratinocytes, a critical protein implied in the formation of a properly stratified epidermis. DMKN, a component of the stratified secreted epithelium complex family, is implicated in the accurate formation and development of the human epidermis (Matsui et al., 2004). Previous research has indicated the potential role of MMP10 in promoting keratinocyte migration during re-epithelialization in wound healing (Krampert et al., 2004; Murphy et al., 1991). Furthermore, *Schlage et al.* provided evidence that MMP10 cleaves DMKN, both *in-vitro* and *in-vivo*, potentially modulating keratinocyte migration (Schlage et al., 2015). In detail, DMKN is implicated to play a part in the proliferation phase of epithelial keratinocyte differentiation, potentially through its cytokine-like domain (Higashi et al., 2012). Our study reveals a pivotal role for DMKN in keratinocyte biology and epidermal stratification in a human skin model. Monitoring DMKN proteotypic peptides in *Dmkn* $\beta/\gamma^{-/-}$ skin organoid models showed decreased abundance of the cytokine-like domain peptide, which was elusive only when both the β and α DMKN isoforms were eliminated. Histological assessment demonstrated a lack of differentiated epidermis in DMKN-truncated skin organoids, a pattern aligned with the expression gradient of DMKN. Global analysis of proteins from *Dmkn* $\beta/\gamma^{-/-}$ keratinocyte skin organoids revealed changes in 904 out of 4253 quantifiable proteins, many associated with the formation of the cornified envelope

and DMKN-associated signalling events. Through an IS-PRM approach, we independently validated these findings in the *Dmkn* $\alpha/\beta^{-/-}$ keratinocyte skin organoid and identified decreased levels of proteins essential for filaggrin processing, cornified envelope assembly, and desquamation. Lastly, we mapped the exact cleavage site of MMP10-dependent modulation in human DMKN, previously only identified in mice (Schlage et al., 2015). Overall, our research highlights the significant role of DMKN in maintaining skin homeostasis and proper epidermal stratification.

First, we investigated the structural characteristics of skin organoids grown with DMKN isoform disrupted keratinocytes by histological assessments. Initial examination of the wildtype organoids through H/E staining revealed a clear stratification of keratinocytes, culminating in a structure similar to the stratum corneum. Wildtype keratinocyte skin organoids analyzed by immunohistochemical (IHC) staining, highlighted the anticipated suprabasal expression gradient of DMKN, peaking close to the stratum corneum (Matsui et al., 2004). In addition, skin organoids including both, the *Dmkn* $\beta\gamma^{-/-}$ and *Dmkn* $\alpha/\beta^{-/-}$ keratinocytes, we observed dramatic distortions from the wildtype (Utsunomiya et al., 2020). Interestingly, the suprabasal layers of keratinocytes appeared to be absent above the stratum spinosum. This pattern resembled the established DMKN expression profile, which is lacking in the basal layer and reaches its highest quantities in the granular stratum (Leclerc et al., 2014). Further, immunohistochemistry stainings confirmed the deficiency of DMKN expression in both knockout models.

Concomitantly, a quantitative proteomics analysis of *Dmkn* $\beta\gamma^{-/-}$ skin organoids compared to models grown with wildtype keratinocytes resulted in 904 differentially abundant proteins out of 4253 quantifiable proteins. Proteins that showed a decreased abundance in knockout skin models are essential for formation of the cornified envelope and also demonstrated once more that DMKN abundance is depleted (de Veer et al., 2014). In contrast, proteins with increased abundance are suggestive of endogenous DMKN-associated events, linked to extracellular matrix organization and signalling by tyrosine kinases.

Subsequent to the proteomics screen, we applied a targeted proteomics approach to validate the recent findings in the DMKN cytokine-like domain elusive keratinocyte skin organoid (Gallien et al., 2015; Higashi et al., 2012). Here, we quantified the abundance of 37 selected proteins and their 107 proteotypic peptides related to epidermal differentiation processes such as filaggrin processing, cornified envelope assembly, and desquamation (de Veer et al., 2014). In the *Dmkn* $\alpha\beta^{-/-}$ model, we identified decreased quantities of proteins associated with filaggrin processing (BLMH, APRV1, KLK5, CASP14) and the assembly of the cornified envelope and desquamation (TGM1, CATL1, TGM3, KLK7, CATG, KLK5, KLK14, KLK6), suggesting a failure to fully stratify, in alignment with the expression gradient of DMKN (Utsunomiya et al., 2020).

Lastly, our work further corroborated our previous studies by pinpointing the precise cleavage site of direct cleavage of human dermokine by MMP10, an finding that was previously established in mice (Schlage et al., 2015). Through a targeted degradomics assay, we were able to monitor the neo-N-terminus and detect a peak only in the presence of MMP10, which was not observed in its absence (Savickas & dem Keller, 2017).

In conclusion, our comprehensive study elucidates DMKN's pivotal role in epidermal stratification, contributing to a healthy and functional epidermis. The comprehensive set of techniques and models used in our study have not only confirmed the vital role of DMKN in epidermal stratification but also highlighted the convoluted balance of molecular processes involved in the formation of the cornified envelope. This further underlines the direct or indirect influence of the bioactive protein DMKN on key mechanisms that maintain skin homeostasis.

2.2.6 Acknowledgments

We thank Susanne Primdahl (Centre for Diagnostics, DTU Health Tech) for her histological and immunohistochemical support. This work was supported

by a Novo Nordisk Foundation Young Investigator Award (NNF16OC0020670 to U.a.d.K) and funding from the LEO Foundation (LF-OC-19-000033 to U.a.d.K). Figure 2.6A and partially figure 2.11A were created by Biorender.

2.2.7 References

A, D. M., C, H. W., Yasushi, I., Vincent, R., Y, W. J., A, W. R., N, L. D., P, L. F., & G, R. J. (2000). Human Keratinocytes That Express hTERT and Also Bypass a p16INK4a-Enforced Mechanism That Limits Life Span Become Immortal yet Retain Normal Growth and Differentiation Characteristics. *Molecular and Cellular Biology*, *20*(4), 1436–1447.

Clevers, H. (2016). Modeling Development and Disease with Organoids. *Cell*, *165*(7), 1586–1597.

Demichev, V., Messner, C. B., Vernardis, S. I., Lilley, K. S., & Ralser, M. (2019). DIA-NN: neural networks and interference correction enable deep proteome coverage in high throughput. *Nature Methods 2019 17:1*, *17*(1), 41–44.

de Veer, S. J., Furio, L., Harris, J. M., & Hovnanian, A. (2014). Proteases: Common culprits in human skin disorders.

Eckl, K. M. (2014). Update: advanced methods in three-dimensional organotypic tissue engineering for congenital ichthyosis and other rare keratinization disorders. *British Journal of Dermatology*, *171*(6), 1289–1290.

Enjalbert, F., Dewan, P., Caley, M. P., Jones, E. M., Morse, M. A., Kelsell, D. P., Enright, A. J., & O'Toole, E. A. (2020). 3D model of harlequin ichthyosis reveals inflammatory therapeutic targets. *Journal of Clinical Investigation*, *130*(9), 4798–4810.

Fuchs, E., & Raghavan, S. (2002). Getting under the skin of epidermal morphogenesis. *Nature reviews. Genetics*, *3*(3), 199–209.

Gallien, S., Kim, S. Y., & Domon, B. (2015). Large-Scale Targeted Proteomics Using Internal Standard Triggered-Parallel Reaction Monitoring (IS-PRM). *Mol Cell Proteomics*, *14*(6), 1630–1644.

Higashi, K., Hasegawa, M., Yokoyama, C., Tachibana, T., Mitsui, S., & Saito, K. (2012). Dermokine-β impairs ERK signaling through direct binding to GRP78. *FEBS Letters*, *586*(16), 2300–2305.

Krampert, M., Bloch, W., Sasaki, T., Bugnon, P., Rulicke, T., Wolf, E., Aumailley, M., Parks, W. C., & Werner, S. (2004). Activities of the matrix metalloproteinase stromelysin-2 (MMP-10) in matrix degradation

and keratinocyte organization in wounded skin (2004/09/17). *Mol Biol Cell*, *15*(12), 5242–5254.

Leclerc, E. A., Huchenq, A., Kezic, S., Serre, G., & Jonca, N. (2014). Mice deficient for the epidermal dermokine β and γ isoforms display transient cornification defects. *Journal of Cell Science*, *127*(13), 2862–2872.

Lichtenthaler, S. F., Lemberg, M. K., & Fluhrer, R. (2018). Proteolytic ectodomain shedding of membrane proteins in mammals—hardware, concepts, and recent developments. *The EMBO Journal*, *37*(15).

MacLean, B., Tomazela, D. M., Shulman, N., Chambers, M., Finney, G. L., Frewen, B., Kern, R., Tabb, D. L., Liebler, D. C., & MacCoss, M. J. (2010). Skyline: an open source document editor for creating and analyzing targeted proteomics experiments (2010/02/12). *Bioinformatics*, *26*(7), 966–968.

Matsui, T., Hayashi-Kisumi, F., Kinoshita, Y., Katahira, S., Morita, K., Miyachi, Y., Ono, Y., Imai, T., Tanigawa, Y., Komiya, T., & Tsukita, S. (2004). Identification of novel keratinocyte-secreted peptides dermokine-α/- β and a new stratified epithelium-secreted protein gene complex on human chromosome 19q13.1. *Genomics*, *84*(2), 384–397.

Mestas, J., & Hughes, C. C. W. (2004). Of Mice and Not Men: Differences between Mouse and Human Immunology. *The Journal of Immunology*, *172*(5), 2731–2738.

Mullan, K. A., Bramberger, L. M., Munday, P. R., Goncalves, G., Revote, J., Mifsud, N. A., Illing, P. T., Anderson, A., Kwan, P., Purcell, A. W., & Li, C. (2021). ggVolcanoR: A Shiny app for customizable visualization of differential expression datasets. *Computational and Structural Biotechnology Journal*, *19*, 5735–5740.

Murphy, G., Cockett, M. I., Ward, R. V., & Docherty, A. J. (1991). Matrix metalloproteinase degradation of elastin, type IV collagen and proteoglycan. A quantitative comparison of the activities of 95 kDa and 72 kDa gelatinases, stromelysins-1 and -2 and punctuated metalloproteinase (PUMP). *Biochem J*, *277 (Pt 1)*, 277–279.

Naso, M. F., Liang, B., Huang, C. C., Song, X. Y., Shahied-Arruda, L., Belkowski, S. M., D'Andrea, M. R., Polkovitch, D. A., Lawrence, D. R., Griswold, D. E., Sweet, R. W., & Amegadzie, B. Y. (2007). Dermokine: An extensively differentially spliced gene expressed in epithelial cells. *Journal of Investigative Dermatology*, *127*(7), 1622–1631.

Picotti, P., & Aebersold, R. (2012). Selected reaction monitoring–based proteomics: workflows, potential, pitfalls and future directions. *Nature Methods*, *9*(6), 555–566.

R Core Team. (2022). R: A language and environment for statistical computing. R Foundation for Statistical Computing.

Richmond, A., & Yingjun, S. (2008). Mouse xenograft models vs GEM models for human cancer therapeutics. *Disease Models & Mechanisms*, *1*(2-3), 78.

Savickas, S., & dem Keller, U. (2017). Targeted degradomics in protein terminomics and protease substrate discovery. *Biol Chem*, *399*(1), 47–54.

Schlage, P., Kockmann, T., Sabino, F., Kizhakkedathu, J. N., & auf dem Keller, U. (2015). Matrix Metalloproteinase 10 Degradomics in Keratinocytes and Epidermal Tissue Identifies Bioactive Substrates With Pleiotropic Functions. *Mol Cell Proteomics*, *14*(12), 3234–3246.

Schlage, P., Egli, F. E., Nanni, P., Wang, L. W., Kizhakkedathu, J. N., Apte, S. S., & Keller, U. a. d. (2014). Time-resolved Analysis of the Matrix Metalloproteinase 10 Substrate Degradome. *Molecular & Cellular Proteomics*, *13*(2), 580.

Tognetti, M., Sklodowski, K., Müller, S., Kamber, D., Muntel, J., Bruderer, R., & Reiter, L. (2021). Biomarker Candidates for Tumors Identified from Deep-Profiled Plasma Stem Predominantly from the Low Abundant Area. *bioRxiv*, 2021.10.05.463153.

Utsunomiya, A., Chino, T., Utsunomiya, N., Luong, V. H., Tokuriki, A., Naganuma, T., Arita, M., Higashi, K., Saito, K., Suzuki, N., Ohara, A., Sugai, M., Sugawara, K., Tsuruta, D., Oyama, N., & Hasegawa, M. (2020). Homeostatic Function of Dermokine in the Skin Barrier and Inflammation. *Journal of Investigative Dermatology*.

Werner, S. (1998). Keratinocyte Growth Factor: A Unique Player in Epithelial Repair Processes. *Cytokine & Growth Factor Reviews*, *9*(2), 153–165.

Werner, S., & Smola, H. (2001). Paracrine regulation of keratinocyte proliferation and differentiation. *Trends in cell biology*, *11*(4), 143–146.

Wieczorek, S., Combes, F., Lazar, C., Gianetto, Q. G., Gatto, L., Dorffer, A., Hesse, A. M., Couté, Y., Ferro, M., Bruley, C., & Burger, T. (2017). DAPAR & ProStaR: Software to perform statistical analyses in quantitative discovery proteomics. *Bioinformatics*, *33*(1), 135–136.

Zhou, Y., Zhou, B., Pache, L., Chang, M., Khodabakhshi, A. H., Tanaseichuk, O., Benner, C., & Chanda, S. K. (2019). Metascape provides a biologist-oriented resource for the analysis of systems-level datasets. *Nature communications*, *10*(1).

Supplemental Figures

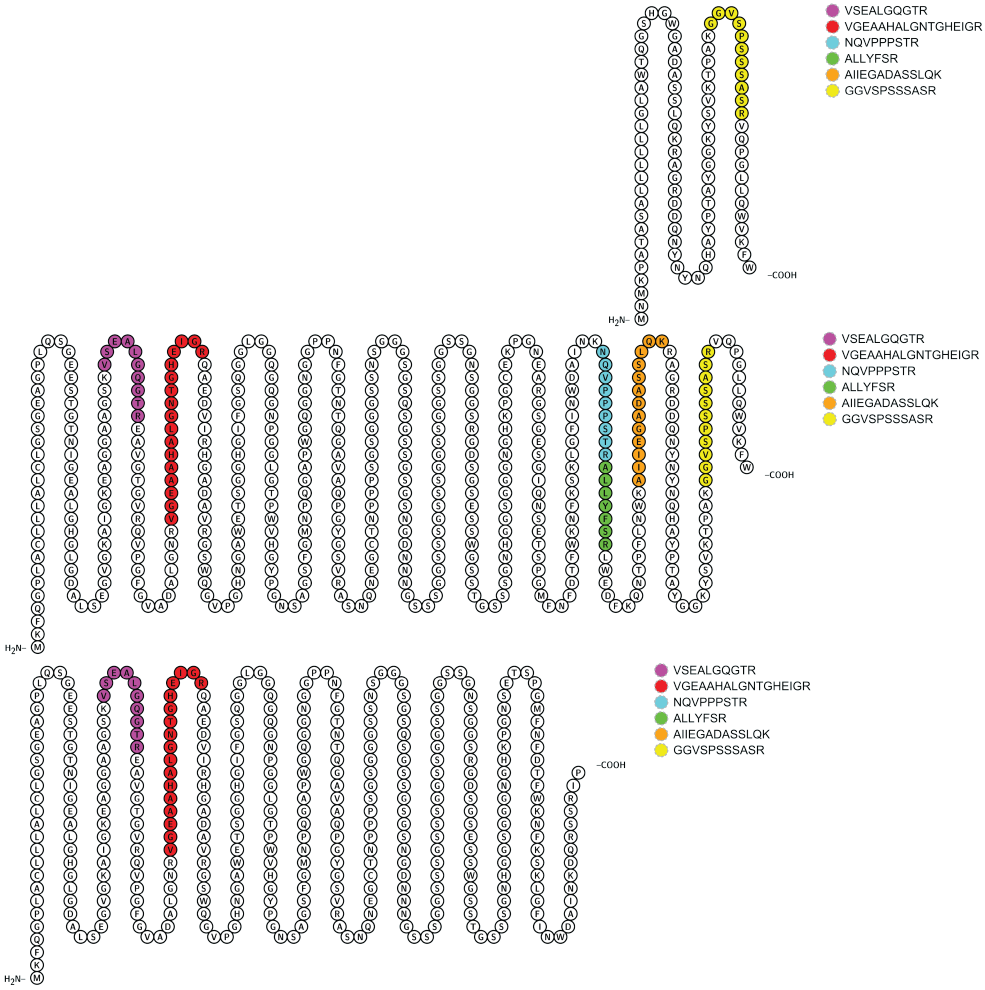

Figure S 2.12. Dermokine isoforms and synthesized proteotypic peptides. Depicting all the synthesized proteotypic peptides utilized in determining the relative abundance of various dermokine isoforms.

Supplemental Files

List of supplemental files uploaded onto Onedrive, attached to this document:

File S1. KO PRMs (.raw) and skyline files.

File S2. Global Proteomics screen (.raw) and Excel files.

Nucleotide Sequence (1431 nt):
ATGAAGTTCCAGGGGCCCCTGGCCTGCCTCCTGCTGGCCCTCTGCCTGGGCAGTGGGGAGGCTGGCCCCC
TGCAGAGCGGAGAGGAAAGCACTGGGACAAATATTGGGGAGGCCCTTGGACATGGCCTGGGAGACGCCCT
GAGCGAAGGGGTGGGAAAGGCCATTGGCAAAGAGGCCGGAGGGGCAGCTGGCTCTAAAGTCAGTGAGGCC
CTTGGCCAAGGGACCAGAGAAGCAGTTGGCACTGGAGTCAGGCAGGTTCCAGGCTTTGGCGTAGCAGATG
CTTTGGGCAACAGGGTCGGGGAAGCAGCCCATGCTCTGGGAAACACTGGGCACGAGATTGGCAGACAGGC
AGAAGATGTCATTCGACACGGAGCAGATGCTGTCCGCGGCTCCTGGCAGGGGGTGCCTGGCCACAATGGT
GCTTGGGAAACTTCTGGAGGCCATGGCATCTTTGGCTCTCAAGGTGGCCTTGGAGGCCAGGGCCAGGGCA
ATCCTGGAGGTCTGGGGACTCCGTGGGTCCACGGATACCCCGGAAACTCAGCAGGCAGCTTTGGAATGAA
TCCTCAGGGAGCTCCCTGGGGTCAAGGAGGCAATGGAGGGCCACCAAACTTTGGGACCAACACTCAGGGA
GCTGTGGCCCAGCCTGGCTATGGTTCAGTGAGAGCCAGCAACCAGAATGAAGGGTGCACGAATCCCCCAC
CATCTGGCTCAGGTGGAGGCTCCAGCAACTCTGGGGGAGGCAGCGGCTCACAGTCGGGCAGCAGTGGCAG
TGGCAGCAATGGTGACAACAACAATGGCAGCAGCAGTGGTGGCAGCAGCAGTGGCAGCAGCAGTGGCGGC
AGCAGTGGCGGCAGCAGTGGTGGCAGCAGTGGCAACAGTGGTGGCAGCAGAGGTGACAGCGGCAGTGAGT
CCTCCTGGGGATCCAGCACCGGCTCCTCCTCCGGCAACCACGGTGGGAGCGGCGGAGGAAATGGACATAA
ACCCGGGTGTGAAAAGCCAGGGAATGAAGCCCGCGGGAGCGGGGAATCTGGGATTCAGAACTCTGAGACG
TCTCCTGGGATGTTTAACTTTGACACTTTCTGGAAGAATTTTAAATCCAAGCTGGGTTTCATCAACTGGG
ATGCCATAAACAAGAACCAGGTCCCGCCCCCCAGCACCCGAGCCCTCCTCTACTTCAGCCGACTCTGGGA
GGATTTCAAACAGAACACTCCTTTCCTCAACTGGAAAGCAATTATTGAGGGTGCGGACGCGTCATCACTG
CAGAAACGTGCAGGCAGAGACGATCAGAACTACAATTACAACCAGCATGCGTATCCCACTGCCTATGGTG
GGAAGTACTCAGTCAAGACCCCTGCAAAGGGGGGAGTCTCACCTTCTTCCTCGGCTTCCCGGGTGCAACC
TGGCCTGCTGCAGTGGGTGAAGTTTTGGTAG

Translation (476 aa):
MKFQGPLACLLLALCLGSGEAGPLQSGEESTGTNIGEALGHGLGDALSEGVGKAIGKEAGGAAGSKVSEA
LGQGTREAVGTGVRQVPGFGVADALGNRVGEAAHALGNTGHEIGRQAEDVIRHGADAVRGSWQGVPGHNG
AWETSGGHGIFGSQGGLGGQGQGNPGGLGTPWVHGYPGNSAGSFGMNPQGAPWGQGGNGGPPNFGTNTQG
AVAQPGYGSVRASNQNEGCTNPPPSGSGGGSSNSGGGSGSQSGSSGSGSNGDNNNGSSSGGSSSGSSSGG
SSGGSSGGSSGNSGGSRGDSGSESSWGSSTGSSSGNHGGSGGGNGHKPGCEKPGNEARGSGESGIQNSET
SPGMFNFDTFWKNFKSKLGFINWDAINKNQVPPPSTRALLYFSRLWEDFKQNTPFLNWKAIIEGADASSL
QKRAGRDDQNYNYNQHAYPTAYGGKYSVKTPAKGGVSPSSSASRVQPGLLQWVKFW

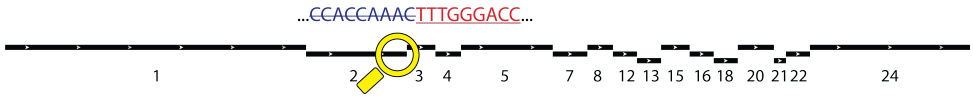

Figure S 2.13. **Dermokine genetic and protein sequence as well as the MMP10 cleavage site.** Evaluating the comparison between the cleavage site and the genetic sequence to elucidate that MMP10 cleaves DMKN in its collagen-like domain (exon2).

File S3. 3D KO epidermal protease panel SureQuant™(.raw) and skyline files.

File S4. MMP10 co-incubation PRMs (.raw) and skyline files.

Abbreviations and Acronyms

APRV1 Retroviral-like aspartic protease 1

BLMH Bleomycin Hydrolase

CASP14 Caspase 14

CATG Cathepsin G

CATL1 Procathepsin L

CO_2 Carbon Dioxide

DIA Data-Independent Acquisition

DIANN Data-Independent Acquisition Neural Networks

DMKN Dermokine

FBS Fetal Bovine Serum

GTPase Guanosine Triphosphatase

HE Hematoxylin and Eosin

IHC Immunohistochemistry

IS-PRM Internal-standard Triggered Parallel Reaction Monitoring

KLK5 Kallikrein-5

KLK6 Kallikrein-6

KLK7 Kallikrein-7

KLK14 Kallikrein-14

LC Liquid Chromatography

MMP10 Matrix Metalloproteinase 10

MS Mass Spectrometry

MS/MS Tandem Mass Spectrometry

PRM Parallel Reaction Monitoring

RNA Ribonucleic Acid

TGM1 Transglutaminase 1

TGM3 Transglutaminase 3

2.3 Dermokine – A Modulator of Adhesion - Manuscript 5

MANUSCRIPT 5 – SUMMARY

Phosphoproteomics of Human Keratinocytes. This study broadens the depth of phosphopeptide identifications in keratinocytes by utilizing automation-aided sample preparation and cutting-edge LC-MS/MS instrumentation coupled to advanced data analysis strategies. These approaches have enabled us to confidently quantify several thousand phosphosites, and we aimed to link phosphorylated serines, threonines, or tyrosines to their specific kinases. We have further improved our data acquisition method by reducing the MS^2 window size, allowing more extensive investigation of the mass spectrum, and increasing the separation of phosphopeptides within our sample using a 140-minute LC gradient. Employing this strategy, we acquired the to our knowledge deepest phosphoproteome of keratinocytes known to date, encompassing 15468 quantified phosphosites. Our comprehensive dataset provides an exhaustive resource for future studies in keratinocyte biology.

Dermokine-Dependent Modulation of Keratinocyte Adhesion. A central focus of this analysis was the investigation of *Dmkn* $\beta\gamma^{-/-}$ and *Dmkn* $\alpha\beta^{-/-}$ keratinocytes, where all cytokine-like domain-containing isoforms had been removed, comparing the mutants to wildtype keratinocytes. In the course of this exploration, we made several interesting findings. Interestingly, under endogenous dermokine (DMKN) levels, we observed increased abundance of several receptor phosphorylations, including proto-oncogene, receptor tyrosine kinase Met (MET) at site S990, erb-b2 receptor tyrosine kinase 2 (ERBB2) at site T701, and insulin like growth factor 2 receptor (IGF2R) at site S2409. These receptors are pivotal to various cellular processes, and their phosphorylation dynamics in the presence of DMKN may provide insights into the

complex regulation of keratinocyte physiology.

Phosphorylation of ERBB2 at T701, for instance, impacts its molecular association and protein conformation, and suppresses receptor internalization, thereby regulating cellular sensitivity to external signals. Phosphorylation of IGF2R at S2409 by the casein Kinase 2 α 1 kinase, which was found to be considerably more active in our study, aligns with previous studies on the receptor. However, the effect of MET phosphorylation at S990 on receptor activity is unclear, its increased abundance was of interest.

Further investigation into the role of adherens junctions in keratinocyte biology and how DMKN levels influence their phosphorylation status resulted in identification of differential abundances in the protein-corrected bona fide phosphorylation events. This study identified an interesting phosphorylation event of SRC at site S17 under endogenous DMKN levels, which could play a considerable role in cell migration.

Concurrently, an increase in the phosphorylation of catenin δ 1 (CTNN δ 1) was observed when DMKN was truncated. This alteration suggests its impact on the associative state with cadherin 1 and thus the adhesive strength of the cells, which is known to increase upon dephosphorylation of CTNN δ 1, which might be mediated by differentially phosphorylated protein tyrosine phosphatase receptor type κ.

These observations suggest a convoluted interaction of cellular processes potentially regulated by DMKN levels. This complex regulation modulates adhesion dynamics in keratinocytes, essential for the physiological responses of keratinocytes and accurate epidermal stratification.

Dermokine drives keratinocyte differentiation by phosphorylation-dependent modulation of cell adhesion

Vahap Canbay[1], Michael Stumpe[2], Jörn Dengjel[2] and Ulrich auf dem Keller[1]

[1]Department of Biotechnology and Biomedicine, Technical University of Denmark, DK-2800, Kongens Lyngby, Denmark
[2]Department of Biology, University of Fribourg, Fribourg, Switzerland

Published in

Canbay V., Stumpe M., Dengjel J., and auf dem Keller U. (2023) Dermokine drives keratinocyte differentiation by phosphorylation-dependent modulation of cell adhesion *In preparation.*

Contribution by VC:
Cell culture, HRMS[1]-DIA phosphoproteomics experiment, performance of the LC-MS/MS measurements, data analysis, bioinformatics, manuscript writing.

2.3.1 Abstract

Dermokine, a protein influencing keratinocyte differentiation and epidermal renewal, has been shown to play a critical role in maintaining skin homeostasis and the skin's barrier function. Despite substantial upregulation of dermokine under conditions of skin injury or inflammation, its exact role in epidermal stratification remains poorly understood. The protein is known to exist in three major isoforms – dermokine-α, dermokine-β, and dermokine-γ, each with unique domain architectures that contribute to diverse biological processes. In this study, we utilized automation-aided phosphoproteomics enrichment to compare phosphoproteomes from *Dmkn* $\alpha\beta^{-/-}$ and *Dmkn* $\beta\gamma^{-/-}$ keratinocytes to those from wildtype cells. We implemented a modified HRMS[1] DIA method to enhance phosphopeptide identifications and quantifications. Our results revealed that disruption of dermokine isoforms led to a decreased phosphorylation of the tyrosine kinase Src and the protein tyrosine phosphatase receptor type κ, along with an increased phosphorylation of catenin δ 1. By integrating this information, we suggest that the binding of dermokine affects adherens junctions within the epidermis. Therefore, this indicates that dermokine influences the differentiation of keratinocytes by acting upon cellular adhesion through kinase-dependent signaling, thus providing a better understanding of its role in maintaining skin homeostasis and potentially revealing novel therapeutic targets for skin diseases.

2.3.2 Introduction

Keratinocyte differentiation and epidermal renewal play critical roles in maintaining skin homeostasis and the skin's barrier function, which can be disrupted by injury or inflammatory skin diseases. Dermokine (DMKN), a protein that is significantly upregulated under these conditions, has not been well-characterized for its role in epidermal stratification (Leclerc et al., 2014). In a physiological context, within the first five days after injury, DMKN-β is

present in relatively high amounts at the wound margin, persisting throughout the wound healing process and re-epithelialization, suggesting a functional contribution of DMKN to the phenotype of wound keratinocytes (Leclerc et al., 2014).

DMKN, along with suprabasin and keratinocyte differentiation-associated protein, forms part of the secreted protein gene complex (SSC), which plays a vital role in the suprabasal layer of stratified epithelium (Matsui et al., 2004; Moffatt et al., 2004; Oomizu et al., 2000; Park et al., 2002; Tsuchida et al., 2004). These genes do not only group tightly together in their genomic locus and transcribe in the same direction, but their resultant gene products are synthesized concurrently during epidermal stratification.

DMKN is expressed in three major isoforms — DMKN-α, DMKN-β, and DMKN-γ, each exhibiting unique domain architectures that play crucial roles in different biological processes. DMKN-β is the longest isoform, encompassing all four key domains: two globular domains (1 and 2), a collagen-like domain, and a keratin-like domain. In contrast, DMKN-γ contains the first three domains (globular 1, collagen-like, and keratin-like), DMKN-α is composed solely of the globular domain 2 also known as cytokine-like domain. The cytokine-like domain, close to the C-terminus of DMKN-β and integral to DMKN-α, contributes significantly to the functionality of this bioactive molecule within the extracellular space (Higashi et al., 2012). Notably, while DMKN-γ is produced by differential splicing of the DMKN-β gene product, DMKN-α is expressed from an alternative promoter and can exert redundant biological activity (Matsui et al., 2004). Consistent with previous findings, it has been demonstrated that the globular C-terminal domain of DMKN-β is essential for modulation of ERK1/2 phosphorylation in cultured keratinocytes (Higashi et al., 2012). However, it was also observed that the treatment of cultured keratinocytes with recombinant DMKN-β did not affect Akt phosphorylation levels (Higashi et al., 2012). These events have been assigned to the direct binding of DMKN-β to GRP78 by immunoprecipitation-mass spectrometry (Higashi et al., 2012).

Notably, GRP78 has also been recognized as a significant contaminant in affinity purification-mass spectrometry experiments, and the observed effects have been relatively minor (Mellacheruvu et al., 2013). Thus, employing a phosphoproteomic approach is needed to elucidate the influence of DMKN on downstream signalling events through receptor interactions in keratinocytes. This comprehensive method of analysis will illuminate the intricate downstream effects induced by DMKN's interaction with these receptors at the level of protein phosphorylation.

Here, we exploited current cutting-edge DIA-based phosphoproteomics techniques to investigate the changes in phosphorylation in human keratinocytes upon disruption of either the DMKN $\beta\gamma$ or the $\alpha\beta$ isoforms. We not only acquired the to our knowledge most comprehensive keratinocyte phosphoproteome with 15468 phosphorylated sites but could also quantify several important keratinocyte regulatory proteins. We could identify changes in adherens junction proteins, such as p120-catenin, Src and receptor-type tyrosine-protein phosphatase κ upon ablation of either the α or β isoform, with more pronounced effects upon depletion of both these isoforms containing the cytokine-like domain.

2.3.3 Experimental Procedures

N/TERT keratinocytes cell culture and lysis. Human keratinocyte telomerase reverse transcriptase immortalized (h/TERT immortalized) N/TERT-1 cells derived from clinically normal foreskin tissue (A et al., 2000) were a kind gift from Prof. Edel O'Toole (Queen Mary University, London, United Kingdom). N/TERT-1 keratinocytes as well as the N/TERT-1 *Dmkn* $\alpha\beta^{-/-}$ and N/TERT-1 *Dmkn* $\beta\gamma^{-/-}$ keratinocytes (see chapter 2.1 for more details) were grown in DMEM/F-12 growth medium supplemented with RM+ (DMEM/F-12 (Thermo Fisher Scientific, Waltham, MA, 11-320-033), 10% FBS (Thermo Fisher Scientific, 11550356), 1% penicillin/streptomycin [P/S] (Sigma-Aldrich, Darmstadt, Germany, P0781), 0.4 μg/mL hydrocortisone

(Sigma-Aldrich, H4881), 0.5 μg/mL insulin (Sigma-Aldrich, I5500), 10 ng/mL epidermal growth factor (Bio-Rad, Hercules, CA, PMP89), 0.1 nM cholera toxin (Sigma-Aldrich, C8052), 5 μg/mL transferrin (Sigma-Aldrich, T2252), 20 pM liothyronine (Sigma-Aldrich, T6397)) and incubated at 37 °C, 5% CO_2. All cell lines were tested mycoplasm negative. Briefly, cells were washed three times with PBS (PAN Biotech, Aidenbach, Germany, P04-361000) and incubated in DMEM/F-12 (Thermo Fisher Scientific) without growth factors for 24 h. Afterwards, cells were scraped from the dishes and the cell suspension was transferred into a falcon tube, centrifuged at 500 x g for 3 min, 4 °C, the supernatant was discarded and the cell pellet was resuspended in PBS, for a total of three washes. The resuspended cells were transferred into an Eppendorf tube (Eppendorf, Hamburg, Germany, 0030 121.023) and once more centrifuged at 500 x g for 3 min, 4 °C to remove the supernatant and frozen in liquid nitrogen.

Sample preparation for MS analysis. Protein concentration was determined by BCA assay (Thermo Fisher Scientific, 23227), and adjusted protein lysates (2 μg/μL in 8 M Urea (Sigma-Aldrich, U5128) and 50 mM tris(hydroxymethyl)aminomethane hydrochloride (Tris-HCl) (Sigma-Aldrich, 1.08219) (pH 8.0)) were stored at -80 °C until further use. 200 μg lysate per sample were reduced with dithiothreitol (DTT) (Sigma-Aldrich, DTT-RO) (1 mM final concentration), alkylated by iodoacetamide (Sigma-Aldrich, I6125) (5 mM final concentration), and digested with Lys-C (FUJIFILM Wako Pure Chemical Corporation, Osaka, Japan, 125-05061) in an enzyme/protein ratio of 1:100 (w/w) for 2 h, shaking, followed by an 8-fold dilution with 50 mM Tris-HCl (Sigma-Aldrich) (pH 8.0) to 1 M Urea (Sigma-Aldrich) and further digested overnight with trypsin (Promega, Madison, WI, V5113) 1:100 (w:w). Protease activity was quenched by acidification with trifluoroacetic acid (Sigma-Aldrich, T650) (TFA) to a final concentration of approximately 1% and peptides were purified by SPE using HR-X columns (Macherey-Nagel, Düren, Germany, 730936P45) in combination with C18 cartridges (Macherey-

Nagel, 731802) (Hu et al., 2021). The peptides were frozen in liquid nitrogen and lyophilized prior to phosphopeptide enrichment.

Automated phospho-peptide enrichment. The enrichment of phosphopeptides was executed automatically through a Bravo Automated Liquid Handling Platform (Agilent, Santa Clara, CA). The Fe (III)-NTA cartridges (Agilent, G5496-60085) (5 μL) were initially primed with 200 μL 0.1% TFA (Sigma-Aldrich) in acetonitrile and then balanced with 0.1% TFA in 80% acetonitrile (Thermo Fisher Scientific, 85174) (equilibration/washing buffer). Peptides were redissolved in 200 μL of equilibration buffer and loaded onto the cartridges at a flow rate of 5 μL/min. Cartridges were then rinsed twice with 200 μL of washing buffer at a flow rate of 10 μL/min. Phosphopeptides were extracted first with 50 μL of 1% ammonia followed by 50 μL of 1% ammonia in 80% acetonitrile (Thermo Fisher Scientific) at a flow rate of 5 μL/min into 5 μL of 99% formic acid (Thermo Fisher Scientific, 270480250). These samples were then concentrated via a lyophilizer and reconstituted in 20 μL of 0.1% formic acid (Thermo Fisher Scientific) for subsequent LC-MS/MS analysis.

Data independent acquisition nanoflow LC-MS/MS for proteome analysis. HRMS^1-DIA proteome data sets were acquired at the DTU Proteomics Core at Technical University of Denmark.

For each resuspended keratinocyte proteome, peptides were analysed using the pre-set '20 samples per day' method on the EvoSep One instrument (EvoSep, Odense, Denmark). Peptides were eluted over an EvoSep One defined 58-min gradient and analysed by mass spectrometry, Orbitrap Exploris 480 (Thermo Fisher Scientific), with following settings: Spray voltage was set to 2.3 kV, funnel RF level at 40, and heated capillary at 240 °C. Full MS spectra were collected at a resolution of 120000, with an AGC target of 300% or maximum injection time set to 'auto' and a scan range of 400–1000 m/z. The MS^2 spectra were obtained in DIA mode in the Orbitrap operating at a resolution of 30000, with an AGC target 1000% or maximum injection time set to

'auto', a normalised HCD collision energy of 32. The isolation window was set to 8 m/z with a 1 m/z overlap and window placement on. Each DIA experiment covered a range of 200 m/z resulting in three DIA experiments (400-600 m/z, 600-800 m/z and 800-1000 m/z). Between the DIA experiments a full MS scan is performed. MS performance was verified for consistency by running complex cell lysate quality control standards, and chromatography was monitored to check for reproducibility.

Data independent acquisition nanoflow LC-MS/MS for phosphopeptide analysis. HRMS^1-DIA phosphoproteomics data sets were acquired at the Metabolomics and Proteomics Platform (MAPP) at University of Fribourg.

Each resuspended enriched keratinocyte phosphoproteome was analysed with an Easy-nLC 1200 (Thermo Fisher Scientific) coupled to an Orbitrap Exploris 480 mass spectrometer (Thermo Fisher Scientific) operated with a DIA method; 5 μL of each sample was injected. Peptides were separated on a fused silica HPLC-column tip (I.D. 75 μm, New Objective, self-packed with ReproSil-Pur 120 C18-AQ, 1.9 μm (Dr. Maisch, Ammerbuch-Entringen, Germany, r119.aq.) to a length of 20 cm) using a gradient of mobile phase A (0.1% formic acid in water) and mobile phase B (0.1% formic acid in 80% acetonitrile in water). The column temperature was maintained at 50 °C using the EASY-Spray oven. The total gradient time was 140 min and went from 6% to 23% acetonitrile (ACN) in 95 min, followed by 30 min to 38%. This was followed by 5 min increase to 60% ACN, and a washout by 10 min increase to 90% ACN. Flow rate was kept at 250 nL/min. Re-equilibration was done prior to sample pickup and prior to loading with a volume of 4 μL of 0.1% FA buffer at a maximum pressure of 750 bar. Spray voltage was set to 1.9 kV, funnel RF level at 40, and heated capillary at 275 °C. Full MS spectra were collected at a resolution of 120000, with an AGC target of 300% or maximum injection time set to 'auto' and a scan range of 400–1400 m/z. The MS^2 spectra were obtained in DIA mode in the Orbitrap operating at a resolution of

60000, with an AGC target 1000% or maximum injection time set to 'auto' and a normalised HCD collision energy of 32. The isolation window was set to 6 m/z with a 1 m/z overlap and window placement on, resulting in 175 DIA windows. Each DIA experiment covered a range of 200 m/z resulting in three DIA experiments (400-600 m/z, 600-800 m/z, 800-1000 m/z, 1000-1200 m/z and 1200-1400 m/z). Between the DIA experiments, a full MS scan was performed. All data were acquired in profile mode using positive polarity, application mode was set to peptide, FAIMS mode was not installed, advanced peak determination was set to true, and default charge state was set to 2. MS performance was verified for consistency by running complex cell lysate quality control standards, and chromatography was monitored to check for reproducibility.

Raw data processing. Two independent searches for the proteome and phosphopeptide samples were performed.

For the proteome, raw files were analysed using Spectronaut™(Biognosys, Schlieren, Switzerland, version 17.4) directDIA+ (deep) default settings, spectra were matched against the homo sapiens reference FASTA database (UP000005640; downloaded from Uniprot on 27th of December 2022). Dynamic modifications were set as Oxidation (M) and Acetyl on protein N-termini. Cysteine carbamidomethyl was set as a static modification. Protein quantitation was done on the MS^1 level, data filtering set to Q-value and the data was normalized by RT-dependent local regression model (Callister et al., 2006) and protein groups were inferred by IDPicker.

For phosphopeptides, raw files were analysed using Spectronaut™ (Biognosys, version 17.4) directDIA+ (deep), spectra were matched against the homo sapiens database (UP000005640; downloaded from Uniprot on 27th of December 2022) with the BGS Phospho PTM workflow with the following modifications: deamidation (NQ) and oxidation (M) were added as dynamic modifications together with Phospho (STY) and Acetyl on protein N-termini. Cysteine carbamidomethyl was set as a static modification. All results were

filtered to a 1% FDR, data filtering set to Q-value and protein quantitation done on the MS^1 level (Xuan et al., 2020). The data was cross-normalized by a RT-dependent local regression model on modified (phospho)-peptides (Callister et al., 2006). The PTM probability cutoff was set to 0.

Bioinformatics analysis. Most of the data analysis was performed using custom scripts in R (R Core Team, 2022).

First, the Spectronaut™(version 17.4) report was filtered for a cutoff of 0.6 for "FG.ShapeQualityScore (MS^1)". Data at protein and phospho-site level were processed using R (version 4.2.0). For kinase substrate enrichment analysis, the filtered Spectronaut™(Biognosys, version 17.4) reports were transformed into modification-specific peptide-like reports using the plugin peptide collapse in Perseus (version 2.0.9.0), with EG.PTMAssayProbability as grouping column (Hogrebe et al., 2018; Tyanova et al., 2016). A localization cutoff of 0.75 was applied and the same variable PTMs as listed above, and summed intensities were $\log_2$-transformed. Downstream data analysis was performed by filtering for a minimum of two valid values in at least one treatment group, and no imputation was performed. The limma package was employed to calculate the fold change as well as the moderated p-value for the comparisons between genotypes (Ritchie et al., 2007). This calculation was conducted for both the phosphopeptides and the $\log_2$-transformed protein abundance values, providing a comprehensive overview of changes (Ritchie et al., 2007). In brief, Next, phosphorylation events were further distinguished between products of kinase/phosphatase activity and changes in global protein quantity by subtracting the fold change of global protein quantities from the fold change of the phosphorylated peptides. The result of this operation allowed identifying those phosphorylation sites whose changes were likely driven by variations in kinase/phosphatase activity (Kauko et al., 2015).

High-throughput phosphoproteomics datasets were aligned with upstream kinases by inferring kinase activity through clustering phosphorylation sites based on either their known kinase targets (profile score) or their common

phosphorylation motifs (motif score) (Casado et al., 2013; Kim et al., 2021).

To calculate the profile score, the quantification of each phosphosite was first z-transformed. Then, these phosphosites were mapped to any previously known *in-vitro* or *in-vivo* kinases acting on the quantified site, by intersecting quantified substrate-kinase pairs from PhosphoSitePlus®. This correlation then informed the calculation of the profile matching scores (Hornbeck et al., 2015; Kim et al., 2021). For the motif score, a motif matching score was computed by ranking the seven preceding and the seven subsequent amino acids of each quantifiable phosphosite against the phosphorylation affinities of kinases. Finally, the combined score for each phosphosite in relation to a specific kinase was determined by averaging the motif and profile matching scores, with due consideration for the quantity of sequences and substrates involved in the computation of the kinase's motif and profile (Kim et al., 2021). Adaptive sampling machine learning was applied to minimize positive-unlabeled phosphorylated sites by iterative estimation of the probability of class mislabeling and generate a predictive score for each phosphosite (Yang et al., 2019).

2.3.4 Results

Experimental setup, spectral processing and data analysis strategy. To identify effects of endogenously expressed dermokine (DMKN) isoforms on phosphorylation in human keratinocytes, we recorded deep quantitative phosphoproteomes from replicates of wildtype cells in comparison to samples from either *Dmkn* $\beta\gamma^{-/-}$ (DTU $\beta\gamma^{-/-}$) or *Dmkn* $\alpha\beta^{-/-}$ (CS $\alpha\beta^{-/-}$) keratinocytes (Figure 2.14A). This allowed us to monitor the activity of the bioactive dermokine β isoform and possible compensatory effects mediated by the alternative promoter driven dermokine α variant (Utsunomiya et al., 2020).

To enrich the samples for phosphorylated peptides, we performed automated Fe(III)-NTA enrichment for each sample to not only reduce variation in sample handling but also increase the pull-out efficiency and robustness

of the experiment. The HRMS^1-DIA strategy employed for this study was modified from the original method to cover a higher mass range (400-1400 m/z) (Figure 2.14B) (Bekker-Jensen et al., 2020; Xuan et al., 2020). The empirically determined median peak width was 0.91 min, and the median full width at half maximum was 0.53 min. Each MS^1 window consisted of 175 MS^2 (6 m/z) DIA windows, achieving a final cycle time of 5.17 s, resulting in 10 median data points per peak on MS^1 level with a gradient length of 140 min (Figure 2.14B). The acquired mass spectra were searched without using a spectral library, utilizing Spectronaut™(version 17.4) that allowed for the fast identification and quantification of phosphopeptides (Figure 2.14C) (Bruderer et al., 2015).

Dermokine isoform ablation leads to differential effects on protein and phosphopeptide abundance in keratinocytes. Deepening our *in-silico* analysis, we simultaneously analysed the non-enriched fraction of each sample, utilizing the same high-resolution mass spectrometry (HRMS^1)-DIA method (Figure 2.14B). This exhaustive proteomic analysis yielded 5522 distinct proteins (Figure 2.16C). Notably, this proteome composition reflected remarkable differences between the two knockout models: in the *Dmkn* $\beta\gamma^{-/-}$, we found 753 significantly differentially abundant proteins, with 343 showing decreased abundance and 410 showing increased abundance (Figure 2.16C). The *Dmkn* $\alpha\beta^{-/-}$, in contrast, displayed even more dramatic changes, with 1612 significantly differentially abundant proteins, of which 490 decreased and 1122 increased in abundance when compared to samples from wildtype cells.

Applying a HRMS^1-DIA phosphoproteomics method and a rigorous data analysis strategy (Figure 2.14C), we identified a total of 41817 phosphopeptides in 4609 proteins, of which 34634 phosphopeptides passed the MS^1 peak shape filter (Figure 2.16A). In addition, we calculated absolute phosphorylation site stoichiometry, utilizing a Perseus plugin which allowed for determination of phosphorylation sites independent of transcription regulation modify-

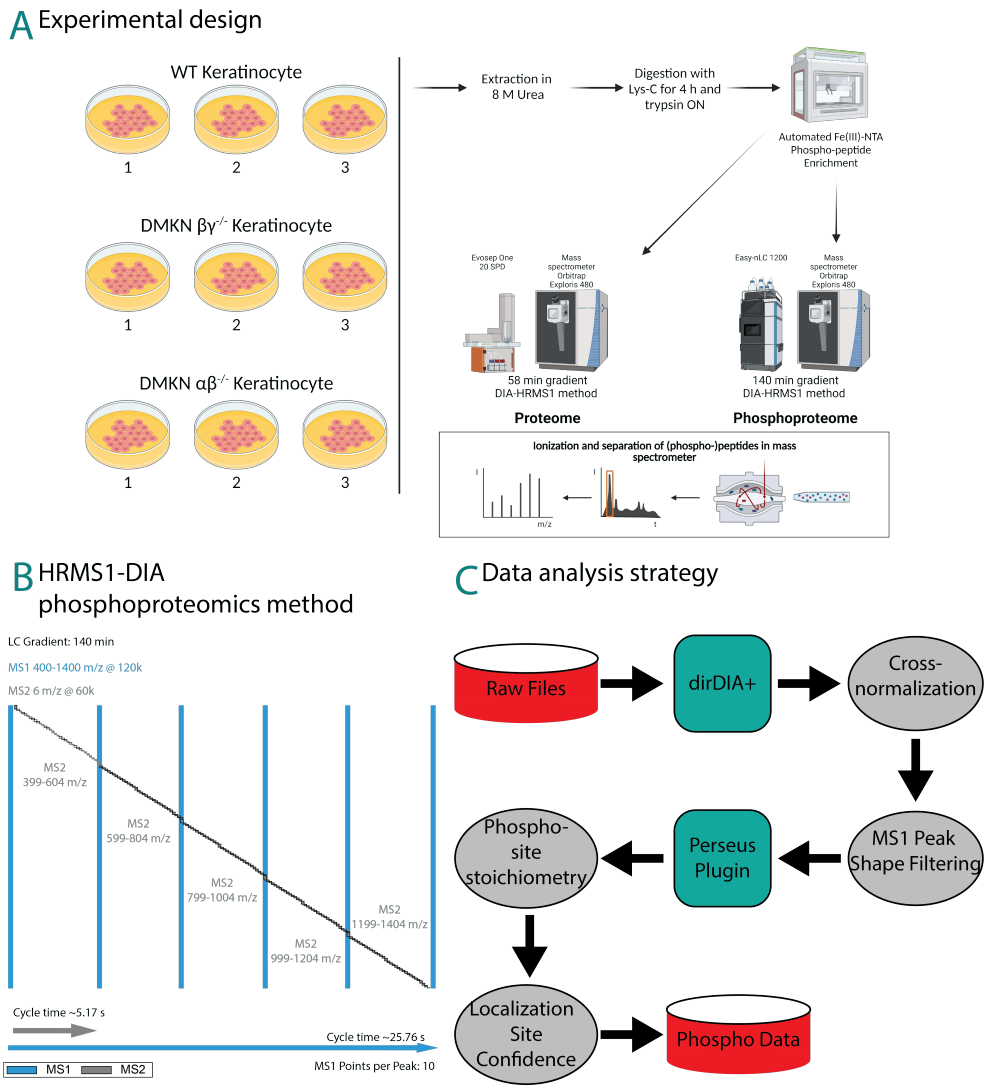

Figure 2.14. (Continued on the following page.)

Figure 2.15. Experimental details of semi-automated HRMS^1-DIA phosphoproteomics of *Dmkn* $\alpha\beta^{-/-}$ and *Dmkn* $\beta\gamma^{-/-}$ keratinocytes. A. The serum-deprived *Dmkn* $\alpha\beta^{-/-}$, *Dmkn* $\beta\gamma^{-/-}$ or wildtype keratinocytes were lysed and digested overnight with trypsin and Lys-C. Utilizing the Agilent Bravo likquid handling system, the samples were enriched using Fe(III)-NTA cartridges and prepared for LC-MS/MS to acquire both the proteome and phosphoproteome. **B.** The HRMS^1-DIA phosphoproteomics raw files were recorded applying a DIA method that utilizes window-wide MS^1 (200 m/z) over a range of 400-1400 m/z with small MS^2 DIA windows (6 m/z) totaling in 175 MS^2 windows. Utilizing a 140 min LC gradient the empirically obtained cycle time was 5.17 seconds resulting in 10 median data points per peak. **C.** The raw files were subjected to spectral library-free directDIA+ searches, applying a cut-off to the parameter "MS^1 Peak Shape Filtering" to determine reliable peaks. A Perseus Plugin was further utilized to calculate absolute phosphorylation site stoichiometry and a filter of 0.75 was applied to remove non-confidently assigned phosphorylation sites.

ing protein abundance (Hogrebe et al., 2018; Tsai et al., 2015). Since a phosphorylated peptide might contain more than one serine, threonine or tyrosine, each potential phosphosite was ranked by a localization score (>0.75), allowing us to keep 15468 confident phosphosites (Figure 2.16A) (Bekker-Jensen et al., 2020). Finally, to remove non-quantified conditions we removed phosphosites that were not 70% present in at least one condition, leaving 11740 high-confidence phosphosite assignments (2.16A). Notably, we successfully obtained 646 tyrosine phosphosites without the need for specific tyrosine specific enrichment methods (Vemulapalli et al., 2022).

In terms of variability within our data, we undertook a coefficient of variance analysis. This revealed that for the proteome level (at a protein base), our data showed less than 20% median CV ratio (Figure S2.21A). On the phosphopeptide level (at a peptide base), we observed less than 30% for the knockouts, and slightly higher at 36% for the wildtype (Figure S2.21B).

We employed an unsupervised machine learning technique, known as Principal Component Analysis (PCA), to visualize the differences among our samples. Interestingly, we observed that both *Dmkn* truncated samples were markedly distinct from the wildtype keratinocytes at both the proteome and phosphoproteome levels (Figure S2.21C and 2.21D). Additionally, we noticed

that the *Dmkn* $\alpha\beta^{-/-}$ clustered closely together and separated distinctly from the *Dmkn* $\beta\gamma^{-/-}$, once again noticeable at both proteome and phosphoproteome levels (Figure S2.21C and 2.21D). This consistent observation along both proteome and phosphoproteome levels underlines the different molecular profiles of these samples.

Applying an absolute fold change cut-off of 1.5 and a limma moderated p-value lower than 0.05 we were able to scrutinize significant differential phosphosites (Figure 2.16D) (Ritchie et al., 2007). We identified 177 significantly increased phosphosites (Figure 2.16D) under endogenous DMKN quantities.

Kinase-enrichment analysis reveals distinct and additive sets of activated kinases by dermokine isoforms in keratinocytes. To align identified phosphosites with upstream kinases, we applied a modified PhosR strategy (Kim et al., 2021) and first investigated the downstream effects of isoform disruption in *Dmkn* $\beta\gamma^{-/-}$ in comparison to wildtype keratinocytes expressing endogenous levels of DMKN. To illustrate the kinase substrate relationships the combined score of the 2 highest ranking phosphorylated sites for each identified kinase in our kinase substrate enrichment analysis (KSEA) were illustrated in a heatmap (Figure 2.17). Hereby, we could identify SRC S17, CAV2 Y19 and PML S38 (Figure 2.17A), of which SRC was not only identified as active kinase but was also increased in abundance in wildtype compared to DMKN $\beta\gamma$ knockout keratinocytes.

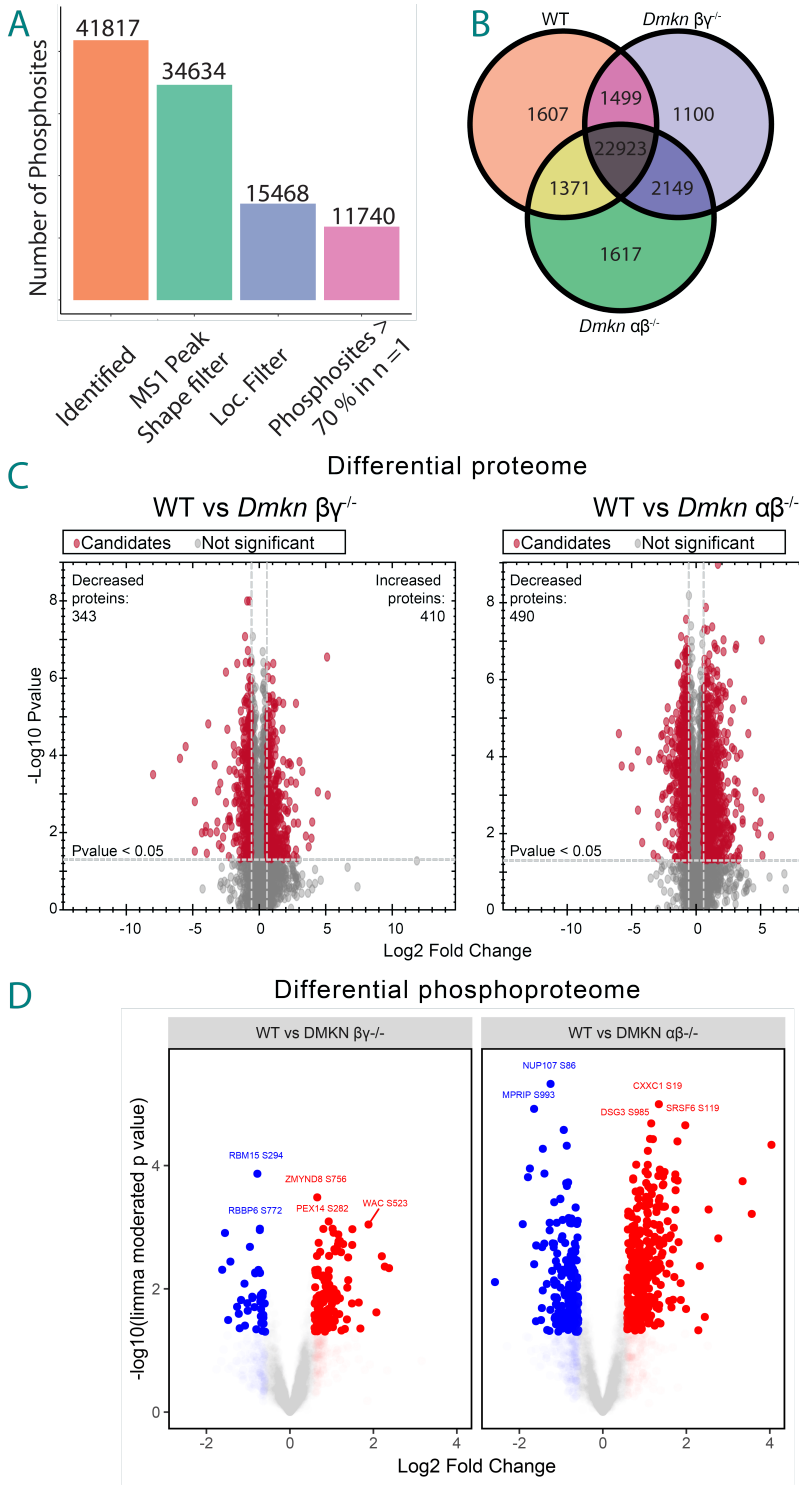

Figure 2.16. (Continued on the following page.)

Figure 2.16. Sensitive HRMS^1-DIA phosphoproteomics for *Dmkn* $\alpha\beta^{-/-}$ and *Dmkn* $\beta\gamma^{-/-}$ keratincytes—identification and quantification. A. Identification of 41817 phosphopeptides after analysis with Spectronaut™(version 17.4) using the library-free directDIA+ algorithm, resulting in 34634 identifications after applying the peak shape filter of 0.6. Removing non-confident phosphorylation sites using a cut-off of 0.75 for the PTM localization score resulted in 15468 reliably quantified phosphosites. Removing phosphosites that are not at least 70% present in at least one condition, the remaining 11740 phosphosites were computed. **B.** The Venn diagram, featuring the 34634 phosphopeptides that passed the MS^1 peak shape filtering criteria, reveals a substantial overlap of 22923 phosphopeptides among all three conditions. **C** provides a detailed depiction of the proteome composition, showcasing a total of 5522 proteins. The comparison of *Dmkn* $\beta\gamma^{-/-}$ and *Dmkn* $\alpha\beta^{-/-}$ keratinocytes to the wildtype reveals 753 and 1612 significantly differentially abundant proteins, respectively. **D.** The two volcano plots visualize phosphopeptides. The p-value was determined using an empirical Bayes method. In grey are non-significant, non-differentially abundant phosphosites. Red illustrates the significantly ($-\log_{10}(0.05)$) increased sites and blue the significantly decreased sites, comparing wildtype keratinocytes to either *Dmkn* $\beta\gamma^{-/-}$ or *Dmkn* $\alpha\beta^{-/-}$ keratinocytes.

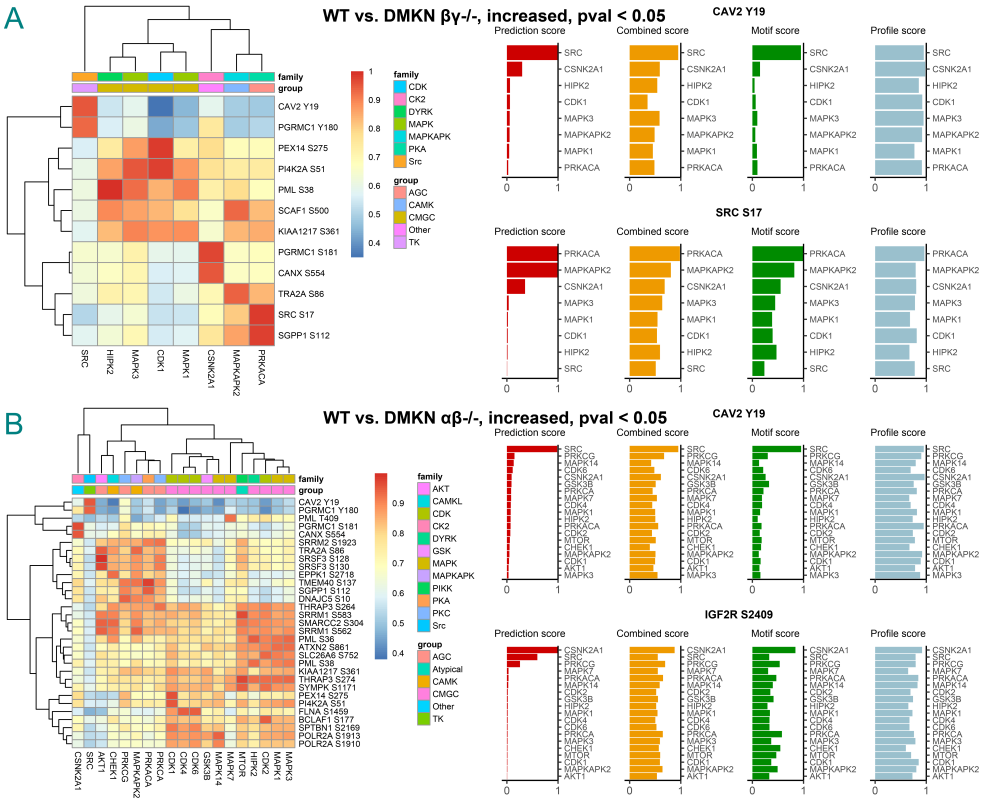

Figure 2.17. (Continued on the following page.)

Figure 2.17. Clustering of DMKN-dependent significantly increased phosphorylation sites. A. Kinase substrate enrichment analysis of phosphosites with significantly ($\log_2(1.5)$ and a limma moderated pvalue lower than 0.05) increased abundance in wildtype compared to *Dmkn* $\beta\gamma^{-/-}$ keratinocytes. The two substrates CAV2 (Y19) SRC (S17) illustrate the kinase profile by aligning the phosphorylation site to prior experimental perturbations (profile score) and comparing the flanking sequence (-7 amino acids, S/T/Y, +7 amino acids) to kinase motif preferences. The weighted combination of both profile and motif score is illustrated in the form of a heatmap, where the substrates are vertically aligned and the kinases are horizontally shown. The predictive score provides means to recognize unlabeled phosphosites that are phosphorylated by a specific kinase. **B.** Kinase substrate enrichment analysis of phosphosites with significantly ($\log_2(1.5)$ and a limma moderated pvalue lower than 0.05) increased abundance in wildtype compared to *Dmkn* $\alpha\beta^{-/-}$ keratinocytes. The two substrates CAV2 (Y19) and IGF2R (S2409) illustrate the assignment of regulating kinases. Identified kinases are illustrated in form of a heatmap, with vertical alignment of substrates and a horizontal illustration of kinases.

Utsunomiya et al. recently described the compensatory effect of the alternative promoter driven DMKN α isoform in DMKN $\beta\gamma$ knockout skin, yet the exact mechanisms of the underlying molecular process are not clear (Utsunomiya et al., 2020). In line with these previous observations, we could observe that the additive deletion of the compensatory DMKN α isoform in the *Dmkn* $\alpha\beta^{-/-}$ keratinocytes had a more pronounced effect on phosphorylation when comparing to the wildtype (Figure 2.16D), which became particularly evident when the two comparisons were superimposed (Figure 2.16E) (Utsunomiya et al., 2020). In detail, we attributed 19 kinases to 382 significantly increased phosphosites in wildtyppe compared to *Dmkn* $\alpha\beta^{-/-}$ keratinocytes, of which 11 were phosphorylated tyrosines (”PGRMC1 Y180 ”, ”PGRMC2 Y210 ”, ”PEX14 Y290 ”, ”MATR3 Y202 ”, ”CAV2 Y19 ”, ”ILF3 Y867 ”, ”PRPF4B Y849 ”, ”NECTIN1 Y418 ”, ”RMDN3 Y53 ”, ”HNRNPUL1 Y216 ” and ”BCLAF1 Y284 ”) and mostly assigned to the tyrosine kinase SRC (Figure 2.17B). As observed in previous studies the tyrosine kinase SRC activity is modulated in the presence of growth factors (Aghib & McCrea, 1995; Mariner et al., 2001; Mendonsa et al., 2020). Interestingly, we observed several kinase groups in our heatmap, sharing combined scores for several

substrates, group 1 (”MAPK3”, ”MAPK1”, ”CDK2”, ”HIPK2”, ”MTOR”), group 2 (”MAPK14”, ”GSK3B”, ”CDK6”, ”CDK4”, ”CDK1”) and group 3 (”PRKCA”, ”PRKCA”, ”PRKACA”, ”MAPKAPK2”, ”PRKCG”, ”CHEK1”, ”AKT1”). SRC and CSNK2A1 exhibited a distinctive grouping or association among themselves.

Monitoring kinase activity indicates significant SRC activity in response to presence of dermokine isoforms. Having established the KSEA to determine the kinase in question for our relevant phosphorylated sites, we analysed kinase activity profiles along their genotypes. For every kinase under consideration, the function identified the corresponding substrates. It then computed the median values of these substrates' quantification across all kinases for each sample and finally pairwise testing was performed to comprehensively analyze the genotype in contrast to the wildtype. In the comparison analysis between wildtype and DMKN $\beta\gamma^{-/-}$ keratinocytes, eight kinases were identified, but only two - CDK1 and MAPK3 - showed significant differences, as depicted in Figure 2.18A. In line with predictions, when wildtype keratinocytes were compared to *Dmkn* $\alpha\beta^{-/-}$ keratinocytes, the results indicated a noteworthy difference in 12 distinct kinases, underscoring the impact of not only DMKN β but also DMKN α on kinase activity in these cells (Figure 2.18B). Beyond CDK1 and MAPK3, our investigation revealed several other kinases - specifically CDK2, CHEK1, CSNK2A1, HIPK2, MAPK1, MAPK14, MAPK3, MAPKAPK2, PRKACA, PRKCA, PRKCG and SRC - that also showed significant differences Figure 2.18B).

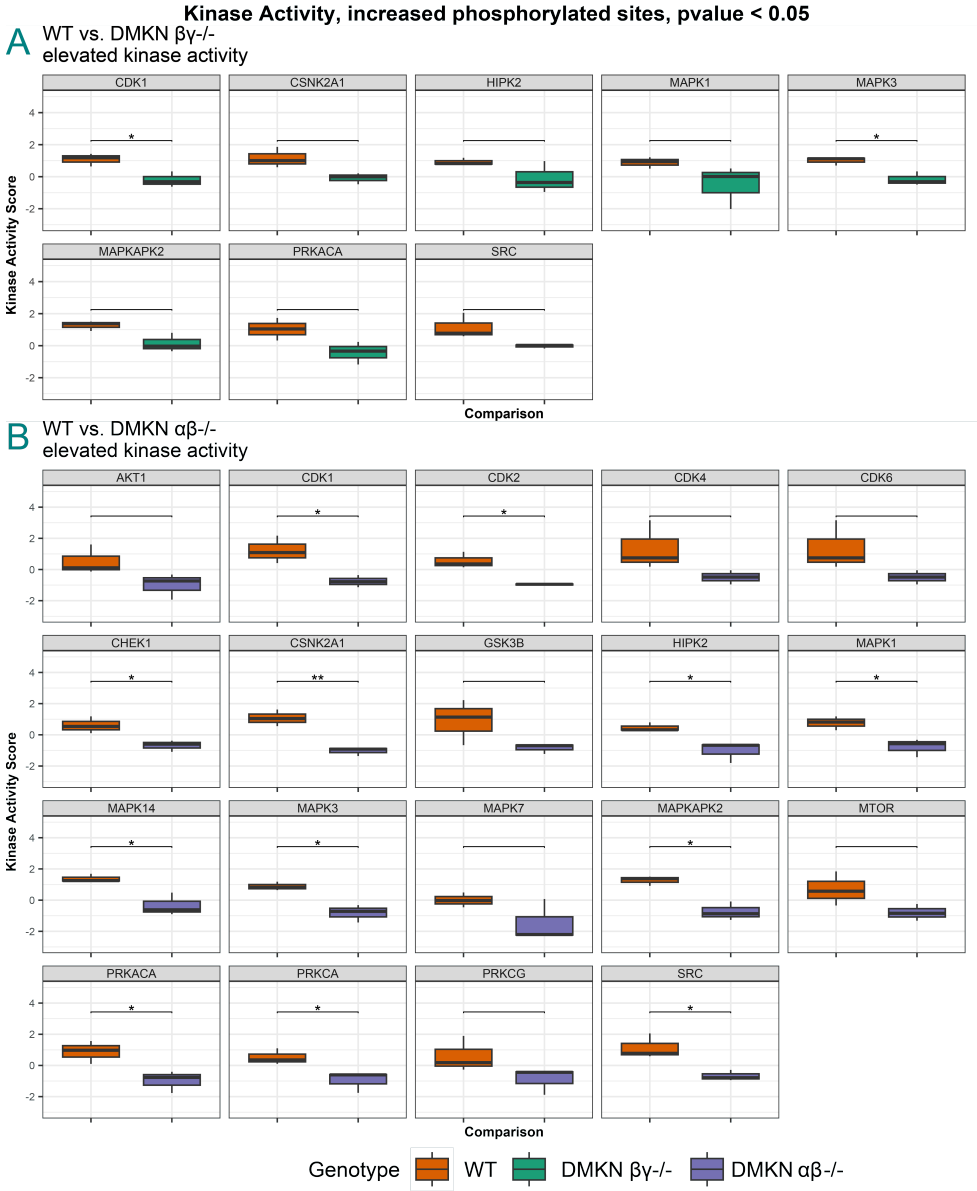

Figure 2.18. **Kinase activity profiles of identified kinases in the kinase substrate enrichment analysis. A.** The median substrates' quantification values were computed for each kinase for comparing wildtype with *Dmkn* $\beta\gamma^{-/-}$ keratinocytes. Two kinases were significantly differentially enriched, CDk1 and MAPK3. **B.** The median substrates' quantification values were computed for each kinase for comparing wildtype with *Dmkn* $\alpha\beta^{-/-}$ keratinocytes. Several kinases were significantly differentially enriched, CDk1, CDK2, CHEK1, CSN2KA1, HIPK2, MAPK1, MAPK14, MAPK3, MAPKAPK2, PRKACA, PRKCA and SRC.

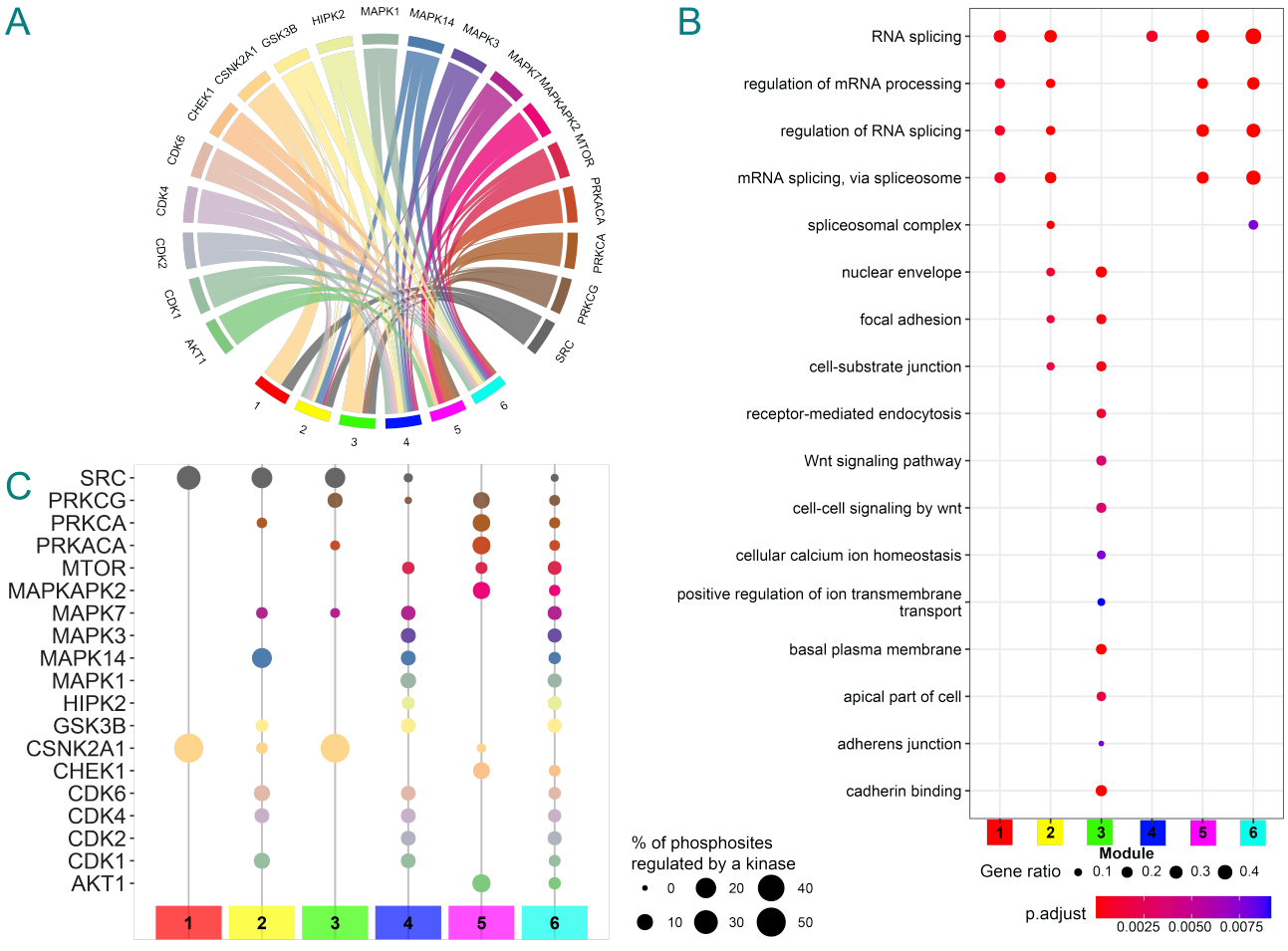

Figure 2.19. (Continued on the following page.)

Figure 2.19. Clustering of DMKN-dependent significantly increased phosphorylation site. A. Hierarchical clustering, applying the "ward.D" method of significantly increased proteins and their respective phosphosite for the comparison wildtype keratinocytes versus *Dmkn* $\alpha\beta^{-/-}$ keratinocytes. Phosphosites assigned to the clusters were above a combined score of 0.8. **B.** Gene Ontology over-representation analysis of protein modules, assigning biological processes mostly associated with modules 1,4,5, and 6. Modules 2 and 3 contain phosphorylated proteins associated with biological processes, such as focal adhesion, cadherin binding, adherens junctions, and wnt signalling pathway. **C.** Kinase profiles of each protein module, marking each module upon the percentage of kinase activity.

Cluster analysis identifies functional modulation of focal adhesions and adherens junctions by dermokine isoforms. Proteins frequently feature multiple phosphorylation sites, each potentially targeted by a different kinase. When analyzing phosphoproteomic data, some methods focus on each phosphosite independently, neglecting the broader context of the host protein. Conversely, other approaches concentrate solely on the overall protein, which can lead to the omission of specific phosphosite details. To address this, we employed a comprehensive kinase-substrate scoring system. This facilitated construction of hierarchical cluster plots 2.19, enabling simultaneous examination of phosphorylation modifications both within a single protein and across different proteins. This integrated approach allowed us to pinpoint proteins experiencing regulation by multiple kinases across phosphosites. We imposed a strict cutoff for the combined score (>0.8), considering only phosphorylated proteins and their sites which maintained a high degree of consistency in their kinase-substrate relationship (Figure 2.19A) (Kim et al., 2021). Our investigative focus was mainly on phosphosites exhibiting a significant increase in the comparison between wildtype and DMKN α/β-ablated cells. This strategic consideration was motivated by our interest in discerning those phosphosites which become notably active following DMKN binding and subsequent induction of downstream phosphorylation. However, our analysis did not extend to β/γ ablated cells owing to the insufficient numbers of differentially abundant phosphosites in this context. Within the 6 defined modules, where numerous kinases are interacting, we identified specific ones – module 1, module 2, and

module 3, which allowed us to expand the analysis, aiming at understanding kinases 'SRC' and 'CSNK2A1' which were particularly influential within these modules (Figure 2.19C). Through Gene Ontology over-representation analysis, we further explored the distinct functionalities of modules 1, 4, 5, and 6 (Figure 2.19B). These modules were primarily associated with terms related to gene expression and RNA splicing, suggesting proteins assigned to these clusters, together with their phosphorylation sites, have key roles in gene transcription into mRNA and subsequent mRNA processing—critical stages in gene expression pathways (Figure 2.19B).

Intriguingly, modules 2 and 3 exhibited a distinct array of terms related to the regulation of focal adhesions, adherens junctions and wnt signalling pathways. Module 2, despite containing multiple kinases, was partially governed by the actions of kinases CSNK2A1, SRC and PRKACA (Figure 2.19C). This hints at the potential involvement of these kinases in processes that determine the cell's functional state, associated with focal adhesion and cell-substrate junction. Conversely, Module 3 exhibited a more well-defined scenario with five clearly attributed kinases - CSNK2A1, MAPK7, PRKACA, PRKCG and SRC - controlling the phosphorylation of specific sites (Figure 2.19C). The presence of these kinases suggests that they play a vital role in the activities of Module 3. The regulation of distinct phosphorylation sites by these kinases could be a determining factor in driving the biological mechanisms related to this module. The functions associated with this module extended beyond focal adhesion, encompassing a diverse range of cellular processes such as receptor-mediated endocytosis, which involves the selective uptake of molecules, the wnt signalling pathway, which is essential for cell differentiation and proliferation, adherens junctions, which contribute to cellular adhesion, and cadherin binding, which plays a significant role in cell-cell adhesion. This broad range of biological activities emphasizes the complex role of this module in controlling and managing various cellular functions (Figure 2.19C). It also suggests the potential influence of DMKN on determining the keratinocyte phenotype. Therefore, it highlights DMKN's possible critical role in guiding the course of

cell behavior in keratinocytes. Table S2.7 illustrates the distinct sites identified to be related to each term. It is worth noting that two EGFR sites (S1042 and T693) were pinpointed within the focal adhesion, along with several ITG β 4 sites (S1474, S1517, T1471 and T1530), and a few CAV2 sites (S20, S23 and S36), one of which is directly phosphorylated by SRC. The EGFR sites also seem to play an essential role in cadherin binding and the wnt signalling pathway.

Differential phosphorylation events reveal DMKN-dependent downstream signalling events. In an effort to consolidate the phosphorylated proteins detected in our *Dmkn* $\alpha\beta^{-/-}$ keratinocytes study, we focused primarily on those identified in the Gene Ontology over-representation analysis (Table S2.7). We paid particular attention to proteins associated with focal adhesion and adherens junctions. Despite our consideration on these aspects, our coefficient analysis, normalized to protein levels, did not reveal any significant changes in the difference between phosphorylation and protein levels within the focal adhesion complex. The coefficient analysis involved calculating the differences of phosphorylation to protein fold changes for each protein, which allowed for a direct comparison of phosphorylation levels across different proteins while accounting for differences in overall protein abundance (Figure 2.20B and 2.20C) (Kauko et al., 2015). This methodology ensured that the analysis did not merely rely on transcriptional regulation but accurately reflected the degree of kinase/phosphatase phosphorylation quantities, enabling a more comprehensive interpretation of our phosphorylation data (Kauko et al., 2015).

We uncovered intriguing alterations in phosphorylation status under endogenous DMKN levels. Most notably, under these conditions, we observed diminished phosphorylation at several CTNN δ 1 sites (S265, S268, Y291, and Y296) (Figure S2.22), likely due to the action of the receptor-type tyrosine-protein phosphatase κ (PTPRκ). This dephosphorylation enhances the affinity of CTNN δ 1 towards CDH1, suggesting a role for DMKN in modulating

cadherin strength and adherens junction stability (Figure 2.20B).

In our current working model, DMKN forms a complex with one of the candidate RTKs. This receptor-ligand interaction induces a phosphorylation cascade involving multiple intracellular effectors. Importantly, the phosphorylation status of PTPRκ (S854, S856 and Y858) was found to be elevated under normal DMKN levels. This suggests that DMKN plays a role in regulating the balance of phosphorylation and dephosphorylation events in keratinocytes (Figure 2.20B).

Most notably, under endogenous DMKN levels, we observed diminished phosphorylation at several CTNN δ 1 sites (S265, S268, Y291 and Y296), likely due to the action of the phosphatase PTPRκ. This dephosphorylation enhances the affinity of CTNN δ 1 towards CDH1, suggesting a pivotal role for DMKN in modulating cadherin strength and adherens junction stability (Figure 2.20B).

2.3.5 Discussion

Dermokine (DMKN) has been identified as a member of the stratified epithelium secreted peptides complex (SSC) and through loss-of-function analyses strongly related to keratinocyte differentiation (Matsui et al., 2004). The protein is produced in several isoforms generated by differential splicing and alternative promoter usage, with three major secreted isoforms in human epidermis α β and γ (Naso et al., 2007), and highly increased in inflammatory skin diseases or upon injury (Leclerc et al., 2014). The α and β isoforms are driven by alternative promoters and both comprise a C-terminal cytokine-like domain that has been implicated in triggering intracellular kinase signalling cascades (Higashi et al., 2012). DMKN γ is driven by the same promoter as β but only comprises an N-terminal domain of β and lacks the cytokine-binding region. A compensatory effect of the α isoform for ablation of dermokine β/γ in mice has been demonstrated (Utsunomiya et al., 2020) and targeted analyses performed to validate DMKN-β dependent effects on protein phosphoryla-

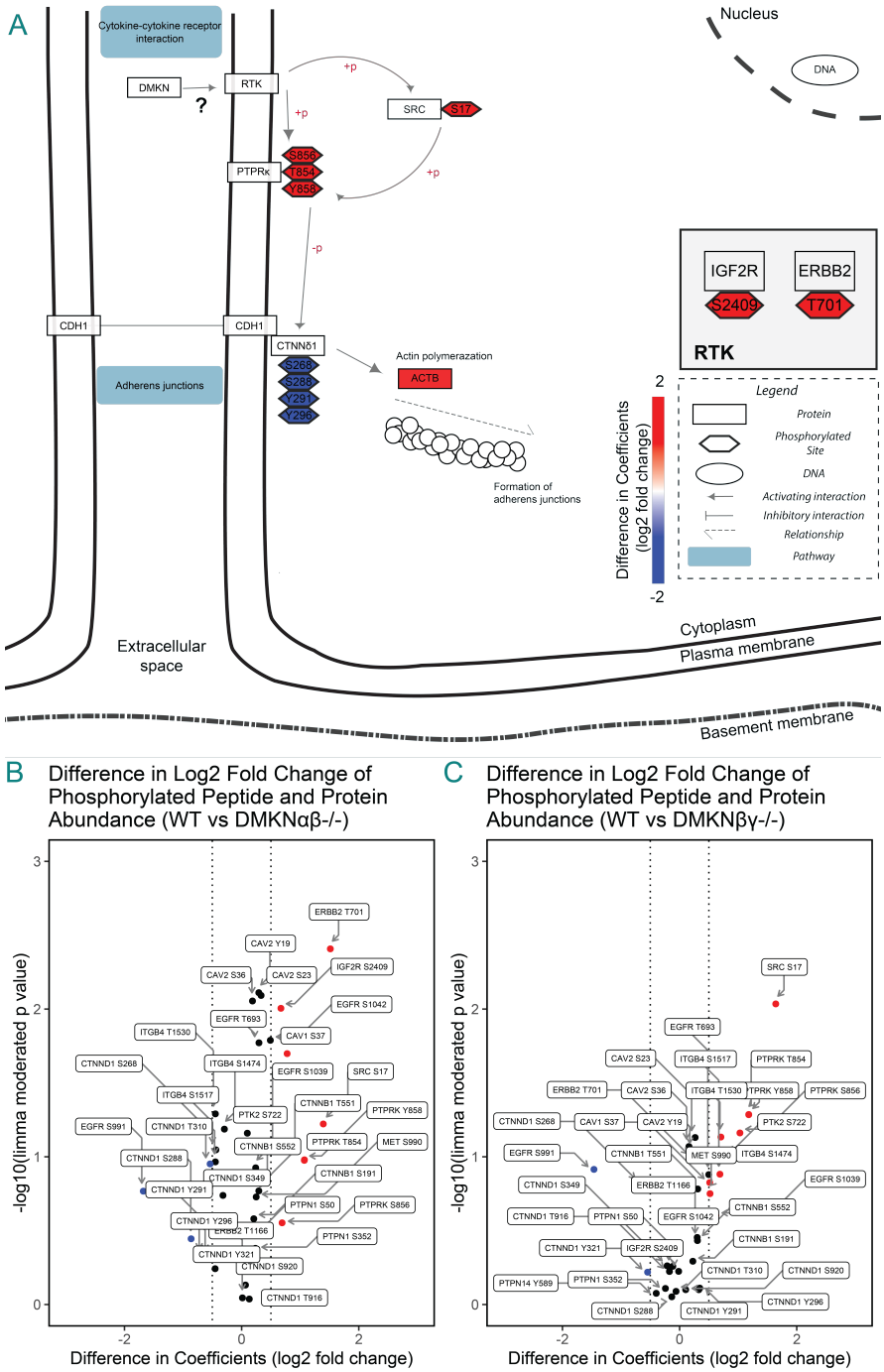

Figure 2.20. (Continued on the following page.)

Figure 2.20. Systems biology graphical notation map of working model for DMKN-dependent downstream signalling events. A. Upon activation by a receptor tyrosine kinase (RTK) such as ERBB2 (T701) or IGF2R (S2409), intracellular phosphorylation cascades are triggered. This leads to the activation of SRC. Simultaneously, the activated RTK induces direct phosphorylation on PTPRκ and possibly indirect via activated SRC, which activates its dephosphorylating activity. This causes the dephosphorylation of CTNN δ 1 at sites S268, Y296, Y291, and S288, increasing its affinity towards CDH1 and strengthening cell-cell adhesion. Please note, the values in the corresponding plot represent the differential phosphorylation levels normalized to the protein abundance ($\log_2$ fold change of WT vs *Dmkn* $\alpha\beta^{-/-}$). Specifically, the plot showcases the differential phosphorylation status of peptides, after subtracting the global changes in protein abundance ($\log_2$ fold change of WT vs KO). This normalization helps to distinguish changes in phosphorylation from overall changes in protein levels. In this study, only phosphorylation sites with a difference coefficient higher than 0.5 were considered significant, except for the sites on CTNN δ 1. Modified from: hsa04520 Pathway - Adherens junction - Homo sapiens (human). **B.** This volcano plot represents the differential phosphorylation status of peptides between the wildtype (WT) and the double knockout of *Dmkn* $\alpha\beta^{-/-}$. The values plotted are derived from the difference between the $\log_2$ fold change of phosphorylated peptides and the $\log_2$ fold change of global protein abundance (WT vs *Dmkn* $\alpha\beta^{-/-}$). This differential visualization highlights changes in phosphorylation status that are beyond changes in overall protein levels. Notably, only phosphorylation sites with an absolute difference coefficient of 0.5 were considered. **C.** This volcano plot depicts the differential phosphorylation status of peptides between the wildtype (WT) and the double knockout of *Dmkn* $\beta\gamma^{-/-}$. The plotted values represent the difference between the $\log_2$ fold change of phosphorylated peptides and the $\log_2$ fold change of global protein abundance (WT vs *Dmkn* $\beta\gamma^{-/-}$). This method of visualization emphasizes changes in phosphorylation status that can't be attributed merely to changes in overall protein levels. Notably, only phosphorylation sites with an absolute difference coefficient of 0.5 were considered.

tion in keratinocytes (Higashi et al., 2012). However, global phosphoproteome analyses of the distinctly expressed and bioactive α and β isoforms are lacking that are needed to understand underlying kinase signalling pathways and relate them to molecular and cellular alterations that might result from or cause abnormalities contributing to pathological skin conditions. Here, we apply an advanced proteomics and phosphoproteomics workflow together with a thorough data analysis strategy on DMKN-β/γ and DMKN-α/β deficient human keratinocytes in comparison to wildtype cells. This analysis provides to our

knowledge the most comprehensive phosphoproteome of this cell type to date, validates the compensatory effect of DMKN-α for β on a molecular level, and reveals an effect of DMKN on keratinocyte adhesion through kinase-dependent signalling (Mishra et al., 2017; Öhman et al., 2014; Patil et al., 2021; Patil et al., 2019).

Recent advances in automation-aided sample preparation and fully-robotic enrichment of phosphorylated peptides as well as state-of-art LC-MS/MS instrumentation have vastly expanded the identification rate of phosphopeptides (Post et al., 2017). Together with high resolution data independent acquisition methods and sophisticated data analysis strategies we can reliably quantify not only novel phosphosites but link known phosphorylated serines, threonines or tyrosines to a specific kinase (Xuan et al., 2020). Kinase substrate enrichment analysis (KSEA) provides the means to link protein substrates to kinases, thus generating insightful phosphorylation patterns (Casado et al., 2013). In a first step, we aimed at further enhancing our existing strategy for phosphopeptide acquisition.

Our methodological change involved reducing the MS^2 window size to 6 m/z. The purpose of this reduction was to allow a broader exploration of the mass spectrum, expanding the mass range from the previous 400 to a more comprehensive 1400 m/z (Bekker-Jensen et al., 2020). This expansion contributed to the high coverage, as it included phosphopeptides that might have been lost due to a slightly elevated mass. In our subsequent step, we introduced a 140-minute liquid chromatography (LC) gradient, specifically chosen to enhance the separation of the compounds within our sample. These methodological adjustments presumably contributed to the comprehensive coverage of high-confidence phoshopeptide identifications in keratinocytes, exceeding numbers identified in previous studies (Mishra et al., 2017; Öhman et al., 2014; Patil et al., 2021; Patil et al., 2019). To further support these findings, detailed method comparisons are needed that were not primary aim of our study.

Guided by the Gene Ontology (GO) annotations, we scrutinized each term,

focusing on the specific phosphorylation sites that we had quantified (Carbon et al., 2019). Initially, we considered an increase in the abundance of several receptors under endogenous DMKN levels, including MET at site S990, ERBB2 at site T701, and IGF2R at site S2409 (Bohnsack et al., 2014; Chmielowiec et al., 2007; Dahlhoff et al., 2017; Haensel & Dai, 2018; Ramírez Moreno & Bulgakova, 2022). These receptors with key functions in various cellular processes such as proliferation, survival, and differentiation, constitute essential components of the cell signalling network. Understanding their phosphorylation mechanism in response to DMKN could provide new insights relating its activity to the regulation of keratinocyte proliferation and differentiation. ERBB2, at phosphorylation site T701, undergoes phosphorylation by kinases such as MAPK1/3, which plays an considerable role in its molecular association and protein conformation (Chen et al., 2017; Kawasaki et al., 2016). Additionally, this phosphorylation event is known to suppress ERBB2 receptor internalization, an essential process modulating cell surface receptor quantities and their responsiveness to external signals (Capparelli et al., 2018; Chen et al., 2017; Kawasaki et al., 2016).

IGF2R, specifically at phosphorylation site S2409, is targeted by CSNK2A1, a kinase that was found to be considerably more active under endogenous DMKN quantities. This observation aligns with previous studies on the cytoplasmic domain of the 300 kDa mannose-6-phosphate receptor (Rosorius et al., 1993). Despite the increased abundance of MET at phosphorylation site S990, our study found that the impact of its phosphorylation on receptor activity or its involvement in cellular processes was elusive (Organ & Tsao, 2011).

Focal adhesions are fundamental structures in keratinocyte biology to establish dynamic junctions between a cell and its surrounding extracellular matrix, providing both physical support and facilitating communication (Turner, 2000; Wu, 2007). However, upon correcting the phosphorylation levels of focal adhesion proteins by their protein abundance, our data did not reveal any differential changes in the phospho-protein-to-protein ratio, suggesting that the DMKN levels did not greatly mediate the phosphorylation status of these

proteins, yet modifications are because of transcriptional regulation.

Adherens junctions represent critical structures within cellular architecture, contributing to the maintenance of tissue coherence (Niessen, 2007). The cohesive function is especially critical in the context of keratinocytes, where adherens junctions are instrumental in their development and in defining their phenotypic attribute (Zijl et al., 2022). *Zijl et al.* elucidated the pivotal purpose of adhesion mechanisms in the differentiation of keratinocytes. Their findings illustrate that keratinocytes considerably rely on their adhesive competence for proper stratification. When adhesion levels decrease, keratinocytes experience a substantial phenotypic transformation, transitioning towards a migratory state, which is indicative of the phenotype of transient amplifying keratinocytes throughout wound healing (Usui et al., 2008; Zijl et al., 2022).

Furthermore, we observed an increase in the β-actin (ACTβ) protein expression in the presence of DMKN, which presents interesting possibilities for understanding cellular adhesion mechanisms, given the established link between elevated ACTβ and the formation of more robust focal adhesions (Vedula et al., 2021). Such increased ACTβ quantities might provide a mechanistic explanation for DMKN-associated modulations in cellular adhesion and motility (Vedula et al., 2021).

Under such circumstances, we detected several dephosphorylated sites on catenin δ 1 (CTNN δ 1) protein. Also known as p120-catenin, CTNN δ 1 is a critical factor of adherens junctions, contributing to their stability and function (Kourtidis et al., 2013). It is acknowledged to strengthen cell adhesion by dephosphorylation through its interaction with cadherins, a family of proteins that mediate cell-cell adhesion (Mendonsa et al., 2020). Interestingly, we noticed a decrease in CTNN δ 1 phosphorylation at multiple sites (S265, S268, Y291 and Y296), indicating a change in the regulation of adherens junctions in keratinocytes (Shashikanth et al., 2015). Interestingly, this decrease might be orchestrated by the activity of the protein tyrosine phosphatase receptor type κ (PTPRκ), which was also found to be phosphorylated in our analysis (Fearnley et al., 2019).

Indeed, the phosphorylation of PTPRκ can lead to its enzymatic activation, which can then dephosphorylate targets such as p120-catenin and enhance their association with cadherin, promoting cell-cell adhesion (Xu et al., 2005).In the interaction between PTPRκ and growth factor signalling, growth factor stimulation has been established to activate the tyrosine phosphorylation of PTPRκ (Fearnley et al., 2019). This phosphorylation, possibly through the inhibition of protein-tyrosine phosphatases (PTPs) by oxidation induced by receptor tyrosine kinases, may have a considerable impact on cellular signalling (Fearnley et al., 2019). Thereby, PTPRκ phosphorylation could alter its phosphatase activity, enhancing PTPRκ's efficiency in removing phosphate groups from its substrates, such as CTNN δ 1 (Hay et al., 2022). This would lead to a decrease in CTNN δ 1 phosphorylation, as observed in our analysis. It is known that the dephosphorylation of CTNN δ 1 improves its ability to reinforce cell adhesion via interactions with cadherins (Oas et al., 2013). Consequently, the observed decrease in CTNN δ 1 phosphorylation, potentially induced by the activated PTPRκ, could increase adhesive contact area, possibly facilitating the formation and stabilization of adherens junctions (Mendonsa et al., 2020; Reynolds & Roczniak-Ferguson, 2004).

In our study, the increased activity and phosphorylation of SRC, at site S17, were also detected, especially under the influence of endogenous DMKN levels. SRC, a critical factor in modulating adherens junctions, has a considerable effect on cell migration and interactions with the extracellular matrix (Arias-Salgado et al., 2003; Shattil, 2005). Of note, the S17 site on SRC is phosphorylated by cAMP-dependent protein kinase catalytic subunit α (PRKACA), according to PhosphoSitePlus® (Gould & Hunter, 1988). Hereby, PRKACA was found to phosphorylate SRC on S17, which inhibits ERKs and cell proliferation illustrating the crucial anti-proliferative function of SRC (Schmitt & Stork, 2002). In light of these results, the phosphorylation of SRC at S17 in the context of endogenous DMKN levels indicates a potential regulation of adhesion modulation and cell proliferation. The implications of this phosphorylation event, particularly in relation to DMKN levels, require

further analyses.

As part of our investigation, we first examined the abundance of quantifiable phosphopeptides. This analysis allowed us to gain an essential understanding of potential phosphorylation sites present in our samples and which kinase and phosphatase might be inducing the phosphorylation. In order to further explore the complexities of phosphorylation regulation by upstream kinases and phosphatases, we then corrected these results by protein levels. This step proved to be critical in our understanding of the correlation between phosphorylation, regulated by upstream kinases and phosphatases and transcriptionally-mediated protein abundance (Kauko et al., 2015). As such, the phosphorylation of CTNN δ 1, SRC, and PTPR κ was not influenced by protein abundances, as their levels remained constant. In contrast, the increased phosphorylation observed in ITG β 4 was attributable to the increase in ITG β 4 protein quantities, suggesting that the ratio of phosphorylated to non-phosphorylated molecules of ITG β 4 was not the determining factor, as opposed to changes in the rate of the phosphorylation process itself.

Finally, our research indicates that DMKN orchestrates cell adhesion via intricate downstream phosphorylation pathways through the modulation of adhesive junctions. This regulatory mechanism has significant implications for epidermal biology, where reliable adhesion is crucial for cohesive differentiation (Zijl et al., 2022). In the context of keratinocyte biology, the induction of robust cell adhesion by DMKN is an essential process ensuring differentiation and stratification. This observed effect aligns with the necessity for keratinocytes to firmly adhere to each other, thereby establishing the multilayered structure of the epidermis, consecutively with the suprabasal DMKN expression in the epidermis (Hasegawa et al., 2013). Our results indicate that cell adhesion is active under normal DMKN quantities through a convoluted, multi-modal system involving the dephosphorylation of CTNN δ 1 - through PTPRκ, inducing the polymerization of ACTβ thus the formation of adherens junctions. We propose this complex network of interactions that elucidates a calibrated mechanism in which these proteins altogether function to regu-

late cellular adherence. This emphasizes the intricate level of governance in cellular adhesion mechanisms, highlighting the elaborateness and specificity of cellular signalling in response to DMKN and its subsequent downstream signalling events. However, further validations of uncovered phosphorylation events are necessary to corroborate the results.

2.3.6 Acknowledgments

We thank Dr. Valdemaras Petrosius (Technical University of Denmark, Denmark) for the discussions regarding MS[1] peak picking data analysis. This work was supported by a Novo Nordisk Foundation Young Investigator Award (NNF16OC0020670 to U.a.d.K) and funding from the LEO Foundation (LF-OC-19-000033 to U.a.d.K). Figure 2.14A was created by Biorender. UadK and JD are members of the SKINTEGRITY.CH collaborative research program.

2.3.7 References

A, D. M., C, H. W., Yasushi, I., Vincent, R., Y, W. J., A, W. R., N, L. D., P, L. F., & G, R. J. (2000). Human Keratinocytes That Express hTERT and Also Bypass a p16INK4a-Enforced Mechanism That Limits Life Span Become Immortal yet Retain Normal Growth and Differentiation Characteristics. *Molecular and Cellular Biology*, *20*(4), 1436–1447.

Aghib, D. F., & McCrea, P. D. (1995). The E-cadherin Complex Contains the src Substrate p120. *Experimental Cell Research*, *218*(1), 359–369.

Arias-Salgado, E. G., Lizano, S., Sarkar, S., Brugge, J. S., Ginsberg, M. H., & Shattil, S. J. (2003). Src kinase activation by direct interaction with the integrin β cytoplasmic domain. *Proceedings of the National Academy of Sciences*, *100*(23), 13298–13302.

Bekker-Jensen, D. B., Bernhardt, O. M., Hogrebe, A., Martinez-Val, A., Verbeke, L., Gandhi, T., Kelstrup, C. D., Reiter, L., & Olsen, J. V. (2020). Rapid and site-specific deep phosphoproteome profiling by data-independent acquisition without the need for spectral libraries. *Nature Communications*, *11*(1), 1–12.

Bohnsack, R. N., Warejcka, D. J., Wang, L., Gillespie, S. R., Bernstein, A. M., Twining, S. S., & Dahms, N. M. (2014). Expression of Insulin-Like Growth Factor 2 Receptor in Corneal Keratocytes During Differentiation and in Response to Wound Healing. *Investigative Ophthalmology & Visual Science*, *55*(12), 7697.

Bruderer, R., Bernhardt, O. M., Gandhi, T., Miladinović, S. M., Cheng, L.-Y., Messner, S., Ehrenberger, T., Zanotelli, V., Butscheid, Y., Escher, C., Vitek, O., Rinner, O., & Reiter, L. (2015). Extending the Limits of Quantitative Proteome Profiling with Data-Independent Acquisition and Application to Acetaminophen-Treated Three-Dimensional Liver Microtissues * [S]. *Molecular & Cellular Proteomics*, *14*(5), 1400–1410.

Callister, S. J., Barry, R. C., Adkins, J. N., Johnson, E. T., Qian, W. J., Webb-Robertson, B. J. M., Smith, R. D., & Lipton, M. S. (2006). Normalization approaches for removing systematic biases associated with mass spectrometry and label-free proteomics. *Journal of proteome research*, *5*(2), 277–286.

Capparelli, C., Purwin, T. J., Heilman, S. A., Chervoneva, I., McCue, P. A., Berger, A. C., Davies, M. A., Gershenwald, J. E., Krepler, C., & Aplin, A. E. (2018). ErbB3 Targeting Enhances the Effects of MEK Inhibitor in Wild-Type BRAF/NRAS Melanoma. *Cancer Research*, *78*(19), 5680–5693.

Carbon, S., Douglass, E., Dunn, N., Good, B., Harris, N. L., Lewis, S. E., Mungall, C. J., Basu, S., Chisholm, R. L., Dodson, R. J., Hartline, E., Fey, P., Thomas, P. D., Albou, L. P., Ebert, D., Kesling, M. J., Mi, H., Muruganujan, A., Huang, X., … Westerfield, M. (2019). The Gene Ontology Resource: 20 years and still GOing strong. *Nucleic Acids Research*, *47*(D1), D330–D338.

Casado, P., Rodriguez-Prados, J.-C., Cosulich, S. C., Guichard, S., Vanhaesebroeck, B., Joel, S., & Cutillas, P. R. (2013). Kinase-substrate enrichment analysis provides insights into the heterogeneity of signaling pathway activation in leukemia cells. *Sci Signal*, *6*(268), rs6.

Chen, C.-H., Hsia, T.-C., Yeh, M.-H., Chen, T.-W., Chen, Y.-J., Chen, J.-T., Wei, Y.-L., Tu, C.-Y., & Huang, W.-C. (2017). MEK inhibitors induce Akt activation and drug resistance by suppressing negative feedback ERK-mediated HER2 phosphorylation at Thr701. *Molecular Oncology*, *11*(9), 1273–1287.

Chmielowiec, J., Borowiak, M., Morkel, M., Stradal, T., Munz, B., Werner, S., Wehland, J., Birchmeier, C., & Birchmeier, W. (2007). c-Met is

essential for wound healing in the skin. *The Journal of Cell Biology*, *177*(1), 151.

Dahlhoff, M., Gaborit, N., Bultmann, S., Leonhardt, H., Yarden, Y., & Schneider, M. R. (2017). CRISPR-assisted receptor deletion reveals distinct roles for ERBB2 and ERBB3 in skin keratinocytes. *The FEBS Journal*, *284*(19), 3339–3349.

Fearnley, G. W., Young, K. A., Edgar, J. R., Antrobus, R., Hay, I. M., Liang, W.-C., Martinez-Martin, N., Lin, W., Deane, J. E., & Sharpe, H. J. (2019). The homophilic receptor PTPRK selectively dephosphorylates multiple junctional regulators to promote cell–cell adhesion (T. Hunter, J. A. Cooper, T. Hunter, A. Yap, & M. Tremblay, Eds.). *eLife*, *8*, e44597.

Gould, K. L., & Hunter, T. (1988). Platelet-derived growth factor induces multisite phosphorylation of pp60c-src and increases its protein-tyrosine kinase activity. *Molecular and Cellular Biology*, *8*(8), 3345–3356.

Haensel, D., & Dai, X. (2018). Epithelial-to-mesenchymal transition in cutaneous wound healing: Where we are and where we are heading. *Developmental Dynamics*, *247*(3), 473–480.

Hasegawa, M., Higashi, K., Yokoyama, C., Yamamoto, F., Tachibana, T., Matsushita, T., Hamaguchi, Y., Saito, K., Fujimoto, M., & Takehara, K. (2013). Altered expression of dermokine in skin disorders (2012/06/01). *J Eur Acad Dermatol Venereol*, *27*(7), 867–875.

Hay, I. M., Mulholland, K. E., Lai, T., Graham, S. C., Sharpe, H. J., & Deane, J. E. (2022). Molecular mechanism of Afadin substrate recruitment to the receptor phosphatase PTPRK via its pseudophosphatase domain (T. Hunter, J. A. Cooper, T. Hunter, & S. Knapp, Eds.). *eLife*, *11*, e79855.

Higashi, K., Hasegawa, M., Yokoyama, C., Tachibana, T., Mitsui, S., & Saito, K. (2012). Dermokine-β impairs ERK signaling through direct binding to GRP78. *FEBS Letters*, *586*(16), 2300–2305.

Hogrebe, A., Von Stechow, L., Bekker-Jensen, D. B., Weinert, B. T., Kelstrup, C. D., & Olsen, J. V. (2018). Benchmarking common quantification strategies for large-scale phosphoproteomics. *Nature Communications 2018 9:1*, *9*(1), 1–13.

Hornbeck, P. V., Zhang, B., Murray, B., Kornhauser, J. M., Latham, V., & Skrzypek, E. (2015). PhosphoSitePlus, 2014: mutations, PTMs and recalibrations. *Nucleic Acids Res*, *43*(Database issue), 512–520.

Hu, Z., Sankar, D. S., Vu, B., Leytens, A., Vionnet, C., Wu, W., Stumpe, M., Martínez-Martínez, E., Stork, B., & Dengjel, J. (2021). ULK1 phospho-

rylation of striatin activates protein phosphatase 2A and autophagy. *Cell Reports*, *36*(13).

Kauko, O., Laajala, T. D., Jumppanen, M., Hintsanen, P., Suni, V., Haapaniemi, P., Corthals, G., Aittokallio, T., Westermarck, J., & Imanishi, S. Y. (2015). Label-free quantitative phosphoproteomics with novel pairwise abundance normalization reveals synergistic RAS and CIP2A signaling. *Scientific Reports 2015 5:1*, *5*(1), 1–17.

Kawasaki, Y., Sakimura, A., Park, C. M., Tomaru, R., Tanaka, T., Ozawa, T., Zhou, Y., Narita, K., Kishi, H., Muraguchi, A., & Sakurai, H. (2016). Feedback control of ErbB2 via ERK-mediated phosphorylation of a conserved threonine in the juxtamembrane domain. *Scientific Reports*, *6*(1), 31502.

Kim, H. J., Kim, T., Hoffman, N. J., Xiao, D., James, D. E., Humphrey, S. J., & Yang, P. (2021). PhosR enables processing and functional analysis of phosphoproteomic data. *Cell Reports*, *34*(8).

Kourtidis, A., Ngok, S. P., & Anastasiadis, P. Z. (2013). p120 catenin: an essential regulator of cadherin stability, adhesion-induced signaling, and cancer progression. *Progress in molecular biology and translational science*, *116*, 409.

Leclerc, E. A., Huchenq, A., Kezic, S., Serre, G., & Jonca, N. (2014). Mice deficient for the epidermal dermokine β and γ isoforms display transient cornification defects. *Journal of Cell Science*, *127*(13), 2862–2872.

Mariner, D. J., Anastasiadis, P., Keilhack, H., Böhmer, F.-D., Wang, J., & Reynolds, A. B. (2001). Identification of Src Phosphorylation Sites in the Catenin p120ctn*. *Journal of Biological Chemistry*, *276*(30), 28006–28013.

Matsui, T., Hayashi-Kisumi, F., Kinoshita, Y., Katahira, S., Morita, K., Miyachi, Y., Ono, Y., Imai, T., Tanigawa, Y., Komiya, T., & Tsukita, S. (2004). Identification of novel keratinocyte-secreted peptides dermokine-α/- β and a new stratified epithelium-secreted protein gene complex on human chromosome 19q13.1. *Genomics*, *84*(2), 384–397.

Mellacheruvu, D., Wright, Z., Couzens, A. L., Lambert, J. P., St-Denis, N. A., Li, T., Miteva, Y. V., Hauri, S., Sardiu, M. E., Low, T. Y., Halim, V. A., Bagshaw, R. D., Hubner, N. C., Al-Hakim, A., Bouchard, A., Faubert, D., Fermin, D., Dunham, W. H., Goudreault, M., … Nesvizhskii, A. I. (2013). The CRAPome: a contaminant repository for affinity purification-mass spectrometry data (2013/08/08). *Nat Methods*, *10*(8), 730–736.

Mendonsa, A. M., Bandyopadhyay, C., & Gumbiner, B. M. (2020). p120-catenin phosphorylation status alters E-cadherin mediated cell adhesion and ability of tumor cells to metastasize. *PLOS ONE*, *15*(6), e0235337–.

Mishra, A., Oulès, B., Pisco, A. O., Ly, T., Liakath-Ali, K., Walko, G., Viswanathan, P., Tihy, M., Nijjher, J., Dunn, S. J., Lamond, A. I., & Watt, F. M. (2017). A protein phosphatase network controls the temporal and spatial dynamics of differentiation commitment in human epidermis. *eLife*, *6*.

Moffatt, P., Salois, P., St-Amant, N., Gaumond, M.-H., & Lanctôt, C. (2004). Identification of a conserved cluster of skin-specific genes encoding secreted proteins. *Gene*, *334*, 123–131.

Naso, M. F., Liang, B., Huang, C. C., Song, X. Y., Shahied-Arruda, L., Belkowski, S. M., D'Andrea, M. R., Polkovitch, D. A., Lawrence, D. R., Griswold, D. E., Sweet, R. W., & Amegadzie, B. Y. (2007). Dermokine: An extensively differentially spliced gene expressed in epithelial cells. *Journal of Investigative Dermatology*, *127*(7), 1622–1631.

Niessen, C. M. (2007). Tight junctions/adherens junctions: basic structure and function. *The Journal of investigative dermatology*, *127*(11), 2525–2532.

Oas, R. G., Nanes, B. A., Esimai, C. C., Vincent, P. A., García, A. J., & Kowalczyk, A. P. (2013). p120-catenin and β-catenin differentially regulate cadherin adhesive function. *Molecular Biology of the Cell*, *24*(6), 704–714.

Öhman, T., Söderholm, S., Hintsanen, P., Välimäki, E., Lietzuén, N., MacKintosh, C., Aittokallio, T., Matikainen, S., & Nyman, T. A. (2014). Phosphoproteomics combined with quantitative 14-3-3-affinity capture identifies SIRT1 and RAI as novel regulators of cytosolic double-stranded RNA recognition pathway. *Molecular & Cellular Proteomics : MCP*, *13*(10), 2604–2617.

Oomizu, S., Sahuc, F., Asahina, K., Inamatsu, M., Matsuzaki, T., Sasaki, M., Obara, M., & Yoshizato, K. (2000). Kdap, a novel gene associated with the stratification of the epithelium. *Gene*, *256*(1-2), 19–27.

Organ, S. L., & Tsao, M. S. (2011). An overview of the c-MET signaling pathway. *Therapeutic Advances in Medical Oncology*, *3*(1 Suppl), S7.

Park, G. T., Lim, S. E., Jang, S. I., & Morasso, M. I. (2002). Suprabasin, a novel epidermal differentiation marker and potential cornified envelope precursor (2002/09/14). *Journal of Biological Chemistry*, *277*(47), 45195–45202.

Patil, S., Bhat, M. Y., Advani, J., Mohan, S. V., Babu, N., Datta, K. K., Subbannayya, T., Rajagopalan, P., Bhat, F. A., Al-hebshi, N., Sidransky, D., Gowda, H., & Chatterjee, A. (2021). Proteomic and phosphoproteomic profiling of shammah induced signaling in oral keratinocytes. *Scientific Reports 2021 11:1*, *11*(1), 1–12.

Patil, S., Rajagopalan, P., Patel, K., Subbannayya, T., Babu, N., Mohan, S. V., Advani, J., Sathe, G., Bhandi, S., Solanki, H. S., Sidransky, D., Chatterjee, A., Gowda, H., & Ferrari, M. (2019). Chronic shisha exposure alters phosphoproteome of oral keratinocytes. *Journal of Cell Communication and Signaling*, *13*(3), 281.

Post, H., Penning, R., Fitzpatrick, M. A., Garrigues, L. B., Wu, W., MacGillavry, H. D., Hoogenraad, C. C., Heck, A. J. R., & Altelaar, A. F. M. (2017). Robust, Sensitive, and Automated Phosphopeptide Enrichment Optimized for Low Sample Amounts Applied to Primary Hippocampal Neurons. *Journal of Proteome Research*, *16*(2), 728–737.

R Core Team. (2022). R: A language and environment for statistical computing. R Foundation for Statistical Computing.

Ramírez Moreno, M., & Bulgakova, N. A. (2022). The Cross-Talk Between EGFR and E-Cadherin. *Frontiers in Cell and Developmental Biology*, *9*, 3968.

Reynolds, A. B., & Roczniak-Ferguson, A. (2004). Emerging roles for p120-catenin in cell adhesion and cancer. *Oncogene*, *23*(48), 7947–7956.

Ritchie, M. E., Silver, J., Oshlack, A., Holmes, M., Diyagama, D., Holloway, A., & Smyth, G. K. (2007). A comparison of background correction methods for two-colour microarrays (2007/08/28). *Bioinformatics*, *23*(20), 2700–2707.

Rosorius, O., Mieskes, G., Issinger, O. G., Körner, C., Schmidt, B., von Figura, K., & Braulke, T. (1993). Characterization of phosphorylation sites in the cytoplasmic domain of the 300 kDa mannose-6-phosphate receptor. *Biochemical Journal*, *292*(3), 833–838.

Schmitt, J. M., & Stork, P. J. S. (2002). PKA Phosphorylation of Src Mediates cAMP's Inhibition of Cell Growth via Rap1. *Molecular Cell*, *9*(1), 85–94.

Shashikanth, N., Petrova, Y. I., Park, S., Chekan, J., Maiden, S., Spano, M., Ha, T., Gumbiner, B. M., & Leckband, D. E. (2015). Allosteric Regulation of E-Cadherin Adhesion *. *Journal of Biological Chemistry*, *290*(35), 21749–21761.

Shattil, S. J. (2005). Integrins and Src: dynamic duo of adhesion signaling. *Trends in Cell Biology*, *15*(8), 399–403.

Tsai, C. F., Wang, Y. T., Yen, H. Y., Tsou, C. C., Ku, W. C., Lin, P. Y., Chen, H. Y., Nesvizhskii, A. I., Ishihama, Y., & Chen, Y. J. (2015). Large-scale determination of absolute phosphorylation stoichiometries in human cells by motif-targeting quantitative proteomics. *Nature Communications 2015 6:1*, *6*(1), 1–8.

Tsuchida, S., Bonkobara, M., McMillan, J. R., Akiyama, M., Yudate, T., Aragane, Y., Tezuka, T., Shimizu, H., Cruz, P. D., & Ariizumi, K. (2004). Characterization of Kdap, A Protein Secreted by Keratinocytes. *Journal of Investigative Dermatology*, *122*(5), 1225–1234.

Turner, C. E. (2000). Paxillin and focal adhesion signalling. *Nature Cell Biology 2000 2:12*, *2*(12), E231–E236.

Tyanova, S., Temu, T., Sinitcyn, P., Carlson, A., Hein, M. Y., Geiger, T., Mann, M., & Cox, J. (2016). The Perseus computational platform for comprehensive analysis of (prote)omics data. *Nature Methods 2016 13:9*, *13*(9), 731–740.

Usui, M. L., Mansbridge, J. N., Carter, W. G., Fujita, M., & Olerud, J. E. (2008). Keratinocyte Migration, Proliferation, and Differentiation in Chronic Ulcers From Patients With Diabetes and Normal Wounds. *Journal of Histochemistry and Cytochemistry*, *56*(7), 687.

Utsunomiya, A., Chino, T., Utsunomiya, N., Luong, V. H., Tokuriki, A., Naganuma, T., Arita, M., Higashi, K., Saito, K., Suzuki, N., Ohara, A., Sugai, M., Sugawara, K., Tsuruta, D., Oyama, N., & Hasegawa, M. (2020). Homeostatic Function of Dermokine in the Skin Barrier and Inflammation. *Journal of Investigative Dermatology*.

Vedula, P., Kurosaka, S., Mactaggart, B., Ni, Q., Papoian, G. A., Jiang, Y., Dong, D., & Kashina, A. (2021). Different translation dynamics of β-and γ-actin regulates cell migration. *eLife*, *10*.

Vemulapalli, V., Blacklow, S., Gygi, S., & Erickson, A. (2022). Enrichment of Tyrosine Phosphorylated Peptides for Quantitative Mass Spectrometry Analysis of RTK Signaling Dynamics.

Wu, C. (2007). Focal Adhesion: A Focal Point in Current Cell Biology and Molecular Medicine. *Cell Adhesion & Migration*, *1*(1), 13.

Xu, Y., Tan, L. J., Grachtchouk, V., Voorhees, J. J., & Fisher, G. J. (2005). Receptor-type protein-tyrosine phosphatase-kappa regulates epidermal growth factor receptor function. *The Journal of biological chemistry*, *280*(52), 42694–42700.

Xuan, Y., Bateman, N. W., Gallien, S., Goetze, S., Zhou, Y., Navarro, P., Hu, M., Parikh, N., Hood, B. L., Conrads, K. A., Loosse, C., Kitata, R. B., Piersma, S. R., Chiasserini, D., Zhu, H., Hou, G., Tahir, M.,

Macklin, A., Khoo, A., … Conrads, T. P. (2020). Standardization and harmonization of distributed multi-center proteotype analysis supporting precision medicine studies. *Nature Communications*, *11*(1), 5248.

Yang, P., Ormerod, J. T., Liu, W., Ma, C., Zomaya, A. Y., & Yang, J. Y. H. (2019). AdaSampling for Positive-Unlabeled and Label Noise Learning With Bioinformatics Applications. *IEEE Transactions on Cybernetics*, *49*(5), 1932–1943.

Zijl, S., Salameti, V., Louis, B., Negri, V. A., & Watt, F. M. (2022). Chapter Four - Dynamic regulation of human epidermal differentiation by adhesive and mechanical forces. In T. Kornberg (Ed.), *Current topics in developmental biology* (pp. 129–148). Academic Press.

Supplemental Figures and Tables

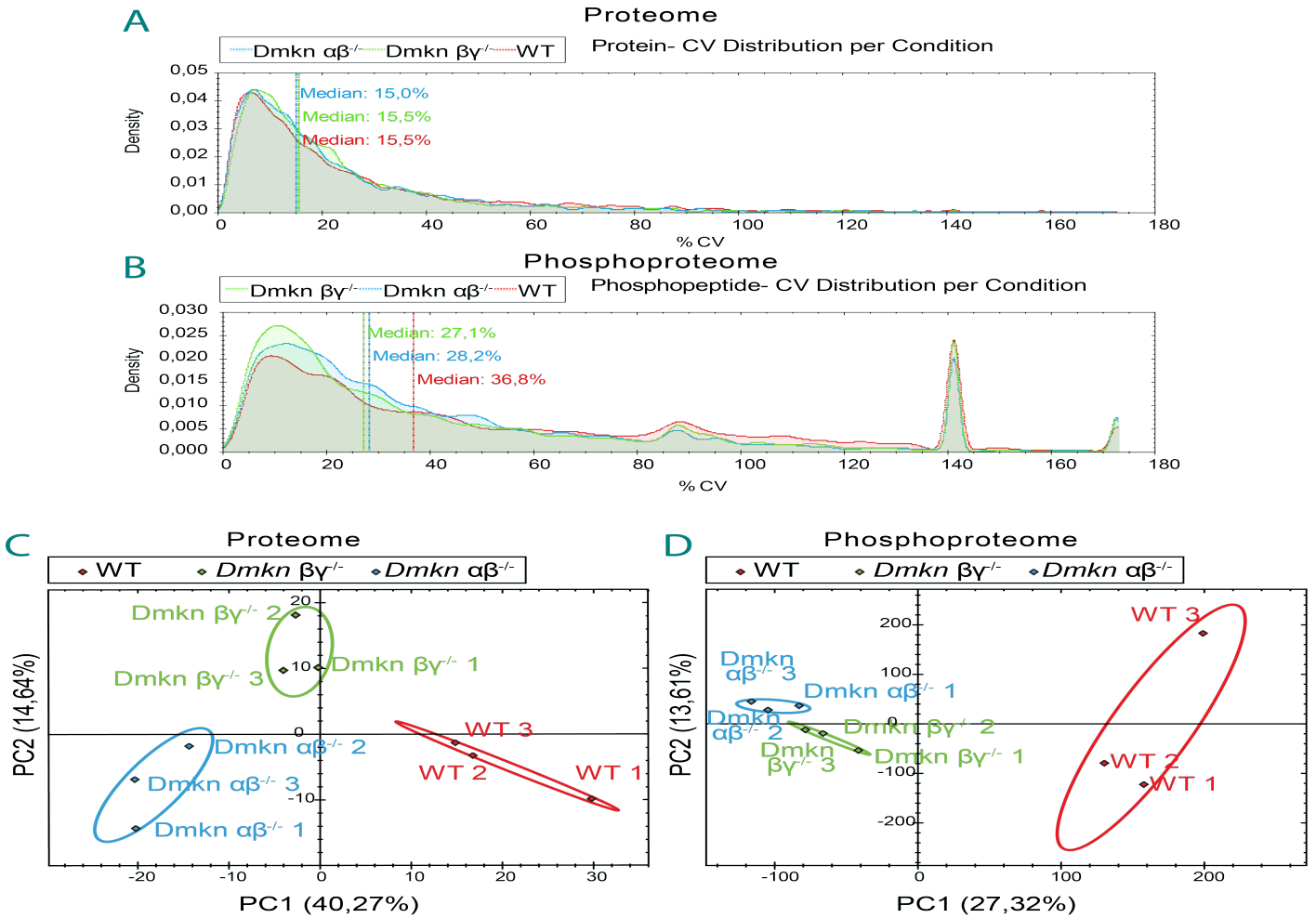

Figure S 2.21. (Continued on the following page.)

Figure S 2.21. Coefficient of variance and principal component analysis. **A** presents the results of the coefficient of variance (CV) analysis performed on the proteome (on a protein base). Notably, all median CV ratios were under 20%. **B** provides a CV analysis, focused on the phosphoproteome (at a peptide base). The CV analysis shows a relatively higher degree of variability, with a median CV for the *Dmkn* truncated keratinocytes below 30% and around 36% for the wildtype samples. **C** illustrates the results of the Principal Component Analysis (PCA) conducted on the proteome data. The plot exhibits distinct clustering patterns.
D extends the PCA to the phosphoproteome level. A clear separation between wildtype and knockout samples can be observed, with the *Dmkn* $\alpha\beta^{-/-}$ distinctly separated from the *Dmkn* $\beta\gamma^{-/-}$.

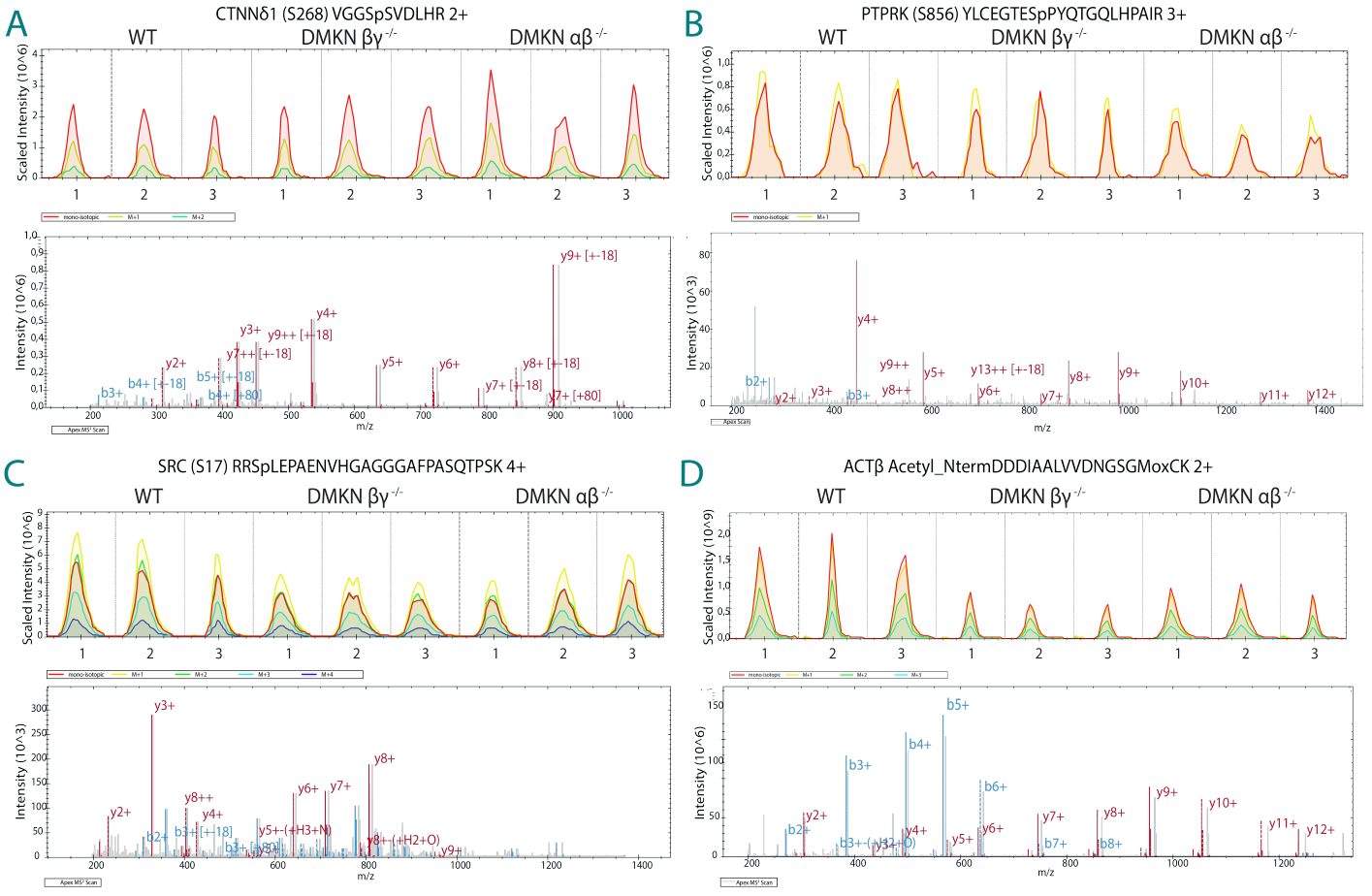

Figure S 2.22. (Continued on the following page.)

Figure S 2.22. Total Ion Chromatogram Traces across. In this figure, ion traces are compared side by side, specifically selected due to their implication in adherens junctions. **A** depicts the ion trace for the phosphopeptide of catenin δ 1, showing an increase in abundance upon the ablation of dermokine. **B** presents the ion trace for the phosphopeptide of PTPRκ. Upon dermokine ablation, a decrease in its abundance is observed. **C** portrays the ion trace for the SRC phosphopeptide. Similar to Figure B, a decrease in abundance is shown upon the ablation of dermokine. **D** exhibits the overall protein abundance, which is observed to decrease upon dermokine ablation.

Table S 2.7. GO over-representation analysis results of DMKN-dependent significantly increased phosphorylation events. Identifying several biological processes associated with each protein. Focal adhesion/Cell-substrate junction includes ADD1 (T614), AHNAK (S332 and S5110), CAV2 (S20, S23, S36 and Y19), CHP1 (T7), EGFR (S1042 and T693), FLNA (S1459), ITG β 4 (S1474, S1517, T1471 and T1530), MARCKS (T150), SNTB2 (S222) and TGFB1I1 (T33). Proteins associated with cadherin binding include AHNAK (S332 and S5110), EGFR (S1042 and T693), EPS15 (S107 and S108), ESYT2 (S691 and S693), KTN1 (S75), PKP4 (S214), PSEN1 (S43) and SPTAN1 (S1031). Receptor-mediated endocytosis proteins include ACKR3 (S350), ANXA2 (S12), CANX (S554, S564, S583 and T562), CAV1 (S37), CAV2 (S20,S23,S36 and Y19), EPS15 (S107 and S108) and IGF2R (S2409). The wnt signalling pathway includes the terms, CAV1 (S37), EGFR (S1042 and T693), LEO1 (S212), PBXIP1 (S43 and S45), PSEN1 (S43) and SLC9A3R1 (S288 and S290). Adherens junctions include the proteins, ANXA2 (S12), NECTIN1 (S422, S435 and Y418) and PKP4 (S214).

Focal adhesion/ Cell-substrate junction			Receptor-mediated endocytosis			Cadherin binding			Wnt signalling pathway			Adherens junctions		
Protein	Site	Module	Protein	Site	Module	Protein	Site	Module	Protein	Site	Module	Protein	Site	Module
ADD1	T614	2	ACKR3	S350	3	AHNAK	S332	2	CAV1	S37	3	ANXA2	S12	3
AHNAK	S332	2	ANXA2	S12	3	AHNAK	S5110	2	EGFR	S1042	3	NECTIN1	S422	2
AHNAK	S5110	2	CANX	S554	3	ANXA2	S12	3	EGFR	T693	2	NECTIN1	S435	2
CAV2	S20	3	CANX	S564	3	EPS15	S107	3	LEO1	S212	3	NECTIN1	Y418	2
CAV2	S23	3	CANX	S583	2	EGFR	S1042	3	PBXIP1	S43	3	PKP4	S214	3
CAV2	S36	3	CANX	T562	2	EGFR	T693	2	PBXIP1	S45	3			
CAV2	Y19	2	CAV1	S37	3	EPS15	S108	4	PKD2	S812	3			
CHP1	T7	2	CAV2	S20	3	ESYT2	S691	3	PSEN1	S43	3			
EGFR	S1042	3	CAV2	S23	3	ESYT2	S693	2	SLC9A3R1	S288	3			
EGFR	T693	2	CAV2	S36	3	KTN1	S75	3	SLC9A3R1	S290	3			
FLNA	S1459	2	CAV2	Y19	2	PKP4	S214	3						
ITG β 4	S1474	2	EPS15	S107	3	PSEN1	S43	3						
ITG β 4	S1517	3	EPS15	S108	4	SPTAN1	S1031	3						
ITG β 4	T1471	2	IGF2R	S2409	3									
ITG β 4	T1530	2												
MARCKS	T150	2												
SNTB2	S222	2												
TGFB1I1	T33	2												

Supplemental Files

List of supplemental files uploaded onto Onedrive, attached to this document:

File S1. List (.tsv) of 41817 phosphopeptides identified by HRMS^1-DIA phosphoproteomics of *Dmkn* $\alpha\beta^{-/-}$, *Dmkn* $\beta\gamma^{-/-}$ and wildtype keratinocytes.

File S2. List (.xlsx) of 15468 phosphosites identified by HRMS^1-DIA phosphoproteomics of *Dmkn* $\alpha\beta^{-/-}$, *Dmkn* $\beta\gamma^{-/-}$ and wildtype keratinocytes.

File S3. List (.xlsx) of 5522 proteins identified by HRMS^1-DIA phosphoproteomics of *Dmkn* $\alpha\beta^{-/-}$, *Dmkn* $\beta\gamma^{-/-}$ and wildtype keratinocytes.

File S4. Acquisition files (.raw) for the proteome of HRMS^1-DIA phosphoproteomics of *Dmkn* $\alpha\beta^{-/-}$, *Dmkn* $\beta\gamma^{-/-}$ and wildtype keratinocytes.

File S5. Acquisition files (.raw) for the phosphoproteome of HRMS^1-DIA phosphoproteomics of *Dmkn* $\alpha\beta^{-/-}$, *Dmkn* $\beta\gamma^{-/-}$ and wildtype keratinocytes.

File S6. Spectronaut™experiment file (.SNE) for the phosphoproteome of HRMS^1-DIA phosphoproteomics of *Dmkn* $\alpha\beta^{-/-}$, *Dmkn* $\beta\gamma^{-/-}$ and wildtype keratinocytes.

File S7. Spectronaut™experiment file (.SNE) for the proteome of HRMS^1-DIA phosphoproteomics of *Dmkn* $\alpha\beta^{-/-}$, *Dmkn* $\beta\gamma^{-/-}$ and wildtype keratinocytes.

Abbreviations and Acronyms

ACKR3 Atypical Chemokine Receptor 3

ACTβ Actin β

ADD1 Adducin 1

AHNAK AHNAK Nucleoprotein

AKT1 AKT Serine/Threonine Kinase 1

ANXA2 Annexin A2

BCLAF1 BCL2 Associated Transcription Factor 1

CAV1 Caveolin 1

CAV2 Caveolin 2

CDH1 Cadherin 1

CDK1 Cyclin-Dependent Kinase 1

CDK2 Cyclin-Dependent Kinase 2

CDK4 Cyclin-Dependent Kinase 4

CDK6 Cyclin-Dependent Kinase 6

CHEK1 Checkpoint Kinase 1

CHP1 Calcineurin Like EF-Hand Protein 1

CO_2 Carbon Dioxide

CSNK2A1 Casein Kinase 2 α 1

CTNN δ 1 Catenin δ 1

DIA Data-Independent Acquisition

DMKN Dermokine

EGFR Epidermal Growth Factor Receptor

EPS15 Epidermal Growth Factor Receptor Pathway Substrate 15

ERBB2 Erb-b2 Receptor Tyrosine Kinase 2

ERK Extracellular Signal-Regulated Kinase

ESYT2 Extended Synaptotagmin 2

FBS Fetal Bovine Serum

FLNA Filamin A

GSK3B Glycogen Synthase Kinase 3 β

HIPK2 Homeodomain Interacting Protein Kinase 2

HNRNPUL1 Heterogeneous Nuclear Ribonucleoprotein U Like 1

HRMS[1] High Resolution Mass spectrometry

IGF2R Insulin Like Growth Factor 2 Receptor

ITG α 6 Integrin Subunit α 6

ITG β 4 Integrin Subunit β 4

KRTDAP Keratinocyte Differentiation Associated Protein

KTN1 Kinectin 1

LC Liquid Chromatography

LEO1 Leo1, Paf1/RNA Polymerase II Complex Component

MAPK1 Mitogen-Activated Protein Kinase 1

MAPK3 Mitogen-Activated Protein Kinase 3

MAPK14 Mitogen-Activated Protein Kinase 14

MAPKAPK2 Mitogen-Activated Protein Kinase-Activated Protein Kinase 2

MARCKS Myristoylated Alanine Rich Protein Kinase Substrate

MATR3 Matrin 3

MET Tyrosine-Protein Kinase Met

MS Mass Spectrometry

MS/MS Tandem Mass Spectrometry

MTOR Mechanistic Target of Rapamycin Kinase

NECTIN1 Nectin Cell Adhesion Molecule 1

PBXIP1 PBX Homeobox Interacting Protein 1

PEX14 Peroxisomal Biogenesis Factor 14

PKD2 Polycystin 2, Transient Receptor Potential Cation Channel

PKP4 Plakophilin 4

PGRMC1 Progesterone Receptor Membrane Component 1

PGRMC2 Progesterone Receptor Membrane Component 2

PRKACA Protein Kinase cAMP-Activated Catalytic Subunit α

PRKCA Protein Kinase C α

PRKCG Protein Kinase C γ

PRPF4B Pre-mRNA Processing Factor 4B

PSEN1 Presenilin 1

PTPRκ Protein Tyrosine Phosphatase Receptor Type κ

RAP1 Ras-related protein Rap-1b

RMDN3 Regulator of Microtubule Dynamics 3

SBSN Suprabasin

SLC9A3R1 SLC9A3 Regulator 1

SNTB2 Syntrophin β 2

SRC Src Proto-Oncogene, Non-Receptor Tyrosine Kinase

SPTAN1 Spectrin α, Non-Erythrocytic 1

TGFβ1I1 Transforming Growth Factor β 1 Induced Transcript 1

CHAPTER 3

Concluding discussion and outlook

Dermokine (DMKN) and its several gene products, crucial members of the secreted protein gene complex family, play a pivotal role in the development and stratification of suprabasal layers of the stratified epithelium (Matsui et al., 2004). Further, DMKN displays a large number of isoforms, with the major isoforms DMKN-α, DMKN-β and DMKN-γ, of which both the β and γ isoform are highly expressed towards the granular layer, whereas the α isoform is synthesized throughout the epidermis (Leclerc et al., 2014; Naso et al., 2007). However, besides its implications in keratinocyte differentiation, its exact biological mechanism has not been unraveled (Utsunomiya et al., 2020). In addition, our laboratory recorded the matrix metalloproteinase 10 (MMP10)-dependent proteolytic modulation of DMKN *in-vitro* and *in-vivo*, indicating a purported function of DMKN in migratory keratinocytes (Schlage et al., 2015). Therefore, we selected DMKN as the candidate protease substrate and conducted detailed functional characterizations of DMKN in epidermal differentiation.

To elucidate a protein's function within a cellular system, it is critical to establish a control model depleted of the protein of interest. Modern approaches utilize CRISPR/Cas9-based gene truncations within the cellular model system to ensure that the gene product is inaccurately synthesized, supporting the study of the protein through loss-of-function. In addition, novel cell culturing techniques such as the multi-cellular *in-vivo*-like skin organoids allow studying crosstalk between human keratinocytes and fibroblasts, supporting keratinocyte differentiation. However, to characterize downstream signalling of a putative bioactive protein, such as DMKN, phosphoproteomics presents itself as a current means to not only enrich phosphorylated proteins but also apply appropriate kinase substrate enrichment analysis methods to elucidate putatively related upstream kinases. To address the contribution of DMKN to keratinocyte differentiation, we initially employed CRISPR/Cas9 gene editing strategies to generate DMKN-α, DMKN-β and DMKN-γ truncated knockouts. Next, we intended to determine the conclusive function that DMKN assumes throughout the development of epidermal stratification. For this, we

employed skin organoids as a model system to explore the activity of both DMKN-β and DMKN-α in keratinocyte differentiation. Finally, we aimed to investigate the convoluted process, by which extracellular dermokine initiates intracellular phosphorylation events. We utilized an automation-assisted sample preparation platform in combination with mass spectrometry-based phosphoprotemics to study phosphorylation events in both *Dmkn* $\beta\gamma^{-/-}$ and *Dmkn* $\alpha\beta^{-/-}$ mutants compared to wildtype keratinocytes.

For the development of isoform-specific DMKN ablated human keratinocytes, we simultaneously exploited several lentivirus-free gene editing workflows, namely the introduction of CRISPR/Cas9 plasmids into keratinocytes via transfections as well as a multiplexed CRISPR approach that employs the direct administration of multiple CRISPR RNP complexes into the nucleus of keratinocytes in collaboration with Cytosurge AG, Switzerland.

We optimized several parameters to increase the transfection-based approach, which culminated in doubling the efficacy of transfection relative to present methods and a lowering in the total duration necessary to create a single truncated mutant by 7 weeks (Enjalbert et al., 2020; Tuladhar et al., 2019). We sequenced 42 distinct keratinocyte populations, each obtained from a single-cell clone, allowing the generation of 4 unique isoform-specific DMKN knockouts. Together with Cytosurge AG, Switzerland, we utilized their proprietary FluidFM® technology, to develop an independent DMKN-truncated keratinocyte mutant. This approach not only allows for direct nano-injection of CRISPR RNP complexes into the nucleus but also simplifies multiplexed CRISPR applications (Meister et al., 2009). Our results demonstrate the potential of FluidFM® nano-injection to concurrently administer multiple gRNAs into targeted single cells, enabling simultaneous exon ablation. Furthermore, FluidFM® proposes considerable time optimization, reducing the period needed to generate relevant monoclonal cell lines. However, we experienced substantial difficulties regarding the segregated truncation of the DMKN-α isoform. While previous studies efficiently accomplished this, an obstacle became evident when exon 17 of DMKN-α isoform was ablated (Utsunomiya

et al., 2020). The results concluded in an unforeseen truncation at the intron site of the DMKN-β isoform, subsequently resulting in a posterior truncation of the DMKN-β isoform itself. Consequently, these outcomes obstructed the successful implementation of an isolated deletion of the DMKN-α isoform. Of note, we deliberately excluded a sole truncation of the DMKN-γ isoform, due to our focus on the cytokine-like domain contained in isoforms, DMKN-α and DMKN-β, as prior research indicated a lack of bioactive domains within the DMKN-γ isoform (Higashi et al., 2012). We obtained several DMKN isoform-specific knockout keratinocytes. These mutants form the foundation for future studies to elucidate the intricate function of dermokine in epidermal differentiation.

By utilizing our novel DMKN isoform-specific mutants, namely *Dmkn* $\beta\gamma^{-/-}$ and *Dmkn* $\alpha\beta^{-/-}$, in combination with wildtype keratinocytes, we were able to generate DMKN isoform-deficient skin organoids (Clevers, 2016). This model system provided us with an effective approach to explore the conclusive role of DMKN in the stratification of the epidermis using skin organoids (Enjalbert et al., 2020). Monitoring DMKN proteotypic peptides in *Dmkn* $\beta\gamma^{-/-}$ skin organoids utilizing targeted proteomics, displayed a decrease in abundance of the peptide in the cytokine-like domain, which became more evident when both DMKN-β and DMKN-α were removed. This finding corroborates the assumption that DMKN-α, being regulated by its unique promoter, compensates for the loss of DMKN-β (Utsunomiya et al., 2020). The histological evaluation of these skin organoids exhibited the absence of suprabasal layers in both *Dmkn* $\beta\gamma^{-/-}$ and *Dmkn* $\alpha\beta^{-/-}$ mutants in comparison to the wildtype, mirroring the expression gradient of DMKN. A global mass spectrometry based-proteomics assay in *Dmkn* $\beta\gamma^{-/-}$ skin organoids revealed significantly differential abundance changes in 904 out of the 4253 measurable proteins, of which several are linked to the formation of the cornified envelope and DMKN-associated signalling events. Using an IS-PRM assay, we independently validated these findings in the *Dmkn* $\alpha\beta^{-/-}$ skin organoid and could confirm the decreased abundance in regulatory proteins for filaggrin processing, cornified

envelope assembly, and desquamation. In addition, we identified the precise cleavage site of MMP10-dependent modulation in human DMKN, something previously only recorded in murine models (Schlage et al., 2015).

Although our comprehensive proteomics screening in DMKN isoform-truncated skin organoids provided observations into DMKN's contributions in keratinocyte differentiation, this strategy did not present any perspective into the intricate mechanism substantial to DMKN-dependent keratinocyte differentiation. Therefore, we employed a cutting-edge proteomics and phosphoproteomics approach, in combination with exhaustive data analysis, to study the *Dmkn* $\beta\gamma^{-/-}$ and *Dmkn* $\alpha\beta^{-/-}$ keratinocytes, comparing our results with those from wildtype cells (Bekker-Jensen et al., 2020; Xuan et al., 2020). Hereby, we observed several DMKN-dependent dephosphorylation sites on catenin δ 1 (CTTN δ 1), critical for the proper activity of adherens junctions. We identified decreased phosphorylation in CTNN δ 1 at various sites, indicating an alteration in keratinocyte adherens junction control (Zijl et al., 2022). This modulation might be mediated by the protein tyrosine phosphatase receptor type κ (PTPRκ), which was phosphorylated under endogenous DMKN quantities (Hay et al., 2022). The activation of PTPRκ could contribute to the dephosphorylation of CTNN δ 1, mediating cell adhesion (Fearnley et al., 2019). In addition, we recorded the phosphorylation of SRC in our study, affected by endogenous DMKN levels. SRC, a critical factor in the regulation of adherens junctions, mediates cellular migration and interactions with the extracellular matrix. To the best of our knowledge, this study provides the most exhaustive phosphoproteome of keratinocytes so far. It corroborates the compensatory function of DMKN-α for DMKN-β at the molecular level and reveals DMKN's potential influence on keratinocyte adhesion through phosphorylation (Mishra et al., 2017; Öhman et al., 2014; Patil et al., 2021; Patil et al., 2019). However, comprehensive insight into these complex pathways requires further research, especially to elucidate how they can be utilized for therapeutic applications.

Although we thoroughly examined the function of several DMKN iso-

forms in our investigation, we did neither study the implications of MMP10-dependent proteolytic processing of DMKN, nor the subsequent consequences of the cleavage event. In detail, the proteolytic cleavage of DMKN by MMP10 and the subsequent modulation of DMKN activity could potentially provide an alternative mechanism of phenotypic keratinocyte plasticity in wound healing (Schlage et al., 2015). Particularly, this could have a considerable influence on the proliferative phase of wound healing, eventually modulating wound healing progression. Future research emphasizing this element could provide important insights into the intricate biology of MMP10-processed DMKN and the effect it has on wound healing.

3.0.1 References

Bekker-Jensen, D. B., Bernhardt, O. M., Hogrebe, A., Martinez-Val, A., Verbeke, L., Gandhi, T., Kelstrup, C. D., Reiter, L., & Olsen, J. V. (2020). Rapid and site-specific deep phosphoproteome profiling by data-independent acquisition without the need for spectral libraries. *Nature Communications*, *11*(1), 1–12.

Clevers, H. (2016). Modeling Development and Disease with Organoids. *Cell*, *165*(7), 1586–1597.

Enjalbert, F., Dewan, P., Caley, M. P., Jones, E. M., Morse, M. A., Kelsell, D. P., Enright, A. J., & O'Toole, E. A. (2020). 3D model of harlequin ichthyosis reveals inflammatory therapeutic targets. *Journal of Clinical Investigation*, *130*(9), 4798–4810.

Fearnley, G. W., Young, K. A., Edgar, J. R., Antrobus, R., Hay, I. M., Liang, W.-C., Martinez-Martin, N., Lin, W., Deane, J. E., & Sharpe, H. J. (2019). The homophilic receptor PTPRK selectively dephosphorylates multiple junctional regulators to promote cell–cell adhesion (T. Hunter, J. A. Cooper, T. Hunter, A. Yap, & M. Tremblay, Eds.). *eLife*, *8*, e44597.

Hay, I. M., Mulholland, K. E., Lai, T., Graham, S. C., Sharpe, H. J., & Deane, J. E. (2022). Molecular mechanism of Afadin substrate recruitment to the receptor phosphatase PTPRK via its pseudophosphatase domain (T. Hunter, J. A. Cooper, T. Hunter, & S. Knapp, Eds.). *eLife*, *11*, e79855.

Higashi, K., Hasegawa, M., Yokoyama, C., Tachibana, T., Mitsui, S., & Saito, K. (2012). Dermokine-β impairs ERK signaling through direct binding to GRP78. *FEBS Letters*, *586*(16), 2300–2305.

Leclerc, E. A., Huchenq, A., Kezic, S., Serre, G., & Jonca, N. (2014). Mice deficient for the epidermal dermokine β and γ isoforms display transient cornification defects. *Journal of Cell Science*, *127*(13), 2862–2872.

Matsui, T., Hayashi-Kisumi, F., Kinoshita, Y., Katahira, S., Morita, K., Miyachi, Y., Ono, Y., Imai, T., Tanigawa, Y., Komiya, T., & Tsukita, S. (2004). Identification of novel keratinocyte-secreted peptides dermokine-α/- β and a new stratified epithelium-secreted protein gene complex on human chromosome 19q13.1. *Genomics*, *84*(2), 384–397.

Meister, A., Gabi, M., Behr, P., Studer, P., Vörös, J., Niedermann, P., Bitterli, J., Polesel-Maris, J., Liley, M., Heinzelmann, H., & Zambelli, T. (2009). FluidFM: Combining Atomic Force Microscopy and Nanofluidics in a Universal Liquid Delivery System for Single Cell Applications and Beyond. *Nano Letters*, *9*(6), 2501–2507.

Mishra, A., Oulès, B., Pisco, A. O., Ly, T., Liakath-Ali, K., Walko, G., Viswanathan, P., Tihy, M., Nijjher, J., Dunn, S. J., Lamond, A. I., & Watt, F. M. (2017). A protein phosphatase network controls the temporal and spatial dynamics of differentiation commitment in human epidermis. *eLife*, *6*.

Naso, M. F., Liang, B., Huang, C. C., Song, X. Y., Shahied-Arruda, L., Belkowski, S. M., D'Andrea, M. R., Polkovitch, D. A., Lawrence, D. R., Griswold, D. E., Sweet, R. W., & Amegadzie, B. Y. (2007). Dermokine: An extensively differentially spliced gene expressed in epithelial cells. *Journal of Investigative Dermatology*, *127*(7), 1622–1631.

Öhman, T., Söderholm, S., Hintsanen, P., Välimäki, E., Lietzuén, N., MacKintosh, C., Aittokallio, T., Matikainen, S., & Nyman, T. A. (2014). Phosphoproteomics combined with quantitative 14-3-3-affinity capture identifies SIRT1 and RAI as novel regulators of cytosolic double-stranded RNA recognition pathway. *Molecular & Cellular Proteomics : MCP*, *13*(10), 2604–2617.

Patil, S., Bhat, M. Y., Advani, J., Mohan, S. V., Babu, N., Datta, K. K., Subbannayya, T., Rajagopalan, P., Bhat, F. A., Al-hebshi, N., Sidransky, D., Gowda, H., & Chatterjee, A. (2021). Proteomic and phosphoproteomic profiling of shammah induced signaling in oral keratinocytes. *Scientific Reports 2021 11:1*, *11*(1), 1–12.

Patil, S., Rajagopalan, P., Patel, K., Subbannayya, T., Babu, N., Mohan, S. V., Advani, J., Sathe, G., Bhandi, S., Solanki, H. S., Sidransky,

D., Chatterjee, A., Gowda, H., & Ferrari, M. (2019). Chronic shisha exposure alters phosphoproteome of oral keratinocytes. *Journal of Cell Communication and Signaling*, *13*(3), 281.

Schlage, P., Kockmann, T., Sabino, F., Kizhakkedathu, J. N., & auf dem Keller, U. (2015). Matrix Metalloproteinase 10 Degradomics in Keratinocytes and Epidermal Tissue Identifies Bioactive Substrates With Pleiotropic Functions. *Mol Cell Proteomics*, *14*(12), 3234–3246.

Tuladhar, R., Yeu, Y., Tyler Piazza, J., Tan, Z., Rene Clemenceau, J., Wu, X., Barrett, Q., Herbert, J., Mathews, D. H., Kim, J., Hyun Hwang, T., & Lum, L. (2019). CRISPR-Cas9-based mutagenesis frequently provokes on-target mRNA misregulation. *Nature Communications*, *10*(1), 4056.

Utsunomiya, A., Chino, T., Utsunomiya, N., Luong, V. H., Tokuriki, A., Naganuma, T., Arita, M., Higashi, K., Saito, K., Suzuki, N., Ohara, A., Sugai, M., Sugawara, K., Tsuruta, D., Oyama, N., & Hasegawa, M. (2020). Homeostatic Function of Dermokine in the Skin Barrier and Inflammation. *Journal of Investigative Dermatology*.

Xuan, Y., Bateman, N. W., Gallien, S., Goetze, S., Zhou, Y., Navarro, P., Hu, M., Parikh, N., Hood, B. L., Conrads, K. A., Loosse, C., Kitata, R. B., Piersma, S. R., Chiasserini, D., Zhu, H., Hou, G., Tahir, M., Macklin, A., Khoo, A., … Conrads, T. P. (2020). Standardization and harmonization of distributed multi-center proteotype analysis supporting precision medicine studies. *Nature Communications*, *11*(1), 5248.

Zijl, S., Salameti, V., Louis, B., Negri, V. A., & Watt, F. M. (2022). Chapter Four - Dynamic regulation of human epidermal differentiation by adhesive and mechanical forces. In T. Kornberg (Ed.), *Current topics in developmental biology* (pp. 129–148). Academic Press.

Appendices

Journal Articles

The FEBS Journal

FEBS PRESS science publishing by scientists

COMMENTARY

New links for meprin β within the protease web

Vahap Canbay and Ulrich auf dem Keller

Department of Biotechnology and Biomedicine, Technical University of Denmark, Kongens Lyngby, Denmark

Keywords
ADAM; ectodomain shedding; epidermis; meprin; MT1-MMP; protease web

Correspondence
U. auf dem Keller, Department of Biotechnology and Biomedicine, Technical University of Denmark, Søltofts Plads, 2800 Kongens Lyngby, Denmark
Tel: +45 21 12 61 45
E-mail: uadk@dtu.dk

(Received 31 August 2022, accepted 5 September 2022)

doi:10.1111/febs.16621

Proteases are organised in interconnected networks, together forming the protease web whose disturbance can have detrimental consequences for tissue homeostasis and response to environmental insults. Membrane-anchored sheddases are proteases that themselves can be released into the pericellular space by ectodomain shedding. Werny et al. have uncovered unexpected promiscuity in ectodomain shedding of meprin β, a metalloprotease with critical functions in inflammation and fibrosis. These findings suggest new links within complex proteolytic networks like the epidermal protease network with potential implications for skin homeostasis, inflammation and response to injury.

Comment on: https://doi.org/10.1111/febs.16586

Proteases play pivotal roles in development, cellular signalling, tissue homeostasis and responses to environmental stimuli in health and disease. Either by degradation or by specific processing of target substrates, they irreversibly modulate extracellular environments or orchestrate intracellular processes to critically determine cell behaviour. Together with their inhibitors, proteases do not act alone but in cascades, circuits and complex networks, mutually affecting activity, localization and substrate repertoires. Classic examples of interconnected protease networks are blood coagulation and caspase-mediated programmed cell death, which control seminal tissue and cellular responses and whose disturbance is inevitably associated with life-threatening diseases. However, they are only parts of a higher order network, termed the protease web, that integrates all proteases (> 550 in humans) and inhibitors (> 150 in humans) and their complex interactions [1]. Despite rapid advances in high-throughput degradomics technologies that have significantly contributed to deconvolution of the protease web [2], only a tiny fraction of its complexity has been unravelled. Hence, many missing links need to be established to devise effective strategies for personalised treatment for aberrant proteolysis in devastating diseases, such as cancer, neurodegeneration and chronic inflammatory disorders.

In this issue of *The FEBS Journal*, Werny et al. [3] provide new insight into the intricate interplay of the membrane-anchored proteases meprin β, MT1-MMP (membrane-type-I matrix metalloproteinase) and ADAMs 10/17 (a disintegrin and metalloproteinase) that have all been associated with carcinogenesis, inflammation and Alzheimer's disease (AD). Acting in the pericellular space, meprin β, MT1-MMP and ADAMs 10/17 are sheddases, which can modulate extracellular

Abbreviations
AD, Alzheimer's disease; ADAM, a disintegrin and metalloproteinase; CASP, caspase; CD109, cluster of differentiation 109; CST, cystatin; CTS, cathepsin; ELA, elastase; IL-6R, interleukin-6 receptor; KLK, kallikrein; LGMN, legumain; MEP, meprin; MMP, matrix metalloproteinase; MT1-MMP, membrane-type-I matrix metalloproteinase; PLG, plasmin; PRSS8, prostasin; SASP, senescence-associated subtilisin protease; SERPIN, serine protease inhibitor; SPINK, serine protease inhibitor Kazal-type; ST14, suppressor of tumorigenicity 14; TMPRSS6, trans-membrane serine protease 6; TREM2, triggering receptor expressed on myeloid cells 2.

environments by releasing bioactive ligands from the cell surface. Interestingly, the catalytically active ectodomains of all these sheddases are also shed themselves, not only controlling their activity in close proximity to the plasma membrane, but also extending their proteolytic activity further into the protease-rich extracellular space. As shedding is mediated by proteolysis, these shedding events are critical links within the protease web and significantly contribute to dynamics of protease signal propagation. Thus, they must be tightly regulated in space and time to prevent uncontrolled proteolysis, potentially causing, or resulting from disease.

High flexibility in controlling ectodomain shedding can be conferred by multiple proteases cleaving the same substrate, allowing individual spatiotemporal regulation of expression and activity in complex tissue responses. Werny et al. now provide evidence for a striking overlap of ADAM10/17 and MT1-MMP activity towards meprin β ectodomain shedding, using the exact same cleavage site. Consistently, all three sheddases can only release inactive but not active meprin β from the cell surface, indicating a similar effect of the meprin β propeptide on susceptibility to proteolysis by ADAM10/17 and MT1-MMP. With MT1-MMP, a new meprin β sheddase has been discovered, which allows fine-tuning both the cell surface sheddase activity of meprin β to cleave bioactive mediators, such as IL6R (interleukin-6 receptor), CD109 (cluster of differentiation 109) and TREM2 (triggering receptor expressed on myeloid cells 2), and the amount of soluble pro-meprin β that eventually is activated by secreted tryptic proteases to functionally modulate the extracellular matrix [4].

Another and particularly interesting new link that has been established for meprin β within the protease web is its *vice versa* activity on MT1-MMP to shed the ectodomain of this major collagenase, sheddase of bioactive ligands and facilitator of MMP activation [5]. Interestingly, MT1-MMP ectodomain shedding has been described as a physiological event [6], generating an active soluble protease with enhanced activity in the pericellular space [7]. Data suggest that the MT1-MMP ectodomain sheddase is a membrane-anchored metalloprotease, but a defined candidate has not been identified yet [8]. Although focussing on meprin β rather than MT1-MMP ectodomain shedding, Werny et al. now present convincing data that suggest meprin β as a potent candidate to fill this void. Importantly, in addition to taking part in proMMP9 activation [9], meprin β now connects to the complex MMP network also through MT1-MMP, one of whose major functions is the zymogen activation of proMMP2 that in turn can activate other MMPs, thereby further transmitting the proteolytic signal [5].

As the authors have established these new links within the protease web in cell-based systems, major questions arise on whether, where and under which conditions they are relevant *in vivo*. Since MT1-MMP, as well as ADAM10/17, are expressed with low tissue

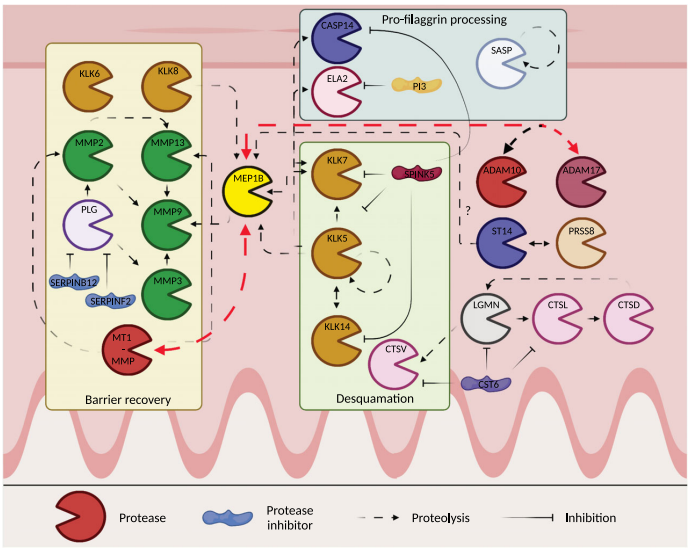

Fig. 1. Connectivity of meprin β within the epidermal protease network. Red connections indicate new links analysed by Werny et al. [3]. Figure inspired by [11]. Created with BioRender.com. ADAM, a disintegrin and metalloproteinase; CASP, caspase; CST, cystatin; CTS, cathepsin; ELA, elastase; LGMN, legumain; MEP, meprin; MMP, matrix metalloproteinase; MT1-MMP, membrane-type-I matrix metalloproteinase; PLG, plasmin; PRSS8, prostasin; SASP, senescence-associated subtilisin protease; SERPIN, serine protease inhibitor; SPINK, serine protease inhibitor Kazal-type; ST14, suppressor of tumorigenicity 14; TMPRSS6, transmembrane serine protease 6.

specificity in many cell types and under many conditions, there might be hardly situations where meprin β ectodomain shedding is exclusively mediated by either of the three sheddases. Thus, the tissue specificity of meprin β will guide the search for the most relevant tissues and responses to physiological or pathological stimuli. Meprin β is part of protease networks in the brain, intestine, kidney and skin with high expression in the epidermal compartment [4]. The latter is of special interest, since, in addition to MT1-MMP and ADAM10/17, it includes several member proteases such as kallikreins that are involved in the regulation of meprin β activity [10,11] (Fig. 1). Upon injury or in inflammatory skin diseases, the epidermal protease network undergoes significant changes in expressed proteases and proteolytic interactions. Wound healing phenotypes in mice with genetic ablation of either MT1-MMP or meprin β in epidermal keratinocytes are mild [12,13], but both proteases are increased in abundance during the redifferentiation phase, whereas ADAM17 also plays important roles in keratinocyte differentiation [14]. Activities with similar functional consequences have been assigned to matriptase-1 (ST14 (suppressor of tumorigenicity 14)) [15] that is closely related and shares cleavage specificity with matriptase-2 (TMPRSS6), a major activator of membrane-anchored meprin β [4], making it a potential candidate for meprin β activation in the epidermal compartment. As a caveat, most of these studies have been performed using mouse models, whereas Werny et al. could only demonstrate mutual shedding of meprin β and MT1-MMP using human proteins. However, as the authors mention, this might be related to dynamic O-glycosylation and thus could add another level of control to the complex system. Together, current evidence and the high connectivity of meprin β within the epidermal protease network (Fig. 1) warrant further analyses of its contributions to this very robust network with interconnected and redundant proteolytic activities. These might be addressed using humanised model systems and multiplexed gene editing strategies to understand complex rewiring of epidermal protease signalling in healing impairments and inflammatory skin disorders.

Acknowledgements

The authors acknowledge support by a Novo Nordisk Foundation Young Investigator Award (NNF16OC0020670) to UadK and funding from the LEO Foundation (LF-OC-19-000033).

Conflict of interest

The authors declare no conflict of interest.

Author contributions

VC and UadK wrote, reviewed and edited the manuscript.

References

1 Fortelny N, Cox JH, Kappelhoff R, Starr AE, Lange PF, Pavlidis P, et al. Network analyses reveal pervasive functional regulation between proteases in the human protease web. *PLoS Biol*. 2014;**12**:e1001869.
2 Canbay V, auf dem Keller U. New strategies to identify protease substrates. *Curr Opin Chem Biol*. 2021;**60**:89–96.
3 Werny L, Grogro A, Bickenbach K, Bülck C, Armbrust F, Koudelka T, et al. MT1-MMP and ADAM10/17 exhibit a remarkable overlap of shedding properties. *FEBS J*. 2022. https://doi.org/10.1111/febs.16586
4 Arnold P, Otte A, Becker-Pauly C. Meprin metalloproteases: molecular regulation and function in inflammation and fibrosis. *Biochim Biophys Acta Mol Cell Res*. 2017;**1864**:2096–104.
5 Itoh Y. Membrane-type matrix metalloproteinases: their functions and regulations. *Matrix Biol*. 2015;**44–46**:207–23.
6 Toth M, Osenkowski P, Hesek D, Brown S, Meroueh S, Sakr W, et al. Cleavage at the stem region releases an active ectodomain of the membrane type 1 matrix metalloproteinase. *Biochem J*. 2005;**387**:497–506.
7 Pahwa S, Bhowmick M, Amar S, Cao J, Strongin AY, Fridman R, et al. Characterization and regulation of MT1-MMP cell surface-associated activity. *Chem Biol Drug Des*. 2019;**93**:1251–64.
8 Toth M, Sohail A, Mobashery S, Fridman R. MT1-MMP shedding involves an ADAM and is independent of its localization in lipid rafts. *Biochem Biophys Res Commun*. 2006;**350**:377–84.
9 Geurts N, Becker-Pauly C, Martens E, Proost P, van den Steen PE, Stöcker W, et al. Meprins process matrix metalloproteinase-9 (MMP-9)/gelatinase B and enhance the activation kinetics by MMP-3. *FEBS Lett*. 2012;**586**:4264–9.
10 Nauroy P, Nyström A. Kallikreins: essential epidermal messengers for regulation of the skin microenvironment during homeostasis, repair and disease. *Matrix Biol Plus*. 2019;**6-7**:100019.
11 de Veer SJ, Furio L, Harris JM, Hovnanian A. Proteases: common culprits in human skin disorders. *Trends Mol Med*. 2014;**20**:166–78.
12 Kruppa D, Peters F, Bornert O, Maler MD, Martin SF, Becker-Pauly C, et al. Distinct contributions of meprins to skin regeneration after injury – meprin α a physiological processer of pro-collagen VII. *Matrix Biol Plus*. 2021;**11**:100065.

13 Zigrino P, Ayachi O, Schild A, Kaltenberg J, Zamek J, Nischt R, et al. Loss of epidermal MMP-14 expression interferes with angiogenesis but not with re-epithelialization. *Eur J Cell Biol*. 2012;**91**:748–56.
14 Tholen S, Wolf C, Mayer B, Knopf JD, Löffek S, Qian Y, et al. Skin barrier defects caused by keratinocyte-specific deletion of ADAM17 or EGFR are based on highly similar proteome and degradome alterations. *J Proteome Res*. 2016;**15**:1402–17.
15 Touati A, Saeidian AH, Youssefian L, Faghankhani M, Niaziorimi F, Pajouhanfar S, et al. The matriptase-prostasin proteolytic cascade in dermatologic diseases. *Exp Dermatol*. 2020;**29**:580–7.

Available online at www.sciencedirect.com

ScienceDirect

Current Opinion in Chemical Biology

New strategies to identify protease substrates

Vahap Canbay and Ulrich auf dem Keller

Abstract

Proteome dynamics is governed by transcription, translation, and post-translational modifications. Limited proteolysis is an irreversible post-translational modification that generates multiple but unique proteoforms from almost every native protein. Elucidating these proteoforms and understanding their dynamics at a system-wide level is of utmost importance because uncontrolled proteolytic cleavages correlate with many pathologies. Mass spectrometry–based degradomics has revolutionized protease research and invented workflows for global identification of protease substrates with resolution down to precise cleavage sites. In this review, we provide an overview of current strategies in protease substrate degradomics and introduce the concept of workflow, mass spectrometry–based and *in silico* enrichment of protein termini with the perspective of full deconvolution of digital proteome maps for precision medicine, and degradomics biomarker diagnostics.

Addresses

Department of Biotechnology and Biomedicine, Technical University of Denmark, DK-2800, Kongens Lyngby, Denmark

Corresponding author: auf dem Keller, Ulrich. (uadk@dtu.dk)

Current Opinion in Chemical Biology 2021, **60**:89–96

This review comes from a themed issue on **Omics**

Edited by **Nichollas Scott** and **Laura Edgington-Mitchell**

For a complete overview see the Issue and the Editorial

Available online 18 November 2020

https://doi.org/10.1016/j.cbpa.2020.09.009

Keywords

Proteoform, Protease, Degradomics, COFRADIC, TAILS, HUNTER, Targeted degradomics, *In silico* enrichment.

Introduction

Data from the human genome project impressively demonstrated that in addition to canonical proteins an enormous number of diverse proteoforms generated by alternative splicing and protein post-translational modifications (PTMs) contribute to the complexity of the human proteome [1]. To globally understand the myriads of human proteins and proteoforms, the Human Proteome Organization and its associated Human Protein Project have been established. The chromosome-centric Human Protein Project aims at characterizing the leading proteoforms, which have distinct and, sometimes, even contradictory biological activities in a physiological context compared with their unmodified protein of origin. The proteome analysis of dynamic regulation of proteoforms in a biological system could be a potential approach to discover novel biomarkers, unveiling differential abundance in specific diseases and provide solutions for the treatment of cancer and other disorders [2].

Over the last few years, cutting-edge mass spectrometry (MS)-based proteomics has become a robust and versatile tool to scrutinize the biological functions of proteins and for the quest for biomarkers [3]. Particularly, MS-based proteomics is used to investigate divergent proteoforms generated from PTMs with phosphoproteomics as the most prominent example [4]. Yet, these proteoforms are frequently under-sampled and thus neglected without proper enrichment protocols [5].

With roughly 560 estimated proteases derived from 3% of human protein-coding genes, this enzyme class is characterized by hydrolysis of the peptide bond linkage of amino acid residues in a polypeptide chain [6]. If uncontrolled, for example, through disturbances of protease regulation, proteolysis might be associated with pathologies, such as cancer, neurodegenerative and chronic inflammatory diseases [7]. Therefore, pathological protease cleavage events might be a manifestation of a continuous disease, making proteases important candidates for drug targets [8].

Limited proteolysis is a pivotal biological mechanism in maintaining cellular homeostasis through control of protein activities and contributes to decisive biological processes, such as cell cycle regulation and apoptosis [9]. Generation of protein neo-N and neo-C termini is a result of proteolytic cleavage, and thus characterization of protein termini is critical in revealing novel protease–substrate relations and understanding of regulatory proteolytic networks. The broad interest in proteases and their substrates established the field of degradomics, aiming at identifying not only proteases but also their substrates using system-wide analytical methods and, in particular, MS-based proteomics [10].

However, the low abundance of these PTMs is a hindrance in their identification, and therefore specific protocols are necessary to record proteolytic signatures. Hereafter, we will focus on extensive protease substrate

enrichment workflows and give an outlook on targeted degradomics and *in silico* enrichment.

Degradomics technologies

Typically, to characterize proteome dynamics in a biological system, a discovery-driven proteomics approach is put into practice [3]. A classical bottom—up proteomics workflow involves seclusion of the proteome from the biological sample and subsequent digestion into peptides using sequence-specific proteases, such as trypsin, LysargiNase, LysN, or GluC [11]. The newly generated peptides are fractionated by reversed-phase (RP) liquid chromatography (LC), ionized, and fragmented to be analyzed by tandem mass spectrometry (MS/MS) based on their mass-to-charge (m/z) ratio. Both identified peptide sequences and their abundances are used to computationally infer and relatively quantify the original protein. Still, the complexity of the whole biological sample proteome prevents comprehensive identification of low-abundance proteins because of the intrinsic mechanisms of the MS analysis, masking low-abundance peptides by peptides generated from highly abundant proteins. Consequently, the differentiation of sparse proteolytically spawned proteoforms requires additional experimental workflows to reduce sample complexity, such as supplementary sample fractionation and prior enrichment of protein termini [12].

Identification of crucial spatiotemporally confined proteolytic processes resulting in scarce neo-N— and neo-C—terminal proteoforms is challenging, and dedicated positional degradomics techniques have been developed to limit purification steps leading to general protein losses and prevent redundant contaminations of enriched fractions [10]. Positional degradomics methods follow either a positive enrichment strategy to directly select protein termini or negative selection protocols, removing internal tryptic peptides to enrich for proteolytically generated neo-N and neo-C termini. Whereas positive enrichment methods focus on selective affinity tagging of protein N-terminal α-amines over lysine side-chain ε-amines, negative selection approaches chemically label both free ε- and α-amines at the protein level and subsequently remove internal tryptic peptides exploiting reactivity of their newly generated N-terminal primary amine groups.

Positive enrichment strategies

Various positive enrichment workflows have been developed to selectively enrich N-terminal peptides relying on biotin—avidin affinity purification (Figure 1). With great success, subtiligase has been engineered to enzymatically label protein N termini with a biotinylated tagging peptide, while chemical biotinylation exploits differences in reactivity of ε- and α-amines toward amine-reactive coupling groups [13,14]. Subtiligase-based N-terminomics has been applied to record the first N-terminome of human blood [15], extensively map caspase cleavages in apoptosis [16] and monitor proteolytic fragments as biomarkers in serum from cancer patients [17]. Recently, efficacy and versatility of subtiligase for global enzymatic modification of protein N termini in complex samples have been further extended by introduction of novel engineered mutant enzymes, which expand its application in several fields of research including protease substrate discovery [18].

As an alternative strategy for positive enrichment of N-terminal peptides, N-terminalomics by chemical labeling of the α-amine of proteins (N-CLAP) uses selective deblocking of N-terminal α-amines after whole protein full amine labeling followed by chemical biotinylation and avidin-functionalized solid-phase extraction [19]. More recently, Griswold et al. [20] used a 2-pyridinecarboxaldehyde—biotin probe to selectively label protein N termini in a chemical approach termed chemical enrichment of protease substrates (CHOPS) that is particularly suited to study dipeptidyl peptidases because binding is prohibited by proline as the penultimate N-terminal residue.

Despite constant development of novel workflows, an inherent drawback of most positive enrichment strategies is the need of customized reagents, complicating introduction of isotopic labels and often limiting multiplexing capabilities. Some of these limitations have been addressed by a novel immuno-N-terminomics (miNterm) approach using tandem mass tags (TMTs) for whole protein labeling and anti—TMT-antibody resins for N-terminal enrichment [21]. On the other hand, positive enrichment has advantages in identification of intracellular neo-N termini that might be masked by the huge number of naturally Nα-acetylated protein N termini co-enriched in negative enrichment workflows.

Negative enrichment strategies

Negative enrichment workflows rely on removal of internal tryptic peptides rather than capture of chemically modified protein termini and thus also allow for annotation of natural N-terminal modifications, such as Nα-acetylation and N-terminal glutamine cyclization [22]. Widely applied negative enrichment strategies use either fractional chromatography, amine-reactive polymers, or solid-phase extraction upon chemical alteration of hydrophobicity and focus on N-terminal peptides for protease substrate discovery. Of these, combined fractional diagonal chromatography (COFRADIC) and terminal amine isotopic labeling of substrates (TAILS) have been extensively applied in positional proteomics [23], whereby high-efficiency undecanal-based N-termini enrichment (HUNTER) has been introduced more recently [24].

Figure 1

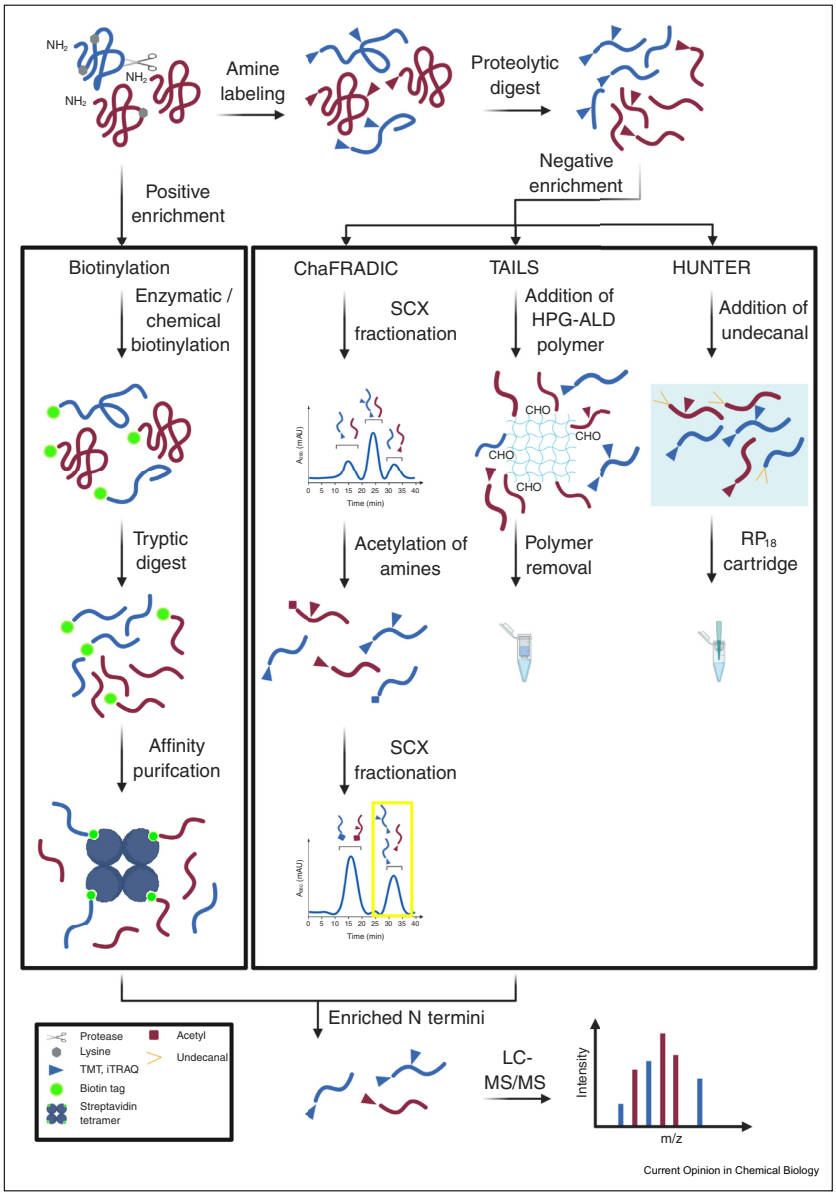

Overview of N-terminal enrichment workflows. Positive enrichment strategies selectively attach affinity tags to N-terminal primary peptide α-amines allowing for affinity purification. Negative enrichment workflows rely on whole protein amine-labeling and subsequent removal of internal endoproteinase-generated peptides using amine-reactive polymers (TAILS) or exploiting changes in chromatographic elution times upon chemical derivatization (ChaFRADIC, HUNTER). Created with BioRender.com. ChaFRADIC, charge-based fractional diagonal chromatography; HPG-ALD, amine-reactive soluble hyperbranched polyglycerol aldehyde polymer; HUNTER, high-efficiency undecanal-based N-termini enrichment; LC, liquid chromatography; MS, mass spectrometry; SCX, strong cation exchange; TAILS, terminal amine isotopic labeling of substrates.

Combined fractional diagonal chromatography

COFRADIC depends on chemical conversion of internal peptides altering their hydrophobicity, subsequently using two consecutive chromatography steps, which in turn enrich for proteolytically generated protein N termini [25]. Essentially, all primary amines of proteins are acetylated; subsequently the sample is tryptically digested and prefractionated by strong cation exchange (SCX) chromatography, which is used to enrich for acetylated N termini because of the low binding capacity of neo-N−terminal peptides to the SCX resin in comparison with unblocked, tryptic peptides. The fractions undergo a primary RP high-performance liquid chromatography (HPLC) separation, and 2,4,6-trinitrobenzenosulfonic acid is introduced to each enriched fraction, hydrophobically tagging the remaining internal peptides and thus enabling their efficient depletion in a consecutive RP-HPLC run, while initially acetylated neo-N termini are collected based on their shorter retention time on the RP-HPLC resin.

The initial acetylation step limits multiplexing capabilities of COFRADIC, which has been overcome by a more recent variant termed charge-based fractional diagonal chromatography (ChaFRADIC) [26]. The ChaFRADIC approach can use isobaric tags for relative or absolute quantitation (iTRAQ) or TMTs for labeling of N-terminal peptides, followed by a primary SCX run to fractionate peptides based on their charge state, deutero-acetylation of tryptic peptides upon digest and an additional SCX step to pull out fractions exclusively containing blocked neo-N−terminal peptides [26,27]. Simplifying ChaFRADIC, charge-based fractional diagonal chromatography in tip format (ChaFRAtip) miniaturizes the workflow, requiring only a pipette tip and SCX beads to significantly decrease sample amounts to below 5 μg total protein per sample [28]. This presents a possibility to circumvent the use of expensive HPLC systems, which are linked to investment expenses and maintenance costs [28].

Terminal amine isotopic labeling of substrates

The workflow that has been most widely applied for systematic discovery of new protease substrates in complex biological samples [23] was introduced by Kleifeld et al. [29] and termed TAILS. TAILS employs commonly used reagents, such as formaldehyde (reductive dimethylation), iTRAQ and TMTs, for labeling of lysine ε- and protein N-terminal α-amines at the protein level, enabling flexible experimental designs optimized for costs and multiplexing capabilities [30]. Labeled proteomes are combined, digested with site-specific endoproteinases (mostly trypsin) and the generated internal peptides covalently captured using a commercially available amine-reactive soluble hyperbranched polyglycerol aldehyde polymer (HPG-ALD). Subsequent ultrafiltration collects N-terminal peptides in the flow-through, the so-called TAILS fraction, that together with LC-MS/MS analysis of an aliquot of the nonenriched preTAILS fraction provides a comprehensive positional annotation of the sample proteome [31]. TAILS' extensive multiplexing capabilities have been applied to perform time-resolved analyses [32] and to record N-terminomes from patient samples [33].

Over the years, the TAILS workflow has been continuously improved to increase proteome and N-terminome coverage, combined with different labeling modalities [34] and adapted for analysis of samples from several species, tissues, and body fluids [35−37]. Moreover, a recent variant of the HPG-ALD polymer that is susceptible to precipitation significantly improved N-terminal enrichment, enabling higher efficiency and lowering potential sample losses [38].

After the principle of TAILS, Ju et al. introduced a novel workflow termed iNrich that replaces the HPG-ALD polymer by N-hydroxysuccinimide beads and has been adapted to an encapsulated format with the potential for automated processing [39].

High-efficiency undecanal-based N-termini enrichment

HUNTER, a sensitive and automatable assay, is based on chemical alteration of hydrophobicity to remove internal peptides by RP-HPLC and achieved a remarkable enrichment of 1000 N-termini from as little as 2 μg total protein per biological replicate [24]. HUNTER also introduced reversible capturing to magnetic SP3 beads for proteome purification and labeling [40] to degradomics workflows and exploited data-independent acquisition for label-free quantification. Thus, through its adaptability to automatic liquid-handling systems, HUNTER has the potential to drive forward high-throughput protease substrate discovery and N-terminal proteoform mapping in clinical degradomics.

C-terminomics

Not all protease substrate cleavages are accessible by analysis of the resulting N-terminal peptide, which might not be possible to be generated in an appropriate length, might lack suitable physicochemical properties for MS-based analysis or might be too short for unambiguous identification in complex proteomes. Thereby, a particular challenge is the detection of events resulting from carboxypeptidase activities. Therefore, despite an unfavorable chemistry COFRADIC, ChaFRADIC, and TAILS have been modified for analysis of C-terminal peptides [41].

C-terminal COFRADIC replaces 2,4,6-trinitrobenzenosulfonic acid with an amine-reactive derivate of butyrate, allowing to separately recover N-

and C-terminal peptides in the second RP-HPLC run [42]. C-TAILS removes internal tryptic and N-terminal peptides via their (1-ethyl-3-(3-dimethylaminopropyl) carbodiimide hydrochloride)—functionalized free carboxyl groups using an amine-reactive polymer upon blocking of free C-terminal and side-chain carboxyl groups at the protein and all primary amines at both the protein and the peptide level [43]. Application of multiple enzymes for site-specific proteome digest further increased identification rates of C termini using the C-TAILS approach [44]. Only recently, ChaFRADIC has been modified to allow for negative enrichment of C termini by reducing charge states of non-C—terminal peptides through enzymatic removal of trypsin-generated basic amino acids in C-terminal position [45].

Targeted degradomics and *in silico* enrichment

Positive and negative enrichment workflows separate terminal from internal peptides in proteome digests to facilitate their detection in complex mixtures. Targeted degradomics moves this separation inside the mass spectrometer by selective analysis of predefined peptide precursors based on mass and LC retention time utilizing the principles of selected or parallel reaction monitoring (S/PRM) [46]. Because neo-terminal peptides are preselected in the PRM mode, targeted degradomics is mostly applied for validation of newly identified protease cleavage events rather than to discover new protease substrates [47]. However, with the rapid improvements in MS instrumentation and PRM workflows such as internal standard—triggered

Figure 2

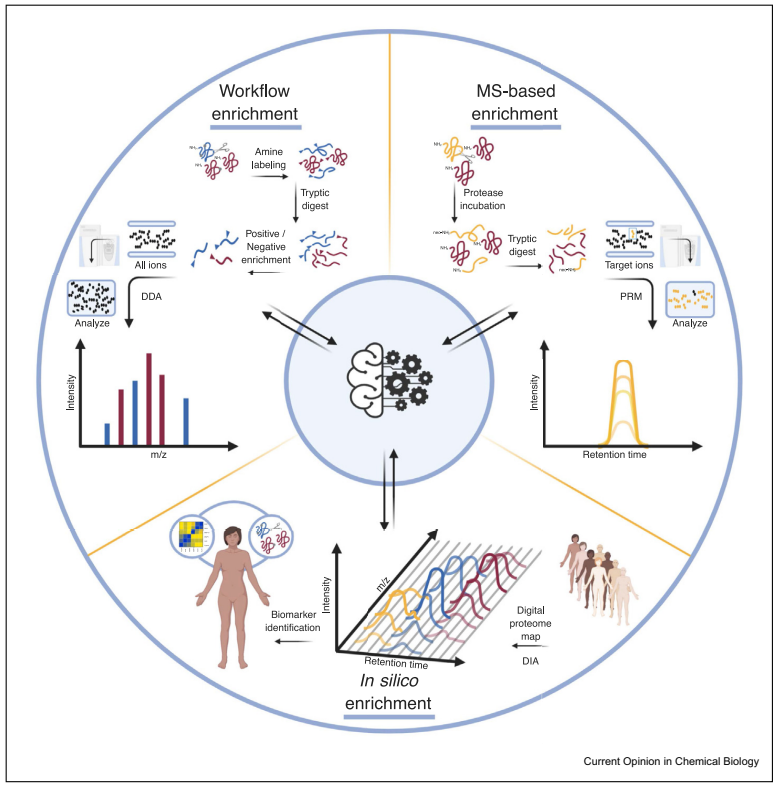

Concept of enrichment strategies for positional proteomics. Workflow enrichment combines chemical proteome modification with separation techniques to physically isolate protein termini before proteomics analysis. Mass spectrometry (MS)–based enrichment relies on separation of selected peptide ions within the instrument, allowing quantitative monitoring of hundreds of cleavage events by concomitant analysis of neo-termini and cleavage-site spanning peptides. *In silico* enrichment utilizes digital proteome maps recorded by data-independent acquisition (DIA) to correlate differential abundances of proteolytically spawned proteoforms in individual patients with large patient cohorts. Enrichment strategies use machine learning algorithms and artificial intelligence to computationally infer proteoform identification. Created with BioRender.com. DDA, data-dependent acquisition; MS, mass spectrometry; PRM, parallel reaction monitoring.

PRM (IS-PRM) [48], numbers of targets that can be monitored with high sensitivity are rapidly increasing, enabling discovery-like analyses using extensive target libraries for assay development (Figure 2). Such peptide libraries might be synthetically produced or generated from proteomes exposed to differential protease activities. Thereby, machine learning algorithms and artificial intelligence will help to extend into the discovery domain based on growing datasets deposited in proteolysis databases, such as TopFIND [49].

In future, similar libraries might be used to query digital proteome maps [50] that are recorded using DIA from cellular assay systems, animal models, and patient cohorts for proteolytic events by *in silico* enrichment of indicative proteoforms. This principle has recently been demonstrated by Ye et al. [51] who used glycopeptide libraries to identify and quantify hundreds of glycopeptides in human serum without prior enrichment.

Conclusion and perspectives

Identification of proteolytic proteoforms has gained immense momentum over the last years, aiming at understanding limited proteolysis as a decisive signaling event and uncovering novel proteoform biomarkers generated by specific cleavage. Unveiling regulatory proteolytic networks will divulge a hidden level in the complex interplay of regulatory cellular functions.

Prevailing degradomics strategies allow unprecedented insights into cleavage events in cells and tissue and provide information about specific protease–substrate relations. Several existing degradomics methods have been improved and spun out either new techniques or modified versions. Yet, protease substrate identification proves to be challenging, and more recently developed targeted degradomics approaches have the potential to extend into the discovery domain, exploiting the increased sensitivity of state-of-the-art mass spectrometers to identify and quantify proteolytically spawned proteoforms. Growing knowledge of cleavage events and bona fide protease substrates deposited in common repositories together with advancements in machine learning algorithms and further improvements in instrumentation will pave the way for systematic querying of digital proteome maps for limited proteolysis and significantly reduce time and efforts in global protease substrate discovery.

Declaration of competing interest

Nothing declared.

Acknowledgement

Ulrich auf dem Keller acknowledges support by a Novo Nordisk Foundation Young Investigator Award [NNF16OC0020670].

References

Papers of particular interest, published within the period of review, have been highlighted as:

* of special interest
** of outstanding interest

1. Paik YK, Lane L, Kawamura T, Chen YJ, Cho JY, Labaer J, Yoo JS, Domont G, Corrales F, Omenn GS, Archakov A, Encarnación-Guevara S, Lui S, Salekdeh GH, Cho JY, Kim CY, Overall CM: **Launching the C-HPP neXt-CP50 pilot project for functional characterization of identified proteins with No known function**. *J Proteome Res* 2018, **7**:4042–4050, https://doi.org/10.1021/acs.jproteome.8b00383.
2. Macklin A, Khan S, Kislinger T: **Recent advances in mass spectrometry based clinical proteomics: applications to cancer research**. *Clin Proteomics* 2020, **17**, https://doi.org/10.1186/s12014-020-09283-w.
3. Aebersold R, Mann M: **Mass-spectrometric exploration of proteome structure and function**. *Nature* 2016, **537**:347–355, https://doi.org/10.1038/nature19949.
4. Hosp F, Mann M: **A primer on concepts and applications of proteomics in neuroscience**. *Neuron* 2017, **96**:558–571, https://doi.org/10.1016/j.neuron.2017.09.025.
5. Pieroni L, Iavarone F, Olianas A, Greco V, Desiderio C, Martelli C, Manconi B, Sanna MT, Messana I, Castagnola M, Cabras T: **Enrichments of post-translational modifications in proteomic studies**. *J Separ Sci* 2020, **43**:313–336, https://doi.org/10.1002/jssc.201900804.
6. Vizovišek M, Vidmar R, Drag M, Fonović M, Salvesen GS, Turk B: **Protease specificity: towards in vivo imaging applications and biomarker discovery**. *Trends Biochem Sci* 2018, **43**:829–844, https://doi.org/10.1016/j.tibs.2018.07.003.
7. Eckhard U, Marino G, Butler GS, Overall CM: **Positional proteomics in the era of the human proteome project on the doorstep of precision medicine**. *Biochimie* 2016, **122**:110–118, https://doi.org/10.1016/J.BIOCHI.2015.10.018.
8. Drag M, Salvesen GS: **Emerging principles in protease-based drug discovery**. *Nat Rev Drug Discov* 2010, **9**:690–701, https://doi.org/10.1038/nrd3053.
9. Turk B, Turk D, Turk V: **Protease signalling: the cutting edge**. *EMBO J* 2012, **31**:1630–1643, https://doi.org/10.1038/emboj.2012.42.
10. Klein T, Eckhard U, Dufour A, Solis N, Overall CM: **Proteolytic cleavage - mechanisms, function, and "omic" approaches for a near-ubiquitous posttranslational modification**. *Chem Rev* 2018, **118**:1137–1168, https://doi.org/10.1021/acs.chemrev.7b00120.
11. Huesgen PF, Lange PF, Rogers LD, Solis N, Eckhard U, Kleifeld O, Goulas T, Gomis-Rüth FX, Overall CM: **LysargiNase mirrors trypsin for protein C-terminal and methylation-site identification**. *Nat Methods* 2014, **12**:55–58, https://doi.org/10.1038/nmeth.3177.
12. Luo SY, Araya LE, Julien O: **Protease substrate identification using N-terminomics**. *ACS Chem Biol* 2019, **14**:2361–2371, https://doi.org/10.1021/acschembio.9b00398.
13. Yoshihara HA, Mahrus S, Wells JA: **Tags for labeling protein N-termini with subtiligase for proteomics**. *Bioorg Med Chem Lett* 2008, **18**:6000–6003, https://doi.org/10.1016/j.bmcl.2008.08.044.
14. Timmer JC, Enoksson M, Wildfang E, Zhu W, Igarashi Y, Denault JB, Ma Y, Dummitt B, Chang YH, Mast AE, Eroshkin A, Smith JW, Tao WA, Salvesen GS: **Profiling constitutive proteolytic events in vivo**. *Biochem J* 2007, **407**:41–48, https://doi.org/10.1042/BJ20070775.
15. Wildes D, Wells JA: **Sampling the N-terminal proteome of human blood**. *Proc Natl Acad Sci U S A* 2010, **107**:4561–4566, https://doi.org/10.1073/pnas.0914495107.

16. Mahrus S, Trinidad JC, Barkan DT, Sali A, Burlingame AL, Wells JA: **Global sequencing of proteolytic cleavage sites in apoptosis by specific labeling of protein N termini**. *Cell* 2008, **134**:866–876, https://doi.org/10.1016/j.cell.2008.08.012.

17. Wiita AP, Hsu GW, Lu CM, Esensten JH, Wells JA: **Circulating proteolytic signatures of chemotherapy-induced cell death in humans discovered by N-terminal labeling**. *Proc Natl Acad Sci U S A* 2014, **111**:7594–7599, https://doi.org/10.1073/pnas.1405987111.

18. A. M. Weeks, J. A. Wells, N-terminal modification of proteins with subtiligase specificity variants, *Curr Protoc Chem Biol* 12, e79. https://doi.org/10.1002/cpch.79.

19. Xu G, Shin SB, Jaffrey SR: **Global profiling of protease cleavage sites by chemoselective labeling of protein N-termini**. *Proc Natl Acad Sci U S A* 2009, **106**:19310–19315, https://doi.org/10.1073/pnas.0908958106.

20. * Griswold AR, Cifani P, Rao SD, Axelrod AJ, Miele MM, Hendrickson RC, Kentsis A, Bachovchin DA: **A chemical strategy for protease substrate profiling**. *Cell Chemical Biology* 2019, **26**:901–907, https://doi.org/10.1016/j.chembiol.2019.03.007.
This study describes a novel and efficient positive enrichment strategy with particular advantages for dipeptidyl peptidase substrate discovery.

21. * Shin S, Hong JH, Na Y, Lee M, Qian W-J, Kim VN, Kim J-S: **Development of multiplexed immuno-N-terminomics to reveal the landscape of proteolytic processing in early embryogenesis of Drosophila melanogaster**. *Anal Chem* 2020, **92**:4926–4934, https://doi.org/10.1021/acs.analchem.9b05035.
This work makes use of commercially available reagents including highly specific anti-TMT antibodies to implement a novel positive enrichment strategy with multiplexing capabilities.

22. Rogers LD, Overall CM: **Proteolytic post-translational modification of proteins: proteomic tools and methodology**. *Mol Cell Proteomics* 2013, **12**:3532–3542, https://doi.org/10.1074/mcp.M113.031310.

23. Savickas S, Kastl P, auf dem Keller U: **Combinatorial degradomics: precision tools to unveil proteolytic processes in biological systems**. *Biochim Biophys Acta Protein Proteonomics* 2020, **1868**:140392, https://doi.org/10.1016/j.bbapap.2020.140392.

24. ** Weng SSH, Demir F, Ergin EK, Dirnberger S, Uzozie A, Tuscher D, Nierves L, Tsui J, Huesgen PF, Lange PF: **Sensitive determination of proteolytic proteoforms in limited microscale proteome samples**. *Mol Cell Proteomics* 2019, **18**:2335–2347, https://doi.org/10.1074/mcp.TIR119.001560.
This paper is of outstanding interest, since it introduces significant improvements to the TAILS workflow and opens up new possibilities for automation.

25. Staes A, Van Damme P, Timmerman E, Ruttens B, Stes E, Gevaert K, Impens F: **Protease substrate profiling by n-terminal cofradic**. *Methods Mol Biol* 2017, **1574**:51–76, https://doi.org/10.1007/978-1-4939-6850-3_5.

26. Venne AS, Vögtle FN, Meisinger C, Sickmann A, Zahedi RP: **Novel highly sensitive, specific, and straightforward strategy for comprehensive N-terminal proteomics reveals unknown substrates of the mitochondrial peptidase Icp55**. *J Proteome Res* 2013, **12**:3823–3830, https://doi.org/10.1021/pr400435d.

27. Venne AS, Solari FA, Faden F, Paretti T, Dissmeyer N, Zahedi RP: **An improved workflow for quantitative N-terminal charge-based fractional diagonal chromatography (ChaFRADIC) to study proteolytic events in Arabidopsis thaliana**. *Proteomics* 2015, **15**:2458–2469, https://doi.org/10.1002/pmic.201500014.

28. * Shema G, Nguyen MT, Solari FA, Loroch S, Venne AS, Kollipara L, Sickmann A, Verhelst SH, Zahedi RP: **Simple, scalable, and ultrasensitive tip-based identification of protease substrates**. *Mol Cell Proteomics* 2018, **17**:826–834, https://doi.org/10.1074/mcp.TIR117.000302.
In this work, the authors present significant improvements to ChaFRADIC by miniaturizing the workflow and adjusting to small sample sizes.

29. Kleifeld O, Doucet A, auf dem Keller U, Prudova A, Schilling O, Kainthan RK, Starr AE, Foster LJ, Kizhakkedathu JN, Overall CM: **Isotopic labeling of terminal amines in complex samples identifies protein N-termini and protease cleavage products**. *Nat Biotechnol* 2010, **28**:281–288, https://doi.org/10.1038/nbt.1611.

30. Kleifeld O, Doucet A, Prudova A, auf dem Keller U, Gioia M, Kizhakkedathu JN, Overall CM: **Identifying and quantifying proteolytic events and the natural N terminome by terminal amine isotopic labeling of substrates**. *Nat Protoc* 2011, **6**:1578–1611, https://doi.org/10.1038/nprot.2011.382.

31. auf dem Keller U, Prudova A, Eckhard U, Fingleton B, Overall CM: **Systems-level analysis of proteolytic events in increased vascular permeability and complement activation in skin inflammation**. *Sci Signal* 2013, **6**, https://doi.org/10.1126/scisignal.2003512. rs2.

32. Schlage P, Egli FE, Nanni P, Wang LW, Kizhakkedathu JN, Apte SS, auf dem Keller U: **Time-resolved analysis of the matrix metalloproteinase 10 substrate degradome**. *Mol Cell Proteomics* 2014, **13**:580–593, https://doi.org/10.1074/mcp.M113.035139.

33. Klein T, Fung SY, Renner F, Blank MA, Dufour A, Kang S, Bolger-Munro M, Scurll JM, Priatel JJ, Schweigler P, Melkko S, Gold MR, Viner RI, Regnier CH, Turvey SE, Overall CM: **The paracaspase MALT1 cleaves HOIL1 reducing linear ubiquitination by LUBAC to dampen lymphocyte NF-kappaB signalling**. *Nat Commun* 2015, **6**:8777, https://doi.org/10.1038/ncomms9777.

34. Schlage P, Kockmann T, Kizhakkedathu JN, auf dem Keller U: **Monitoring matrix metalloproteinase activity at the epidermal-dermal interface by SILAC-iTRAQ-TAILS**. *Proteomics* 2015, **15**:2491–2502, https://doi.org/10.1002/pmic.201400627.

35. Bell PA, Solis N, Kizhakkedathu JN, Matthew I, Overall CM: **Proteomic and N-terminomic TAILS analyses of human alveolar bone proteins: improved protein extraction methodology and LysargiNase digestion strategies increase proteome coverage and missing protein identification**. *J Proteome Res* 2019, **18**:4167–4179, https://doi.org/10.1021/acs.jproteome.9b00445.

36. Sabino F, Hermes O, auf dem Keller U: **Body fluid degradomics and characterization of basic N-terminome**. *Methods Enzymol* 2017, **585**:177–199, https://doi.org/10.1016/bs.mie.2016.09.018.

37. Bundgaard L, Savickas S, auf dem Keller U: **Mapping the N-terminome in tissue biopsies by PCT-TAILS**. *Methods Mol Biol* 2020, **2043**:285–296, https://doi.org/10.1007/978-1-4939-9698-8_24.

38. Solis N, Parambath A, Abbina S, Kizhakkedathu J, Overall CM: **Simplified high yield TAILS terminomics using a new HPG-ALD 800k-2000 polymer with precipitation**. *Methods Enzymol* 2019, **6262**:429–446, https://doi.org/10.1016/bs.mie.2019.07.030.

39. * Ju S, Kwon Y, Kim JM, Park D, Lee S, Lee JW, Hwang CS, Lee C: **INrich, rapid and robust method to enrich N-terminal proteome in a highly multiplexed platform**. *Anal Chem* 2020, **92**:6462–6469, https://doi.org/10.1021/acs.analchem.9b05653.
This study presents important novelties in N-terminomics by introducing single-staged multiplexed parallel N-terminal enrichment as a prerequisite for high-throughput analyses.

40. Hughes CS, Moggridge S, Müller T, Sorensen PH, Morin GB, Krijgsveld J: **Single-pot, solid-phase-enhanced sample preparation for proteomics experiments**. *Nat Protoc* 2019, **14**:68–85, https://doi.org/10.1038/s41596-018-0082-x.

41. Tanco S, Gevaert K, Van Damme P: **C-terminomics: targeted analysis of natural and posttranslationally modified protein and peptide C-termini**. *Proteomics* 2015, **15**:903–914, https://doi.org/10.1002/pmic.201400301.

42. Van Damme P, Staes A, Bronsoms S, Helsens K, Colaert N, Timmerman E, Aviles FX, Vandekerckhove J, Gevaert K: **Complementary positional proteomics for screening substrates of endo- and exoproteases**. *Nat Methods* 2010, **7**:512–515, https://doi.org/10.1038/nmeth.1469.

43. Schilling O, Huesgen PF, Barré O, Overall CM: **Identification and relative quantification of native and proteolytically generated**

protein C-termini from complex proteomes: C-terminome analysis. *Methods Mol Biol* 2011, **781**:59–69, https://doi.org/10.1007/978-1-61779-276-2_4.

44. * Zhang Y, Li Q, Huang J, Wu Z, Huang J, Huang L, Li Y, Ye J, Zhang X: **An approach to incorporate multi-enzyme digestion into C-TAILS for C-terminomics studies**. *Proteomics* 2018, **18**: 1700034, https://doi.org/10.1002/pmic.201700034.

Here, an elegant approach is presented that combines specific enzymatic reduction of charge states of non-C-terminal peptides with ChaFRADIC for large-scale C-terminome analysis.

45. Chen L, Shan Y, Yang C, Sui Z, Zhang X, Zhang L, Zhang Y: **Carboxypeptidase B-assisted charge-based fractional diagonal chromatography for deep screening of C-terminome**. *Anal Chem* 2020, **92**:8005–8009, https://doi.org/10.1021/acs.analchem.0c00762.

46. Bourmaud A, Gallien S, Domon B: **Parallel reaction monitoring using quadrupole-Orbitrap mass spectrometer: principle and applications**. *Proteomics* 2016, **16**:2146–2159, https://doi.org/10.1002/pmic.201500543.

47. Sabino F, Hermes O, Egli FE, Kockmann T, Schlage P, Croizat P, Kizhakkedathu JN, Smola H, auf dem Keller U: **In vivo assessment of protease dynamics in cutaneous wound healing by degradomics analysis of porcine wound exudates**. *Mol Cell Proteomics* 2015, **14**:354–370, https://doi.org/10.1074/mcp.M114.043414.

48. Gallien S, Kim SY, Domon B: **Large-scale targeted proteomics using internal standard triggered-parallel reaction monitoring (IS-PRM)**. *Mol Cell Proteomics* 2015, **14**:1630–1644, https://doi.org/10.1074/mcp.O114.043968.

49. Lange PF, Overall CM: **TopFIND, a knowledgebase linking protein termini with function**. *Nat Methods* 2011, **8**:703–704, https://doi.org/10.1038/nmeth.1669.

50. Guo T, Kouvonen P, Koh CC, Gillet LC, Wolski WE, Röst HL, Rosenberger G, Collins BC, Blum LC, Gillessen S, Joerger M, Jochum W, Aebersold R: **Rapid mass spectrometric conversion of tissue biopsy samples into permanent quantitative digital proteome maps**. *Nat Med* 2015, **21**:407, https://doi.org/10.1038/nm.3807.

51. ** Ye Z, Mao Y, Clausen H, Vakhrushev SY: **Glyco-DIA: a method for quantitative O-glycoproteomics with in silico-boosted glycopeptide libraries**. *Nat Methods* 2019, **16**:902–910, https://doi.org/10.1038/s41592-019-0504-x.

This work is of outstanding interest, since it demonstrates how PTM libraries can be used to query digital proteome maps for PTM-modified peptides without enrichment.